The Physiology and Computation of Pyramidal Neurons

Thesis by
Adam Shai

In Partial Fulfillment of the Requirements for the degree of
Bioengineering

CALIFORNIA INSTITUTE OF TECHNOLOGY
Pasadena, California
2016
(Defended December 8, 2015)

ACKNOWLEDGEMENTS

"Sitting in the gaudy radiance of those windows hearing the organ play and the choir sing, his mind pleasantly intoxicated from exhaustion, Daniel experienced a faint echo of what it must be like, all the time, to be Isaac Newton: a permanent ongoing epiphany, an endless immersion in lurid radiance, a drowning in light, a ringing of cosmic harmonies in the ears."

Neal Stephenson in Quicksilver

Sometimes it feels as if graduate school was designed specifically to keep a certain type of soul happy. Those of us whose obsessions tend to overtake polite conversation, betraying either a slight social ineptitude or quirky personality trait, depending on who you ask, tend to find a home in the academic life. That such a setting was afforded to me requires my unrelenting thanks. I cannot think of a more joyous situation than the last six years of my life, where I was expected and able to be thinking intensely about what I wanted to think about.

I came to Caltech primarily as a result of an interesting conversation with Christof Koch, about consciousness, quantum mechanics, and art, when I first visited during the winter of 2009. That he became my advisor guaranteed that I would be cared for during my graduate studies. Christof takes the calling of *Doktorvater* seriously. The environment of K-lab, by Christof's example and design, was one of intense intellectual playfulness. During lab lunches we could plausibly expect to hear a talk on NMDA receptors in single neuron computation, the tuning of neurons in the human brain to Jennifer Aniston, information theory measurements of consciousness, or fMRI studies on face processing. The breadth and depth of conversation in the lab was something inspiring and unique. At every step of the way Christof supported me and made sure I was provided for. That I had such a unique graduate experience, being able to call four different labs, in three different locations home, was his doing. Upon joining K-lab, Christof introduced me to Costas Anastassiou, at that time a postdoc in the lab. Costas would become a mentor and friend for the duration of my studies. At every step of the way he has been there for support, both scientific and personal. I will always have fond memories of sitting in the same space, working late, and blasting Stan Getz or Biggie Smalls. I have no doubt that the contents of this thesis would look substantially worse were it not for Costas' direction and motivation. I have been extremely lucky that both Christof and Costas have remained integral parts of my advising, even after K-lab ceased, and we moved to the Allen Institute in Seattle.

I owe a debt of gratitude to many in K-lab (including Christof and Costas). Costas, Erik Schomburg, Yazan Billeh (who bore the brunt of my incessant semi-understandable rantings about whatever topic happened to have caught my attention that day), and Jiannis Taxidis, formed the biophysics group, and were a constant source of help and friendship. Nathan Faivre, Michael Hill, Liad Mudrik, Xiaodi Hu, and Virgil Griffith, were always available to discuss topics ranging from philosophy of consciousness and psychophysics to the mathematics of information or gut bacteria and theories of humor.

During my time at Caltech, a group outside of K-lab provided friendship. In Sandy Nandagopal I found someone to discuss systems biology, and the similarities and differences between neuroscience and genetic regulatory networks. More importantly, he was a sounding board for complaints about science, sharing musical tastes, and making jokes at the others' expense. Elizabeth Jensen, Naomi Kraemer, Emzo De Los Santos, Jerzy Szablowski, Gustavo Rios, Devin Trudeau, and Naeem Husain were all vital friends during my graduate school years. The administrative staff at Caltech were the best I have ever seen. Special thanks to Linda Scott, who was always available and ready to help. My thesis also owes an obvious debt to my committee members, Christof Koch, Costas Anastassiou, Markus Meister, Vivianna Gradinaru, and Doris Tsao. They all provided important feedback throughout my studies.

In my third year, I had the incredible pleasure of spending a year in Matthew Larkum's lab in Bern, Switzerland, and then in Berlin, Germany. Before leaving for Europe I already knew that I was lucky to learn patching from the world's best, but I was unaware of how inspirational my time in the Larkum lab would be. Matthew is a world-class experimentalist who is not scared of thinking big and speculating on how details of physiology could fit into larger-scale phenomenon, even consciousness. Always with a child's wonder and excitement, Matthew showed a purity of scientific curiosity that was infectious. Aside from long hours at the rig patching cells, I will cherish long conversations about morality and consciousness. Matthew's lab also ended up being a source of great friendships and collaborations. Lucy Palmer, Sean Murphy, Jan Schulz, Tim Zolnick, and Julie Seibt were all there for my constant questions and fun lunch outings. I've benefited greatly from continued communication with Lucy and Sean and they have played an important part in my graduate work and life beyond my time in Berlin, and I hope that continues.

During my time in Europe, Christof began his position as Chief Scientific Officer at the Allen Institute in Seattle. I was incredibly fortunate to be able to continue working on my projects there. During my two years in Seattle, I had the honor of constantly being the most ignorant person in the room. Hongkui Zheng graciously accepted me into her group. Tim Jarsky and Gilberto Soler-Llavina were both helpful beyond any reasonable expectation of lab-companionship, constantly giving advice and answering questions about electrophysiology and life. Natalia Orlova and Corrine Teeter were especially good friends, helping me out both scientifically and outside of the lab. Whether going for hikes, bike rides, or dinners, their companionship was a great boon for my sanity and happiness. The list of friends I've made at the Institute is long, and I will undoubtedly forget someone. Ram Iyer, Severine Durandt, Rylan Larson, Marina Garret, Soumya Chaterjee, Nick Cain, Bosiljka Tasic, all became companions in the lab. Adrian Cheng, Jim Berg, Elliot Mount, Marty Mortrud, Ben Oullette, Phil Bohn, Jonathan Ting, and Lu Li all helped in setting up various parts of my experiment and providing scientific support. In addition, my roommates, Christa Fagnant and Dan Meyers, were an indispensable part of my life, providing a home to unwind at, and dinners that had all the supportive roles of a family.

While working on the experiment in Seattle, I still had an academic home back at Caltech due to the graciousness of Markus Meister. I was provided with a desk, but more importantly a lab environment to be part of. Being able to present, and watch, lab meetings was an important part of my time at Caltech. More generally, I was the beneficiary of many great discussions about

neuroscience (and even sometimes about topics that weren't quite neuroscience), with Markus and his lab. Many Meister lab members became good friends, particularly Brenna Kreiger, Melis Yilmaz, and Margarida Agrochao.

During my graduate work, I had a number of different organizations provide funding for me and the projects I worked on. The National Science Foundation, the Whitaker Foundation, the Mather's Foundation, the Swiss National Fund, and Paul and Jody Allen all contributed immensely to my work.

Finally, I owe a great debt to my family and friends. Due to the impressive technology that is Whatsapp, a tight group of high school friends has been a source of daily humor and companionship during my graduate tenure. My family (we also happen to have an active Whatsapp group), has been the defining influence on every aspect of my personality. How I think and laugh is due to their ever-present love and support. Our family is one of constant laughing and poking fun at eachother and the world. More importantly, they displayed an unwavering encouragement, when tolerance would have sufficed, of my eclectic interests over the years. My curiosity is entirely a function of my family environment. My father, mother, sister, and grandmother have provided this bedrock of love and support for my entire life. This thesis would be inconceivable without them.

ABSTRACT

A variety of neural signals have been measured as correlates to consciousness. In particular, late current sinks in layer 1, distributed activity across the cortex, and feedback processing have all been implicated. What are the physiological underpinnings of these signals? What computational role do they play in the brain? Why do they correlate to consciousness? This thesis begins to answer these questions by focusing on the pyramidal neuron. As the primary communicator of long-range feedforward and feedback signals in the cortex, the pyramidal neuron is set up to play an important role in establishing distributed representations. Additionally, the dendritic extent, reaching layer 1, is well situated to receive feedback inputs and contribute to current sinks in the upper layers. An investigation of pyramidal neuron physiology is therefore necessary to understand how the brain creates, and potentially uses, the neural correlates of consciousness. An important part of this thesis will be in establishing the computational role that dendritic physiology plays. In order to do this, a combined experimental and modeling approach is used.

This thesis beings with single-cell experiments in layer 5 and layer 2/3 pyramidal neurons. In both cases, dendritic nonlinearities are characterized and found to be integral regulators of neural output. Particular attention is paid to calcium spikes and NMDA spikes, which both exist in the apical dendrites, considerable distances from the spike initiation zone. These experiments are then used to create detailed multicompartmental models. These models are used to test hypothesis regarding spatial distribution of membrane channels, to quantify the effects of certain experimental manipulations, and to establish the computational properties of the single cell. We find that the pyramidal neuron physiology can carry out a coincidence detection mechanism. Further abstraction of these models reveals potential mechanisms for spike time control, frequency modulation, and tuning. Finally, a set of experiments are carried out to establish the effect of long-range feedback inputs onto the pyramidal neuron. A final discussion then explores a potential way in which the physiology of pyramidal neurons can establish distributed representations, and contribute to consciousness.

Table of Contents

Chapter 1

INTRODUCTION

"Once, probably, I used to think that vagueness was a loftier kind of poetry, truer to the depths of consciousness, and maybe when I started to read mathematics and science back in the mid-70s I found an unexpected lyricism in the necessarily precise language that scientists tend to use. My instinct, my superstition is that the closer I see a thing and the more accurately I describe it, the better my chances of arriving at a certain sensuality of expression.

And I think the key to all this is precision. If the language is precise, the sentence will not (in theory) seem self-conscious or overworked. At some point (in my writing life) I realized that precision can be a kind of poetry, and the more precise you try to be, or I try to be, the more simply and correctly responsive to what the world looks like -- then the better my chances of creating a deeper and more beautiful language."

- Don Delilo letter to David Foster Wallace on precision in writing, February 5, 1997

CONSCIOUSNESS

It would be difficult for even the most hard-nosed materialist to deny the primacy of the qualitative aspects of life. Many of the actions we knowingly take are directed toward the manipulation of our conscious state. The scientist who says we eat only to pay an advance towards metabolic costs neglects the most intimate and well-known facts about ourselves, and one of the fundamental mysteries in his field. We eat to feel satiated. That is to say we eat for the same reason we put so much effect into planning and ultimately taking many of our actions, to *feel* a certain way (and what should we make of that scientist who explains sex in the human species without mention of lust or love?). That our plans for actions are ultimately attempts to manipulate our own conscious states in certain ways underlies the central importance of consciousness in our lives. Indeed we have little else.

Given how intimate our conscious experience is, it perversely seems to have eluded scientific description. There are many philosophers today who claim that consciousness will necessarily escape a wrangling-in by science. For the most part, centuries of philosophical and more recent experimental work[1] have not lessened that mystery. It might even seem hard to imagine what a mature science of consciousness would look like. Consider, though, the state of affairs of energy physics in the 17th century. At that time, Descartes and Leibnez each held contradictory views on the nature of motion, and in particular, on what exactly were the conserved quantitates of motion. Today we might see this argument, known now as the *vis-viva controversy*, as one between

[1] This all depends on where exactly you want to draw the lines between experimental and non-scientific exploration. Because of the subjective nature of consciousness, some would consider intense self-reflection like those seen in various meditative practices as experiments on consciousness.

momentum, *mv,* and kinetic energy, mv^2. However, at the time the debate carried much more serious ontological underpinnings. Conservation laws were understood to exist on first principles, due to gods perfect nature. The argument was then one of figuring out what quantity, *motion* (mv) or *force* (mv^2), was real, and actually existed. Today, of course, we are quite happy to use momentum and kinetic energy in our equations and to feel secure in our understanding of mechanics, without the intellectual burden of ontology. Then though, the debate often did not concern itself with experimental results, but instead with considerations on what must necessarily be true, philosophically. The purpose of this example is not to explore the specifics of Leibniz's monodalogy or Cartesian views on extension and motion (for that see Iltis 1971). Instead, imagine a Leibniz or Descartes watching an introductory college lecture on mechanics, and being baffled at the lack of discussion on what constitutes the *true* nature of reality. Has the triumph of physics been in answering those questions, or in disregarding them?

Consider the word *energy*. It has all the mysterious and supernatural connotations that the word consciousness has. Today, there are *still* philosophers who argue that the nature of energy means that it will forever escape scientific explanation. This position, called *mysterianism*, is one philosophical argument used to explain the ultimately unknowable nature of consciousness. But how many of us are ready to call the attempts of physicists to understand energy a failure? Our current understanding of energy has left us not only with concepts and equations that describe and help us engineer systems of billiard balls and inclined planes, but is equally applicable to chemical reactions, heat, electricity, magnetism, star-nebulae, etc. One wonders if anyone other than a philosopher could possibly consider our current understanding of energy mysterious. If

this is the type mystery left over after science is done with consciousness, then bring it on. The world and our understanding of ourselves will be much better for it.

All the same, there is no denying that consciousness is today quite a mystery. What is the way forward?

A WAY FORWARD – THEORY AND EXPERIMENT

In 1920, a 21 year old Friedrich Hayek (later to become the famous economist and winner of the 1974 Nobel Prize in Economic Sciences), wrote one of the first explicit proposals linking the coordinated activity of neural assemblies to consciousness and the representation of percepts in the brain (Hayek 1991). Though Hayek would devote the majority of his adult life to economic theory[2], he would, some three decades later in 1953, publish an extended book on those same ideas in *The Sensory Order: An Inquiry into the Foundations of Theoretical Psychology* (Hayek 1999)[3]. The general "problem of theoretical psychology" that Hayek introduced in *The Sensory Order* was to first describe what, and then explain how, physical states of the brain give rise to sensory perception. To satisfy these criteria he postulated a conceptual mechanism for how the collective action of individual neurons could carry out a highly complex hierarchical classification function, and how such aggregate activity binds sensory primitives to represent percepts – a defining problem still fundamental to modern neuroscience. By recasting the problem of perceptual representation in terms of classification, Hayek made a great leap forward in suggesting a specific framework of neural processing that accounts for the psyche. The mechanistic descriptions offered by Hayek point to unparalleled insightfulness at the conceptual level, ultimately bridging the gap between the seemingly ineffable psyche and the algorithmic framework of computation.

---

[2] There has been some discussion on the relationship between his thought in theoretical psychology and economics, especially as it relates to the distribution of information in complex networks of individual nodes, e.g. neurons in the brain or humans in a society (Butos and Koppl 2007; Caldwell 2004; Horwitz 2000).

[3] Interestingly, Hayek considered this work to be of his most important intellectual achievements, and was disappointed that it did not reach the popularity of his others works (Caldwell 2004).

Theoretical (and often philosophical) work has continued in the decades since Hayek's work, but perhaps the most progress has been in identifying biophysical signals that correlate to different behavioral and psychological states. Most typically, electrical activity as measured via electroencephalography (EEG) or fluctuations of magnetism assayed via magnetoencelography (MEG) gathered from the scalp of humans have been shown to correlate to behavioral and psychological states. An offspring of such studies is the well-known framework of the *neural correlates of consciousness* (or NCC), i.e. the minimal set of neural events and mechanisms jointly sufficient for a specific conscious percept. The NCC framework, first proposed by one of the discoverers of DNA structure and Nobel prize winner, Francis Crick, and his colleague Christof Koch, was suggested as a scientific framework in which to study consciousness (Crick and Koch 1990; Crick and Koch 2003). Generally, the study of consciousness can be separated into studying *contents* and *level*. The *contents* of consciousness refer to those perceptual objects that a subject is conscious of, for instance, when a subjects reports being aware of a tree in their visual field. *Level*, on the other hand, refers to the continuum spanning from dreamless sleep to normal waking life.

The use of NCC, studying both contents and level, has yielded a fruitful but extremely nuanced list of candidate signals that correlate (in varying degrees and with varying evidence) consciousness and other related subjects, like attention and decision-making. Due to the necessary use of noninvasive techniques in humans, these signals are often found using EEG, or fMRI. Alternatively, in a clinical setting human patients that have to undergo brain surgery (e.g. to treat epilepsy) live days with intracranial depth electrodes implanted in their brains,

allowing neuroscientists to work with them and study how cognitive processing is related to neural signals. Thus, when measured with EEG, MEC, or depth electrodes, the NCC usually consist in modulations of amplitude in the extracellular signal (alongside their timing), or modulations of oscillatory power in certain frequency bands of the extracellular signals. When measured with fMRI, blood-oxygen level dependent (BOLD) signals are used as a proxy for neural activity, and to find spatial locations in the primate brain. Despite the immense advances in this kind of research, they have taken place largely independent from more theoretical concerns, like those discussed by Hayek.

In order to understand consciousness, neuroscience must find mechanistic explanations for how the NCC reflect, support or even constitute the conscious mind, ultimately explaining theoretical concerns through an understanding of the function of neurons and the circuits they compose. Moreover, this thesis will show that an investigation of the details of physiology and anatomy of the brain can drive the creation of experimentally testable psychological theories. Importantly, neuroscience is now at a point where biophysical and anatomical details can be used to close the gap between experimental neuroscience, psychology and theoretical concerns. Although much work has been done to find explanations that relate signals to psychological phenomena, it is important to realize that it is the physiology and anatomy of neurons and the networks they create that actually compute and perform tasks in the brain. In other words, the neural substrate of psychology are cells and their networks, and not (directly) extracellular fields, oxygenation levels, or frequencies in certain bandwidths (though alternative ideas exist (Hameroff 1994; McFadden 2002; Pockett 2012)). Thus, theories of consciousness and perception acknowledge that the signals mentioned are proxies for the activity of cells and

their networks. The method is thus easily described by a triumvirate of areas of study (in no particular order), related to each other, as shown in **Figure 1**.

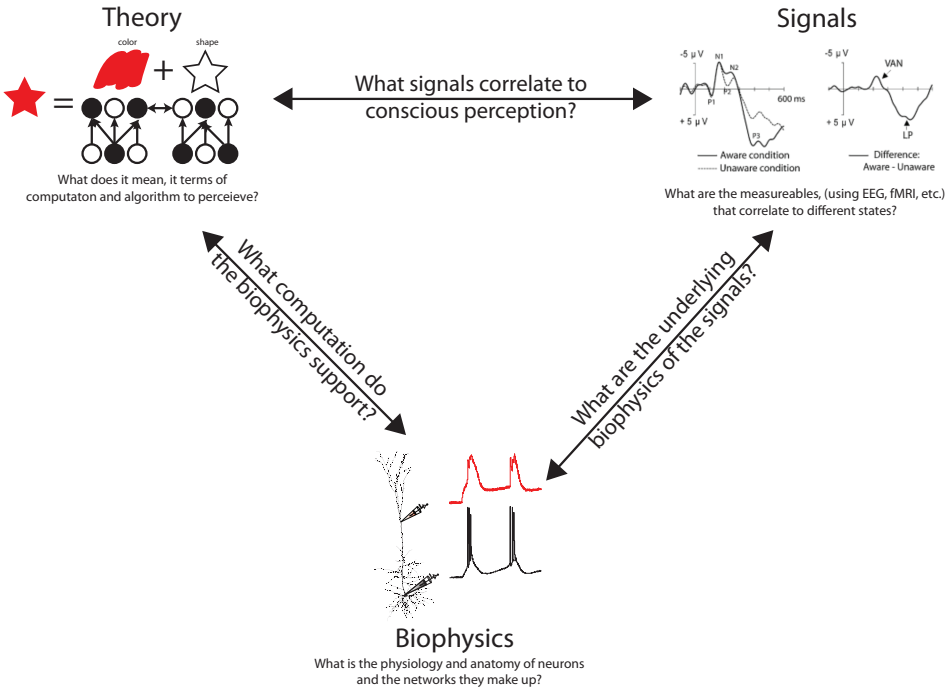

Figure 1: Signals correlated to conscious perception and theoretical concerns can be connected by considering the biophysics of signals and the computations they perform. Theory concerns itself with what it means in terms of computation and algorithm to consciously perceive something. Signals refers to the population level measurements found in the psychophysics literature (e.g. EEG, fMRI, ECoG). The underlying biophysics of these signals can be uncovered using the tools of experimental neuroscience, and then the computational functionalities of networks made from those biophysics can be explored in order to bridge theory and signals.

First are the empirically reported signals that correlate with psychological phenomena. As discussed, these can include signatures of the EEG, locations found via fMRI, extracellular recorded spiking of cells in the thalamocortical system, and power spectrum analysis in different bands. Second are the theoretical considerations regarding psychological phenomena. These include questions regarding computational and functional concerns - for example, what does it mean in terms of a general algorithm to attend to something, or represent a conscious percept? Answers to these questions are often given using some mathematical framework, for instance Bayesian inference (Knill and Pouget 2004; Ma et al. 2006; Yuille and Kersten 2006), predictive coding (Carandini and Ringach 1997; Rao and Ballard 1999), integrated information theory (Oizumi, Albantakis, and Tononi 2014), the free-energy principle (Friston 2010), or can take a more conceptual form such as neural Darwinism (Edelman 1993), global workspace theory (Baars 2005), or indeed the ideas of Hayek and their modern extensions like the cognit (Fuster 2003; Fuster 2006).

Bridging the empirical signals and theoretical concerns are the biophysical mechanisms. One natural area of study arises in elucidating the physiological underpinnings of signals that correlate to specific psychological states. For instance, given a specific EEG amplitude occurring over the visual cortex, what subnetworks, cell types, transmembrane currents, etc. contribute to that signal? Because these anatomical and physiological details are the substrate of neural computation, we can then delve into the the computational role these physical mechanisms play. These questions connect high-level theory, low-level biophysical details, and mid-level psychophysical signals.

This thesis will explore the use of biophysics in order to elucidate and build the connection between signals and psyche, using the physiology and anatomy of pyramidal neurons in the neocortex in order to explain a mechanism for perceptual binding.

THE NEURAL CORRELATES OF CONSCIOUSNESS

What processes in the brain accompany conscious perception? In the attempt to answer this question, scientists have carried out more than a century's work, often under the area of study called psychophysics, to find measurable signals in the brain that correlate to consciousness. In particular, we discuss the evidence for three such neural signatures: (1) late extracellular signals, (2) distributed information sharing in cortex, and (3) long-range feedback connections within the cortex. As we will see, the boundaries between these topics are often overlapping, but they have been studied in an independent enough manner to discuss them individually (though not necessarily independently).

Late extracellular signals

In 1964, Haider, Spong, and Lindsley (Haider, Spong, and Lindsley 1964) used scalp electrodes to record extracellular signals from humans during a simple detection task. Dim flashes of light were shown to the subjects, who were asked to report perception of these stimulii. When comparing the averaged extracellular signature of seen and unseen trials, a significant difference was found in the amplitude of a negative wave occurring approximately 160 ms after the signal onset, with the amplitude of the negative wave being positively correlated to perception. These visual results were later reproduced in the auditory cortex (Spong, Haider, and Lindsley 1965).

Similar conclusions were formed in a series of papers in the 80s and 90s. Cauller and Kulics performed a go/no-go discrimination task on forepaw stimulation in monkeys (Kulics and Cauller 1986; Kulics and Cauller 1989). They compared the extracellular signal in the somatosensory cortex, and found that an early positive component (called P1, occurring about 50ms after the stimulus) correlated well to the signal strength whereas a later negative component (called N1) correlated to the behavioral report of the signal (interpreted as the conscious perception). In a later study using depth electrodes, the laminar structure of these signals was examined using current source density analysis. Interestingly, the early P1 signal was found to be attributed to a current sink in layer 4, while the later N1 signal was attributed to a current sink in layer 1. Later work also showed that the later N1 signal was absent during sleep and anesthesia (Cauller and Kulics 1988).

More recent psychophysical work, using a spectrum of masking techniques, has suggested a variety of different extracellularly recorded signals that might correlate to consciousness. Two of the most plausible seem to be the Visual Awareness Negativity (VAN) (Koivisto et al. 2008) and the p3b (also known as p300 or late potential). Discussion of whether these signals correlate to consciousness itself, or pre- or post-conscious events, is ongoing (for review see (Koivisto and Revonsuo 2010; Railo, Koivisto, and Revonsuo 2011)). The p3b is a signal occurring in a largely all-or-none fashion from 300-400 ms after stimulus onset (**Figure 2**A), but can occur earlier based on expectation (Melloni et al. 2011)[4].The VAN (**Figure 2**A) shows a more graded response than p3b, and occurs from 100-200 ms after the stimulus, but has

[4] Debate over the p3b and what it correlates to has increased recently, with evidence both pointing to (Gaillard et al. 2009; Salti et al. 2015) and against (Silverstein et al. 2015) its status as an NCC.

been shown to occur as late as 400 ms given the right stimulus conditions. One study asked subjects to report the subjective awareness of a change in a visual stimulus. EEG signals in aware and unaware trials from the occipital lobe were compared (**Figure 2**A). Both the p3b (referred to as P3 in their figure) and the VAN can be seen to clearly signify the difference in awareness. We will not review all the differences between these signals, and all the evidence for their correlation (or absence of correlation) to conscious perception here, but suffice it to say, there seems to be an NCC in a late signal occurring at least 100 ms after the stimulus onset, extracellularly measurable from the scalp. The VAN is particularly interesting as the timing of this signal corresponds to the timing of the signals measured in the Haider et al., study as well as the Kulics and Cauller work discussed above. As argued below, the VAN or p3b might even correspond to recent measurements in behaving rodents.

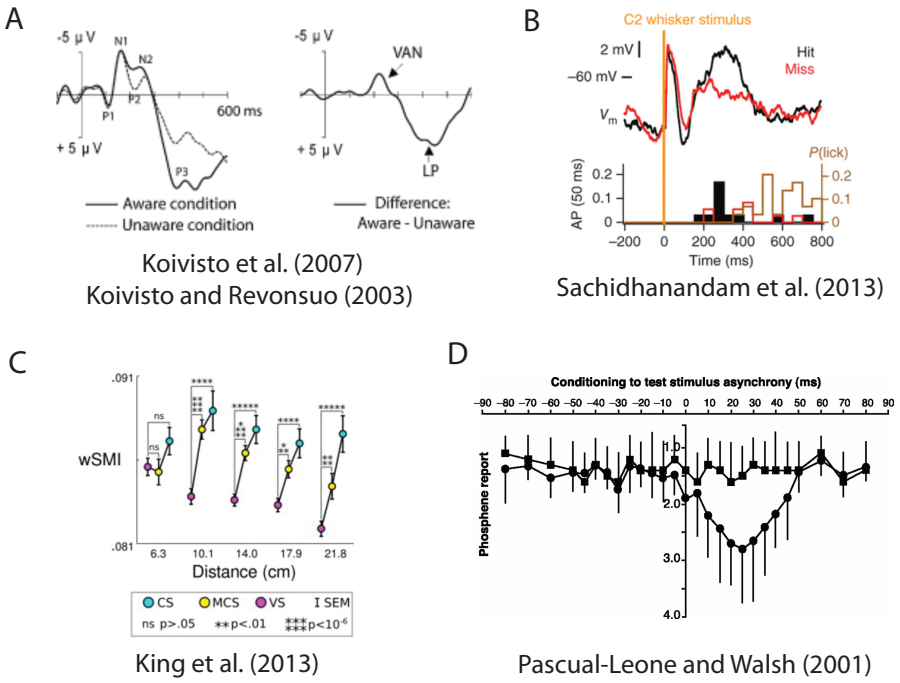

Figure 2: The neural correlates of consciousness. A) EEG signals taken from occipital sites during a change blindness task. On the left are averaged responses from trials where the subject was aware or unaware of the change. On the right is the difference between aware and unaware trials. Data from Koivisto and Revonsuo (2003), figure from Koivisto et al. (2007). B) The subthreshold membrane potential of a mouse L2/3 pyramidal neuron during a whisker stimulus task. Behavioral hits and misses are shown in black and red. There are two epochs of depolarization, with the late epoch correlating to the behavioral output. Figure from Sachidhanandem et al. (2013). C) Weighted symbolic mutual information between EEG sites in control (CS), minimally conscious (MCS), and vegetative (VS) patients. As the distance between sites increases, the differences in wSMI become more and more significant between the different conscious states. Figure from King et al. (2013) D) Phosphene report after TMS stimulation in area V5 followed by V1, after a time delay shown on the x-axis. When V1 stimulation followed V5 stimulation within ~50ms, phosphene report was abolished. Figure from Pascual-Leone and Walsh (2001).

One of the main advantages of primate experiments is the relatively direct knowledge of what the subjects' perception is, though of course this advantage is offset by more limited access to physiological properties. Rodent experiments have been used as a model organism for cortical

physiology at the synaptic, single-neuron (including dendrites), and small network level. Recent genetic tools (e.g. cre-lines, opsins) have made the mouse a preferred animal in cellular and systems neuroscience, despite the relative difficulty in establishing complicated behavior and inferring perceptual state. By establishing measurable (often population or indirect) signals in primates, experimentalists are now able to find analogous signals in the rodent cortex, attempting to establish links between behavior and perception. One recent example is from Sachidhanandam et al. (Sachidhanandam et al. 2013) (**Figure 2**B). In this experiment, mice were trained to report a whisker stimulus during whole-cell patch recording of single pyramidal neurons in the barrel cortex. Two periods of depolarization were found. The first, occurring within 50 ms of stimulus onset, correlated well to stimulus strength. The second signal, occurring 50-400 ms after stimulus onset, correlated well to the behavioral report. Taking advantage of the animal preparation, optogenetics was used to silence pyramidal neurons during both the early or the late epoch. Both types of inhibition abolished the behavioral report. In a control experiment, inactivation of the forepaw somatosensory cortex (and not the whisker cortex) had no effect on performance. These experiments established a causal influence of the late depolarization specifically in the whisker cortex for the perception of whisker deflection.

Taken together, this body of work suggests a potential NCC in a late (~150 ms) signal that originates in the upper layers of the neocortex.

Distributed processing in the cortex

How distributed is the cortical representation for a given conscious percept? What are the necessary and sufficient conditions related to the communication between different areas of the brain and representation of such percepts? Here we review the evidence pointing to the distributed nature of cortical percepts.

Perhaps the earliest work hinting at the distributed mode in which cortex operates was given by the pioneering physiologist Flourens, who sought to test the theory of localized function in the brain made popular by phrenologists like Gall and Spurzheim around the turn of the 19th century[5]. Flourens removed different parts of the brain in rabbits and pigeons, and assessed a range of behavioral abilities. Although he was able to ascribe differences in function between the cerebellum and cerebrum, for instance, he was unable to relate different parts of the cerebrum to different cognitive and memory-dependant behaviors, ultimately positing that memory and cognition were highly distributed throughout the cerebrum (Flourens 1842).

Alongside medical results from the injured soldiers of WW1 (Goldstein 1942), and a number of famous case studies (Harlow 1999), this line of study was continued a century later by Lashley. In this body of work (Lashley 1929; Lashley 1950), Lashley aimed to study the relationship between cerebral damage and cognitive behavior, wanting to more quantitatively explain results in human patients with cortical damage who had their visual discrimination assessed, by using more invasive experiments in rodents, very similar to those of Flourens. In this work, rats were trained to run through a maze. Upon removing varying volumes of cortex

[5] This task was actually assigned to Flourens by the French Academy of Sciences in Paris, on order of Napoleon Bonaparte. Gall was not seen to have carried out his experiments with ample scientific rigor by the Academy (Pearce 2009).

in different areas, rats were reintroduced into the maze, and their ability to complete the maze was assessed. Lashley found that the maze-running ability was related to the volume, but importantly not the location, of the cortical lesion. He thus posited that the ability to run through the maze was not contained in any specific local part of the cerebrum, but was instead distributed amongst the entirety of the cortex.

One caveat of the work presented so far is that it is often not explicitly testing the distributed nature of a conscious percept per se, but instead a more general cortex-dependent behavior. More recently, psychophysical experiments in humans have suggested that widely distributed cortical activity is associated with conscious perception, while activity more localized to the primary sensory areas is not. Using intracortical EEG, Gaillard et al. (Gaillard et al. 2009), used a masking paradigm to compare conscious vs. unconscious extracellular signatures. They found that conscious perception of the stimulus was associated with widely distributed voltage deflections sustained across the cortex, increased beta (12-20 Hz) synchrony across the cortex, as well as gamma (30-60 Hz) power. The timing of these changes was late, occurring most obviously 300 ms after stimulus presentation (this was interpreted as being the p3b, though significant differences could be measured starting at 200 ms). Other similar studies show that more localized gamma band activity relegated to the visual cortex accompanies conscious perception (Fisch et al. 2009), though follow up studies argue that these signals are related more with pre- or post-conscious processing (e.g. decision making and report, Aru et al. 2012) than with conscious perception itself, a general weakness of the contrastive method (Aru et al. 2012; de Graaf, Hsieh, and Sack 2012; Tsuchiya et al. n.d.).

Two recent studies used mathematical concepts related to information sharing across the cortex to successfully quantify the amount of consciousness in patients. King et al., (King et al. 2013) used weighted symbolic mutual information, a novel measure of information sharing, between pairs of EEG recording sites (**Figure 2**C). Importantly, in comparing this information measure using different distances between electrodes, it was found that differences between different levels of consciousness (e.g. vegetative vs. minimally conscious vs. healthy) were most significant for mid to long-range distances, implicating information sharing between far-away parts of cortex in consciousness. Casali et al., (Casali et al. 2013) used TMS evoked potentials to assess the amount of integration and differentiation distributed across the scalp EEG of patients. Importantly, this method was able to accurately and quantifiably assess the level of consciousness in patients undergoing anesthesia, sleep (Massimini et al. 2005), and varying degrees of brain-injury. Similar results were more recently shown by Sarasso et al., (Sarasso et al. n.d.), comparing propofol and xenon anesthesia, which induce states of unconsciousness with no dreams, to dream-inducing ketamine anesthesia. In propofol and xenon anesthesia, integration and differentiation measures were found to be low, while in ketamine, these same measures were high. These two studies show that the concept of long-range distributed information sharing is not only a qualitatively useful correlate of consciousness, but is also quantifiable and workable in a medically applicable setting. Similar studies using transfer entropy measures have been used to study anesthesia in rats (Imas et al. 2005).

How distributed the representation for a conscious percept needs to be is a matter of ongoing debate. For visual perception, it is quite clear that V1 is generally necessary but not in itself

sufficient to support a conscious content (Blake and Fox 1974; Crick and Koch 1995; Cumming and Parker 1997; Gawne and Martin 2000; Rees, Kreiman, and Koch 2002), though it is unclear if information processing needs to reach extrastriate areas or the most frontal regions or the entirety of cortex. Whatever the case, long-range communication in the cortex[6] between at least several centimeters in a human (or on the order of a millimeter in the mouse) is a necessary condition for representation of a conscious percept.

Feedback processing

A separable but not completely independent area of study from the distributed nature of processing in the cortex is the study of feedback processing of extrastriate areas or frontal regions to primary visual cortex. Here, the data in any one study does not often explicitly implicate feedback processing, but is instead interpreted to be feedback from considerations like timing and anatomy.

The timing of extracellularly measured potentials that correlate to consciousness, like the VAN discussed previously, suggest that they might have their origin in long-range feedback connections from other areas of cortex. The sensory driven, feedforward step of information processing follows a stereotyped succession of cortical areas, and is completed in ~100 ms (Lamme & Roelfsema, 2000). Indeed, many theories of consciousness rest on this fact, and

[6] One interesting possibility is that such long-range communication is mediated through the thalamus via L5b pyramidal neurons, and not directly within the cortex. Some evidence exists that such a pathway is indeed the main mode in which different areas of cortex communicate with each other (Sherman and Guillery 2002; Sherman and Guillery 2011a).

some even go so far as to equate recurrent processing with consciousness (Lamme 2006). Experiments using TMS and other stimulation techniques have tested the causal influence of late, presumably long-range feedback processing, on perception. Multiple studies using different sensory paradigms have now shown interruption of perception by TMS over V1, during two distinct time periods, the early one interpreted to be the feedforward sweep, and a later one (>200 ms) interpreted to be a feedback sweep (Heinen, Jolij, and Lamme 2005; Juan and Walsh 2003). Additionally, phosphenes induced by TMS over V5 (an extrastriate visual area) can be reduced by a lagging TMS pulse over V1, presumably interrupting the feedback of information from V5 to V1 (**Figure 2**D) (Pascual-Leone and Walsh 2001).

Another line of evidence comes from single cell recordings, showing that cells in the cortex continue spiking past initial feedforward activity. Many cells in macaque V1 have been found to possess dynamic orientation tuning, having precise tuning to one orientation starting at around 50 ms, and then inverting at 120 ms (Ringach et al. 1997). Network simulations have shown that feedback, but not feedforward, networks can recapitulate these dynamic tuning curves (Carandini and Ringach 1997). Furthermore, single unit recordings have shown that the early firing of cells codes for the general category (e.g. face), while later spiking, ~165 ms, was tuned for specific identity (Sugase et al. 1999). Finally, inactivation of higher areas of cortex (e.g. area MT) greatly alters the response properties of cells in lower areas (e.g. V1 and V2) where feedback axons project (Nowak and Bullier 1997).

A host of studies using a technique called backwards masking might also be explained by the necessity of feedback processing in consciousness. In backwards masking, a target stimulus is

followed, after ~50ms, by a mask (Breitmeyer and Ogmen 2000). The subject is not aware of the target stimulus, even though on trials without a mask the target is consciously perceived. One explanation for this phenomenon is that while the feedforward information flow through the cortex is preserved, theR feedback signals conflict with the mask, rendering the target unconscious. A similar effect is found in patients with V1 lesions. These so called *blindsight* patients retain the ability to perform forced choice tasks even though they can no longer consciously perceive visual stimuli into the affected visual field (Weiskrantz 1986). Although the exact neural underpinnings of *blindsight* are unknown, one candidate mechanism implicates the largely intact feedforward sweep in the retained information processing capabilities, and the disturbed feedback processing in the absence of consciousness (Lamme 2001). Feedback processing has also been implicated in *contextual modulation*, which is the altering of cellular responses by changes of the stimuli outside of their classical receptive field. Interestingly, blindsight of stimulus that would normally create contextual modulation abolishes such modulation (Zipser, Lamme, and Schiller 1996), and so does anesthesia (Lamme, Zipser, and Spekreijse 1998).

THE STRUCTURE OF CORTEX

The NCC discussed in the previous section arise due to the electrical activity of the neocortex. It will be helpful to understand the basic structure of the cortex as a foundation to our inquiry into consciousness. The neocortex of a mouse is 1-1.5 mm thick and forms the outer shell of the brain. Flattened, it would have the surface area of one side of a quarter, and is home to ~4 million neurons. Despite the fact that our own human neocortex is about 2-5 mm thick, has a surface area closer to the size of a large pizza, and is made of ~20 billion neurons, the internal structure of the mouse neocortex is remarkably similar to our own. What follows is a description of that internal structure, most specifically of the mouse neocortex. When appropriate, for instance in the discussion of high-level abstract tuning properties like the concept of Jennifer Aniston, human and non-human primate results will be mentioned.

The tissue of the mouse neocortex can be separated into different areas. For instance, the *visual cortex*, located in the back of the brain, is the area associated with the processing of information from the retina, and the *sensory cortex*, located in front of the visual cortex, is most associated with sensory input onto the skin (or whiskers) such as air puffs on the hindlimb. The visual cortex is further divided into a hierarchy of *visual areas.* Visual input, relayed into the visual cortex from retinal ganglion cells via the dorsal lateral geniculate nucleus of the thalamus, first reaches an area of the visual cortex known as the *primary visual cortex,* or *V1.* V1 takes up a surface area of about 2 mm by 3 mm. Neurons in V1 are arranged such that two visual inputs near in space create responses in groups of neurons that are near to each other within V1. This structure, called a *retinotopic map*, allows the borders of each visual area to be determined. In this way, within

the borders of V1, the full visual space is continuously accounted for. So to in the surrounding visual areas.

From V1, processed visual information is sent into other areas of the visual cortex. In the mouse, the properties of these areas are still being understood, and in some cases, are yet to be discovered or well-defined. The hierarchy in the monkey visual cortex is, however, well established, and a generally analogous situation is expected in the mouse. Details aside, it is known that the mouse visual cortex has at least 9, and probably more, visual areas beyond V1, each with a complete map of the visual space. The response properties of these areas differ in terms of their preferred temporal and spatial frequencies. These areas are also known to have different locations in the hierarchy. For instance, the *latero-medial area* (area LM), which is bordering the entire lateral side of V1, receives direct input from V1, and thus is considered part of the second level of the visual hierarchy. Importantly, the hierarchy contains recurrent connections, so that higher areas can transmit information back to lower areas, for instance from LM back to V1.

Staining the tissue of the neocortex for cell bodies reveals a 6 layered laminar structure of different densities. These 6 layers are enumerated from the surface (right below the skull), starting with *Layer 1*, and then down in depth towards the subcortical structures, ending with *Layer 6*. Each layer has distinct cell types, distinguishable by their morphology, physiology, connectivity, and genetic makeup. All neurons can be separated into two large classes: excitatory and inhibitory neurons. Excitatory neurons, so named due to their excitatory (i.e. depolarizing) postsynaptic effect, make up the vast majority of neurons in the neocortex, taking up 80% of the neural count. Of the different types of excitatory neurons, the *pyramidal neuron* will be the

most important, in this thesis. The remaining 20% of neurons in the neocortex are *inhibitory neurons*, so called due to their inhibitory (i.e. hyperpolarizing or shunting) postsynaptic effects.

A complete review of the different cell types, their laminar positions, and their functional roles in the cortical circuit is beyond the scope of this introduction, but some facts, especially about pyramidal neurons, will form the foundation for everything to come. Pyramidal neurons are the main mode of long-range (>300 um parallel to the surface) communication in the neocortex. They are referred to by the location of their cell body in the laminar structure, for instance, a layer 5 pyramidal neuron is a pyramidal neuron whose cell body resides in layer 5. Pyramidal neurons exist in every layer except layer 1. No matter where they are in the neocortex, they have a similar dendritic structure, despite differences in size. From the cell body, or *soma*, protrudes an *apical dendrite* looking very much like a tree trunk, rising up towards layer 1. A set of thin dendrites, called the *basal dendrites*, protrude off the soma radially, extending out no more than 100 um. The apical dendrite bifurcates 100-500 um up from the soma, depending on which layer the cell body resides in. A layer 5 pyramidal neuron will bifurcate in layer 2/3, approximately 400 um up from the soma. The bifurcations branch out into another set of thing dendrites, called the *tuft dendrites*. Layer 6, layer 5, and layer 4, and layer 2/3 pyramidal neurons have dendrites that reach layer 1. However, there is some significant fraction of layer 6 pyramidal neurons that only reach layer 4.

If these extensive dendritic structures suggest an important integrative role for pyramidal neurons, and they do, they also poise some problems with respect to understanding how this integrative function could work. Consider the layer 5 pyramidal neuron. A synapse in the tufts must cause a depolarization at the axon hillock, some 500 um away! The solution to this issue

will come in a detailed look at the nonlinear electrical properties of the dendrites, and is a major focus of this thesis. By virtue of various ion channels - some synaptic and some non-synaptic - embedded in the dendritic membrane with different spatial distributions, the single neuron will be found to be an incredibly powerful computational device.

As we will see in the results of this thesis, the structure of long-range connections also has lamination. Feedforward axons are generally considered to most strongly activate layer 4, though recent results show that the basal dendrites of layer 5 pyramidal neurons are very strongly depolarized by feedforward input. On the other hand, feedback axons innervate layer 1 and layer 6. Already we begin to see a potential connection between feedback input, the late current sink in layer 1, and the physiology of pyramidal neuron dendrites.

One way to think of the neocortex is to imagine it as a large network of pyramidal neurons interacting with each other via long-distances. Under the assumption that information-sharing over long-distances, in order to establish a distributed representation, is a necessary part of cortical computation, especially when consciousness is involved, we can indeed treat the pyramidal neuron as a cornerstone on which to build up our theories. In this view, the local circuit (including all inhibitory neurons with a 300 um cylinder) is important insofar as it manipulates the activity of pyramidal neurons, which shuttle information far away. In modeling diction, we could in effect have a model where only the pyramidal neuron is explicitly modeled, and all the activity of the local inhibitory circuit is represented as parameterizations of that model. Although this type of model will not be constructed in this thesis, it is an important conceptual tool that will be used to extend the results into a larger theory of cortical computation.

AN OUTLINE OF THE APPROACH TAKEN IN THIS THESIS

Given that layer 1 current sinks, distributed activity, and feedback processing are all NCC, the basic structure of the neocortex immediately points to some important questions. First, given that the tuft dendrites of many pyramidal neurons reside in layer 1, what is their physiology? Can they support signals like the large current sink found in layer 1? Following these physiological concerns, we can ask what computation the physiology of pyramidal neuron dendrites supports. How does the long-range and local network interact with this physiology in order to create the activity of pyramidal neurons? Since these pyramidal neurons are themselves responsible for long-range communication, the answers to these questions should have important implications for how distributed activity over many areas of the cortex is established.

The topics of this thesis can be separated into four questions:

1. What is single cell physiology of pyramidal neurons that have dendrites in layer 1 of the neocortex?

2. What single cell computations does that physiology support?

3. How do long range feedback inputs combine with single cell physiology to create the output of pyramidal neurons?

4. What are the network level implications of such a scheme with regards to cortical function?

We build in logical progression from the biophysics of single cells, to computation in those cells, to the interaction of that cell with local and long-range synaptic inputs, and finally, to network computation as a whole (**Figure 3**). Given the wide range of scale in these questions, and the technical difficulties associated with purely experimental approaches, this thesis will have a large modeling component. But models are not simply tools for a lazy experimentalist. As we will see, a model, rightly constructed, can give incredible insight into the potential functioning of real cells. This dual experimental and modeling approach is especially useful in the attempt to describe how cells compute on a large and varying set of dynamic and spatially distributed inputs, first by virtue of the exquisite control over every variable afforded by computer simulations, and then, by the ability to compare and construct alternative (often substantially simpler) models that act in similar ways to the experiments or more complex models. The distilling of models into their simplest forms, while still being able to account for the relevant behaviors of higher-parameter models, is the quantitative realization of Occam's razor, and serves as the basis for abstraction and ultimately understanding.

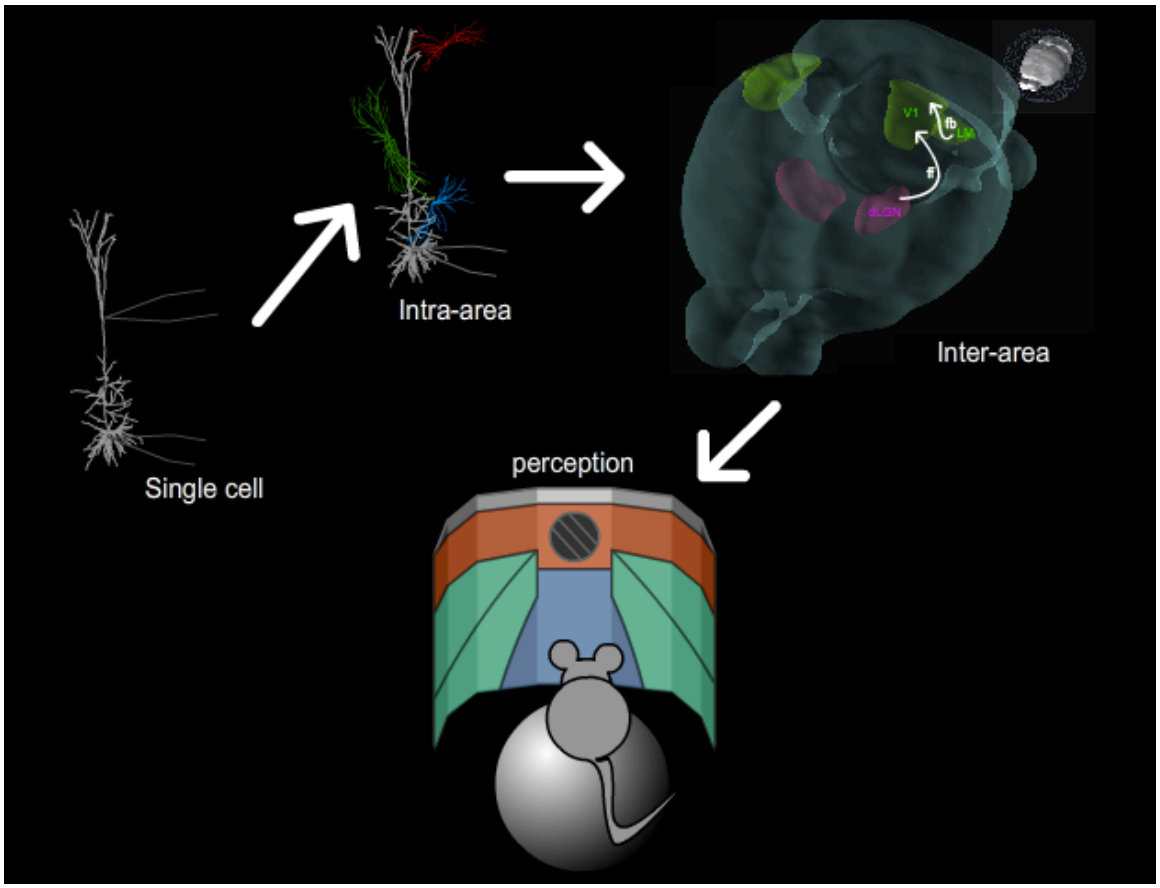

Figure 3: Different levels of inquiry in neuroscience. Neuroscience can study the single cell in isolation, as the atomic unit of computation in the brain. Zooming out, the single cell interacts with the local circuit. Further out still long-range interactions, both feedforward and feedback, impinge on the local circuit. Ultimately, the activity at all of these levels gives rise to perception and behavior.

Chapter 2

BIOPHYSICS OF PYRAMIDAL NEURONS

The role of pyramidal neurons in the cortex is twofold. First, given their large dendritic extent spanning multiple layers, pyramidal neurons act as the main integrator of local cortical column computation. Second, their long-range axons allow them to act as the main conduit of long-range information sharing between distant regions of the cortex. Given their import in both local computation and long-range information sharing, the biophysics of pyramidal neurons will serve as the foundation to our understanding of how the neocortex works. Indeed, considering their placement in the neocortical architecture, and assuming that a foundational part of neocortical computation is the long-range sharing of information between distant areas[7], one can go so far as to make the claim that we only care about cells that make local connections (for instance interneurons) insofar as they support and modify the activity of pyramidal neurons. Thus, a conceptual stance taken here and in the rest of the thesis is that a pyramidal centric view is justified. By the end of this thesis we will explore just how far this point of view can lead us to explanations of cortical computation, and even psychophysical considerations.

For now, this chapter reports on experimental results at the single neuron level. All experiments herein use the whole-cell patch clamp technique, allowing direct electrical access to the somatic compartment of a single neuron. In many of these experiments a second patch,

[7] A justification for this assumption is given in the introductory chapter, at least with respect to conscious perception.

or calcium imaging, is introduced into the thin dendrites. These technically challenging techniques allows a direct look into the highly nonlinear structure of the dendrite, uncovering both synaptic and intrinsic nonlinearities that are unable to be probed with a more standard somatic patch or somatic calcium imaging. All of the experiments discussed in this chapter will form the basis for further modeling and experiments, discussed in later chapters.

This chapter begins with a look at the electrogenic structure of layer 5 pyramidal neurons in the mouse primary visual cortex. In the last decade, the mouse visual cortex has risen to become one of the most popular experimental testbeds for those interested in cortical function, due to the ability to control visual stimulus as well as to probe and manipulate neuronal activity with a host of genetic, electrical, and pharmacological tools. Given the enormous amount of studies that have come out and continue to come out reporting the activity of many neurons in the visual cortex of mice, it is imperative that we understand the physiology of these cells, and how they create the output which is reported (either directly or indirectly) in these papers. We report that the dendritic physiology of layer 5 pyramidal neurons in the mouse primary visual cortex includes two important nonlinearities, NMDA spikes as well as calcium spikes. Additionally, other subthreshold and action potential properties and quantifications of channels such as I_h will be shown. In later chapters, we will create a multicompartmental model to quantify computation in these cells, and discuss mechanisms for spike timing control and frequency modulation. The biophysical work presented here is a foundational step in understanding computation not only in these cells, but also in the networks in which they participate.

Next, the *in vivo* physiology of layer 2/3 pyramidal neurons in the rat somatosensory cortex will be discussed[8]. In this project, an *in vivo* patch clamp was performed, as well as calcium imaging of the dendrites. These experiments looked specifically at the NMDA nonlinearities in the dendrites, and found that NMDA spikes are local events in the dendrites, which can collectively cause action potential outputs during sensory stimulus.

[8] This project was performed with Lucy Palmer and Matthew Larkum.

LAYER 5 PYRAMIDAL NEURONS OF THE MOUSE VISUAL CORTEX

Methods

Experiments were performed in primary visual cortex (V1) neocortical slices from postnatal day (P)35–62 C57BL/6 mice.

Establishing the primary visual cortex slice.

Intrinsic imaging was used to localize V1 (**Figure 4**). Visual stimuli are created using MGL, a freeware Matlab suite for psychophysics (http://gru.brain.riken.jp/doku.php/mgl/). Sinusoidal gratings were shown to the left eye of the mouse, positioned 20 cm from a 13 inch MacBook Pro (Apple Inc., CA) monitor. Gratings were vertically oriented or oblique (45 or 135 degrees), and have a spatial and temporal frequency of 0.045 cycles per degree and 0.069 Hz respectively (Marshel, Garrett, Nauhaus, & Callaway, 2011). Each grating was presented for 5 seconds, and was followed by 30 seconds of a black screen. Results were averaged over 30 trials. V1 (monocular) was found to be a region centered at 2.3 mm lateral from the midline, and 0.3 mm anterior to lambda, and extended at least 1 mm in the lambda direction and 1.5 mm parallel to the midline (**Figure 4**). These results agree with reported stereotaxic coordinates (Dong, 2008). After intrinsic imaging, a bolus of Oregon Green Bapta was injected 500 μm below the pial surface to confirm positions of slices with respect to V1. Parasagittal slices, 300 μm thick, were taken at 12-14 degrees. L5 pyramidal neurons were patched at the soma with intracellular solution containing

Alexa594 (Invitrogen) to visualize the entire dendritic tree of patched cells. The tenth or eleventh slice from the lateral edge was found to contain both the bolus injection as well as L5 apical tuft dendrites that reached the pia, confirming that we have a parallel V1 slice. This method was shown in **Figure 4**.

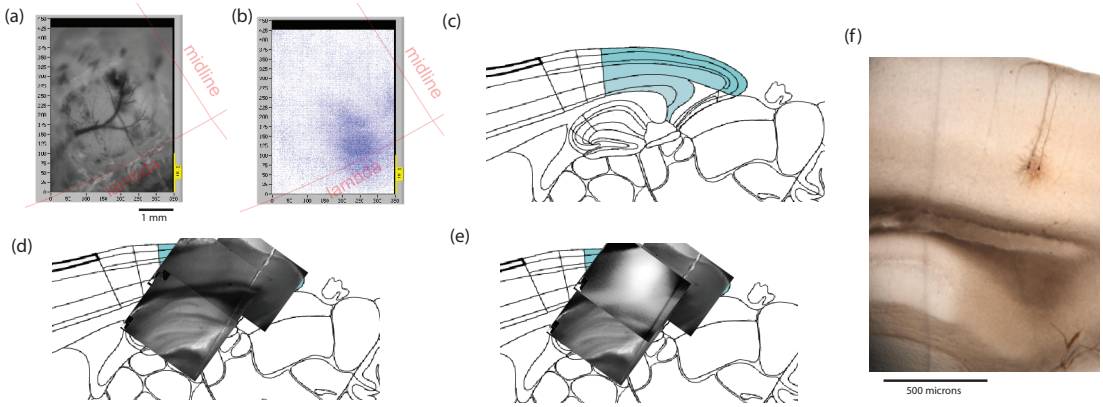

Figure 4: Intrinsic imaging to find a parallel V1 slice. In order to perform this study, we first established a V1, 300 micron slice, which had the full dendritic extent of L5 pyramidal neuron dendrites (ie. The slice had to be normal to the brain surface). To find V1, we used intrinsic imaging with visual stimulus (details in Materials and Methods). a, Image of the craniotomy used during the intrinsic imaging experiment. b, the difference in intrinsic signal between visual stimulus and darkness conditions. c, Allen Brain Reference Atlas sagittal section with visual cortex in green. d, Brightfield image of the V1 slice. e, Fluorescence signal of injected Oregon Green BAPTA bolus into the V1 area found in the intrinsic imaging experiment, verifying that the slice contains V1. f, Biocytin stain of a L5 pyramidal neuron in the V1 slice, verifying that we have a V1 slice with the entire extent of the L5 dendritic tree.

Slice preparation

Slice preparation for electrophysiology was performed using procedures described previously (Ledergerber & Larkum, 2010b). Briefly, mice were decapitated and the brain was quickly removed into cold (0–4°C), oxygenated physiological solution containing (in mM), 125 NaCl, 2.5 KCl, 1.25 NaH2PO4, 25 NaHCO3, 1 MgCl2, 2 CaCl2, and 25 glucose, pH 7.4. Parasagittal slices, 300 μm thick, were cut from the tissue block with a vibratome (Leica VT1200S) and kept at 37°C for 30 min and then at room temperature until use.

Electrophysiology

All experiments were performed at 32.0 ± 0.5°C. Single L5 pyramidal neurons were identified using infrared oblique illumination and a CCD camera (CoolSnap EZ; Roper Scientific). Slices were perfused with the same extracellular solution mentioned above. Recording pipettes were filled with intracellular solution containing the following (in mM): 130 K-gluconate, 5 KCl, 30 HEPES, 10 phosphocreatine, 4 MgATP, 0.3 GTP, pH 7.3. In addition, the somatic pipette contained the following: 10–50 μM Alexa 594 (Invitrogen) to visualize the dendritic arbor for dendritic patching, and 0.2% Biocytin (Sigma). Dual whole-cell voltage recordings were performed from the soma and dendrites (6–10 and 20–40 MΩ pipette resistances, respectively) using Axoclamp 2A (Molecular Devices) and Dagan BVC-700A amplifiers (Dagan Corporation). Access resistances for the dendritic recordings were 15–90 MΩ on break-through. Data was acquired with an ITC-18 board (Instrutech) and custom software written for the Igor environment (Wavemetrics).

Data analysis

Data analysis was performed using Igor software (Wavemetrics) and Matlab (MathWorks). Statistical tests were performed with Matlab using, if not otherwise indicated, a Student's t test in comparison of two datasets, a statistical test comparing the slope of a least squares linear best fit line to 0, or a least squares regression to an exponential function when such a trend was expected (subthreshold and action potential attenuation). Statistical tests were two-tailed unless a reason was explicitly stated to expect a directional relationship between two datasets.

The membrane time constant (τ_m) was measured by fitting a double exponential equation to the voltage response to a long, hyperpolarizing current injection (−200 to −300 pA) and choosing the longer time constant (Ledergerber & Larkum, 2010b).

Sag response was calculated with the equation:

$$Sag = \frac{V_{baseline} - V_{steady-state}}{V_{baseline} - V_{\min}}$$

using V_m recorded at baseline ($V_{baseline}$), the minimum value reached soon after the beginning of the stimulus (V_{min}), and the steady-state value averaged between 400 and 900 ms after the beginning of the stimulus ($V_{steady\text{-}state}$). Sag is thus a heuristic measure that describes the initial dip in membrane potential before a steady-state value is reached in response to long DC current injections.

Following (Waters & Helmchen, 2006) we calculated the input resistance by fitting the following quadratic equation to the steady-state voltage deflection as a function of the responses to long (1000 ms) current injections:

$$\Delta V = R_{N,0}\Delta I + C_{AR}\Delta I^2$$

where $R_{N,0}$ is the slope of the curve at I = 0 (i.e. input resistance at resting membrane potential) and C_{AR} is the coefficient of anomalous rectification and has units of MΩ/nA. Solving for C_{AR} in the previous equation gives us the exact form of the second order correction term:

$$C_{AR} = \frac{\Delta V - R_{N,0}\Delta I}{\Delta I^2} = \frac{\Delta V}{\Delta I^2} - \frac{R_{N,0}}{\Delta I} = \frac{R(V) - R_{N,0}}{\Delta I}$$

where R(V) = ΔV/ΔI. Thus, the second order correction term CAR is a purely phenomenological measure of the deviation of the voltage dependence of the input resistance, and vanishes if the input resistance at all subthreshold current injections is equal to the input resistance measured at rest. We further define a variable $\alpha = C_{AR}/R_{N,0}$ which has units nA^{-1} in order to write:

$$\Delta V = \Delta I R_{N,0}(1 + \alpha\Delta I)$$

which explicitly shows how α describes the deviation from a linear I-V relationship. Thus if $\alpha = 0\ nA^{-1}$ we recover the linear V=IR relationship.

To estimate the occurrence of dendritic plateau potentials in the apical dendrite with long dendritic current injection, we determined the longest depolarization sustained at 20% or more above the baseline level (defined as the most hyperpolarized membrane potential during the dendritic current injection). This includes the effects of backpropagating APs as well as their interplay with the dendritic depolarization.

Results

We investigated the electrophysiological properties of single L5 pyramidal neurons in area V1 in adult mice (P35-62) by whole cell patch clamping the somata and the axial dendrites. The cell bodies were located at cortical depth (mean +/- std) 617 +/- 45 μm (range: 460-715 μm) below the pia. In experiments with dendritic patching, electrodes were placed between 72 and 497 μm from the soma with a mean of 270 +/- 149 μm (n = 13) between the soma and the first bifurcation point along the apical dendrite.

Subthreshold properties

To investigate the subthreshold properties of L5 pyramidal neurons in V1, we injected long (1000 ms) DC current injections through either the dendritic or somatic electrode (**Figure 5** 1a). The results of the analysis of subthreshold properties is given in **Figure 5** and Table 1. Passive cables have a linear relationship between voltage and current (Koch, 1999). Here,

steady-state voltage deflection shows inward rectification (**Figure 5**a, **Table 1**), which is quantified using a coefficient of anomalous rectification ((Waters & Helmchen, 2006), see Methods); C_{AR} = 42.5 +/- 34.7 MΩ nA^{-1} for soma (n=66) and $_{AR}$ = 36.2 +/- 17.3 MΩ nA^{-1} for dendrites (n=13). To further characterize the deviation from the passive case in the subthreshold regime, we used parameter $\alpha = C_{AR}/R_{N,0}$, which describes a second order correction term for the current in the V=IR relationship (e.g. α = 0.5 nA^{-1} implies a 50% deviation from linearity for every 1 nA current injected; see Methods). The cable is found to deviate from linearity with no significant difference between somatic and dendritic regions (**Figure 5**b, α_{soma} = 0.62 +/- 0.30 pA^{-1}, α_{dend} = 0.52 +/- 0.21 pA^{-1}, p = 0.28).

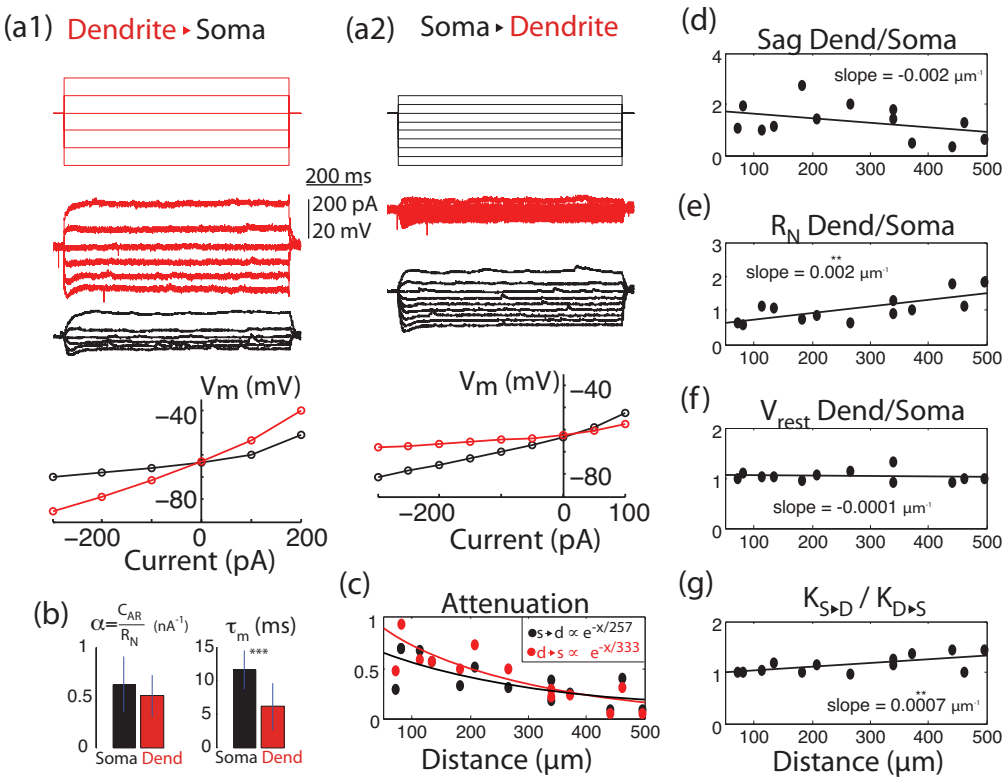

Figure 5: Subthreshold properties of L5 pyramidal neurons in mouse V1. (a) 1 s current steps (top) to the dendrite (a1) and soma

(a2), and the voltage responses (middle) in the dendrites (red traces) and soma (black traces). Bottom, the steady state I-V relationships at the dendrite and soma for current injections into the dendritic (a1) or somatic (a2) electrode in an exemplar L5 cell. (b) Left, Bar graph comparing somatic (n=66) to dendritic (n=13) (= CAR/RN, specifying the deviation from non-linearity see methods) values. Right, bar graph comparing somatic to dendritic time constants, which are significantly different ($p<0.001$, denoted by ***). (c) Attenuation of the steady state voltage from the dendrites to the soma during dendritic current injection (red), and from the soma to the dendrites during somatic current injection (black) as a function of distance from the soma. Curves are exponential fits, and effective length constants shown are derived from those fits. (d) Ratio of sag at the dendrite to sag at the soma as a function of dendritic distance from the soma. The slope of the best-fit line is not significantly different from 0. (e) Ratio of the input resistance at the dendrite to the input resistance at the soma as a function of dendritic distance from the soma. The slope of the best fit line is significantly different from 0 ($p<0.01$, denoted by **). (f) Ratio of the resting membrane potential in the dendrite and soma. The slope of the best-fit line is not significantly different from 0. (g) Ratio of the transfer resistance, KSD/KDS (transfer resistance of the dendritic response to a somatic injection to the transfer resistance of the somatic response to a dendritic injection). The slope of the best-fit line is significantly different from 0 ($p<0.01$)

	Soma Mean	*Soma StDev*	*Dendrite Mean*	*Dendrite StDev*
V_{rest} (mV)	-63.7	5.3	*-69.0 (n=12)*	*7.6*

R_N (MΩ)	67.8	30.9	*89.0*	*45.2*
τ_m (ms)	11.5	3.2	*6.6*	*3.3*
α (1/nA)	*0.62*	*0.30*	*0.52*	*0.21*
C_{AR} (MΩ/nA)	*42.5*	*34.7*	*36.2*	*17.3*
Sag (%)	19.1	6.2	*20.1*	*9.6*
AP threshold (mV)	-44.6	6.3	-41.1	6.7
AP rheobase (pA)	242.4	105.4	357.1	113.4
AP amplitude (mV)	76.2	10.4	48.6	26.5
AP half width (ms)	0.76	0.21	2.62	1.24
Dendritic Recording Distance (μm)	-	-	*270.0*	*149.1*

Table 1: Summary of n=66 somatic and n=13 dendritic physiological properties.

Local membrane time constants were significantly longer at the soma than at the dendrite (**Figure 5**b, 11.5 +/- 3.2 ms vs. 6.6 +/- 3.3, p=1.8e-5). Steady-state voltage attenuation was quantified by finding the effective length constant for somatic or dendritic current injections (λ_{eff} = 257 for somatic and 333 μm for dendritic injections, **Figure 5**c). The ratio of dendritic to somatic sag as a function of distance from the soma (Figure 5d, see Methods) was found to be independent of location (slope -0.002 μm^{-1}, p=0.07). Similarly, a t-test comparing the dendritic (n=13) to somatic (n=66) patches showed no significant difference (sag_{soma} = 19.1 +/- 6.2, sag_{dend} = 20.06 +/- 9.58, p = 0.64), and a paired t-test on the 13 somatic-dendritic dual patches also showed no significant difference (p = 0.93). Mean input resistance in the soma was 68 +/- 30 MΩ, which was significantly different than dendritic input resistance,

found to be 89 +/- 45 MΩ (p=0.034). Similarly, dendritic to somatic input resistance ratio increases as a function of distance from the soma (**Figure 5**e, slope of best fit line is 0.002 μm^{-1}, p = 0.0042).

The dendrites of mature L5 pyramidal neurons in rat somatosensory (SS) cortex are depolarized relative to the soma (Kole, Hallermann, & Stuart, 2006; Zhu, 2000). To test if this is the case in mouse V1, we measured the resting membrane potential (V_{rest}) upon whole cell patch breakthrough. The slope of the best-fit line was not significantly different from zero when we plotted the ratio (**Figure 5**f, slope = -0.0001 μm^{-1}, p = 0.72). The difference between dendritic and somatic resting membrane potential as a function of distance from the soma was also statistically insignificant (p=0.68), suggesting that there is no distance dependence of V_{rest}. Additionally, both paired (n=12; Soma V_{rest} = -67 +/- 5; Dend V_{rest} = -70 +/- 8 mV; p=0.80) and unpaired (Table 1, Soma: n=66, V_{rest} = -64+/-5; Dend: n=12; p=0.96) t-tests fail to show a depolarized dendrite relative to the soma.

To test whether the steady state transfer resistance is symmetric along the dendritic axis (implying that the subthreshold cell acts like a passive cable), we plotted the ratio of soma→dendrite (K_{SD}) to dendrite→soma (K_{DS}) transfer resistance (to -300 pA injections, **Figure 5**g). Interestingly, the slope of the best-fit line was significantly different from 0 and positive (slope = 0.0007 μm^{-1}, p = 0.02), while the y-intercept of that line was not different from 1 (y-intercept = 0.95, p = 0.57), implying that one or multiple nonlinear conductances play a role in the subthreshold regime.

Backpropagation of action potentials

Injections of long current steps (1000 ms) elicited trains of somatic action potentials which backpropagate into the dendrites (**Figure 6**a). The amplitude of the backpropagating action potential (bAP) varies significantly throughout the DC current injections, with the largest amplitude bAP always occurring within the first 3 spikes, and the smallest amplitude bAPs always occurring in the last half of the spike train. The ratio of the dendritic to somatic amplitude of the smallest bAP has an effective length constant of 306 μm, while the amplitude ratio of the largest bAP has an effective length constant of 1013 μm (**Figure 6**b). Similarly, the bAP amplitudes of the smallest and largest bAP decrease with effective length constants of 309 and 1148 μm (**Figure 6**c).

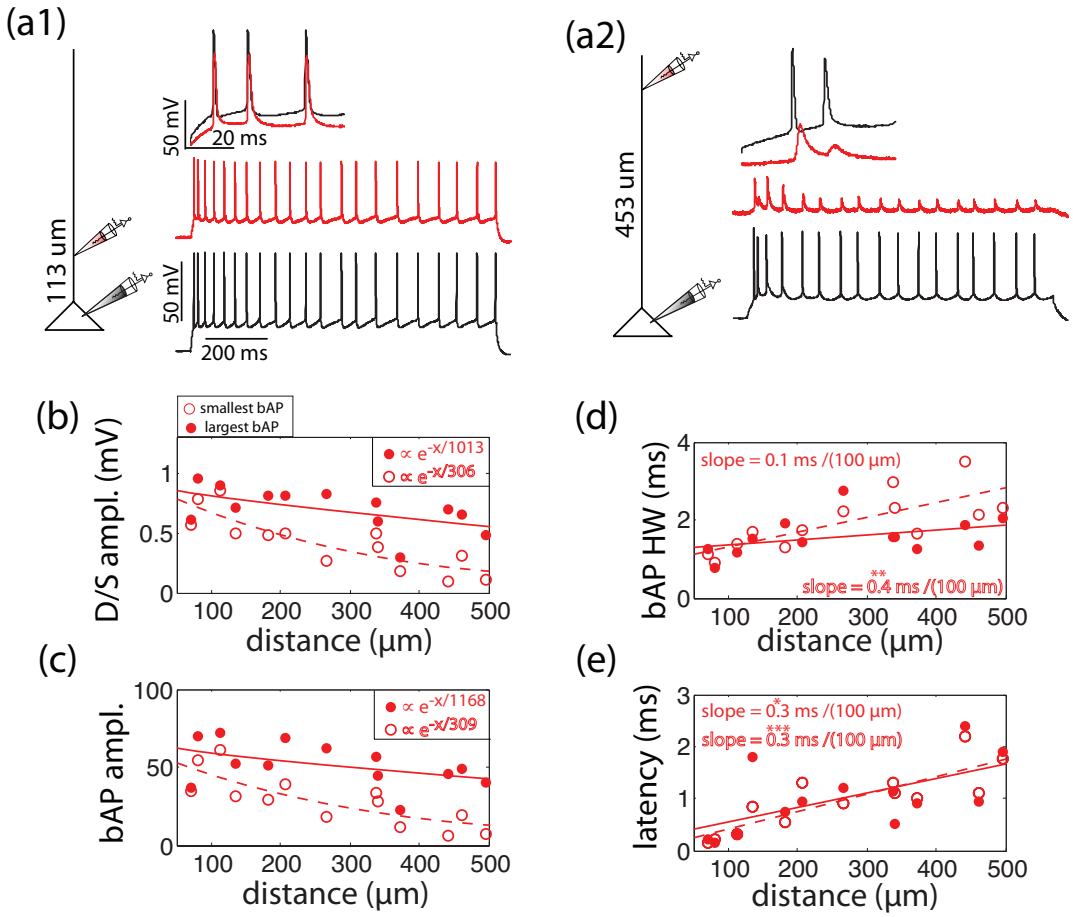

Figure 6: Backpropagation of action potentials into the dendrite. (a) Examplar 1 s DC current injections at the soma. Red traces show the dendritic and black traces show the somatic membrane potentials. Insets show the first spikes at the soma and bAPs in the dendrite. (a1: a dendritic recording 113 µm from the soma; a2: a dendritic recording 453 µm from the soma). (b) The ratio of the dendritic bAP to somatic AP amplitude for the largest (filled circles) and smallest (outlined circles) bAP. Lines (largest bAP data is filled, smallest bAP data is dashed) are exponential fits, and the effective length constant shown is derived from that fit. (c, d) The amplitude and halfwidth of the bAPs (exponential and linear fits respectively). * ($p<0.05$), ** ($p<0.01$), *** ($p<0.001$) denote

significance of the slope from 0. (e) The latency of the bAP as a function of distance from the soma.

The halfwidth of the bAPs (**Figure 6**d) increase significantly as a function of distance for the smallest bAP (slope = 0.004 ms μm^{-1}, p = 0.0025), but not for the largest bAP (slope = 0.001 ms μm^{-1}, p = 0.19). The latency of the bAPs as a function of distance from the soma has a slope that significantly deviates from zero for both the largest and smallest bAPs (slopes = 0.3 ms μm^{-1} and 0.3 ms μm^{-1}, p = 0.029, and 3.7e-4, respectively).

Intrinsic electrogenesis in the dendrites

Injections of DC current through dendritic pipettes can trigger somatic spiking and bAPs (**Figure 7**a), and can, in some cases, induce nonlinear dendritic electrogenesis that precedes somatic spiking (**Figure 7**b). 1 s long dendritic current injections (n = 13) elicit trains of 18.38 +/- 8.52 spikes at the soma. The width of the largest dendritic potential (DP) increases when current is injected farther from the soma (**Figure 7**c, slope = 0.20 ms μm^{-1}, p = 0.0043). This is also the case for the coefficient of variation (CV) of the interspike intervals (ISIs) (**Figure 7**d, slope = 0.0015 μm^{-1}, p = 0.02), and the ratio of voltage threshold for triggering somatic action potentials between dendritic and somatic step current injection (**Figure 7**e, slope = 0.0040 μm^{-1}, p = 3.8e-4). Importantly, both the DP width and the CV of ISIs for the dendrite-first cases (i.e. when dendritic electrogenesis precedes somatic spiking, **Figure 7**b inset; compare to the soma-first case, e.g. **Figure 7**a, inset.) are significantly different than in the soma-first cases (**Figure 7**fg, p = 0.0039 and 4.4e-4 respectively). Additionally, the dendrite-

first cases occur at significantly different distances from the soma than the soma-first cases (**Figure 7**h, p = 0.0016), suggesting that the occurrence of long dendritic potentials and variable somatic ISIs occurs during dendritic injections farther from the soma.

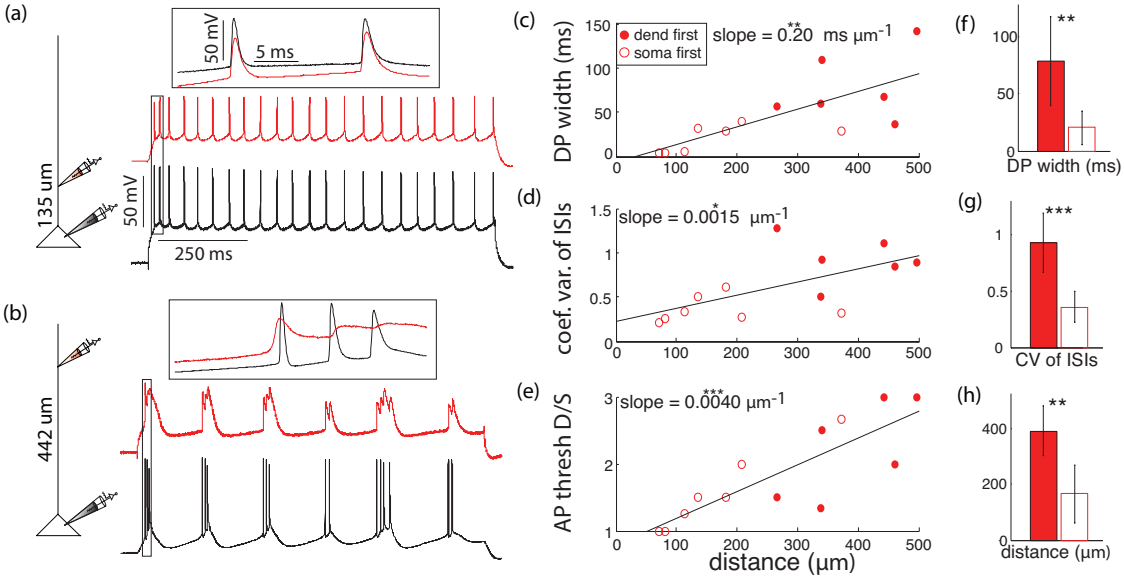

Figure 7: Current injections into the far apical dendrites elicit dendritic electrogenesis. (a,b) Examples of 1 second DC current injections into the dendrites. Red traces show dendritic and black traces show somatic membrane potentials. Insets show details of action potentials and dendritic response of the squared area. (a) Membrane response to dendritic current injections at 135 µm from the soma show somatic spiking with relatively constants ISIs giving rise to bAPs in the dendrite. (b) Membrane response to dendritic current injections 442 µm from the soma show burst firing at the soma and dendritic electrogenesis which precedes action potential firing at the soma. (c,d,e) Filled circles corresponds to cases where dendritic spikes precede the somatic spike (e.g. inset b), while open circles correspond to cases where somatic spikes precede the dendritic event (e.g. inset a). Lines are linear fits. * ($p<0.05$), ** ($p<0.01$), ***

($p<0.001$) denote significance of the slope from 0. (c) Width of dendritic potentials including bAPs (see Methods). (d) Coefficient of variation of the inter spike intervals. (e) The ratio of the current threshold to elicit a somatic action potential via dendritic over somatic current injection. (f,g,h) Comparison of the DP width (f), coefficient of variation of the ISIs (g), and the distance from the soma (h) of current injections of cases where somatic spiking preceded dendritic events (open bar, n = 7), and where dendritic electrogenesis preceded somatic spiking (filled bar, n = 6). *, **, *** Indicate significant differences between the two bars.

Previous work has shown that bursts of bAPs cause calcium channel-dependent spiking in the dendrites of L2/3, L5, and L6 pyramidal neurons in rat somatosensory cortex (Larkum, Kaiser, & Sakmann, 1999; Larkum, Waters, Sakmann, & Helmchen, 2007a; Ledergerber & Larkum, 2010b). Here we use the critical frequencies method to detect the presence of a calcium spike hotzone in the dendrites of mouse V1 L5 pyramidal neurons (Larkum et al., 1999). We administer 3 short (2 ms each) DC current pulses at increasing frequencies (between 10 and 200 Hz, intervals of 10 Hz) at the soma. By aligning the somatic responses to the last AP, a nonlinear increase in the amplitude of the after-depolarization (ADP) is observed (**Figure 8**a-d). The frequency at which the nonlinearity in ADP occurs, called *critical frequency*, is indicative of a calcium spike in the apical dendrites (Larkum et al., 1999), and can be measured explicitly with a dendritic patch (**Figure 8**b). ADP at the soma is 4.4 +/- 3.2 mV greater at critical frequencies than lower frequencies (**Figure 8**df), and the critical frequency is 89.7 +/- 17.1 Hz (**Figure 8**e). The sharp change in ADP suggests nonlinear recruitment of dendritic current,

and the ADP at the soma is clearly dependent on dendritic electrogenesis, since a dendritic nonlinearity occurs for similar critical frequency in all experiments with a dendritic patch.

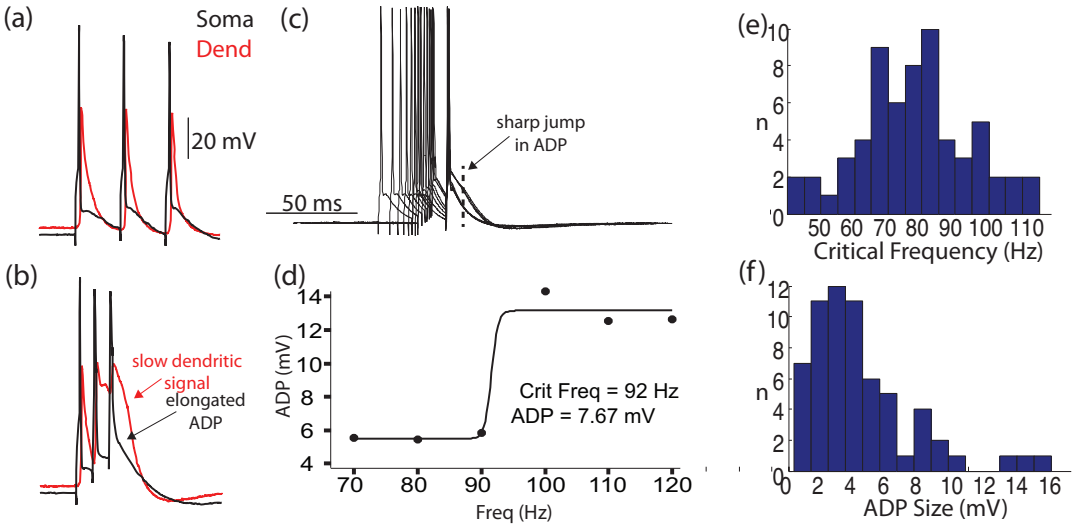

Figure 8: Calcium spiking in the dendrites in response to bursts of action potentials. (a) The somatic (red) and dendritic (black) response to three short current pulses at the soma at a slow frequency (70 Hz). (b) As in (a) except for three pulses above the critical frequency (100 Hz). Note the slow dendritic signal following the last somatic spike as well as the elongated somatic afterdepolarization (ADP) compared to (a). (c) Ten somatic responses to increasing frequencies of 3 short DC current injections at the soma, aligned by the final AP. Note the sharp nonlinear jump in ADP shape (broken line). (d) ADP size shown at the time of the dotted line in (c) as a function of frequency. The critical frequency is defined as the inflection point of the sigmoidal fit, and ADP size is defined as the difference between the two plateaus. (e) Histogram of the critical frequency for all 66 cells. (f) Histogram of the ADP size for all cells.

NMDAr-dependent nonlinearities in the dendrites

NMDA spiking in the dendrites of somatosensory L5 pyramidal neurons of mouse can be evoked with extracellular 50 Hz stimulation that causes presynaptic axon terminals to elicit EPSPs in patched postsynaptic cells (Schiller, Major, Koester, & Schiller, 2000). Here we test whether the dendrites of mouse V1 L5 pyramidal neurons support similar synaptically evoked electrogenesis by stimulating with two extracelluar pulses (**Figure 9**a, theta pipette 50 Hz stimulation) at increasing strengths. Stimulation above a threshold leads to long lasting (~40 ms) and increased amplitude (factor of ~2) responses at the soma compared to stimulation below threshold (**Figure 9**bc, black). The suprathreshold response is blocked by AP-5 bath application (50 μM) indicating the NMDAr dependence of the nonlinear signal (**Figure 9**bc, red).

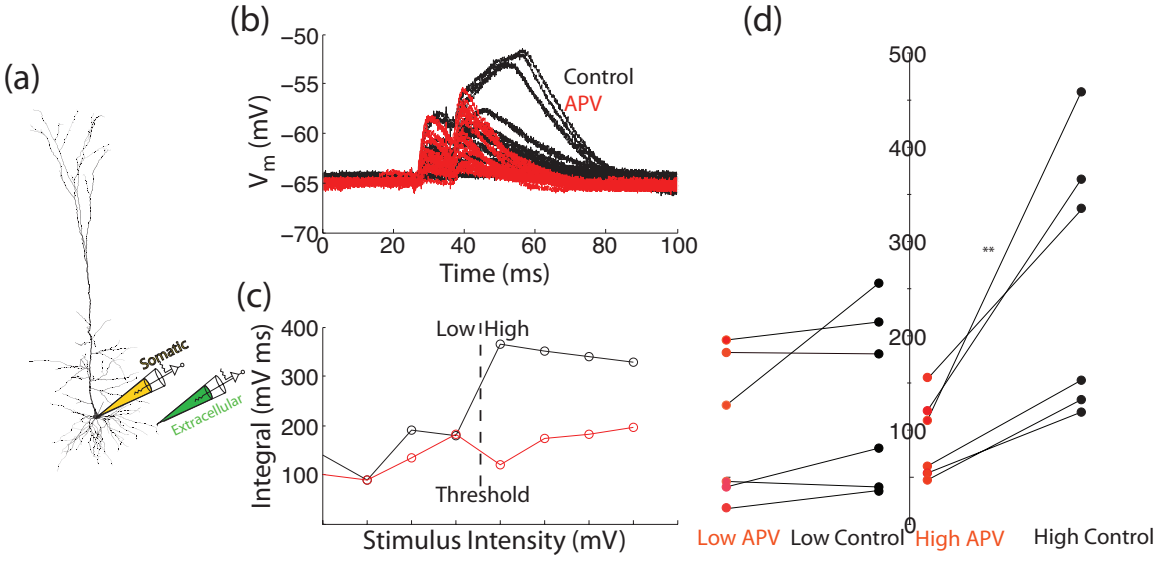

Figure 9: Nonlinear synaptic electrogenesis in the dendrites is NMDA dependent. (a) Diagram of the experimental setup. A glass

theta pipette (green) is used for local extracellular stimulation, while a somatic whole cell patch (yellow) recorded in current clamp at the soma. (b) Two short extracellular pulses at 50 Hz elicited two EPSPs at the soma. In control cases (black), a sharp nonlinear increase in both the duration and amplitude of the second EPSP occurs past some threshold. Bath application of AP-5 (red), an NMDAr antagonist, eliminates this nonlinear effect. (c) The integral of the second EPSP as a function of extracellular stimulus intensity. Note the sharp nonlinear increase in the integral past some threshold only in the control case. (d) Summary of the extracellular stimulation for 6 cells. Left, subthreshold comparison of AP-5 (red circles) and control (black circles) integrals of the second EPSP. Lines connecting circles indicate pairs from the same cell and extracellular stimulus location. The difference between AP-5 and control conditions for the subthreshold case is insignificant. Right, suprathreshold comparison of AP-5 and control integrals of the second EPSP. Control suprathreshold EPSP integrals are significantly bigger than under AP-5 conditions ($p<0.01$).

The integral of the subthreshold EPSPs is not significantly different after AP-5 application (**Figure 9**d left, n = 6, paired t-test, p = 0.17). AP-5 reduces the integral of high threshold responses (**Figure 9**d right, n = 6, paired t-test, p = 0.007), suggesting that suprathreshold, but not subthreshold, electrogenesis is NMDAr-dependent. Additionally, the maximum halfwidth duration of the suprathreshold potential at the soma is 33.2 +/- 7.1 ms (n = 6), and does not resemble the response to direct EPSP-shaped current injection (not shown). AP-5 responses at double the threshold intensity also do not elicit a broadening of the second EPSP

(not shown), further suggesting that synaptic stimulation recruits an additional NMDAr-dependent regenerative component to the EPSP.

Discussion

Recent advances in genetic and imaging techniques have provided experimental access to aspects of cortical processing in mouse vision (Andrew D. Huberman, 2011), and have, for example, given experimentalists the ability to see how functional maps (e.g. orientation maps) relate to long range connectivity (Bock et al., 2011; Glickfeld, Andermann, Bonin, & Reid, 2013). However, to relate functional maps and the phenomenology of vision to computation and biophysics, it is important to know how (i.e. by what physical mechanism) and why (i.e. the computational role) single neurons in the visual cortex respond to different types of inputs. Ultimately, we wish to describe computations that L5 pyramidal neurons perform given their input, how this supports visual perception, and to relate such computation to the biophysical details of the neuron. Understanding computation in terms of biophysics allows for direct experimental testing of network level computational hypotheses (Carandini, 2012). Given the unique role of L5 pyramidal neurons as one of the main integrators in the neocortical network, the electrophysiological properties of these cells hold special interest. We use the rat somatosensory (SS) cortex as a main point of comparison, since it is has the most widely studied dendritic physiology of any cortical area (Larkum et al., 1999; Larkum, Nevian, Sandler, Polsky, & Schiller, 2009; Larkum et al., 2007a; Ledergerber & Larkum, 2010b; Schiller, Schiller, Stuart, & Sakmann, 1997; G. Stuart, Spruston, Sakmann, & Hausser, 1997; Zhu, 2000).

Our main finding regarding single-cell physiology is that L5 pyramidal neurons of the mouse primary visual cortex (V1) broadly share many of the nonlinear properties of their counterparts in hippocampus, somatosensory cortex, and prefrontal cortex of mice and other mammals (Magee, Hoffman, Colbert, & Johnston, 1998; Milojkovic, Zhou, & Antic, 2007; Seamans, Gorelova, & Yang, 1997). Yet, with respect to subthreshold properties, some important differences are observed. The mean input resistance of mouse V1 L5 neurons studied here is higher (mean of 68 MΩ) at the soma than those found in rat somatosensory cortex (mean of 23 MΩ) (Zhu, 2000). One reason for this may be that rat SS neurons are larger, both in soma surface area and in dendritic length, than mouse V1 neurons. Although the higher input resistance suggests an electrically compact cell, this is offset by the effective length constant, which is substantially lower in mouse V1 L5 (257 and 333 um measured by somatic and dendritic current injection respectively, **Figure 5**c) than in rat the SS cortex (438 and 457 um) (Ledergerber & Larkum, 2010b). Assuming an average dendritic distance (from soma to the first bifurcation point) of approximately 500 um, this would give an electrotonic length between 1.50 and 1.95, similar to rat SS cortex (between 1.62 and 1.69). Interestingly, L2/3 pyramidal neurons of the rat SS cortex have a lower electrotonic length (between 0.58 and 1.07) (Larkum et al., 2007a) despite having dendritic lengths more comparable to mouse V1 L5 pyramids than rat SS L5 pyramids (Ledergerber & Larkum, 2010b).

	Mouse V1 L5	**Rat SS L5**	**Rat SS L2/3**
Dendritic Height	450 – 600 um	~ 1 mm	~500 um
Length Constant	~300 um	~450 um	~700 um

Electrotonic Distance	~1.7	~1.65	~0.7

L5 pyramidal neurons of mouse V1 have three main subthreshold properties that are not found in rat SS cortex. (*1*) Rat SS cortex has a ~4-fold change in sag amplitude (from ~5 to ~20 mV) (Zhu, 2000) along the dendritic axis. Here, there is no detectable increase in sag (**Figure 5**d). (*2*) Rat SS cortex has no detectable change in input resistance (R_N) along the dendritic axis (Berger, Larkum, & Luscher, 2001). Here, R_N increases at a rate of 20% relative to somatic R_N every 100 microns along the dendritic axis (**Figure 5**e). (*3*) The resting potential of rat SS cortex depolarizes at a rate of ~10 mV/mm along the dendritic axis (G. J. Stuart & Sakmann, 1994). Here, no change in resting membrane potential as a function of distance from the soma is measurable (**Figure 5**f).

The absence of increasing sag suggests a more spatially homogenous distribution of I_h channels in the dendrites of mouse V1 than in rat SS L5 pyramidals, where I_h concentration exponentially increases up the dendrites (Kole et al., 2006). This spatial concentration of I_h in rat SS cortex is responsible for a dendritic depolarization relative to the soma as well as an absence of an increasing input resistance into the dendrites, since the added conductance counteracts the effect of decreasing diameter (Berger et al., 2001; Zhu, 2000). Thus, the absence of exponentially increasing I_h conductance in the dendrites of mouse V1 L5 pyramidal neurons might explain both the constant resting membrane potential as well as the increase in input resistance. Later, in Chapter 3, we will be able to test this hypothesis with a multi-compartmental model.

This data is also in line with the finding that C_{AR} (the second derivative of the V-I relationship, see Methods) and α (C_{AR}/R_N) is the same in both the soma and dendrites, since I_h is a main source of inward rectification of the L5 pyramidal I-V relationship. Although the functional implications of the subthreshold changes are not explicitly studied here, the changes might reflect a more functionally compact soma-dendrite communication scheme compared to rat SS-cortex (Berger et al., 2001).

We find that mouse V1 L5 pyramidal neurons support the backpropagation of APs into the dendrites (**Figure 6**), Ca^{2+} spiking in the tuft dendrites (**Figure 7**, **Figure 8**), and local NMDAr-dependent spiking in the thin dendrites (**Figure 9**). The attenuation of bAPs into the dendrite decreases with effective length constants of 306 and 1013 μm for the smallest and largest bAPs in a train, respectively. This suggests that the smallest bAP, which always occurs in the last 500 ms of the 1000 ms current injection, attenuates according to subthreshold dynamics (subthreshold effective length constant is 257 or 333 μm, **Figure 5**). Alternatively, the largest bAP, which is always associated with one of the first 3 APs in the train, is most likely actively propagated into the dendrites by voltage-dependent Na+ channels (G. Stuart et al., 1997), and thus has an effective length constant ~3 times larger than the subthreshold dynamics. Similarly, the halfwidth of the smallest, but not the largest, bAP significantly increases as a function of distance from the soma (**Figure 7**d). Importantly, dendritic current injections farther than 250 μm from the soma are associated with longer dendritic depolarizing events which preceded burst firing of APs at the soma, while current injections at the soma and into the dendrite less than 250 μm from the soma are instead associated with regular trains of single APs propagating as bAPs into the dendrites (**Figure 7**). Our experiments support a

conception of single L5 pyramidal neurons in mouse V1 as containing two distinct areas: the perisomatic region within 250 μm of the soma and the dendritic region farther than 250 μm from the soma (**Figure 10**). This conception of a single neuron will prove useful, in Chapter 4, when we find abstract models that recreate many of the important behaviors of these cells.

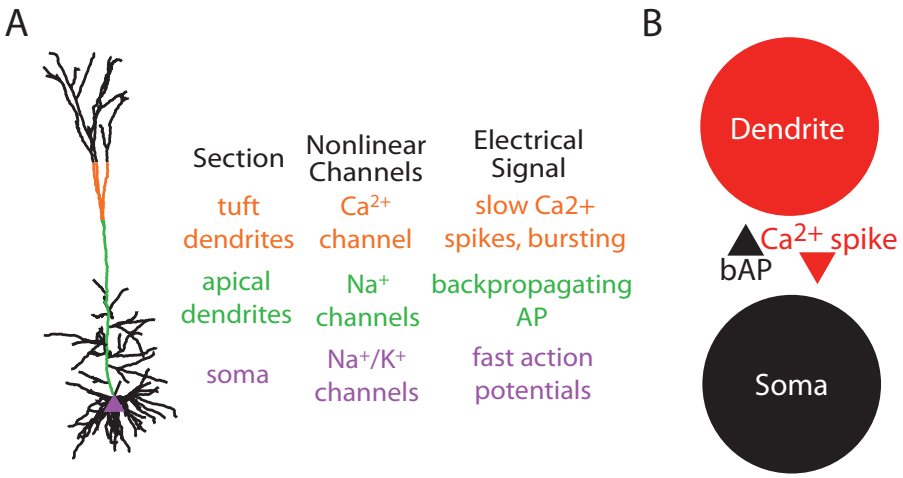

Figure 10: The biophysics of layer 5 pyramidal neurons in mouse V1. A) The experimental results show that the pyramidal neuron can be separated into three electrophysiological sections: the tuft dendrites (orange) supporting slow regenerative calcium spikes, the soma (purple) supporting fast sodium mediated action potentials, and the apical dendrite (green) supporting the active transfer of electrical signals between the soma and tuft dendrites. B) One conceptual understanding of the layer 5 pyramidal neuron is that it is made up of two compartments, each acting as largely independent integrators. The integration at the soma and dendrite result in action potential and calcium spike generation, respectively. The apical trunk then acts as a communication channel between the two compartments.

LAYER 2/3 PYRAMIDAL NEURONS DURING SENSORY INPUT

In the previous section I described the biophysics of layer 5 pyramidal neurons in the mouse visual cortex. Importantly, those experiments were carried out in slice. The *in vitro* prep is essentially analogous to a comatose brain. Here we wish to describe the physiology of pyramidal neuron dendrites during sensory input in the living animal. Due to reasons of technical feasibility, we focus on the layer 2/3 (L2/3) pyramidal neurons of the rat somatosensory cortex. However, L2/3 pyramidal neurons are known to have many of the same dendritic properties as layer 5 pyramidal neurons. In particular, the apical dendrites of L2/3 pyramidal neurons, which also reside in layer 1, support NMDA spiking and calcium spikes (though importantly the density of the nonlinear calcium channels is substantially less than in layer 5 pyramidal neurons). The *in vitro* studies looking at the NMDA spikes in the dendrites have shown that synaptic input to the distal tuft dendrites of pyramidal neurons has very little effect on either the axonal Na^+ initiation zone (Williams & Stuart, 2002) or the closer Ca^{2+} initiation zone in the apical dendrite (Larkum et al., 2009). This raises the question as to how synaptic input onto tuft dendrites can influence action potential (AP) generation. One possibility is that local NMDA receptor-dependent potentials, here referred to as NMDA spikes (Schiller et al., 2000), enhance the generation of APs at the soma. This could explain why NMDA receptors are vital for the processing of feedback signals arriving in L1 (Self, Kooijmans, Super, Lamme, & Roelfsema, 2012).

Although NMDA spikes can be readily evoked in pyramidal neuron dendrites *in vitro* (Antic, Zhou, Moore, Short, & Ikonomu, 2010; Schiller et al., 2000) (**Figure 9**), their existence has

never been conclusively demonstrated *in vivo* nor whether the conditions even exist for their generation (Chen, Leischner, Rochefort, Nelken, & Konnerth, 2011; Hill, Varga, Jia, Sakmann, & Konnerth, 2013; Jia, Rochefort, Chen, & Konnerth, 2010). Recent studies *in vivo* have demonstrated the importance of NMDA receptor activation in layer 4 (L4) somatosensory and L2/3 visual neurons for the tuning properties of cells implying an importance for active dendritic processing (Lavzin, Rapoport, Polsky, Garion, & Schiller, 2012; Smith, Smith, Branco, & Hausser, 2013). Nevertheless, it is still unclear whether NMDA receptor activation leads directly to local NMDA spikes in these cases or whether it plays a more general role in widely activating the dendritic tree (Branco, Clark, & Hausser, 2010; Branco & Hausser, 2011) and/or stimulating other kinds of dendritic spikes (Larkum et al., 2009). NMDA spikes are so named because of the major conductance responsible, although like other types of spikes, other channels may open during the process (Schiller et al., 2000). The important feature of any spike, in terms of the integrative process, is that it involves a thresholded event resulting in a positive feedback loop of local membrane potential and current influx (Major, Larkum, & Schiller, 2013; Schiller & Schiller, 2001) often referred to as electrogenesis. A key characteristic of NMDA spikes is that they require both the binding of glutamate to NMDA receptor channels and the voltage-dependent ejection of Mg^{2+} ions from the channel pore (Mayer, Westbrook, & Guthrie, 1984). The consequence of these two simultaneous conditions is that NMDA spikes tend to be local without propagating actively for any distance and this in turn has vital computation consequences for patterned synaptic input (Larkum & Nevian, 2008; Major et al., 2013; Mel, 1993; Rhodes, 2006).

In this work, we introduce the first experiments with a two-photon activatable version of the caged compound, tc-MK801, that enables the specific block of NMDA receptors on the postsynaptic membrane in a restricted region of the dendritic tree(Reeve, Kohl, Rodriguez-Moreno, Paulsen, & Anderson, 2012b; Rodriguez-Moreno et al., 2011). This allowed us to investigate whether local NMDA receptor-dependent electrogenesis occurs in the tuft dendrites of L2/3 pyramidal neurons under *in vivo* conditions. We found that NMDA spikes occur in multiple dendritic branches both spontaneously and due to sensory input and play a major role in enhancing neuronal output.

Methods

*Anaesthetized **in vivo** and **in vitro** surgical preparation*

All experiments were conducted in strict accordance with the guidelines given by the veterinary office of the canton Bern, Switzerland and The Florey Institute of Neuroscience and Mental Health Animal Ethics Committee, Australia. For *in vivo* experiments under anaesthesia, Wistar rats (P28 –P39) were initially anaesthetized with isoflurane (3%; Abbott*)* before urethane anaesthesia (1.4 g/kg; Sigma) was administered intraperitoneally and lidocaine (1%; Braun) was administered around the surgical site. Body temperature was maintained at ~36 °C and the depth of anaesthesia was monitored throughout the experiment and when necessary anaesthesia was topped-up with 10% of the initial urethane dose. Once anaesthetized, the head was stabilized in a stereotaxic frame by a head-plate attached to the skull with dental cement (paladur, Heraeus). A craniotomy was then performed above the primary somatosensory cortex (~1.5 x 1.5 mm square), centered at 1.5 mm posterior to bregma and

2.2 mm from midline and the dura mater surgically removed. The craniotomy was filled with 2% agarose (Sigma) in a solution containing (in mM): 125 NaCl, 5 KCl, 2 $CaCl_2$, 1 $MgSO_4$, 10 HEPES and 10 glucose, adjusted to pH 7.3-7.4 with NaOH, and covered with a coverslip. The area was then submerged with rat ringer for the entire experiment (in mM: 135 NaCl, 5.4 KCl, 1.8 $CaCl_2$, 1 $MgCl_2$, 5 HEPES).

For *in vitro* experiments, Wistar rats (P30-P35) were anaesthetized with 95% CO_2 / 5% O_2 before decapitation. The brain was then rapidly transferred to ice-cold, oxygenated artificial cerebrospinal fluid (ACSF) containing (in mM) 125 NaCl, 25 $NaHCO_3$, 2.5 KCl, 1.25 NaH_2PO_4, 1 $MgCL_2$, 25 glucose and 2 $CaCl_2$ (pH 7.4). Parasagittal slices of the primary somatosensory cortex (300 μm thick) were cut with a vibrating microslicer (Leica) and incubated at 37 ºC for 30 minutes and subsequently maintained at room temperature (~22 ºC). Somatic whole-cell patch recordings were made from visually identified layer 2/3 pyramidal neurons using infared Dodt gradient contrast and a CCD camera (Coolsnap ES; Roper Scientific). During recordings, slices were bathed in ACSF maintained at 33-35 ºC.

Virus injection and chronic window surgery for awake in vivo experiments

Mice (p9-13) were anaesthetized with isoflurane (~2% by volume in O_2) and a small hole (~0.5 x 0.5 mm) was made over the primary somatosensory cortex (~2 mm posterior and 0.5 mm lateral to bregma). The dura was left intact and the genetic Ca^{2+} indicator GCaMP6 (AAV1.Syn.GCaMP6s.WPRE.SV40; UPen Vecotr Core, AV-1-PV2824) was slowly injected from a microcapillary pipette (~50 nl) at a depth of 400 m. The skin was then sutured and the pup returned to the mother for ~ 2-3 weeks. After this recovery/expression period, a cranial window was performed. Mice were anaesthetized with isoflurane (~2% by volume in

O_2) and a craniotomy (3 mm diameter) was made over the primary somatosensory cortex where the virus was injected. The craniotomy was covered with a circular coverslip (diameter 3 mm; size #1) and a head-post was attached to the skull with dental acrylic to permit head fixation. Mice were allowed to recover for at least 3 days before water restriction (5-2 cycle; 1 ml a day on restricted days; unlimited access to food) and head-restraint habituation. Mice were slowly and carefully trained for head-restraint for up to 14 days before two-photon imaging over the cranial window was performed.

Intrinsic optical imaging

In all *in vivo* experiments, intrinsic optical imaging was first performed to identify the hindlimb sensorimotor cortex. The cortical surface was visualized with green (~530 nm) light to enhance contrast and switched to red (~600 nm) light for functional imaging captured with a CCD camera (Teli) coupled to a 50 mm and 25 mm lens (Navitar). The signal was measured in alternating sweeps before and during contralateral hindlimb stimulation (300 ms; 30 ISI). The intrinsic signal was measured as the difference in the reflected light before and during stimulus and was mapped onto the blood vessel pattern to be targeted during experiments.

Electrophysiological methods

For both *in vivo* and *in vitro* experiments, whole-cell patch-clamp recordings were obtained from pyramidal neurons using a patch pipette (resistance 6-9 MΩ) filled with an intracellular solution containing (in mM): 135 K gluconate, 4 KCl, 10 mM HEPES, 10 Na_2 phosphocreatine, 4 Mg-ATP, 0.3 Na-GTP, 0.2% biocytin, adjusted to pH 7.3-7.4 with NaOH. To measure Ca^{2+} activity, Oregon Green BAPTA 1 (OGB1; 200-500 μM; Invitrogen) was

included in the *in vivo* patch pipette and to aid visualization, Alexa Fluor 594 (Invitrogen; 75 μM) was included in all the *in vitro* and most *in vivo* patch pipettes. *In vitro* and *in vivo* whole-cell voltage recordings were performed from the soma using Dagan BVC-700A amplifiers and were filtered at 10 kHz. For *in vivo* recordings, the pipette was inserted at a 30-degree angle into the brain to a vertical depth of 400 μm before being advanced at steps of 1 μm until a cell was encountered (initial access resistance upon whole-cell were typically ~ 50 MΩ). Because the *in vivo* recordings were performed blind, pyramidal neurons were identified according to both their voltage response to current steps and where possible, biocytin Neurolucida reconstruction. On occasion, holding current was applied to the neuron *in vivo* via the whole-cell recording pipette (~50 pA) to increase cell excitability. Custom written Igor software was used for both acquisition and analysis and no correction was made for the junction potential.

Two-photon Ca^{2+} imaging

In the anaesthetized preparation, neurons were passively filled with the Ca^{2+} indicator OGB1 using the blind, whole-cell patch method (see above). To limit background fluorescence, recordings were typically made within the first 3 pipette insertions into the brain. After greater than 45 min filling, Ca^{2+} dynamics in dendrites at different depths were measured *in vivo* using a custom built two-photon microscope with a titanium sapphire laser (860 nm; 140 fs pulse width; SpectraPhysics MaiTai Deepsee) passed through a 40x water immersion objective (Olympus; 0.8 NA). Ca^{2+} signals were typically obtained in full-frame mode (128 x 128 pixels) and were acquired at a frequency of 8 Hz, unless otherwise stated. Faster imaging rates (50-100 Hz) were obtained by restricting the spatial range of the axis (80 x 40 pixels or 128 x 10 pixels). Custom written labview software (National Instruments) controlled the microscope

movement (courtesy of Florent Haiss and Bruno Weber) and scan mirrors (courtesy of Dominik Langer and Fritjof Helmchen). Emission light was collected using photomultiplier tubes (Hamamatsu, Bridgewater, New Jersey). To minimize photodamage, the excitation laser intensity was adjusted to the minimal value possible depending on the depth of the focal plane. The imaging depth was restricted to ~ 500 m which enabled imaging from all dendritic regions of layer 2/3 pyramidal neurons. Individual dendritic branches were only imaged once per experiment to limit branch-specific photodamage and branch morphology was assessed at the start and end of an experiment and the data excluded if photodamage was detected.

Two-photon imaging of the Ca^{2+} dynamics in dendrites transfected with the genetic Ca^{2+} indicator, GCaMP6, was performed with a Thorlabs B-scope (Sterling, Virginia) with a titanium sapphire laser (920 nm; 140 fs pulse width, Coherent Chameleon). Ca^{2+} signals were typically captured at a frequency of 16 Hz (512 x 512 pixels) by a GaAsP photomultiplier tube (Hamamatsu). Experiments with awake mice were performed under head fixation, during which mice could routinely groom and move their limbs. However, the reported Ca^{2+} transients were recorded while the animal was in quiet wakefulness when brain movement (in either x,y, or z axis) was minimal. Background white-noise was continuously played during recording trials to limit acoustic disturbances.

For *in vitro* experiments, neurons (filled with Alexa Fluor 594) were visualized using confocal microscopy (514 nm; argon laser) and uncaging was achieved using a two-photon femtosecond laser source (710-730 nm; SpectraPhysics MaiTai) both which were coupled to a laser scanning microscope (TCS SP2RS, Leica Microsystems) equipped with a 40x water immersion objective

(NA 0.8). Two-photon uncaging was performed in full-frame mode, which was restricted to the dendrite of interest.

Stimulation and drug application

Local block of NMDA receptors restricted to single branches was achieved by filling neurons with a caged form of the intracellular NMDA receptor blocker MK801 (100 M; tc-MK801 (Reeve, Kohl, Rodriguez-Moreno, Paulsen, & Anderson, 2012a; Rodriguez-Moreno et al., 2011)) via the patch pipette. Control conditions were recorded before uncaging tc-MK801 by focusing two-photon light (690 nm; 140 fs pulse width; typically 3 min) onto the dendrite of interest in full frame mode (8 Hz) using the same light path as described above for Ca^{2+} imaging. Global block of NMDA receptors was typically achieved by including MK801 (1 mM; Tocris) in the patch pipette but was also achieved via cortical application of APV (50 M) where stated. Global block of Na^{+} channels was achieved by including QX-314 bromide (1 mM; Tocris) in the patch pipette. For the QX-314 *in vitro* experiments, NMDA spikes were first evoked in neurons patched with control intracellular solution before the neurons were repatched with intracellular solution containing QX-314.

For both *in vivo* and *in vitro* experiments, direct dendritic stimulation was achieved by placing an extracellular stimulating pipette (theta; tip diameter <1 μm; resistance ~ 12 MΩ) in close proximity to the branch of interest and increasing the strength of paired step pulses (1 ms; 50 Hz; 20 s interspike interval) until supralinear responses were recorded. To aid placement of the pipette, Alex Fluor 594 (Invitrogen; 75 μM) was placed in the extracellular stimulating pipette. For direct activation of fibers within Layer 1, an extracellular stimulating pipette (theta;

tip diameter <1 μm; resistance ~ 12 MΩ) was placed approximately above the recorded cell within the top 50 μm of the cortex.

Sensory stimulation was evoked by a single short electrical pulse (1 ms; 100 V) to conductive adhesive strips (approximately 1cm wide by 2cm long) placed on the contralateral hindpaw pad or via targeted airpuff onto the hindpaw (40 psi; 400 ms). Dendrites were considered to have a response to hindpaw stimulation if the Ca^{2+} peak was 3x standard deviation of the noise and occurred within one second of the stimulus.

Data analysis and statistical methods

During whole-cell recordings, custom written Igor software (Wavemetrics) was used for both acquisition and analysis, and ImageJ (National Institutes of Health) and Igor software was used for imaging analysis. Fluorescence background was measured from a region adjacent to the dendrite. Fluorescence traces are expressed as relative fluorescence changes, $F/F = (F-F_0)/F_0$, where F_0 is the background-corrected fluorescence. Reported Ca^{2+} transients had an amplitude greater than 3X the standard deviation of the noise (which was on average 0.35 F/F) and a half-width greater than 128 ms. The Ca^{2+} transient amplitude was similar in all experiments excluding a severe distortion of the results by dye concentration gradients. Peak amplitudes of the background noise were measured from all trials where a large Ca^{2+} transient occurred. For display purposes only, all Ca^{2+} transients were filtered with Savitzky-Golay 5 point 2nd order filter and APs were truncated. No filtering was performed on the Ca^{2+} transients for analysis.

The spatial spread of dendritic Ca^{2+} activity was calculated using regions of interest (ROI) restricted to 5 m and to account for potential differences in resting Ca^{2+} levels, Ca^{2+} spread

is expressed as the relative fluorescence change, $G/R\ (t) = (G(t) - G_0)/R$, where G_0 is the background-corrected green fluorescence.

The firing frequency was determined as the maximum instantaneous firing rate, which occurred during the dendritic Ca^{2+} event. In experiments with QX-314, peak somatic voltage was measured from 10-90% of baseline and only experiments where the amplitude of the somatic voltage response during dendritic Ca^{2+} activity was within 80% of the somatic voltage responses at break-in were included. Measurements of somatic voltage with no Ca^{2+} transients were from a subset of trials chosen randomly. Reported number of contralateral-HS trials with a Ca^{2+} response were from dendrites which had at least one evoked response during control. When comparing evoked with spontaneous Ca^{2+} transients, peak amplitudes were measured from the maximum Ca^{2+} response in each condition. For somatic voltage analysis *in vitro*, the integral of the extracellularly evoked potentials were measured after 3 min of exposure to two-photon laser and APV. For direct comparison, spontaneous activity and measurement of up and down state parameters were reported from 30 min post whole-cell (to enable complete drug fill).

Unless otherwise stated, all numbers (n) refer to the number of dendrites and all values are indicated as mean ± s.e. Significance was determined using paired t-tests at a significance level of 0.05. No statistical tests were run to predetermine sample size, and blinding and ramdomization were not performed.

Histology

After recordings, neurons were typically prepared for biocytin reconstruction. For *in vivo* recordings, the animal was perfused with 4% paraformaldehyde solution immediately after the

experiment and the brain was removed and placed in 4% paraformaldehyde for up to 2 days before being cut into 250-300 μm parasagittal slices and stored in phosphate buffered solution. For *in vitro* recordings, the slices were placed in 4% paraformaldehyde after the experiment for up to 4 days. Slices were then processed for biocytin staining and Neurolucida reconstructions were performed to reveal the morphology of the *in vivo* and *in vitro* recorded neuron.

Results

We recorded dendritic Ca^{2+} activity and action potential output in L2/3 pyramidal neurons in the hindlimb somatosensory cortex of urethane anesthetized rats (either sex) using single-cell two-photon imaging and patch-clamp electrophysiology *in vivo*. Pyramidal neurons located approximately 250 to 450 μm below the cortical surface were passively filled with the Ca^{2+} indicator Oregon Green BAPTA1 (OGB1) via a patch pipette (**Figure 11a**). Using this approach, local dendritic Ca^{2+} changes could be measured from any dendritic region and correlated to APs recorded simultaneously with the patch pipette at the soma. Here, we recorded large spontaneous Ca^{2+} transients (> 3 SD; **Figure 11b, Figure 12** and **supplementary methods**) that were localized to ~30 μm of the dendrite (**Figure 12**), and had stereotypical peak amplitudes (Figure 52). The simultaneous voltage recording from the soma showed that most of the dendritic Ca^{2+} transients (214 out of 229 transients in 42 dendrites from 11 neurons) were associated with somatic APs. However, most somatic APs (74 ± 4 %) were not associated with Ca^{2+} influx(Svoboda, Denk, Kleinfeld, & Tank, 1997; Svoboda, Helmchen, Denk, & Tank, 1999; Waters, Larkum, Sakmann, & Helmchen, 2003) (Figure 52) and the peak amplitude of the Ca^{2+} transients were not correlated to AP frequency which was typically below the critical frequency for Ca^{2+} spikes(Larkum, Waters, Sakmann, & Helmchen, 2007b) (**Figure 11c**). Moreover, the onset of the Ca^{2+} transient typically occurred

before the somatic AP (Figure 52) further suggesting that these dendritic events were not caused by backpropagating APs. All but one of the restricted dendritic Ca^{2+} transients occurred during an up-state. Taken together with their restricted spatial extent, these results suggest that electrogenic events occur spontaneously in the tuft dendrites of L2/3 pyramidal neurons *in vivo*.

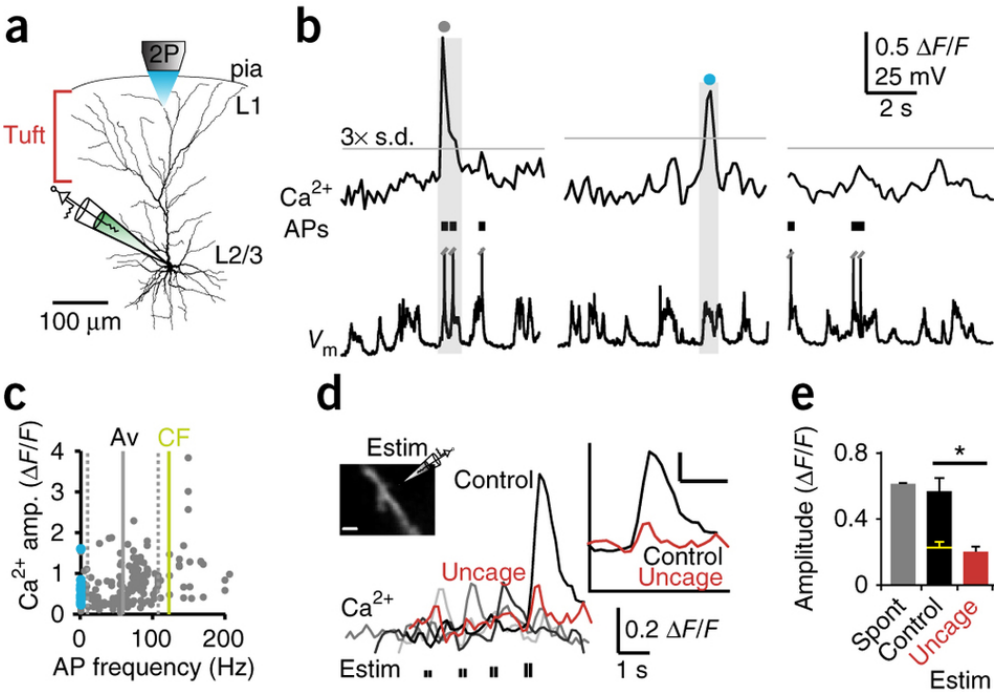

Figure 11: Large NMDA-receptor-dependent Ca2+ transients occur spontaneously in the tuft dendrites of layer 2/3 pyramidal neurons. (a) Schematic of experimental design. Voltage activity was recorded via the somatic whole-cell recording pipette and spontaneous Ca2+ transients were recorded simultaneously in tuft dendrites using two-photon microscopy in vivo. (b) (top) Ca2+ transients in tuft dendrites and (bottom) corresponding somatic voltage during (left) action potentials (APs) and (middle) no APs. (right) APs were typically not correlated with dendritic Ca2+.

Examples are from the same neuron shown in (a). APs are truncated and marked as dashes. Grey lines; threshold criteria for each Ca2+ transient, 3x standard deviation of the noise. (c) AP firing frequency and corresponding amplitude of the Ca2+ transient in tuft dendrites. Isolated Ca2+ transients (0 APs) are indicated in blue. Average and one standard deviation of AP frequency, grey lines. Reported average critical frequency for layer 2/3 pyramidal neurons28, green line. (d) Ca2+ transients in tuft dendrite (inset, left) to increasing extracellular stimulus (Estim) intensity before (control; black) and after (red) block of NMDA receptors by two-photon (690 nm) exposure. Inset, right; overlay of same Estim intensity before (black) and after (red) NMDA block by two-photon uncaging (scale: 1 s, 0.2 F/F). (e) Average Ca2+ transient amplitude during spontaneous transients (grey) and extracellularly evoked suprathreshold transients before (black) and after (red) NMDA block by two-photon uncaging. Yellow bar, average amplitude of the just-subthreshold extracellulary evoked Ca2+ response. * $p < 0.05$. Error bars represent S.E.M.

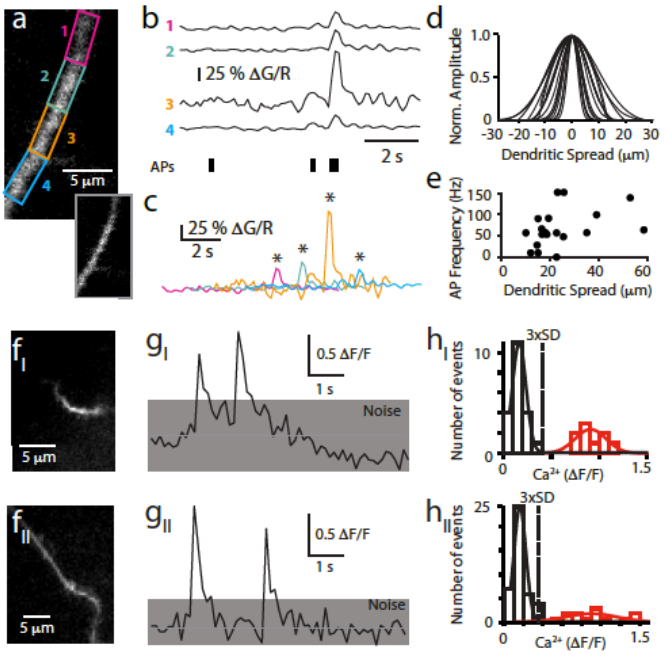

Figure 12: Tuft Ca2+ transients are spatially restricted, have a distinct bimodal distribution, and are not graded in amplitude. In principle, NMDA spikes in multiple branches could be an indication of many NMDA spikes or one very spatially distributed NMDA event. We therefore measured the spatial extent of tuft Ca2+ transients. (a) Twophoton image of a tuft dendrite with spatially restricted regions of interest (ROIs; 5 m length; coloured boxes). (b) Spontaneous Ca2+ transients recorded in the dendritic ROIs shown in (a) and somatic APs indicated by dashes. To compare different dendritic regions, transients are reported as ΔG/R. (c) Overlay of the transients in (b) illustrating the spread of a Ca2+ event along a tuft dendrite. (d) Gaussian distribution of the normalized Ca2+ transient amplitudes at different locations along tuft dendrites. (e) The spatial spread of the Ca2+ transients within a tuft dendrite was not related to the somatic AP firing frequency. (f-h) Since NMDA spikes have a clear threshold, plotting Ca2+ fluorescence amplitudes would result in a bimodal distribution whereas boosted potentials would have a

graded distribution. We therefore plotted the Ca2+ fluorescence amplitude distributions from two example tuft dendrites (I and II). (f) Two-photon image of two example tuft dendrites. (g) Example fluorescence traces with two Ca2+ transients above the noise from tuft dendrite shown in (f). (h) Histogram of the peak amplitude of Ca2+ fluorescence from the tuft dendrite shown in (f) illustrating bimodal distributions. Ca2+ transients were included in the analysis if they had an amplitude larger than 3x the standard deviation of the noise (middle, grey bar; right, dashed line). This criteria separated the reported Ca2+ transients (red) from the fluorescence background noise (black).

Extracellular stimulation is routinely used to evoke NMDA spikes *in vitro* (Gordon, Polsky, & Schiller, 2006; Larkum et al., 2009; Ledergerber & Larkum, 2010a; Polsky, Mel, & Schiller, 2004; Schiller et al., 2000) although their existence has not yet been demonstrated in the tuft dendrites of L2/3 pyramidal neurons. Using this approach (2 pulses at 50 Hz), we showed that the tuft dendrites of L2/3 pyramidal neurons are capable of generating local NMDA spikes *in vitro* (Figure 53). We tested whether the same extracellular stimulus could also evoke tuft electrogenesis *in vivo*. Indeed, large Ca^{2+} transients were evoked at a distinct threshold during paired pulse extracellular stimulation *in vivo* (**Figure 11d** and Figure 54). Next, we examined the NMDA dependence of this electrogenesis using a new caged form of the intracellular NMDA receptor blocker MK801 (100 M; tc-MK801(Reeve et al., 2012b; Rodriguez-Moreno et al., 2011)) which blocked NMDA spikes when two-photon light (690 nm, effectively exciting in the UV range; ~3 min) was focused onto the dendritic branch of interest (Figure 54). Local photoactivation of tc-MK801 prevented the suprathreshold Ca^{2+} response reducing it to the same amplitude (0.20 ± 0.03 dF/F) as the subthreshold response (0.22 ± 0.03 F/F,

Figure 11e). The use of extracellular stimulation *in vivo* allowed us to determine the expected Ca^{2+} transient amplitude during an NMDA spike. Importantly, the average peak Ca^{2+} amplitude of extracellularly evoked NMDA spikes was the same as the spontaneous Ca^{2+} transients (0.56 ± 0.08 F/F versus 0.61 ± 0.01 F/F; P > 0.05; n = 5 dendrites, **Figure 11e**) suggesting that the spontaneous events also arose from NMDA spikes.

The existence of electrogenesis in the tuft dendrites of L2/3 pyramidal neurons in the somatosensory cortex suggests that this mechanism might be important for sensory processing. Indeed, evidence for nonlinear dendritic processing of sensory input has been reported in the dendrites of L2/3, L4 and L5 neurons *in vivo* (Lavzin et al., 2012; Xu et al., 2012). We tested this *in vivo* during sensory stimulation of the contralateral hindpaw (single pulse of 100 V, 1 ms). In half of the neurons tested, we detected at least one tuft branch that responded to hindpaw stimulation with a large local Ca^{2+} transient similar to the spontaneous Ca^{2+} events. Of these, 22 ± 3% of hindpaw stimulation trials had a large local Ca^{2+} transient, which always resulted in an AP at the soma (n = 11 branches; **Figure 13a left, b** and **c**). In contrast, hindpaw stimulation that did not evoke dendritic activity also did not usually evoke APs. In those cases where APs were evoked without a dendritic Ca^{2+} transient, the number of APs was significantly less (2.1 ± 0.2 APs versus 3.9 ± 0.7 APs; n = 11 branches; $p < 0.05$). Similar dendritic sensory responses were evoked during more physiological stimulation provided by air puffs (40 psi) onto the hindpaw. In these experiments, hindpaw stimulation evoked on average 1.2 ± 0.3 APs (**Figure 14**) and we detected large local Ca^{2+} transients similar to the spontaneous Ca^{2+} events in half of the tuft dendrites tested. Of these, air puffs evoked a local Ca^{2+} transient in 18 ± 3 % of hindpaw stimulation trials (n = 16; **Figure 14**). This

suggests that sensory stimuli can reliably evoke NMDA spikes and that these spikes strongly influence the spiking output of the neuron.

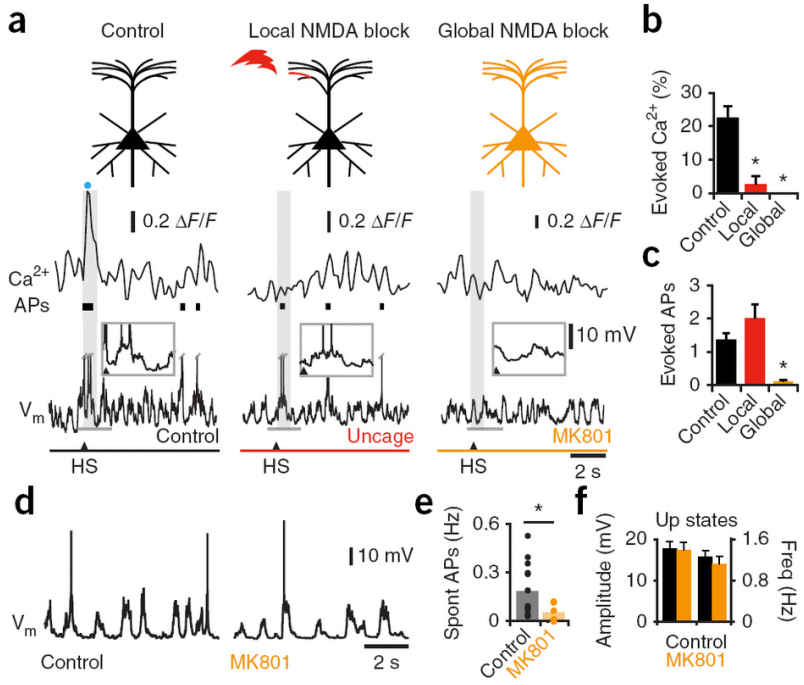

Figure 13: Global, but not local, block of NMDA-receptor-dependent Ca2+ transients in tuft dendrites decreases sensory-evoked neuronal output. (a) (top) Cartoon of L2/3 pyramidal neuron, (middle) Ca2+ transient in tuft dendrite and (bottom) simultaneous somatic voltage in response to contralateral hindpaw stimulation (1 ms; 100 V) during (left) control, (middle) after local NMDA block by two-photon uncaging restricted to a single tuft branch (red) and (right) global NMDA block by intracellular MK801 (orange). Inset: Magnification of somatic voltage (grey bar) during hindpaw stimulation (arrow). Control and local NMDA channel block are from the same neuron. Action potentials (APs) are truncated and marked as dashes. (b) Percentage of hindpaw stimulation trials which resulted in a measurable Ca2+ transient and (c) number of APs

evoked by hindpaw stimulation during control (black), local NMDA block by two-photon uncaging restricted to a single tuft branch (red) and global NMDA block by intracellular MK801 (orange). (d) Spontaneous somatic activity in control (left) and in neurons filled with MK801 (right). (e) The spontaneous firing frequency in control neurons (black) and in neurons filled with MK801 (orange). (f) Average amplitude and frequency of up states in control neurons (black) and in neurons filled with MK801 (orange). * $p < 0.05$. Error bars represent S.E.M.

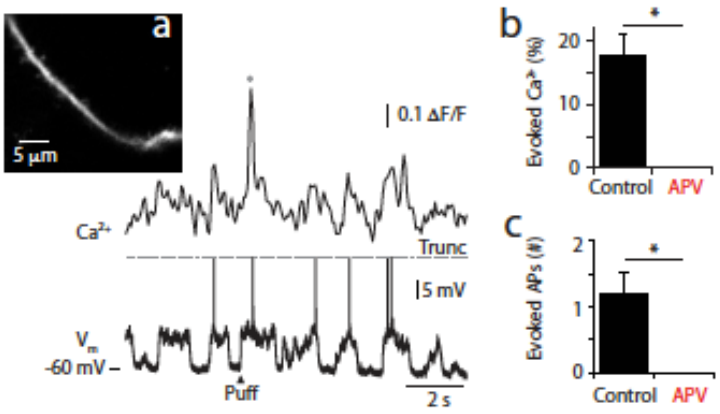

Figure 14: Hindpaw airpuff reliably evokes dendritic and somatic responses which are dependent on NMDA receptors. Despite the different modes of hindpaw stimulation, brief electrical (Figure 2) and airpuff stimulation (40 psi) evoked similar dendritic and somatic responses - approximately one action potential (AP) per stimulation and a dendritic Ca2+ response in approximately 20 % of stimulations. (a) Dendritic Ca2+ fluorescence (top) and somatic voltage (bottom) during airpuff stimulation of the hindpaw. Inset; two-photon image of the imaged tuft dendrite. (b) Percentage of hindpaw stimulation trials which resulted in a measurable Ca2+ transient during control (black; n=16) and NMDA block by cortical

application of APV (red; n = 15). (c) Number of APs evoked by hindpaw stimulation during control (black; n = 5) and NMDA block by cortical application of APV (red; n = 15). Error bars represent S.E.M.

To quantify the influence of local dendritic electrogenesis on somatic output APs, we compared spatially restricted block with global block of NMDA receptors, using tc-MK801 (Figure 57) versus intracellular MK801 (1 mM) (**Figure 13a**). Local uncaging almost completely abolished the Ca^{2+} responses on the affected branch without affecting the electrical responses evoked at the soma (n = 11; $p<0.05$; **Figure 13a-c**) illustrating that isolated NMDA spikes in single tuft branches have little influence on somatic activity as predicted from *in vitro* experiments (Larkum et al., 2009). Conversely, global block of NMDA receptors abolished both local dendritic Ca^{2+} transients and somatic APs in response to both brief electrical (n = 16; **Figure 13a-c**) and airpuff (n = 15; **Figure 14**) hindpaw stimulation. Furthermore, global but not local block of NMDA receptors also significantly decreased the spontaneous firing rate from 0.18 ± 0.05 Hz (n = 11 neurons) to 0.05 ± 0.02 Hz (n = 6 neurons; $p < 0.05$; **Figure 13d** and **e**) without altering the resting membrane potential (control, -71.0 ± 3.4 mV vs MK801, -71.3 ± 5.0 mV). Since blocking all NMDA electrogenesis has a large effect on neuronal activity, dampening both spontaneous and evoked output, this suggests that NMDA receptor-dependent electrogenesis is typically distributed over many branches following sensory stimuli (see also Figure 27). Moreover, global block of NMDA receptors using intracellular MK801 had no effect on either the amplitude (control, 17.7 ± 1.7 mV; MK801, 17.3 ± 1.9 mV), half-width (control, 0.51 ± 0.04 s; MK801, 0.54 ± 0.11 s) or frequency

(control, 1.3 ± 0.1 Hz; MK801, 1.1 ± 0.1 Hz) of up states recorded 30 min post whole-cell in L2/3 pyramidal neurons (n = 11; p > 0.05; **Figure 13f**) consistent with recent data in L2/3 neurons *in vivo* (Chen, Rochefort, Sakmann, & Konnerth, 2013; Smith et al., 2013). Since up-states are generated from barrages of synaptic activity (X. Chen et al., 2013; Plotkin, Day, & Surmeier, 2011), this shows that the effect on AP output by tuft electrogenesis did not arise simply from the reduction of synaptic transmission, per se, and implies a dependence on NMDA-dependent electrogenesis.

The data so far show that NMDA-dependent electrogenesis in the tuft has a strong influence on AP generation. However, is the converse true? That is, does AP activity influence the generation of NMDA spikes in the tuft? To examine this, we blocked AP activity pharmacologically by including the Na^+ channel blocker QX-314 (10 mM) in the patch pipette (**Figure 15a inset**). Without backpropagating APs, spontaneous dendritic Ca^{2+} transients occurred even more frequently in all regions of the tuft (**Figure 15,** Figure 55). These events had the same spatial extent as control transients (~30 μm; Figure 55), occurred in both single and multiple dendrites simultaneously (Figure 55), were blocked by local and global NMDA receptor antagonists (Figure 56), and were synaptic (not Ca^{2+} release from ryanodine-sensitive internal stores, Figure 56). Furthermore, local extracellular stimulation of a tuft dendritic branch with QX-314 evoked local dendritic Ca^{2+} transients at a fixed stimulus threshold that were blocked by local uncaging of tc-MK801 (Figure 56). Large Ca^{2+} transients were also recorded in control dendrites when APs were prevented by hyperpolarizing the soma via the patch pipette (200 - 400 pA; n = 4). Taken together these data show that the generation of NMDA-dependent electrogenesis is not dependent on backpropagating APs.

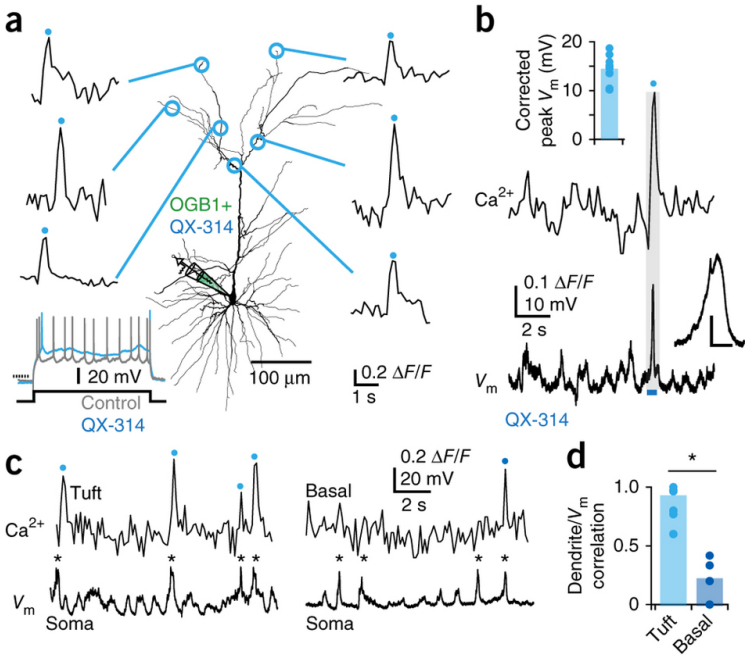

Figure 15: Simultaneous NMDA receptor–dependent Ca2+ transients cause a large voltage event at the soma. (a) Ca2+ transients were recorded in tuft dendrites in L2/3 pyramidal neurons filled with the Na+ channel blocker QX-314 in vivo. Bottom left inset, voltage response to suprathreshold current step (200 pA, 800 ms) in the indicated neuron (blue) compared with a control neuron with action potentials (gray). Dashed line indicates −60 mV. (b) Ca2+ transient recorded in the tuft dendrite (92 µm below pia) and corresponding somatic voltage in a neuron filled with QX-314. Bottom inset, magnification of somatic voltage indicated by blue bar during tuft Ca2+ transient (scale bars represent 10 mV, 100 ms). Top inset, graph of the peak somatic voltage during tuft Ca2+ transients corrected for the increase in input resistance during QX-314. (c) Ca2+ transients (top) and corresponding somatic voltage (bottom) recorded in a tuft (left) and basal (right) dendrite in the same neuron. * indicates large somatic voltage events. (d) Proportion of Ca2+ transients in tuft

(light blue) and basal (dark blue) dendrites that were correlated with large somatic voltage events. *P < 0.05.

What is the spatial extent of NMDA electrogenesis in the tuft dendrites leading to neuronal output? The rare isolated events found under control conditions (**Figure 11b**) depolarized somatic membrane potential by on average only 2.7 mV (n = 15/229 Ca^{2+} transients), which is consistent with the relatively small influence on somatic membrane potential when restricting NMDA receptor block to single branches (**Figure 13**). For this reason, along with the more typical estimated depolarization of ~14 mV, it is likely that events leading to somatic APs typically involve multiple branches simultaneously. We tested this directly by imaging from multiple (2-4) branches revealing that adjacent tuft dendrites were usually simultaneously active (83 ± 2 % of Ca^{2+} transients occurred in multiple branches; n = 36 dendrites; **Figure 16a-d**). There was no difference between the Ca^{2+} transients when they occurred on single or multiple branches in their average amplitude (0.61 ± 0.45 F/F vs 0.74 ± 0.02 F/F, **Figure 16c**) or somatic firing frequency (55.67 ± 7.09 Hz vs 48.50 ± 2.21 Hz; p > 0.05; n = 36). Even though these events were detectable on multiple branches, the calcium transients were not contiguous but were still spatially restricted to ~30 μm. This spatial profile was not influenced by Na^{+} or other voltage-sensitive channels as the spread of the Ca^{2+} transients was similar during intracellular QX-314 (**Figure 16d** and Figure 55). Being both ligand-gated and voltage-dependent, NMDA spikes depend simultaneously on the distribution of extracellular glutamate (Larkum & Nevian, 2008; Mel, 1993) and intracellular membrane potential.

However, since the spatial profile of Ca^{2+} transients did not change with QX-314 (despite the change in synaptic depolarization), NMDA receptor-dependent electrogenesis is most likely predominantly determined by the spatial profile of bound glutamate.

In order to establish the causal role of NMDA spikes in somatic action potential firing, it was necessary to manipulate the activity of NMDA receptors under the tightly controlled conditions provided by anesthesia. It is now clear that active dendritic spikes occur in the awake state in the apical dendrites of pyramidal neurons and are important for behavior (Smith et al., 2013; Xu et al., 2012); however the role of threshold-dependent NMDA spikes in these processes has not yet been established. Establishing whether spatially restricted Ca^{2+} transients occur in the awake state is crucial for determining whether local dendritic electrogenesis contributes to active sensory processing. To investigate this, we used two-photon microcopy to image dendritic Ca^{2+} transients from distal tuft branches of layer 2/3 pyramidal neurons labeled with a genetically encoded calcium indictor (GCaMP6 (T. W. Chen et al., 2013)) through a chronic imaging window in the awake state (see supplemental methods; Figure 58**a-b**). In a subset of tuft dendrites tested, local dendritic Ca^{2+} transients were indeed spatially restricted (26 ± 5 m; n=9; Figure 58**c-e**), highlighting the occurrence of local dendritic signaling in the awake state.

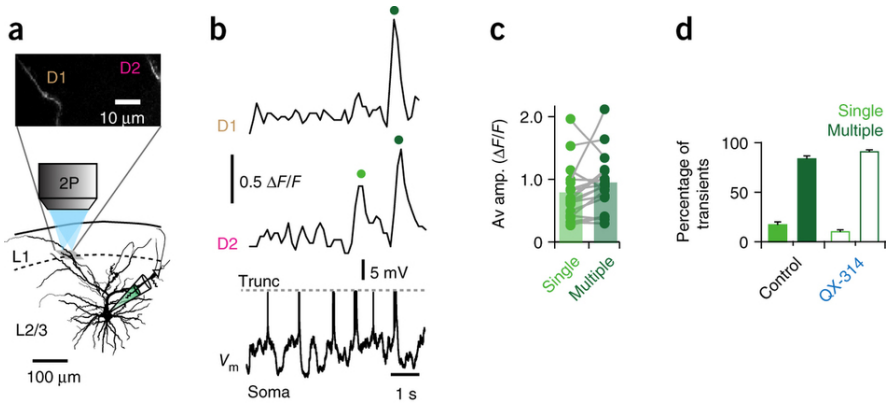

Figure 16: Spontaneous Ca2+ transients occur in both single and multiple tuft branches. (a) Schematic of experimental design. Voltage activity was recorded via the somatic whole-cell recording pipette and spontaneous Ca2+ transients were recorded simultaneously in multiple (2–4) tuft dendrites using two-photon microscopy. (b) Somatic voltage (bottom, action potentials truncated) and corresponding Ca2+ transients recorded in one (light green) or both (dark green) of the dendritic branches shown in a. Action potentials are truncated. (c) Average amplitude of Ca2+ transients in a given dendritic branch that occurred in single (light green) or multiple (dark green) dendrites. (d) Percentage of Ca2+ transients that occurred in single (light green) or multiple (dark green) branches in control neurons (solid) and in neurons filled with QX-314 (empty). Error bars represent s.e.m.

Discussion

The results presented in this study show the existence of large Ca^{2+} transients in the tuft dendrites of L2/3 pyramidal neurons that occur both spontaneously and in response to sensory stimulation, and in both anesthetized and awake animals. These Ca^{2+} transients were localized in single branches of the tuft dendrites and were abolished by a novel caged NMDA receptor antagonist that locally blocked NMDA channels in very confined regions with two-photon activation. These transients were most readily evoked by simultaneous sensory stimulation and activation of L1 feedback fibers.

While NMDA spikes can be evoked in the basal dendrites of L2/3 pyramidal neurons *in vitro*(Gordon et al., 2006), they had so far never been demonstrated in the tuft dendrites *in vitro* or *in vivo* nor under awake conditions. Here, *in vitro* and *in vivo* experiments (as well as computer simulations shown in discussed in Chapter 5) illustrate that the tuft dendrites of L2/3 pyramidal neurons can indeed support local NMDA receptor-dependent electrogenesis in both the anaesthetized and awake state. Previous experiments have demonstrated the existence of Na^{+} and Ca^{2+} spikes in these dendrites (Larkum et al., 2007b; Ledergerber & Larkum, 2010a; Waters et al., 2003). In particular, a recent study *in vivo* using direct patch recordings in the basal dendrites of L2/3 pyramidal neurons of the visual cortex, showed compound dendritic spikes in the apical dendrite that were dependent on dendritic NMDA receptor activity(Smith et al., 2013). In theory, the Ca^{2+} transients we observed in these dendrites *in vivo* could be due to any of the various types of regenerative potentials mentioned above as well as backpropagating APs(Hill et al., 2013). However, there are multiple lines of

evidence indicating that the events we recorded were primarily due to regeneratively evoked NMDA spikes. These include the fact that the dendritic Ca^{2+} transients: 1) were dependent on NMDA receptors, 2) occurred in the absence of backpropagating APs, 3) were restricted to 30 μm of dendrite, 4) appeared in multiple locations, 5) were broader than Ca^{2+} transients expected from Ca^{2+} spikes in these neurons (Larkum et al., 2007b), 6) were evoked in the fine tuft branches (unlike Ca^{2+} spikes (Larkum et al., 2009)), 7) were also found in basal dendrites (unlike Ca^{2+} spikes (Nevian, Larkum, Polsky, & Schiller, 2007)), 8) could be evoked by extracellular stimulus with a distinct threshold, 9) failed to increase after increased extracellular stimulus strength (*in vitro*), and 10) were not blocked by QX-314 that down-regulates both Na^{+} and Ca^{2+} channels. Taken together these results suggest that the dendritic Ca^{2+} transients were not due to back-propagating APs, dendritic Ca^{2+} spikes (plateau potentials) nor local synaptic input, and are instead consistent with the regenerative activation NMDA receptor channels.

NMDA conductances contribute to the amplitude and duration of EPSPs when the membrane potential provides enough depolarization to unblock Mg^{2+} ions from the NMDA receptor channel pore(Mayer et al., 1984). Normally, this would lead to a boosting of the EPSP amplitude that is not "regenerative", i.e. does not recruit neighboring NMDA receptors, because the nearby NMDA receptors do not have bound glutamate and remain closed. Only in the circumstance when enough NMDA receptors bind glutamate in a small area (i.e. when many nearby synapses are activated simultaneously(Larkum & Nevian, 2008)) is it possible for the NMDA receptors to act cooperatively to produce a spike(Schiller & Schiller, 2001). This can be detected in the form of a clear threshold when the input is increased uniformly with extracellular stimulation or uncaging of glutamate(Schiller et al., 2000). To further establish

the spike-like nature of the Ca^{2+} transients recorded in this study, it was therefore crucial to evoke thresholded, NMDA receptor-dependent events with controlled incremental stimulation (both *in vivo* and *in vitro*). This was achieved using extracellular stimulation, which evoked suprathreshold Ca^{2+} transients that had the same amplitude and duration as the spontaneous and sensory stimulus-evoked Ca^{2+} transients. The situation is further complicated by the fact that dendritic NMDA spikes can go on to recruit other channels (Plotkin et al., 2011) and other forms of dendritic electrogenesis (Larkum et al., 2009), which may account for the complex dendritic responses seen under behavioral condi tions(Smith et al., 2013; Xu et al., 2012).

To date, it has been difficult to demonstrate the existence of NMDA-dependent dendritic spikes *in vivo* because wholesale blockade of NMDA receptors significantly changes the profile of synaptic input to the cell. This makes it impossible to distinguish the blockade of regenerative spikes per se from the absence of the driving conditions (sufficient synaptic input) (Hill et al., 2013). Thus, it has been possible to establish that NMDA receptor activation is crucial for dendritic activity(Smith et al., 2013) and for calcium influx during up-states (X. Chen et al., 2013) but not the nature of the underlying NMDA receptor activation. Using a two-photon uncageable NMDA antagonist in this study made it possible to block NMDA receptors locally *in situ* during a physiologically relevant situation and prevent local NMDA spike generation in single branches. This localized block had very little effect on AP spiking in L2/3 pyramidal neurons in contrast to the dramatic effect of global intracellular block of NMDA receptors with MK801. Similar results were reported recently in L2/3 and L4 neurons,

in which global block of NMDA receptors with intracellular MK801 significantly affected the tuning properties of neurons (Lavzin et al., 2012; Smith et al., 2013).

The underlying conductances contributing to NMDA spikes have been well characterized *in vitro* and in computer simulations (Major, Polsky, Denk, Schiller, & Tank, 2008; Rhodes, 2006; Schiller et al., 2000; Schiller & Schiller, 2001). Both voltage-sensitive Ca^{2+} and Na+ channels are activated during NMDA spikes but are not necessary for spike generation (i.e. the NMDA spike remains in the presence of Ca^{2+} and Na^{+} channel blockers (Schiller et al., 2000)). In our experiments, we observed no significant change in the amplitude of the Ca^{2+} transients with the Na^{+} channel blocker QX-314 despite the fact that this compound is known to also partially block voltage-sensitive Ca^{2+} channels (as well as other conductances (Andrade, 1991; Connors & Prince, 1982; Perkins & Wong, 1995; Talbot & Sayer, 1996; Taylor, 1959)). Because of the possible side effects of QX-314 it was impossible to rule out a contribution by voltage-sensitive channels to the Ca^{2+} transients we observed. However, since local and global block of NMDA receptors totally abolished the Ca^{2+} transients and no further regenerative potentials were evoked by increasing extracellular stimulation after addition of APV, we conclude that these channels do not contribute in a significant nor spike-dependent fashion. This is also consistent with the known lack of Ca^{2+} spike initiation in thin tuft dendrites (Larkum et al., 2009) and with the spatially restricted nature of the observed Ca^{2+} transients that were quite unlike the global activation of Ca^{2+} channels during dendritic Ca^{2+} spikes (Xu et al., 2012). Similar spatially restricted Ca^{2+} transients were recorded in both the anaesthetized and awake state, illustrating for the first time local dendritic activity indicative of local spikes during alert wakefulness.

Do NMDA spikes in the tuft dendrites have a crucial influence on AP generation? Global block of NMDA channels postsynaptically had a dramatic influence on the APs evoked by sensory input while having a negligible effect on subthreshold synaptic integration (as determined by the size and duration of up-states). On the other hand, blocking APs with the Na^+ channel blocker QX-314 in the patch pipette or hyperpolarization of the somatic membrane did not prevent the generation of NMDA spikes. Taken together, these two facts point to a causal influence of NMDA spikes on AP generation.

The defining characteristic of NMDA receptor activation is the requirement for simultaneous ligand binding (e.g. glutamate) and depolarization (unblock of Mg^{2+}). It is this requirement that causes the reported spatial restriction and leads to important computational possibilities(Mel, 1993). Since NMDA spikes enable local integration, they therefore make the neuron more sensitive to particular combinations of synaptic input. In this context, NMDA spikes will tend to maximize the influence of input converging on a particular dendritic branch(Larkum & Nevian, 2008). This is consistent with the finding that local NMDA spikes occurred overwhelmingly during up-states (i.e. during barrages of synaptic input). *In vitro* experiments in L5 pyramidal neurons showed that multiple NMDA spikes in the tuft dendrites lead to increased spiking output via the activation of apical dendritic Ca^{2+} spikes(Larkum et al., 2009). Unlike L5 pyramidal neurons(Larkum & Zhu, 2002; Williams & Stuart, 1999), however, L2/3 neurons do not have such a highly electrogenic Ca^{2+} spike initiation zone in the apical dendrite(Ledergerber & Larkum, 2012) which is consistent with the lack of global tuft Ca^{2+} events found in our study in comparison to L5 pyramidal neurons(Xu et al., 2012). It is

therefore not unlikely that NMDA spikes also occur in L5 neurons *in vivo* but are masked by the generation of global Ca^{2+} spikes throughout the tuft dendrite (Xu et al., 2012). The corollary is that NMDA spikes in the tuft dendrites of L2/3 pyramidal neurons appear to have a larger direct influence on AP generation in the axon.

In conclusion, the tuft dendrites of L2/3 pyramidal neurons can sustain local regenerative NMDA-dependent electrogenesis that decisively influences spiking output. Despite the fact that these events are difficult to detect with conventional recordings from the cell body, they are therefore likely to have a significant influence on sensory processing and network activity in the cortex.

Chapter 3

BIOPHYSICALLY DETAILED COMPUTATIONAL MODELS OF PYRAMIDAL NEURONS

In the previous chapter we established the biophysics of pyramidal neurons, both *in vitro*, and *in vivo* during sensory input. Such data, alongside decades of work establishing the general distributions of different channels in pyramidal neurons, allows for the creation of detailed multicompartmental models. Unlike in experiment, every variable is both controllable and easily read from simulations. Similarly, variables that were not part of the experimental paradigm (e.g. spatio-temporal barrages of synapses, extracellular fields, etc.) are all available for simulation. This allows for the implication of variables not directly seen in experiments to explain exerperimental findings, and also in the prediction of certain phenomenon not directly testable by experiment. As we will see in this chapter and the next, these models end up becoming objects of study in and of themselves.

In the first section that follows I establish a mouse primary visual cortex layer 5 pyramidal neuron model based on the experiments shown in the previous chapter. This model recapitulates the subthreshold and nonlinear properties found at both the soma and dendrite of layer 5 pyramidal neurons. Experimentally, it is difficult to precisely control spatio-temporal groups of synapses onto a single neuron. Thus the input-output relationship of the cell, though of upmost importance to understanding the computational properties of a neuron, becomes an experimentally intractable problem. With the model established I then simulate impinging groups of excitatory synapses onto the dendrites, monitoring the output of the cell all the while. A wide range of parameters are searched through, and the input-output relationship of

the cell is found. Additionally, the role of dendritic calcium channels in the input-output relationship is explore.

Next, I establish a somatosensory L2/3 pyramidal neuron model. This model is used to explore the spatial distribution of synaptic inputs leading to NMDA spikes in the dendrites, as well as to the integrative properties which the NMDA nonlinearities affords the cell.

LAYER 5 PYRAMIDAL NEURON MODEL

We use a multi-compartmental pyramidal cell model (Hay, Hill, Schurmann, Markram, & Segev, 2011) to further explore the relationship between the different nonlinearities found in our experiments and their role in the transformation between synaptic input and action potential output. Importantly, the Hay et al. model accurately captures both the backpropagation of action potentials into the dendrites as well as Ca^{2+} electrogenesis in the dendrites and their effect on somatic firing. We first test the model to ensure that the nonlinear signaling, and action potential properties of somatic and dendritic current injections are the same as in our experiments (Figs. 1-5). To recreate these properties, we use a parameter set fit that includes the impact of the axon initial segment (see Hay, Hill et al 2011, their supplemental material Table 2), increases the maximum conductance of the low-threshold voltage-gated calcium channels in the dendrites by a factor of 1.6, and changes the I_h profile from exponentially increasing with distance from the soma to a constant amount in the entirety of the dendritic tree (**Figure 17**). To simulate the effect of NMDAr-dependent nonlinearities, we use an NMDA/AMPA synaptic mechanism previously developed (Larkum, Nevian, Sandler, Polsky, & Schiller, 2009).

Our final model and parameter set captures the subthreshold properties (**Figure 5** and **Figure 17**), bAP innervation into the dendrite (**Figure 6**), the membrane response to suprathreshold somatic and dendritic current injections (**Figure 7** and **Figure 18**), the Ca^{2+} spike caused by a critical frequency of somatic APs (**Figure 8 Figure 19**), and NMDA spiking in the dendrites and their dependence on NMDA conductance (**Figure 9** and **Figure 20**). In the simulations

we ask how much input is needed in the dendritic tufts in order to elicit a burst of somatic action potentials given a certain amount of basal input. Unlike our experiments, we have complete control over every aspect of the simulation (including synaptic input), and can explicitly study the role of specific conductances (e.g. the Ca^{2+} conductances) in the simulations.

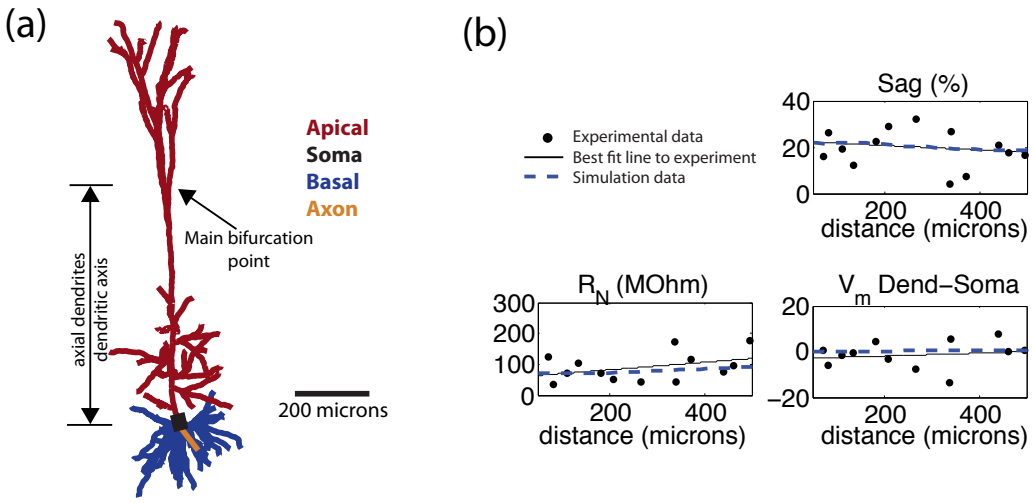

(c) Model parameters

	Soma	Axon	Apical	Basal
cm	1.00	1.00	2.00	2.00
Ra	100.00	100.00	100.00	100.00
g_pas	0.30	0.30	0.60	0.60
Ih*	0.75	0.50	1.50	0.50
Im	0.08	133.22	9.90	
SKv3_1	3380.29	4737.99	18.08	
SK_E2	996.50	0.47	0.02	
K_Tst	0.00	772.74		
K_Pst	0.00	1888.51		
Nap_Et2	0.00	58.34		
NaTa_t	0.00	38961.80		
NaTs2	9989.12		214.89	
Ca_LVA*^	5.57	8.13	22.7	
Ca_HVA	6.44	2.22	7.01	

Membrane capacitance (cm) is in $\mu F/cm^2$, axial resistance (Ra) is in Ω cm, and all conductances are in units of $pS/micron^2$. For details on the model conductances see Hay et al. (2011).

* indicates modified from the original Hay et al. (2011) model in the following ways: after exponential increase of Ih conductance up the apical dendritic axis was removed, somatic, axonal, apical, and basal Ih conductance was multiplied by a factor of 0.75, 0.5, 1.5, and 0.5 respectively. Apical Ca_LVA conductance was multiplied by a factor of 1.6 to lower the critical frequency to agree with experiment.

^ Ca_LVA conductance was increased to 2271.3 $ps/micron^2$ in the 200 microns sourrounding the main bifurcation point in order to recreate the calcium hotspot.

Figure 17: The computational model. (a) Diagram of the computational model colored by section name. (b) The difference in resting membrane potential of dendrite and soma, sag, and input resistance as a function of distance from the soma in experiments

(black) and the model (blue). (c) The computational model parameters. Note that a voltage-gated calcium conductance was increased 100-fold in a 200 micron area around the main bifurcation point to model the calcium hotzone (see Hay et al. (2011), and the exponential increase of Ih conductance was replaced with a flat Ih conductance spatial profile along the main dendritic axis.

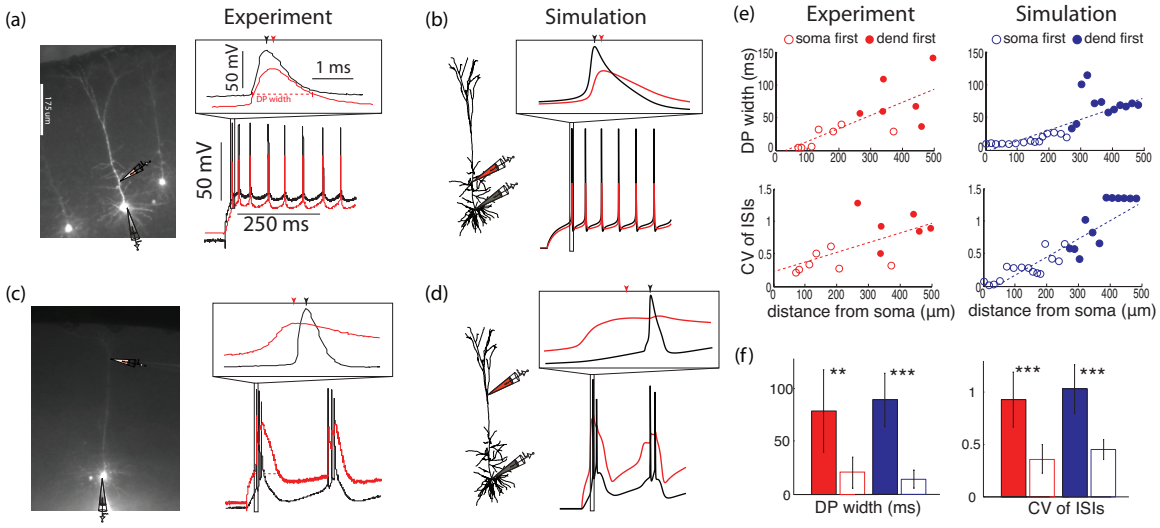

Figure 18: Current injections into the far apical dendrites elicit dendritic electrogenesis. (a,b,c,d) Examples of 1 second DC current injections into the dendrites of a L5 pyramidal neuron in V1 in experiments and computer simulations. Red traces show dendritic and black traces show somatic membrane potentials. Insets show details of individual action potentials and dendritic responses. (a,b) Membrane response to dendritic current injections at 135 μm from the soma show somatic spiking with relatively constant ISIs giving rise to bAPs in the dendrite. (c,d) Membrane response to dendritic current injections 442 μm from the soma show burst firing at the soma and dendritic electrogenesis which precedes action potential firing at the soma. Like in experiments (a,c), in simulations (b,d) injections close

to the soma give rise to APs at a regular frequency that backpropagate, while injections farther into the apical dendrite give rise to large dendritic potentials that precede bursts of APs. (e) Dendritic potential width (illustrated as red dotted lines in (a) and (c)), and ISI coefficient of variations a function of distance of the dendritic current injection from the soma in experiment and simulation. Filled circles corresponds to cases where dendritic spikes precede the somatic spike (e.g. inset c,d), while open circles correspond to cases where somatic spikes precede the dendritic event (e.g. inset a,b). Red and blue circles denote experiment and simulation results respectively. Lines are linear fits. (f) Comparison of the DP width and coefficient of variation of the ISIs of cases where somatic spiking preceded dendritic events (open bars) and where dendritic electrogenesis preceded somatic spiking (filled bars). Experimental data is in red and simulation data is in blue. *, **, *** Indicate significant differences between the two bars.

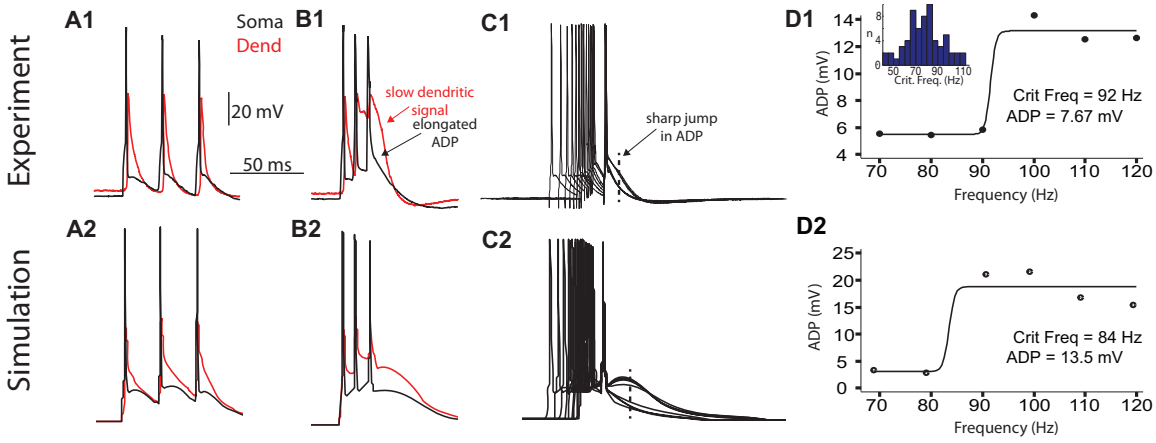

Figure 19: Calcium spiking in the dendrites in response to bursts of action potentials. (a) The somatic (black) and dendritic (red)

response to three short current pulses at the soma at a slow frequency (70 Hz). Analysis of experimental and simulation data are given in rows 1 and 2 respectively. (b) As in (a) except for three pulses above the critical frequency (100 Hz). Note the slow dendritic signal following the last somatic spike as well as the elongated somatic afterdepolarization (ADP) compared to (a). (c) Ten somatic responses to increasing frequencies of 3 short DC current injections at the soma, aligned at the final AP. Note the sharp nonlinear jump in ADP shape (broken line) (d) ADP size shown at the time of the dotted line in (c) as a function of frequency. The critical frequency is defined as the inflection point of the sigmoidal fit, and ADP size is defined as the difference between the two plateaus. The inset in d1 shows a histogram of the critical frequency for all 66 cells. Simulation results of the critical frequency analysis.

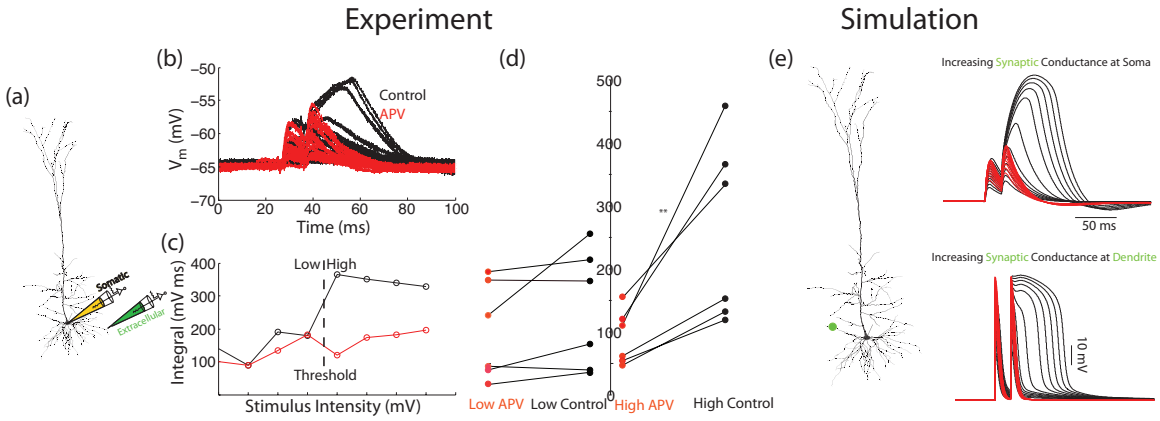

Figure 20: Layer 5 pyramidal neurons in mouse V1 and the computational model have NMDA dependent nonlinearities that produce NMDA spikes in the dendrites. (a) Diagram of the experimental setup. A glass theta pipette (green) is used for local extracellular stimulation, while a somatic whole cell patch (yellow)

recorded in current clamp at the soma. (b) Two short extracellular pulses at 50 Hz elicited two EPSPs at the soma. In control cases (black), a sharp nonlinear increase in both the duration and amplitude of the second EPSP occurs past some threshold. Bath application of AP-5 (red), an NMDAr antagonist, eliminates this nonlinear effect. (c) The integral of the second EPSP as a function of extracellular stimulus intensity. Note the sharp nonlinear increase in the integral past some threshold only in the control case. (d) Summary of the extracellular stimulation for 6 cells. Left, subthreshold comparison of AP-5 (red circles) and control (black circles) integrals of the second EPSP. Lines connecting circles indicate pairs from the same cell and extracellular stimulus location. The difference between AP-5 and control conditions for the subthreshold case is insignificant. Right, suprathreshold comparison of AP-5 and control integrals of the second EPSP. Control suprathreshold EPSP integrals are significantly bigger than under AP-5 conditions ($p<0.01$). (e) diagram of the location of the synapse (green) in the simulation. (top) The somatic membrane potential with (black) and without (red) NMDA conductance, in response to increasing synaptic conductance. (bottom) The membrane potential at the location of the synapse.

Synaptic inputs in the multicompartmental model

We use the multi-compartmental pyramidal cell model (Hay et al., 2011) to further explore the relationship between the different nonlinearities found in our experiments and their role in the transformation between synaptic input and action potential output. In the simulations we ask how much input is needed into the dendritic tuft in order to elicit a burst of somatic action potentials given a certain amount of basal input. Unlike our experiments, we have complete

control over every aspect of the simulation (including synaptic input), and can explicitly study the role of specific conductances (e.g. the Ca^{2+} conductances) in the simulations.

We randomly distribute NMDA/AMPA synapses across the tuft and basal dendrites (**Figure 21**a). 100 tuft and 175 basal synapses of equal postsynaptic conductance are elicited randomly and uniformly (in time) within 100 ms. When basal and tuft inputs impinge along the neuron (**Figure 21**b), a high frequency burst of 4 somatic (black trace) APs and 1 dendritic (red trace) spike occur. Basal input alone (**Figure 21**c) causes a single somatic AP and no dendritic spike, while tuft input alone (**Figure 21**d) causes no spiking. Thus, the neuron acts as a coincidence detector for basal and tuft input, signaling coincident input by a high frequency burst. When the conductance of both high- and low- threshold Ca^{2+} channels in the apical dendrites is halved (**Figure 21**e), somatic output from basal and tuft input reverts from bursting back to a single AP. To visualize the subthreshold responses to the input we inject 200 pA of hyperpolarizing DC current at the soma. The somatic subthreshold response to basal and tuft input both with and without the reduction in apical Ca^{2+} conductance (**Figure 21**fg) is similar, though the dendritic response is slightly smaller when Ca^{2+} conductances are reduced.

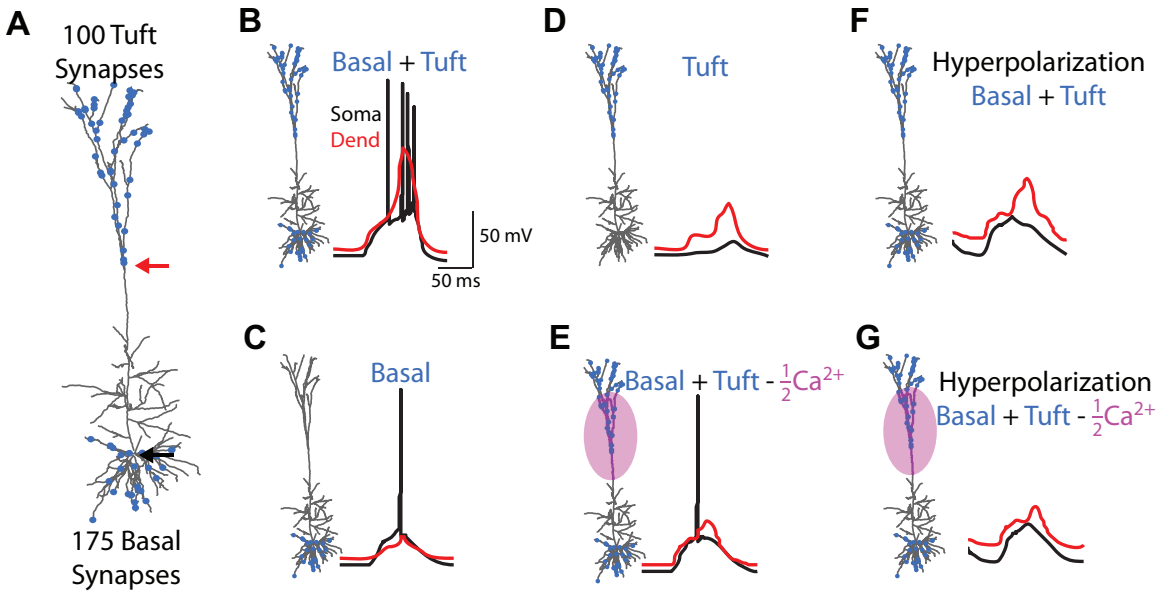

Figure 21: Coincidence detection between basal and apical tuft inputs. (A) 100 tuft and 175 basal NMDA/AMPA synapses are distributed randomly across the apical tuft and basal dendrites of a multi-compartmental L5 pyramidal neuron model. All synapses are randomly and uniformly elicited in time across 100 ms. In the following, somatic traces are in black and dendritic (location shown by the red arrow in (A), are in red. (B) Simultaneous tuft and basal inputs triggers a burst of somatic APs and a dendritic Ca2+ spike, while (C) basal inputs alone evoke only a single somatic spike. (D) Apical tuft inputs alone do not evoke somatic spiking. (E) Reducing Ca2+ channel conductance by 50% during tuft and basal input gives rise to a single somatic spike. (F) When applying a 200 pA hyperpolarizing DC current to the soma, the response of the tuft and basal inputs are similar to the case with Ca2+ conductances reduced shown in (G), even though the suprathreshold (B,C) cases are remarkably different.

We quantify the manipulation and robustness of output spike frequency by tuft inputs via simulations by varying the number of activated basal and tuft synapses. Specifically, we vary the number of tuft synapses from 0 to 200, and basal synapses from 0 to 300 per 100 ms (**Figure 22**a left). We also study the impact of blocking Ca^{2+} conductances in the dendrites on tuft modulation. When Ca^{2+} conductances are reduced by 75% of the control condition (**Figure 22**a right) in the apical dendrites, output frequencies above 100 Hz are abolished. At 50% of the Ca^{2+} conductances (**Figure 22**a middle), frequencies from 100-150 Hz are only reached when there are (at least) 120 basal and 120 tuft inputs onto the cell. No amount of input tested resulted in >150 Hz output. The control case (**Figure 22**a left) reaches outputs > 100 Hz with >80 basal and >70 tuft inputs. Spiking output of >150 Hz is reached when > 110 of basal and >90 tuft inputs, impinged on the cell. A wide range of synaptic input levels allow for tuft modulation to change somatic spiking from below to higher than 100 Hz, and, in the control case, even from no spiking to more than 100 Hz.

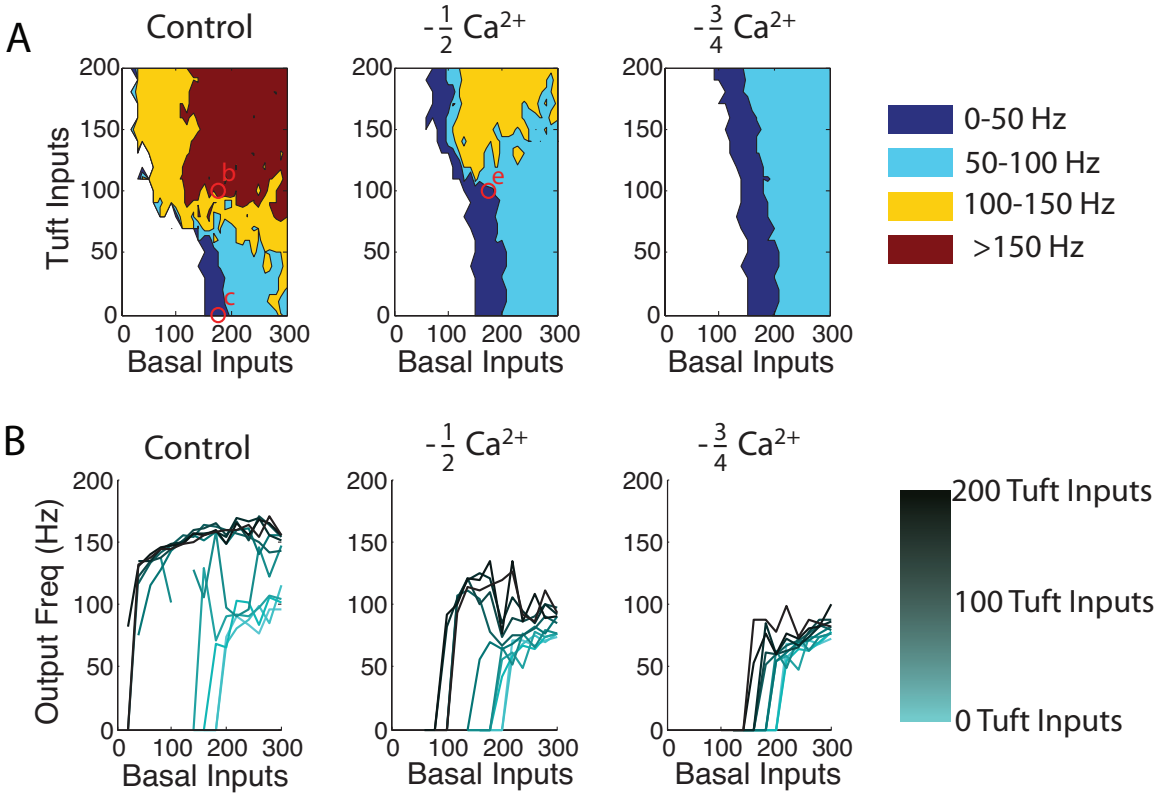

Figure 22: Coincidence detection details. (a) The output frequency of the L5 simulated cell over a wide range of tuft and basal inputs into a control cell (left), a cell with half (middle), and a quarter (right) of the Ca2+ conductance along the apical tuft. Open red circles correspond to **Figure 21** (b), (c), and (e). (b) The modulation of the input-output relationship as function of basal and apical tuft input. Different lines correspond to different amounts of tuft input (from light to dark, 0-200 tuft inputs).

In **Figure 22**b we show the effect of blocking Ca^{2+} conductance, which is twofold: (1) a decrease in the maximum achievable somatic spike frequency, and (2) a requirement for additional basal inputs to elicit somatic spiking for high, but not low, levels of tuft input. In

both cases, this is due to the synergistic effect of somatic and dendritic depolarization. When tuft input is low, basal input alone dictates the somatic output and, thus, changes in dendritic Ca^{2+} conductance make little difference (compare light teal lines in **Figure 22**b). If, instead, there is substantial tuft input (**Figure 22**b dark lines), the somatic output is a function of the interaction of the soma and dendrites. That is, the somatic response for a given number of basal inputs increases substantially as dendritic Ca^{2+} conductance increases. Importantly, when tuft input increases, large increases in output spike frequency are observed. Furthermore, the extent of these increases is reduced as Ca^{2+} conductance is reduced (compare dark lines in **Figure 22**b).

As discussed in the Introduction of this thesis, one of the neural correlates of consciousness is a large, late, and relatively long-lasting current sink, in layer 1. Given the location of the dendrites of pyramidal neurons, what is their extracellular signature, and might they be a major contributor of such current sinks? The model was used to simulate the extracellular signature of a Ca-spike. Synapses were randomly distributed along the dendritic tufts of the model, until threshold for a Ca-spike was reached (**Figure 23**). The extracellular signature of such a simulation was compared to the same simulation with the Ca-hotzone removed. As can be seen, the Ca-spike causes a large, slow, extracellular depolarization in the upper layers of cortex.

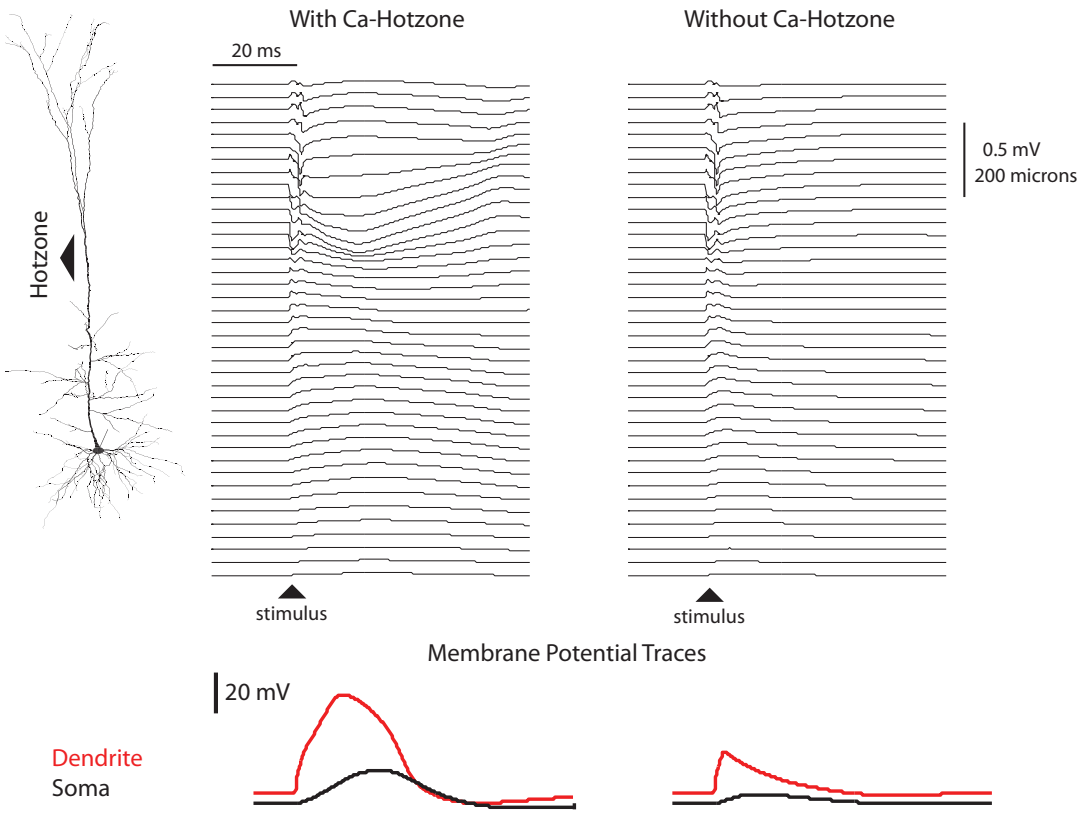

Figure 23: Extracellular calcium spike. Impact of Ca-dependent dendritic spikes on extracellular voltage recordings. A computational model of a layer 5 pyramidal neuron in the presence (left) and absence (right) of the Ca-hotzone (location shown by the arrow) is used to emulate the electric field produced by a single neuron. The simulated depth LFP for the two cases is shown by the traces. It is observed how the presence of the Ca-hotzone and elicitation of a Ca-spike gives rise to a strong, long-lasting event in the superficial regions of the cortex.

Discussion

In this section we have used the whole cell patch clamp results to establish a detailed multicompartmental model of a layer 5 pyramidal neuron. In doing so, the plausible distribution of I_h channels in particular proves to be interesting. The absence of increasing sag in the experimental data suggests a more spatially homogenous distribution of I_h channels in the dendrites of mouse V1 than in rat SS L5 pyramidals, where I_h concentration exponentially increases up the dendrites (Kole, Hallermann, & Stuart, 2006). This spatial concentration of I_h in rat SS cortex is responsible for a dendritic depolarization relative to the soma as well as an absence of an increasing input resistance into the dendrites, since the added conductance counteracts the effect of decreasing diameter (Berger, Larkum, & Luscher, 2001; Zhu, 2000). Thus, the absence of exponentially increasing I_h conductance in the dendrites of mouse V1 L5 pyramidal neurons might explain both the constant resting membrane potential as well as the increase in input resistance. The multicompartmental model provides a way to test this hypothesis. Indeed, when the exponentially increasing I_h conductance is replaced by a constant value in a multi-compartmental model, the values and trends for resting membrane potential, sag, and input resistance are found to coincide with the experimental results (**Figure 17**).

In this work, we focus on the conditions and mechanisms that give rise to high-frequency (>100 Hz) burst firing in L5 pyramidal neurons. Such high-frequency burst firing has been found to occur in rodent pyramidal neurons in both awake and anesthetized conditions (de Kock & Sakmann, 2008). L5 pyramidal neurons in particular have firing frequency distributions that go beyond 200 Hz, and can even have bursts of up to 6 spikes where all 6 spikes are > 100 Hz (de Kock & Sakmann, 2008). Are these bursts relevant to neural and

network computation? Indeed, experimental work in the primary visual cortex of cats and monkeys has shown that bursts provide more information about the orientation or the direction of motion of visual stimulus than isolated spikes (Bair, Koch, Newsome, & Britten, 1994; Cattaneo, Maffei, & Morrone, 1981; Livingstone, Freeman, & Hubel, 1996). Some evidence shows that attentional effects on neurons in the visual cortex covary with burstiness (Anderson, Mitchell, & Reynolds, 2011) suggesting a top-down influence on bursting. In this work, we explored the biophysical mechanism and computation in single cells that accompanies such bursting.

To quantify the relationship between synaptic inputs, Ca^{2+} spiking, and bAPs, we adapt a detailed biophysical multi-compartmental model able to emulate and recreate the physiological properties of mouse V1 L5 pyramids (Hay et al., 2011). In our modeling work, we postulate two groups of excitatory, glutamergic synaptic input. One group impinges on the basal dendrites, in the deeper layers of cortex (basal input), and the other on the apical tufts, in the upper layers (tuft input). Figure 3 shows how tuft input changes the somatic output of a L5 pyramidal neuron from single APs (**Figure 21**c) to high frequency bursts (**Figure 21**b). In this way, high frequency bursts indicate a the coincident input of excitatory input onto to distinct areas of the neuron. Additionally, blocking Ca^{2+} channels in the apical dendrites blocks the effect of tuft input, and reverts the neural output back to single spikes (**Figure 21**e). This calcium-spike dependant modulation of output frequency by apical input can act as a mechanism for coincidence detection within individual cortical columns. In this view, a coincident input into the upper and lower layers of the V1 column cause an output of a high-frequency burst (**Figure 21**bc, **Figure 22**). Thus, any postsynaptic cell receives a unique signal,

in the form of a burst, informing of coincident input onto the presynaptic cell. Although we focus on the output of L5 pyramidal neurons, other neurons in the cortical column such as L2/3 pyramidal neurons also support Ca^{2+} dendritic electrogenesis and NMDA spiking (L. M. Palmer et al., 2014), extend tuft dendrites into the upper layers, and, importantly, have long-range axons which project to other cortical areas. Here, concurrent excitatory input into the superficial and deeper layers produces high-frequency bursting, signaling coincident basal and apical input to downstream neurons. Importantly, high-frequency bursting would not occur with only basal or tuft input in isolation. Additionally, modulation of output frequency by tuft input can be vetoed by a direct block of Ca^{2+} conductance in the apical dendrite (**Figure 21** and **Figure 22**), such as that produced via $GABA_B$ inhibition to the distal tuft (Chalifoux & Carter, 2011).

Further quantification of the tuft modulation, and the Ca^{2+} conductance effect on that modulation shows that it is a robust phenomenon that changes no spiking, single spikes and low-frequency spiking output to high frequency output (**Figure 22**). Furthermore, blocking Ca^{2+} conductance has little effect before the nonlinear dendritic event occurs (**Figure 21**fg, **Figure 22**). Such spiking-dependent inhibition has been referred as "silent inhibition" due to the absence of a somatic effect under subthreshold conditions (L. Palmer, Murayama, & Larkum, 2012). Taken together, these simulations suggest a robust mechanism for coincidence detection between basal and tuft input streams. It works by changing the output frequency of the cell from low (or zero) to high firing rates.

The calcium hotspot is home to a high density of nonlinear calcium channels, that are most active when depolarized. As such, the subthreshold contribution of these channels is minimal. Indeed, when looking at the subthreshold response of these simulations, the differences were not noticeable. This suggests the possibility of a mechanism of *silent inhibition*. In such a scheme, inhibition of a suprathreshold channel remains invisible if all activity is subthreshold. Indeed, metabatropic inhibition of the calcium hotzone has been shown to exist via the activity of neurogliaform cells in layer 1, synapsing onto $GABA_B$ receptors on the apical dendrites of pyramidal neurons.

A number of studies have shown that while the tuning properties of some cells are highly specific to certain stimuli, for instance to bars of certain orientations, their subthreshold responses are largely untuned. In trying to explain this curious state of affairs, people have posited an exquisite balance between excitation and inhibition, so that when the right stimulus impinges on the brain, the excitatory drive into the cell pushes the cell just above threshold for firing. Here, another possible explanation is suggested. Inhibition of the calcium hotzone would be invisible to those looking at subthreshold responses, but would, in the suprathreshold case, result in sizeable changes in spiking. Such a mechanism might be a more robust way to establish tunng properties in cells. Indeed, we will see in the next chapter that the existence of two interacting nonlinearities does indeed afford the cell with robust mechanisms for tuning.

Recently, *in vivo* work has shown that dendritic nonlinearities contribute to the orientation tuning of pyramidal neurons in the visual cortex of mice (Smith, Smith, Branco, & Hausser,

2013). In that work, spikes were carried on long-lasting dendritic potential envelopes, such as those we observe in our *in vitro* work (**Figure 7** and **Figure 8**). Additionally, hyperpolarization of the dendrites, as well as block of NMDA-mediated dendritic current (ie. the synaptic currents modeled in our work), both greatly decreased the tuning of single pyramidal neurons. In our modeling work, a decrease of synaptic input led to a loss of the coincident detection mechanism (**Figure 22**).

LAYER 2/3 PYRAMIDAL NEURON MODEL

Establishing the Computational Model

A multi-compartmental computational model of a L2/3 pyramidal neuron was simulated on a biocytin-filled reconstructed cell from the experimental study. The model consisted of 129 segments of average length 4.17 m and was simulated in NEURON (Hines). The cell was divided into 5 sections: soma, tuft dendrite, basal dendrite, trunk, and axon, as shown in (**Figure 24)**. Intrinsic membrane mechanisms were taken from the Hay et. al, (2012) layer 5b pyramidal model (Hay et al., 2011) and consisted of ten active conductances, internal Ca^{2+} dynamics, and passive conductances at values given in the table in **Figure 17**. Values were chosen by starting with the biophysics of the Hay et. al. model, and modifying them according to *in vitro* data both from this study and Larkum et. al., 2007 (Larkum, Waters, Sakmann, & Helmchen, 2007). Specifically, I_h conductances were reduced in order to fit the sag values at the soma found in our studies, and I_h was modified in the tuft dendrites to fit the reported ratio of dendritic to somatic sag in Larkum et. al., 2007 (Larkum et al., 2007). Ca^{2+} conductances (high voltage activated, HVA; low voltage activated, LVA) around the major bifurcation were reduced to fit the dual-patch DC current injection performed in Larkum et. al., 2007 (Larkum et al., 2007). HVA and LVA Ca^{2+} conductances elsewhere in the dendritic tree were a factor of 10 and 2 less than at the bifurcation region respectively. Compared to the L5 model, the bifucation region in our L2/3 model was 10 times less dense in HVAs and 5 times less dense in LVAs. The two S_K channel conductances were increased by a factor of 1.3 in order to eliminate an afterdepolarization which followed AP spiking which was not seen in DC current injection induced spiking *in vitro* in L2/3 cells. Finally, the passive conductance

was modified to fit the input resistance recorded *in vitro*. No changes were made to the internal Ca^{2+} dynamics. All values are reported in **Figure 24**. Membrane capacitance in the dendrites was doubled relative to the somatic value in order to account for the influence of spines (see Hay et. al., 2012). Reported values are corrected for an 11 mV junction potential.

To model the effects of QX-314 we altered conductances according to the previous published experimental data (Taylor, 1959; Connors and Prince, 1982; Perkins and Wong, 1995; Talbot and Sayer, 1996). In our model, we completely blocked all three Na^+ conductances, reduced all K^+ conductances by 80% except for the I_h conductance which was reduced 75%, reduced low voltage activated Ca^{2+} channels (LVA) by 55% and high voltage activated calcium channels (HVA) by 80%, and changed the passive membrane conductance in order to fit the input resistance found in QX-314 application *in vitro* (**Figure 25**).

Excitatory synaptic input was modeled by a voltage dependent NMDA and voltage independent AMPA conductance at each synapse, using a NEURON mechanism created by Alon Polsky on http://senselab.med.yale.edu/ and published in Larkum et. al., 2009 (Larkum et al., 2009). The NMDA conductance was voltage dependent and given by $g_{NMDA} = g_{MAX}(\exp(-t / 70) - \exp(-t / 3)) / (1 + 0.3 \exp(-0.08v))$, and AMPA conductances were modeled with an instantaneous rise time and decay time constant of 0.5 ms (Larkum et al., 2009). Each synapse had a maximum NMDA to maximum AMPA conductance ratio of 1:1. One hundred background synapses were added across the basal and tuft dendrites (**Figure 24** and **Figure 26**), and were given maximum conductances as a function of distance (x) from the soma: $g_{syn} = 0.39 + 0.09 * \exp(x / 158.02$ m) nS. Each background synapse was randomly activated

between 10 and 100 Hz resulting in an average background somatic depolarization of 17.3 mV, which is similar to the UP states recorded *in vivo*. Top-down input (non-background input) was distributed with uniform distribution across the dendritic tufts in simulations unless otherwise stated. To test the effect of input location on the generation NMDA spikes, the spatial spread of 8 synapses (6) ranged from 20 – 50 m. In simulations with the NMDA conductances removed from the top-down inputs, the AMPA conductance was doubled, in order to keep the total conductance of single synapses equal between trials.

Simulations were also used to model the effect of uncaging MK801 near dendritic branches. Any given trial consisted of background input as described above, a number of top down inputs, and a number of chosen branches. Both background and top down inputs on given branches had their NMDA conductance removed to simulate the effect of uncaged tc-MK801. The average length of a single branch where the effect of uncaging tc-MK801 was simulated was 187.4 m.

Results

The experimental data shown in Chapter 2 demonstrate the importance of NMDA electrogenesis for neuronal output. To quantify this effect, we examined the influence of the spatial distribution and NMDA/AMPA composition of synaptic inputs to the tuft in generating AP output using the NEURON simulation platform (**Figure 26** and **Figure 24**). We first modeled local NMDA receptor-dependent dendritic spikes similar to the experimental data using focal dendritic input (**Figure 26a-c**). Here we were able to simulate dendritic NMDA spikes due to ~8 simultaneous synaptic inputs(Larkum et al., 2009) in a 30 μm segment of dendrite.

We next tested the importance of tuft NMDA conductances on neuronal output during network activity. To achieve this, we simulated background subthreshold synaptic input using 100 randomly distributed NMDA/AMPA synapses over the entire dendritic tree (based on experimental data; up-state amplitude, 17.3 ± 1.7 mV and duration, 0.5 ± 0.04 s; n=11; **Figure 26d**). Under these conditions, somatic APs could be evoked with an additional 40 NMDA/AMPA synaptic inputs that were randomly distributed over the tuft dendrite (**Figure 26d-f**). However, using AMPA-only synaptic inputs (adjusted to have the same conductance as the previous NMDA/AMPA inputs), it was necessary to include 4-fold as many inputs (i.e. 160) to evoke somatic APs (**Figure 26f**). The model further demonstrated the importance of tuft NMDA receptor-dependent electrogenesis by revealing that NMDA conductances in several branches of the tuft dendrite were necessary for somatic AP firing (**Figure 27**, compare to experimental data in Figure 13). These results highlight the importance of NMDA receptor-dependent electrogenesis in the tuft dendrite which far outweighs the passive influence of tuft synaptic input on the soma(Stuart & Spruston, 1998; Waters, Larkum, Sakmann, & Helmchen, 2003; Zador, Agmon-Snir, & Segev, 1995).

By preventing APs, it is in principle possible to quantify the influence of spontaneous NMDA-dependent electrogenesis on the somatic membrane potential. However, QX-314 is known to partially block various other conductances such as I_h, voltage-sensitive Ca^{2+} and K^+ channels and G protein-activated inwardly rectifying K^+ channels(Andrade, 1991; Connors & Prince, 1982; Perkins & Wong, 1995; Talbot & Sayer, 1996; Taylor, 1959) which could affect both the active and passive properties of the dendritic tree. We therefore examined the effect of QX-

314 under more controlled conditions *in vitro*. As *in vivo* (Figure 11 and Figure 56), local extracellular stimulation *in vitro* evoked APV-sensitive NMDA spikes before and after inclusion of QX-314 in the patch pipette (**Figure 25**). Further stimulation of the dendrite after APV had no effect showing that NMDA spikes could still be evoked in the presence of QX-314 without additional active conductances. Nonetheless, the amplitude of the somatic voltage due to dendritic NMDA spikes did increase by 2.3 ± 0.2 fold (n = 6; **Figure 25**). We attributed this to the recorded increase in input resistance (by 49 ± 15%) which was confirmed using a multicompartmental model (**Figure 24**). Using this value as the scaling factor for the somatic voltage response recorded simultaneously during tuft Ca^{2+} transients *in vivo*, we calculated that the influence of spontaneous NMDA spikes on somatic voltage is on average 14.4 ± 0.8 mV (n = 11; Figure 15**b**). Most of this somatic voltage was due to synaptic input to the tuft because large somatic voltage potentials nearly always correlated with spontaneous Ca^{2+} transients in the tuft dendrite (92 ± 4 %; n = 11 dendrites) and only rarely with Ca^{2+} activity in the basal dendrites in 21.2 ± 6 % of cases (n = 7 dendrites; $p < 0.05$; Figure 15**c** and **d**). This might indicate that there is typically more input to the tuft than the basal dendrite for the situations we tested (spontaneous or sensory-evoked activity) or that conditions in the tuft are more favorable for electrogenesis.

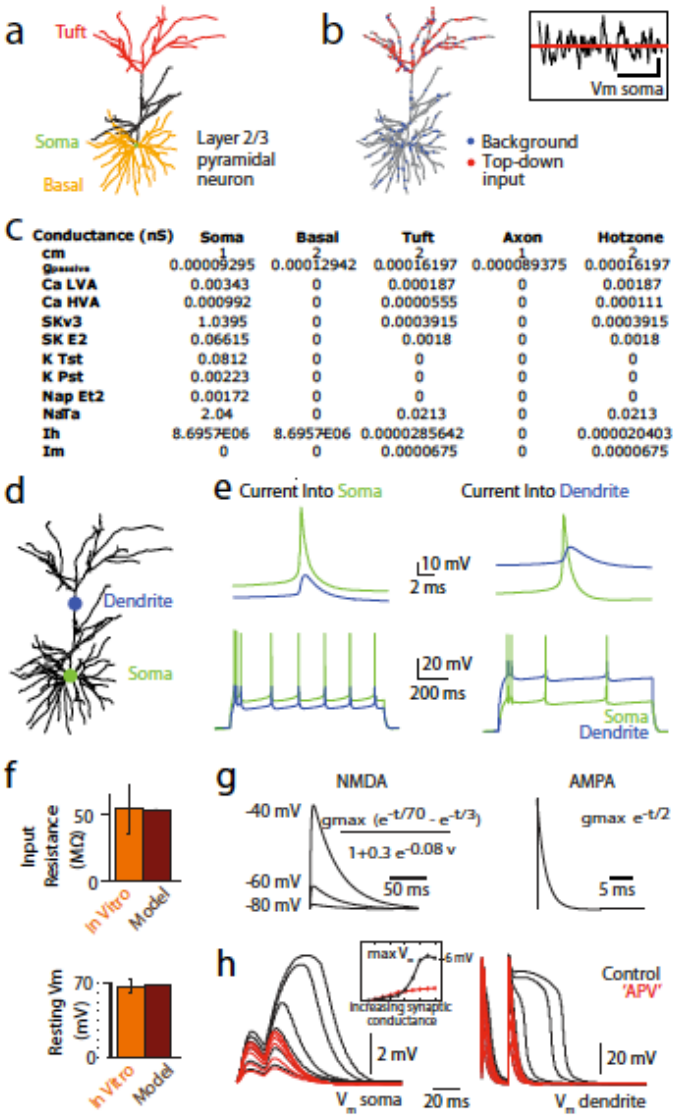

Conductance (nS)	Soma	Basal	Tuft	Axon	Hotzone
cm	1	2	2	1	2
Gpassive	0.00009295	0.00012942	0.00016197	0.000089375	0.00016197
Ca LVA	0.00343	0	0.000187	0	0.00187
Ca HVA	0.000992	0	0.0000555	0	0.000111
SKv3	1.0395	0	0.0003915	0	0.0003915
SK E2	0.06615	0	0.0018	0	0.0018
K Tst	0.0812	0	0	0	0
K Pst	0.00223	0	0	0	0
Nap Et2	0.00172	0	0	0	0
NaTa	2.04	0	0.0213	0	0.0213
Ih	8.6957E06	8.6957E06	0.0000285642	0	0.000020403
Im	0	0	0.0000675	0	0.0000675

Figure 24: Details of the L2/3 multicompartmental model. (a) A reconstructed L2/3 pyramidal neuron from the experimental part of this study was used for simulations in NEURON. (b) Top-down synaptic inputs (red) were placed with uniform probability distribution across the tuft dendrites and a further 100 synaptic inputs were distributed with uniform probability across the entire neuron to simulate background synaptic input (blue). Inset, background membrane potential. Red line: 17.3 mV from rest. Scale, 1 mV; 150

ms. (c) Table of conductance values used in the simulated neuron. All values are in units of nS. (d) A reconstructed L2/3 pyramidal neuron. (e) Computer simulations of the voltage response at the soma (green) and dendrite (blue) during current injection (1 s) into the soma (left) and dendrite (right) for the modeled neuron shown in (d). (f) Comparison of vitro experiments (n = 6) and the model neuron for input resistance and resting membrane potential. Error bars are standard deviation. (g) (left) Nonlinear NMDA conductance used in the model. Note that the conductance is a function of the local membrane potential. Plots are shown at –40, –60, and –80 mV. (Right) Linear AMPA conductance used in the model. Note that the AMPA conductance is voltage independent. (h) Simulated voltage response to paired pulse stimulation (50 Hz) with increasing intensity with (red) and without (black; 'APV') NMDA conductance recorded at the soma (left) and at the site of stimulation (tuft dendrite; right). Inset, maximum voltage response at the soma as synaptic conductance increases. The non linearity in the control condition establishes the event as an NMDA spike, as described in previous work (Schiller et al., 2000, Schiller and Schiller, 2001, Spruston and Kath, 2004, Rhodes, 2006, Major et al., 2008, Larkum et al., 2009, Polsky et al., 2009, Lee, 012).

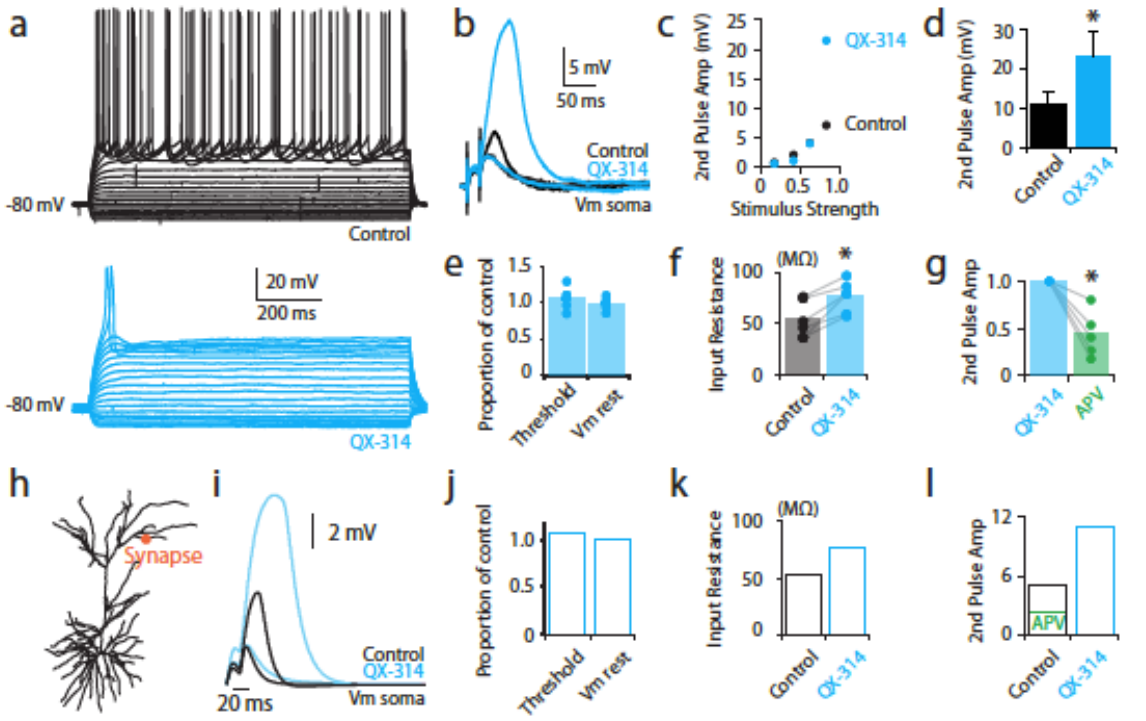

Figure 25: QX-314 increases the amplitude of the somatic voltage during NMDA spikes in tuft dendrites of layer 2/3 pyramidal neurons in vitro and in silico. Intracellular application of QX-314 blocks Na+ channels as well as partially blocks Ca2+, Ih and K+ channels (Perkins and Wong, 1995; Talbot and Sayer, 1996). The eect of QX-314 on NMDA spikes was tested using somatic recordings from layer 2/3 pyramidal neurons which were initially patched with control intracellular solution and then repatched with intracellular solution containing QX-314. Neurons were -lled with Alexa Fluor 594 (50 μM) to aid the placement of an extracellular stimulation pipette in close proximity to a tuft dendrite. (a) Somatic voltage response to somatic current step injections (100 pA steps) before (black) and after (blue) QX-314. Note the lack of action potentials in the presence of QX-314. (b) Sequentially increasing the intensity of paired pulses (2x 1 ms pulses at 50 Hz) to the tuft dendrite resulted in a supralinear voltage response both before (black) and after

QX-314 (blue). A subthreshold and suprathreshold response is shown for each condition. (c) Amplitude of the somatic voltage during sequential increase in stimulus intensity for the example shown in (b). (d) QX-314 significantly increased the amplitude of the voltage response by approximately two-fold (2nd pulse; $n = 5$; $p < 0.05$). (e) There was no signi-cant inuence of QX-314 on the stimulus intensity (threshold) required to evoke a spike ($n = 5$) nor the resting membrane potential ($n = 6$). (f) However, QX-314 significantly increased the input resistance by on average 48 ± 15 % ($n = 6$). (g) Bath application of the NMDA channel agonist APV (50 M; bottom; green) significantly decreased the voltage response. (h) The eects of intracellular QX-314 on synaptic input (location; orange dot) was modeled by completely or partially blocking Na+, Ih, K+ and Ca2+ conductances (see supplemental methods). (i) Subthreshold and suprathreshold somatic responses to increasing NMDA/AMPA input in control (black) and QX-314 (blue) simulations at the synapse shown in (h). Note, the computer simulations are comparable to the experimental data in (b). In the presence of QX-314, the computational model shows no effect on threshold or resting membrane potential (j), an increase in the input resistance (k) and an increase in the amplitude of the second pulse of the paired pulse stimulation which was decreased during bath application of APV in control (l). These computer simulation results are comparable to the in vitro data shown in (a) - (g) and the increase in voltage during QX-314 can be entirely explained by the decrease in input resistance. * indicates $p<0.05$. Error bars represent S.E.M.

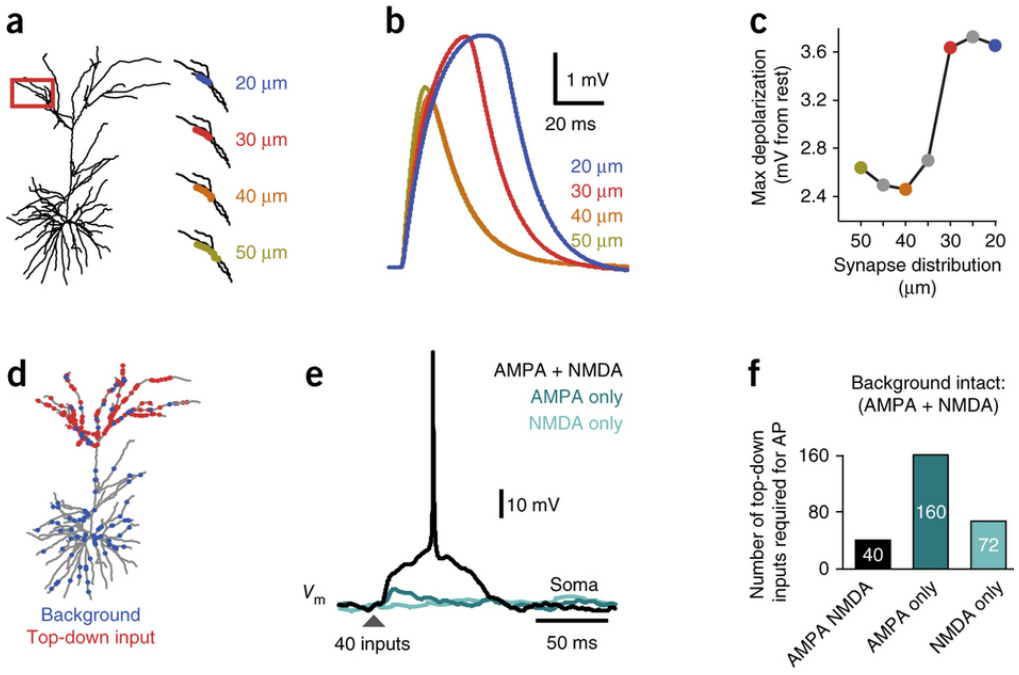

Figure 26: Synaptic input location and NMDA conductance are crucial for NMDA spikes and action potentials. (a) To investigate the spatial spread of the NMDA spike, the spatial location of eight synapses6 were altered in a tuft dendrite of a model L2/3 pyramidal neuron. Right, magnification of boxed region of tuft dendrites (left) illustrating a subset of the different spatial spreads tested. (b) Simulated somatic voltage responses to varying the spatial spread of eight synapses shown in a. (c) Only when synaptic input was spread over a maximum dendritic distance of 30 µm (red) were NMDA spikes initiated. (d) Reconstruction of a L2/3 pyramidal neuron used for computer simulations. Colored dots illustrate randomly distributed synaptic input (blue, background; red, top-down input). (e) Simulated somatic voltage in response to 40 synaptic inputs (plus background) with both AMPA + NMDA (black), AMPA only (teal) and NMDA only (light teal) top-down conductances. Note that the background synaptic input and the overall synaptic conductance were the same for all conditions. (f) The number of randomly distributed

top-down synaptic inputs required to generate a somatic action potential was fourfold greater without NMDA conductances.

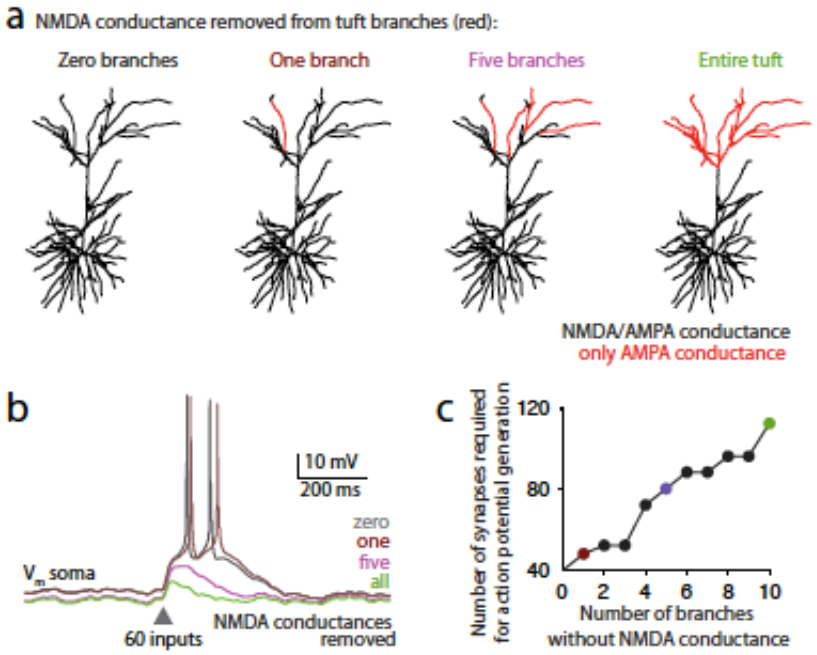

Figure 27: Blocking distributed NMDA conductances in the majority of the tuft affects AP generation. The experimental data showed that locally blocking NMDA channels in a single tuft branch does not affect somatic action potentials (APs). To further investigate this, we used computer simulations in the NEURON simulation platform to manipulate the extent of the tuft experiencing NMDA block and measure the resulting affect on neuronal output. Top-down synaptic inputs were randomly distributed across the tuft dendrites and a further 100 synaptic inputs were distributed with uniform probability across the entire neuron to simulate background synaptic input (see **Figure 24**). (a) A model layer 2/3 pyramidal neuron had NMDA conductances blocked in varying numbers of tuft branches. Synaptic input was randomly distributed for each trial and branches

shown in red had both background and top-down NMDA conductances blocked. (b) Membrane potential traces in response to 60 synaptic inputs randomly distributed onto the tuft dendrite in neurons where NMDA conductances were removed from no (grey), one (brown), five (fuchsia) and all (green) tuft branches. During this simulation, NMDA block in five tuft dendrites is sufficient to substantially change neuronal output. (c) The total number of synapses needed to generate an AP compared to the number of branches with NMDA conductances removed. Colored dots refer to data shown in (b).

Discussion

Using *in vitro* results, statistics of UP-DOWN states, and the results of QX314 pharmacology, a L2/3 multicompartmental model was established. This model was used to quantify the influence of NMDA on action potential generation, which experiments discussed in Chapter 2 showed to be substantial. Experimentally it was found that linearizing single tuft dendrites by blocking NMDA conductances had no influence on action potential generation, even though local NMDA spiking was abolished. On the other hand, complete block of NMDA conductance over the entirety the neurons membrane resulted in the abolishment of action potentials. Modeling allowed us to explore the space between these two extremes.

In particular, it was found that in the case of blocking NMDA in the entire neuron, three times the number of excitatory inputs were required to cause the cell to fire, compared to when only one branch had no NMDA conductance. The increasing need for excitatory input as more branches became linear occurred in a linear fashion, with approximately 8 extra synaptic events

needed for every branch that was linearized. This, despite the fact that the NMDA spike itself is a highly nonlinear event.

There are multiple mechanisms whereby the nonlinearity of individual branches can be controlled. On the path shunting inhibition can work to veto individual branches, such that even if their nonlinearity remains intact, it becomes essentially invisible to the cell body. More recently, computational modeling work has shown that off-path inhibition can be used to strongly inhibit local dendritic branches, by reshaping the spatial profile of conductance in the cell. More direct manipulations are also possible. One of the effects of the metabotropic glutamate receptors (mGluR) is to change NMDA conductance. One subtype of receptor, mGluR1, increases the activity of NMDArs, while mGluR2 and mGluR3 decrease the activity of NMDArs.

The interaction of mGluRs and their influence on NMDA conductance is often studied with respect to neurotoxicity brought about by increased neural activity (e.g. due to increased NMDAr activity). The potential role of mGluRs mentioned here is entirely speculative, but plausible given the lack of focus on single-cell computation by those who study metabotropic signaling. Indeed, the manipulation of the wide varities of nonlinearites that the single cell has at its disposal would be an incredibly powerful computational tool, ripe for discovery, if such manipulations occur. In this case, the effect of mGluR activity would be to shift the neuron left and right across the axis in **Figure 27**c, changing the effective threshold for action potential spiking in the neuron.

Chapter 4

ABSTRACTED MODELS OF PYRAMIDAL NEURONS

Ultimately we wish to understand the functional and computational purposes of the biophysics of single cells. An important part of this process is to distill the single cell into its simplest form, in an effort to describe the abstract computation the physiology carries out. This chapter explore two abstracted models based on the work presented so far in layer 5 pyramidal neurons.

The 2LIF model takes explicit use of the idea presented in **Figure 10**, mainly that the pyramidal neuron consists of two independent integrating areas, that communicate via a nonlinear communication channel. We will explore the use of such a setup specifically for spike-timing control. In particular, noisy excitatory input into the dendrites can interact with noisy somatic inhibition to create precise action-potential output.

After that, we will explore the distilling of the multicompartmental L5 pyramidal neuron model simulations into their simplest forms. In doing so we will test a variety of abstracted model, and find one, the composite model, that explains the simulation results the best. Using this model, we will be able to show a novel mechanism for tuning, in which two untuned inputs can combine to create precisely tuned outputs.

THE 2LIF MODEL

As we've seen in the previous two chapters of this thesis, multiple nonlinear mechanisms exist in the dendrites of excitatory neurons, such as layer 5 cortical pyramidal neurons. In particular, long-lasting plateau potentials far from the soma in the apical, basal, and tuft dendrites, are supported by voltage-gated calcium (Ca) and sodium channels, as well as NMDA receptors (Larkum, Kaiser, & Sakmann, 1999; Larkum, Waters, Sakmann, & Helmchen, 2007; Magee, Hoffman, Colbert, & Johnston, 1998). Importantly, glutamate uncaging experiments have shown a strong correlation between nonlinear dendritic events and long-lasting somatic depolarizations on the order of hundreds of milliseconds and 10-25 mV (Antic, Zhou, Moore, Short, & Ikonomu, 2010; Kamondi, Acsady, Wang, & Buzsaki, 1998). Furthermore, genetically distinct groups of interneurons differentially target perisomatic and dendritic tuft regions of single pyramidal cells in regions like the hippocampus (Freund & Buzsáki, 1996; Royer et al., 2012) and neocortex (Ascoli et al., 2008). Recent in vitro and in vivo work demonstrates that dendritic inhibition can play strikingly different roles than perisomatic inhibition with respect to action potential spiking output (L. M. Palmer et al., 2012; Royer et al., 2012). In addition, computational studies have shown that spatial distributions of inhibitory input can independently affect somatic and dendritic regions such that the effect of plateau potentials on the soma is reduced without directly changing the properties of the dendritic plateau potential itself (Gidon & Segev, 2012; Jadi, Polsky, Schiller, & Mel, 2012).

How can single cells use such a biophysical setup supporting dendritic plateau potentials with spatial distributions of both intrinsic conductances and synaptic inputs to control action

potential output? To study mechanisms of spike timing in pyramidal neurons we compare single neuron processing in a conventional leaky integrate-and-fire (LIF) unit, a two compartment biophysical model with 6 Hodgkin-Huxley mechanisms, and a novel abstracted two-stage LIF model taking into account the relevant aspects of dendritic electrogenesis found in pyramidal neurons. In particular, we study the impact of long-lasting dendritic depolarization on somatic spiking with and without somatic inhibition. We show that a simple 2-stage LIF model, like the more complicated compartmental model it abstracts, gives rise to precise spike timing in the presence of barrages of excitatory and inhibitory inputs. Important to this mechanistic hypothesis are the distinct effects inputs into the dendritic and perisomatic regions produce. We further demonstrate how our model explains recent experimental results in hippocampal place cells where a decrease of dendritic inhibition causes a decrease in phase precession and enforces spiking

Methods

Synaptic inputs into the models

This study features three different single cell models: leaky-integrate-and-fire (1LIF), conventional two compartmental, and a two-component leaky-integrate-and-fire (2LIF, see below, model available for download at https://senselab.med.yale.edu/modeldb/ upon publication). In all models excitatory and inhibitory inputs are implemented as conductance increases described via alpha functions with reversal potentials of 65 mV and -10 mV relative to rest, respectively. Both synaptic types impinge on the membrane with conductance profiles described by

$$g(t) = g_{\max}\left(\frac{t - t_0}{\tau}\right)e^{-(t-t_0-\tau)/\tau}$$

where g_{max} is the maximum conductance of a single synapse, t_0 is the synapse onset time, and τ is the synapse time constant. A ***barrage*** of postsynaptic events is defined as a group of n events sharing the same g_{max}, τ, V_{rev} (reversal potential), and a vector of t_0 s of length n chosen from the same temporal probability distribution. A normal probability distribution with mean time μ_{in} and standard deviation σ_{in} generates a t_0 for each of the n synaptic events in each barrage (Figure 28A). Because spike time is defined as the time at which the membrane potential first crosses threshold relative to μ_{exc} (the mean time μ of the excitatory barrage probability density function), voltage resetting does not affect the analysis and is not included in the simulations.

To compare synapse strengths between different models, the effect of barrages on membrane voltage needs to be normalized. To do so, we divide the synapse strengths (maximum conductance, given in nS) by the threshold synapse strength where an excitatory barrage in the absence of an inhibitory barrage causes a spike. In the 1LIF and 2LIF models this is at 0.97 nS, and in the modified Mainen-Sejnowski two-compartment model this is found to be 0.078 nS (the original Mainen-Sejnowski model has a high input resistance, eliciting spikes with a 10 pA DC current injection into the somatic compartment (Mainen & Sejnowski, 1996), about an order of magnitude lower than in experiment). Hence, for all simulations, the parameter space searched was from 1 to 2 times threshold strength for excitation, and from 0 to 5 times that strength for inhibition.

Parameters for excitatory barrages are σ_{in} = 40 ms, number of synaptic events per barrage n = 100, τ = 0.5 ms, and g_{max} ranging from 1.0 to 2.0 nS. Parameters for inhibitory barrages are σ = 40 ms, number of synaptic events per barrage = 200, τ = 0.75 ms, and g_{max} ranging from 0 to 5 nS. These parameters are comparable to a previous modeling study on the number of synaptic inputs needed to elicit long-lasting regenerative potentials in the tuft dendrites of L5 pyramidal neurons (Larkum, Nevian, Sandler, Polsky, & Schiller, 2009). Every simulation starts with neurons completely at rest. The ***temporal input offset*** is defined as the temporal difference μ_{inh}-μ_{exc} (**Figure 28**A). The ***input jitter***, σ_{in}, is defined as the standard deviation of the excitatory barrage probability distribution and has units of milliseconds. Since the standard deviation of any input distribution, σ, is a defined constant unit of time (in this study 40 ms), all time measurements can be expressed in units of σ_{in} (so that 0.5 σ_{in} would be equivalent to 20 ms and 2.0 σ_{in} would be equivalent to 80 ms). The ***spike time*** is the time of the first voltage threshold crossing relative to μ_{exc}, and is measured in units of σ_{in}. The ***jitter,*** σ_{out}, is defined as the standard deviation of the output *spike times* (**Figure 28**B) (Marsalek, Koch, & Maunsell, 1997), and is also reported in units of σ_{in}. Simulations in the 1LIF and 2LIF are conducted through a range of 6 input offsets, from 0 to 2 σ_{in}, 50 excitatory synapse strengths, and 50 inhibitory synapse strengths, and for 25 excitatory and inhibitory synapse strengths for the two-compartment model. For each parameter triplet, 1000 replicates are conducted in the 1LIF and 2LIF cases (making a total of 15,000,000 simulations), and 20 replicates in the two-compartment model (due to the increased computational time), each with new input times chosen from their temporal probability distributions. Only those experiments where excitation is strong enough to allow for at least half of the replicates to cross spiking threshold are used.

To quantify the ability of the temporal input offset to influence spike timing, we use a measure we term ***shift in spike time due to temporal input offset (*** ST_Δ***).*** ST_Δ is the rate at which changing the temporal input offset changes the mean spike time for fixed excitatory and inhibitory strengths. ST_Δ is calculated by finding the absolute value of the slope of the least squares fit line to the mean spike times as a function of Δ_{IE} for a given excitation and inhibition strength. In other words, ST_Δ reports how many σ_{in} the spike time changes by changing the input offset by 1 σ_{in}, and is thus measured in units of σ_{in}/σ_{in}. The absolute value is taken in order to make ST_Δ a direct measure of spike-time control (in this study, all values of ST_Δ would be negative if the absolute value was not taken, see **Figure 28**B). Importantly, in all 1LIF simulations, the 0 σ_{in} input offset cases produce mean spike times that do not follow the linear trend of the other input offsets (see supplemental materials). Thus, including the 0 σ_{in} input offset data in the ST_Δ calculations would underestimate the ability of input offset to influence spike timing, and so were not included.

To quantify the ability of inhibitory barrages to influence spike timing, we use a measure we term the ***shift in spike time due to inhibition strength (*** ST_{inh}***)***. ST_{inh} is the rate at which the mean spike time changes with changing inhibition strength, for a given excitatory strength. In other words, ST_{inh} is a measure of how many σ_{in} the spike time changes by changing the inhibition strength by 1 nS, and is thus given in units of σ/nS. ST_{inh} is calculated by finding the slope of the least squares linear fit to mean spike time as a function of inhibition strength, for a given excitation strength.

A single leaky-integrate-and-fire unit (1LIF)

A single component leaky-integrate-and-fire neuron (1LIF) is implemented in *Matlab* (The MathWorks Inc., Natick, MA) using the method of finite differences on the dynamic equation $c_m \frac{dV(t)}{dt} = \sum_i g_i(t)\left[V(t) - V_{i,rev}\right] - \frac{V(t)}{r_m}$, where c_m, g_i, r_m, $V_{i,rev}$, and V are the membrane capacitance, conductance change of synapse *i*, membrane resistance, reversal potential of synapse *i*, and the membrane potential, respectively. Simulations exploring how input offset between excitatory and inhibitory barrages affect spike jitter and the dynamic range of spiking use 1LIF with the following parameters, treating the 1LIF as an isopotential sphere (Koch, 1999):, r_m = 80 MΩ, c_m = 13 pF (assuming a radius of 10 μm this is equivalent to 1.035 μF·cm^{-2}), V_{thresh} = 16 mV, and V_{rest} = 0 mV.

A two-compartment Hodgkin-Huxley model supporting dendritic plateau events

A two-compartment model of a pyramidal neuron previously created (Mainen & Sejnowski, 1996) to study the effect of dendrites on action potential output is modified to account for dendritic spiking. The original model features a somatic compartment with sodium (Na) and potassium (K_v) Hodgkin-Huxley style mechanisms to support action-potential spiking, and a dendritic compartment with Na, muscarinic potassium (K_m), calcium-dependent potassium (K_{Ca}), and high-voltage activated calcium (Ca_{HVA}) mechanisms to support dendritic processing. The dendritic compartment additionally contains a linear resistance and capacitance, and the two compartments are joined with a linear resistance (**Figure 30**A). In pyramidal neurons, dendritic calcium electrogenesis has been shown to be dependent on both high and low-

threshold calcium channels (Markram & Sakmann, 1994; Perez-Garci, Larkum, & Nevian, 2013). A low-voltage activated calcium channel Hodgkin-Huxley mechanism is thus added to the dendritic compartment. The channel has the following parameters, based off the Ca_{LVA} mechanism used in (Hay, Hill, Schurmann, Markram, & Segev, 2011): $m_\infty = 1/(1+\exp(-(V+40)/6))$; $h_\infty = 1/(1+\exp((V+90)/6.4))$; $\tau_m = 5 + 20/(1+\exp((V+35)/5))$; $\tau_h = 75 + 50/(1+\exp((V+50)/7))$; $N_m = 2$; $N_h = 1$. This model is implemented in the NEURON programming environment (Carnevale, 2006).

A two-component LIF model (2LIF)

A two-component leaky-integrate-and-fire (2LIF) model is implemented using two coupled 1LIFs (**Figure 30**A). We refer to one component as the *dendritic* and the other as the *somatic component*. These components interact via a single conductance activated in the somatic-unit whenever the dendritic-unit reaches threshold (here set to 16 mV above rest). This conductance, referred to as the *plateau-conductance*, is a constant conductance lasting $3\sigma_{in}$ (120 ms) of strength g_{plat} which, in the absence of any somatic input, gives rise to a V_{thresh} + 1 mV constant depolarization in the somatic component. That is, in the absence of inhibition, the dendritic plateau potential will trigger a somatic spike, as seen with calcium events induced in the dendrites of pyramidal neurons (Antic et al., 2010; Larkum et al., 2009).

Comparisons of temporal offset spike time control in 1LIF and 2LIF models

In the 2LIF model, barrages of input impinge onto the dendritic and somatic components independently. Inhibitory barrages impinging on the dendritic component are named ***direct barrages***, since they directly affect the timing of the plateau conductance. Inhibitory barrages

into the somatic component are named ***gating barrages***, since they gate the effect of the plateau conductance on somatic spiking. Note that unlike a conventional two-compartment model, the somatic membrane potential does not influence the dendritic membrane potential.

Spike and *dendritic plateau timing* are defined as the time of the first threshold crossing in the somatic-unit and dendritic-unit, respectively, relative to the mean of the dendritic excitatory barrage probability density function.

In the analysis of spike time control in the 2LIF model (**Figure 31**), excitatory barrages impinge onto the dendritic compartment, and inhibitory barrages impinge on the somatic one. The same parameters for the barrages in the 1LIF analysis (**Figure 29**) are used in this analysis. In the comparison of gating and direct inhibition in the 2LIF model (**Figure 32**), excitatory barrages have g_{max} = 1.2 nS and inhibitory barrages have g_{max} = 5 nS. 1000 permutations are carried out at each of the 108 input offsets spanning linearly from 0 σ_{in} to 2.5 σ_{in}.

Results

Simulations and analysis exploring mechanisms of spike timing in single cells

How might spatially distributed conductances such as those supporting plateau potentials interact with spatio-temporally distributed inhibitory inputs to give rise to spike time control? In order to establish a method for comparison, we first explain the general simulation and analysis framework used in this work.

In a single cell model, excitatory and inhibitory barrages arrive following σ_{in} = 40 ms probability density functions (**Figure 28**A, for details see methods). We focus on a 40 ms input jitter due to experimental measurement of the distribution of presynaptic cell firing in entorhinal cortex that projects to the hippocampus (Mizuseki, Sirota, Pastalkova, & Buzsaki, 2009). Excitatory and inhibitory barrages arrive with a *temporal input offset* ($\Delta_{IE;}$ **Figure 28**A). For each simulation, excitatory and inhibitory synaptic strengths (g_{inh} in **Figure 28**B) and Δ_{IE} are chosen. Synaptic strengths are given in units of nano-Siemens normalized to the excitation threshold for spiking (denoted nS, see Methods). The output of the simulation is the spike time, measured relative to mean of the excitatory barrage probability density function (**Figure 28**A2), and is thus a negative number if the spike precedes or a positive number if the spike follows the mean time of the excitatory barrage. In order to make the relation of spike output statistics to synaptic input statistics explicit, we analyze spike times in units of σ_{in} (e.g. an output spike time of $-0.5\sigma_{in}$ refers to a spike that occurs 20 ms before the mean of the σ_{in} = 40 ms excitatory synaptic barrage). Multiple simulation replicates are performed for each parameter set, and the parameter space is explored (see Methods). For a given parameter set, *jitter* (σ_{out}) and *mean spike time* (μ_{out}) are defined as the standard deviation and mean of the spike times over all replicates (**Figure 28**B top).

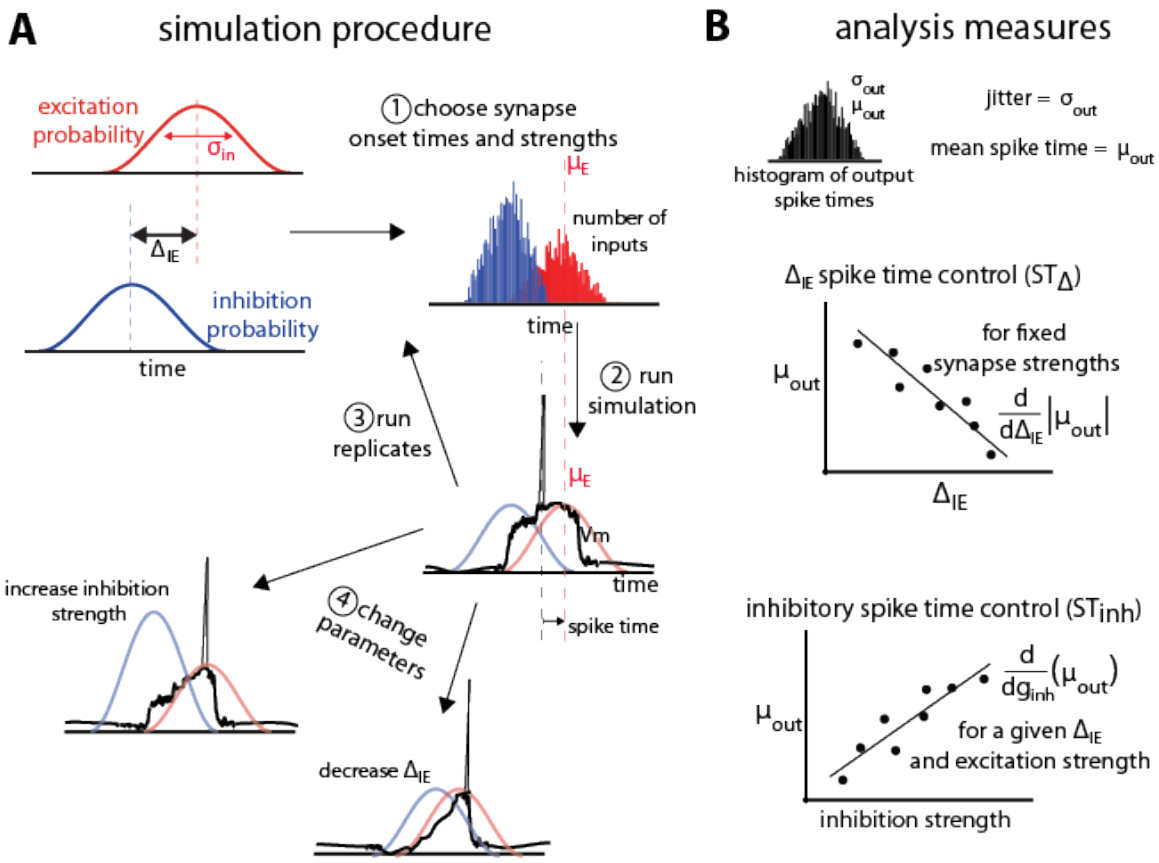

Figure 28: **General protocol for simulations. (A)** Excitatory (red) and inhibitory (blue) synaptic barrages impinge on single neuron models according to temporal probability distributions with standard deviation σ_{in}. Excitatory and inhibitory input barrages are temporally offset by the temporal input offset, Δ_{IE}. After (1) choosing onset times and synaptic strengths for the inputs**,** (2) simulations are conducted and the spike time (measured relative to the mean of the excitatory probability distribution) is recorded. For each parameter triplet of excitatory and inhibitory strengths and Δ_{IE}, (3) replicates are run. (4) Parameter space is explored by choosing new parameter triplets and running new simulations. **(B)** Analysis of the simulations is performed on the output distribution of the spike times over all replicates for a given parameter set. The jitter and mean spike time are defined as the standard deviation and mean of the output spike times. To measure

the control of spike timing by Δ_{IE} (ST_{Δ}) and inhibition strength (ST_{inh}), we find the absolute value of the slope of the best linear fit of the mean spike time as a function of Δ_{IE} or inhibition strength (g_{inh}). These values are thus measures of how much mean spike times shift as the temporal input offset or inhibition strength changes.

Control of spike time is measured in two ways. First, the *shift in spike timing due to temporal input offset* (ST_{Δ}) is the slope of the best-fit line of μ_{out} as a function of Δ_{IE}, and thus estimates the shift in mean spike time by a unit increase in Δ_{IE} (**Figure 28**B, middle). Second, the *shift in spike timing due to inhibition strength* (ST_{Inh}), is the slope of the best-fit line of μ_{out} as a function of the inhibitory barrage synapse strength (g_{inh}), and thus estimates the shift in spike timing by changes in the balance between excitation and inhibition.

Spike time control in a single leaky-integrate-and-fire unit

To establish a baseline for comparison, we begin by quantifying the relationship between barrages of synaptic events and spike timing in a single leaky-integrate-and-fire unit (1LIF, Figure 27A) with no spatial extent of membrane conductances or synapses. In particular, we are interested in the control of spike timing by changes in Δ_{IE} and inhibition strength (**Figure 29**BC).

For each of six values of Δ_{IE} we test (**Figure 29**D), increasing excitation strength shifts spiking to earlier times, while increasing inhibition strength delays spiking (**Figure 29**E). In general, jitter decreases as Δ_{IE} increases (**Figure 29**F). Although spike timing is generally earlier as Δ_{IE}

increases (however the 0 Δ_{IE} case does not follow this trend), the *shift in spike timing due to* Δ_{IE} (ST_{Δ}, i.e. how many σ_{in} later the spike occurs given an increase in input offset of 1 σ_{in}) is weak, with only 30.6% of the parameter space able to change spike timing by more than 0.25 σ_{in} with a 1 σ_{in} increase in Δ_{IE} (**Figure 29**B). In general, increasing the strength of inhibition increases ST_{Δ} (**Figure 29**B).

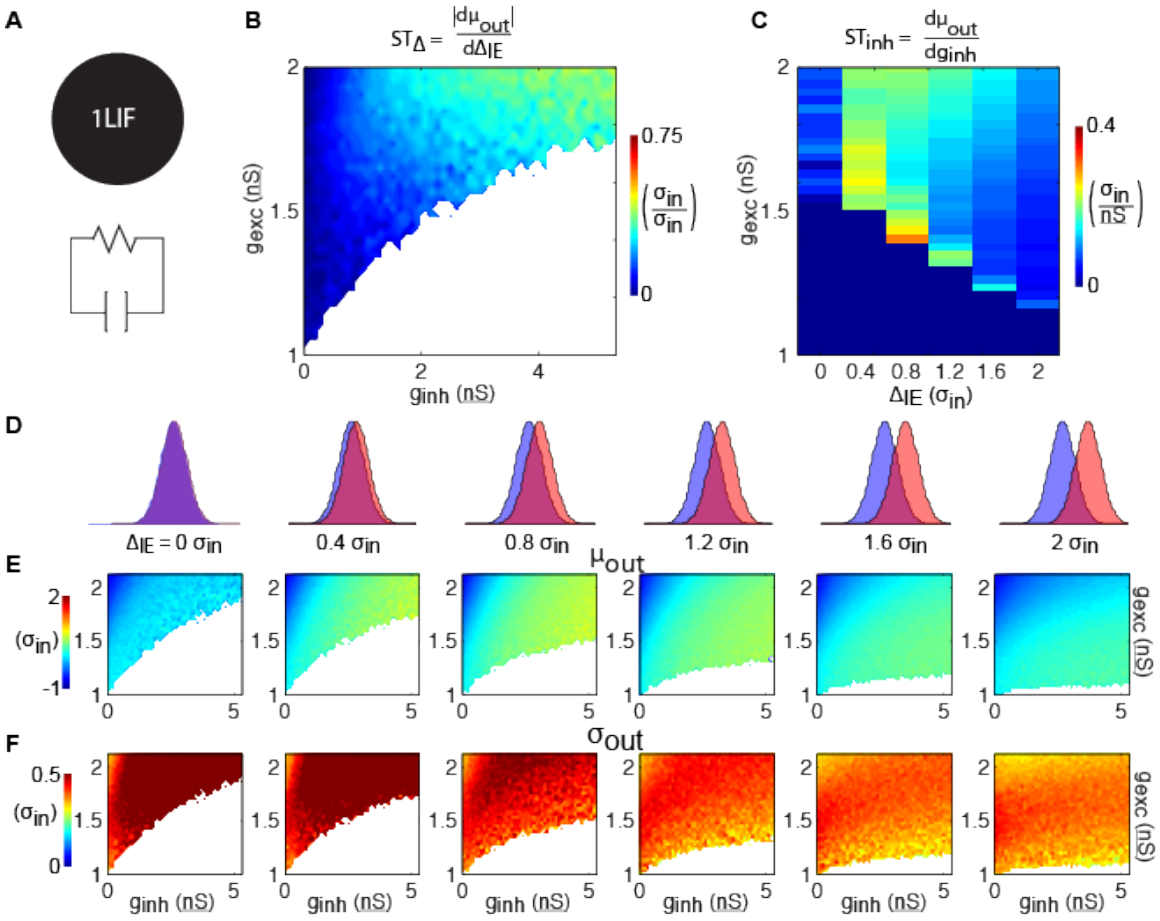

Figure 29: 1LIF simulations. (A) The leaky-integrate-and-fire unit (1LIF) is a single compartment with a leak conductance and membrane capacitance. **(B)** The shift in spike time due to the temporal input offset is plotted as a function of excitatory and inhibitory synapse strength (g_{exc} and g_{inh}). White areas occur due to

the inability of the 1LIF to spike when excitation is not strong enough to elicit a spike given a certain amount of inhibition. **(C)** The shift in spike time due to the inhibitory strength is plotted as a function of temporal input offset and excitatory synapse strength. For each of the 6 input offsets tested **(columns in D)** mean spike time **(E)** and output jitter **(F)** are plotted.

Spike time also varies as a function of the strengths of the inhibitory inputs. When excitatory and inhibitory distributions have no temporal input offset (*i.e.* $\Delta_{IE} = 0$ and their input distributions are the same; **Figure 29**DEF, 1st column), the *shift in spike timing due to inhibition strength (*ST_{Inh}, how many σ_{in} later the spike occurs given a 1 nS increase in inhibition strength) reaches a peak of 0.1 σ_{in}/nS and an average jitter of 0.9 σ_{in} (**Figure 29**C). The no offset condition thus represents an especially poor case of spike time control compared to cases with barrages separated in time, as it has both low ST_{inh} (**Figure 29**C) and high jitter (**Figure 29**F). For every other Δ_{IE}, ST_{inh} is higher, and decreases as Δ_{IE} increases.

Importantly, the decrease in jitter induced by increasing Δ_{IE} (**Figure 29**F) comes with the tradeoff that ST_{inh} is reduced. For example, we find that simulations with Δ_{IE} of 2.0 σ_{in} have ST_{Inh} reaching 0.1 σ_{in}/nS, while simulations with Δ_{IE} of 0.4 σ_{in} reach 0.3 σ_{in}/nS (**Figure 29**C). Although the latter simulations have relatively high ST_{Inh}, they also have higher jitter, reaching σ_{out} of 0.8 σ_{in} for 0.4 σ_{in} input offset, whereas cases with 2.0 σ_{in} input offset have a maximum σ_{out} of 0.5 σ_{in} (**Figure 29**C). Similarly, shifts in mean spike time due to increasing Δ_{IE} (**Figure**

29E, from left to right) do not sustain constant levels of jitter (**Figure 29**F, from left to right) over the range Δ_{IE} where spike timing is shifted.

Increased spike time control achieved with a plateau potential mechanism

Recent experimental results implicate inhibition in the apical and tuft dendrites of pyramidal neurons in the control of spike timing (Royer et al., 2012). Interestingly, this spatially restricted input corresponds to a region in pyramidal neurons known to have a high density of L-type Ca^{2+} channels (Perez-Garci et al., 2013). This "Ca-hotzone" supports a second spiking zone where depolarizations can cause a long-lasting pleateau event (Larkum et al., 2009). To address the potential role of the Ca-hotzone and the associated plateau potentials, we adopt a two-compartment Mainen-Sejnowski pyramidal neuron, originally created to explore the role of the apical dendrites on neural output (Mainen & Sejnowski, 1996). We add an additional Hodgkin-Huxley type low-voltage activated Ca channel to the dendritic compartment to support the regenerative Ca-spike known to occur in the apical dendrites (**Figure 30**A).

The results of simulations with this two-compartment model (**Figure 30**) show both increases in spike time control and decreases in jitter compared to the 1LIF simulations (**Figure 29**). Although the 1LIF also showed earlier spiking as Δ_{IE} increased, here the changes in mean spike time are greater and more sustained across the range of Δ_{IE} tested (**Figure 30**E left to right), thus ST_{Δ} is greater in most of the parameter space (**Figure 30**B). A similarity with the 1LIF is observed in the decreasing ability for inhibition strength to shift spike timing as Δ_{IE} increases (**Figure 30**C). However, in the two-compartment model greater levels of ST_{inh} are found, marking a greater ability to control spike timing by changing either Δ_{IE} or the relative

strengths of excitatory and inhibitory input. Importantly, spike time jitter decreases in the entire parameter space compared to 1LIF simulations. This suggests that separating excitatory and inhibitory inputs into separate electrophysiological regions can be a mechanism for single neurons to control spike output and more effectively decrease jitter.

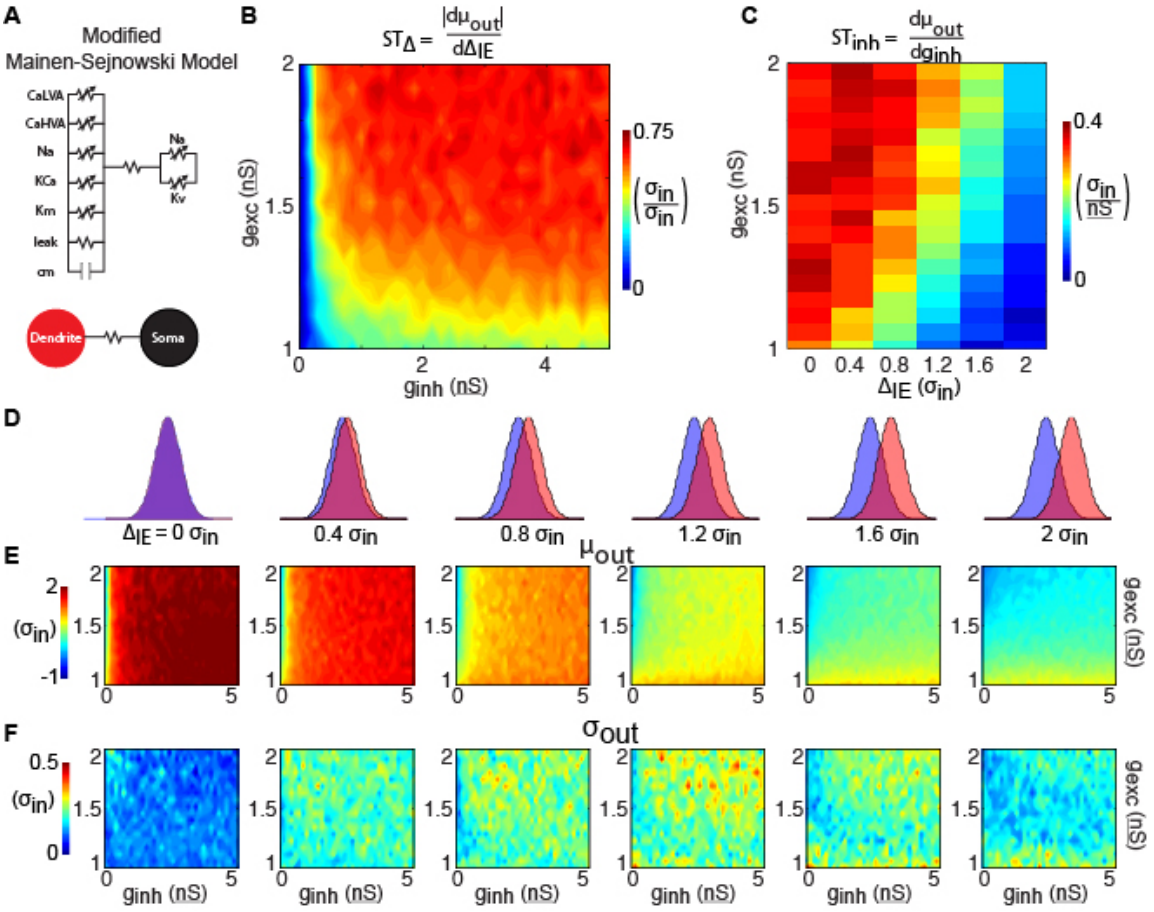

Figure 30: Two-compartment model. (A) The two-compartment model features 6 Hodgkin-Huxley conductances separated into a somatic and dendritic compartment. The two compartments communicate via a linear resistance. **(B)** The shift in spike time due to the temporal input offset is plotted as a function of excitatory and inhibitory synapse strength (g_{exc} and g_{inh}). **(C)** The shift in spike time

due to the inhibitory strength is plotted as a function of temporal input offset and excitatory synapse strength. For each of 6 input offsets tested **(columns in D)** mean spike time **(E)** and output jitter **(F)** are plotted.

Control of spike timing in a two-component LIF model

To study the essential components of the single-cell spike time control mechanism explored in the two-compartment model, we use a two-compartmental LIF abstraction for a single pyramidal cell (2LIF, see Methods; Fig 4A). This model has the additional advantage of a structure more closely related to the 1LIF, thus comparison with the 2LIF is more direct than with the two-compartment model.

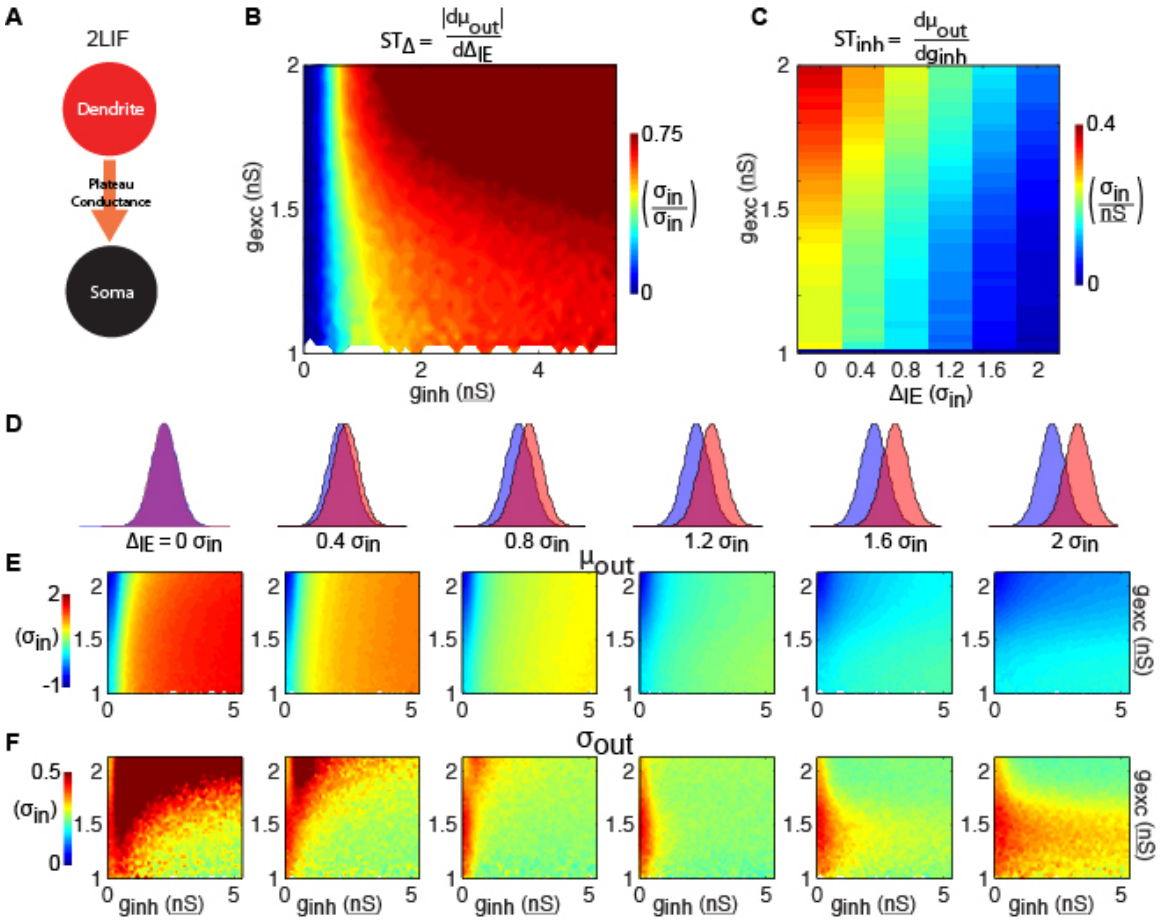

Figure 31: **2LIF model. (A)** The 2LIF consist of 2 leaky-integrate-and-fire units communicating via a long-lasting plateau-conductance. Whenever the dendritic-unit reaches threshold, a plateau-conductance opens in the somatic-unit. **(B)** The shift in spike time due to the temporal input offset is plotted as a function of excitatory and inhibitory synapse strength (g_{exc} and g_{inh}). **(C)** The shift in spike time due to the inhibitory strength is plotted as a function of temporal input offset and excitatory synapse strength. For each of 6 input offsets tested **(columns in D)** mean spike time **(E)** and output jitter **(F)** are plotted.

The 2LIF consists of two LIF units that act independently except when the dendritic-unit reaches threshold, which activates a long-lasting constant plateau-conductance in the somatic-unit (**Figure 31**A, see Methods). As before, increasing inhibition strength delays spiking (**Figure 31**E). Compared to the 1LIF case, increasing excitation has little effect on spike timing (**Figure 31**E), due to the stereotyped amplitude of the plateau-conductance. Importantly, across all Δ_{IE} we observe a decrease in jitter compared to the 1LIF case (**Figure 31**F). Additionally, as Δ_{IE} increases, mean spike time decreases rapidly compared to the 1LIF case. ST_{Δ} is thus greater than 0.6 σ_{in}/σ_{in} for the majority of the parameter space tested (**Figure 31**B), and greater than the 1LIF ST_{Δ} values for 95.9% of parameter space tested (comparing **Figure 31**B to **Figure 29**B). Here, the ST_{Δ} values are greater than 0.25 σ_{in}/σ_{in} for 87.9% of the parameter space tested, compared to 30.6% for the 1LIF simulations. Additionally, in all the parameter space tested in which the somatic inhibitory strength is less than or equal to 0.5 nS, 88.0% of the simulations had an ST_{Δ} less than 0.25 σ_{in}/σ_{in} (**Figure 31**B), whereas only 0.5% of the rest of parameter space tested has such an ST_{Δ}. Thus, somatic inhibition is required for robust spike timing control, and the weakening of somatic inhibition is detrimental for such control.

ST_{inh} decreases as Δ_{IE} increases (**Figure 31**C). Unlike the 1LIF case, this modulation of ST_{inh} by changing Δ_{IE} is not generally accompanied by large increases in jitter, except if there is no offset between excitation and inhibition. For Δ_{IE} of 0.4 σ_{in} or greater, jitter averaged over a given excitation strength remain less than 0.5 σ_{in} in all cases (**Figure 31**F).

Comparing mechanisms of spike time control

Finally, we compare the effect of dendritic ("direct", **Figure 32**A) and somatic ("gating", **Figure 32**B) inhibitory barrages on ST_{Δ}. Importantly, the direct inhibition 2LIF case is equivalent to the 1LIF case with a short time lag (the rise time of the somatic voltage due to the plateau-conductance). This is because there is no synaptic barrage into the soma, so all synaptic integration occurs in the dendrite. The somatic voltage is thus guaranteed to reach threshold whenever the dendritic threshold is crossed.

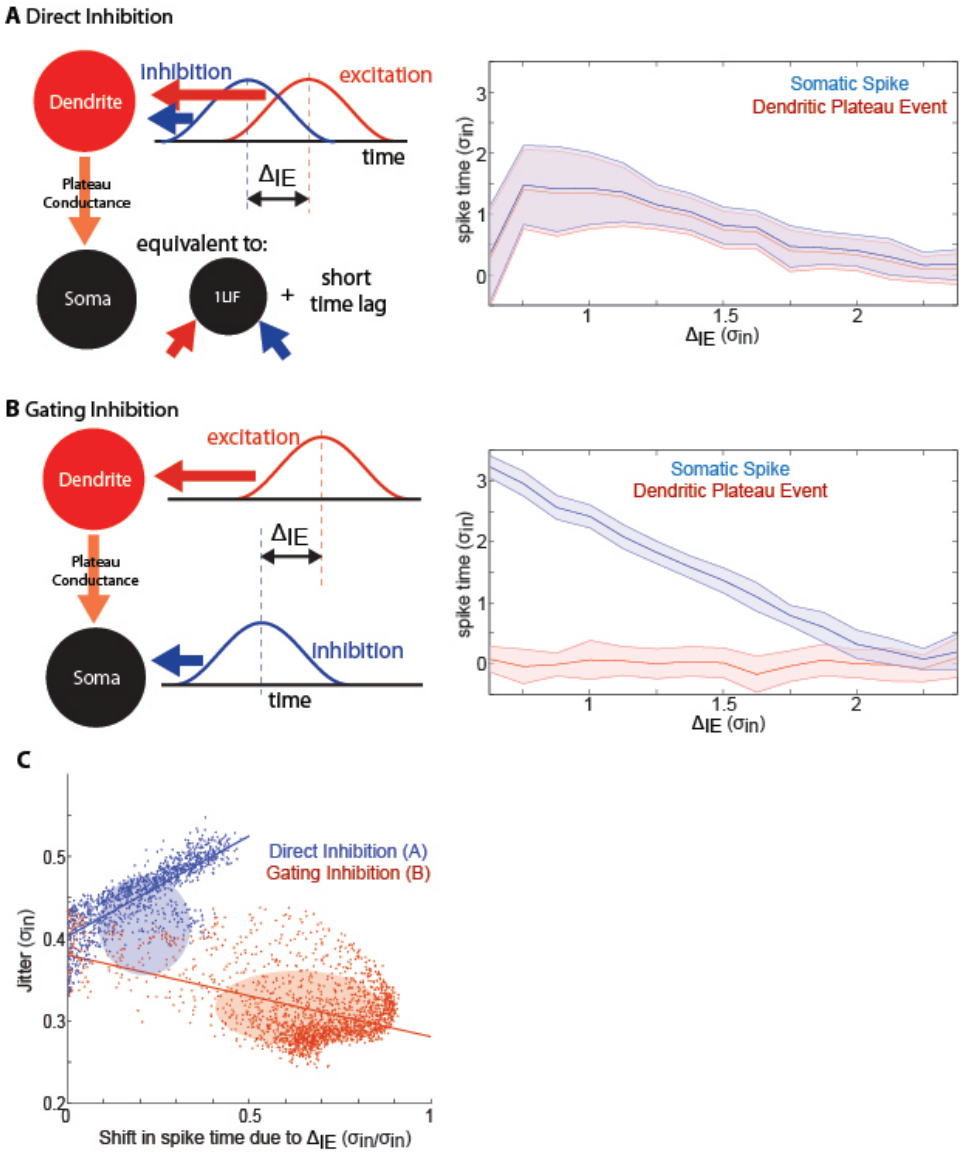

Figure 32: **A mechanism for spike time control (A)** In the direct inhibition case, excitation and inhibition both impinge on the dendritic-unit. This is equivalent to a 1LIF with a short time lag between threshold crossing and spiking. Here, 1000 replications were conducted at each of 108 different input offsets. (right) Plot of the time of the plateau potential (relative to the mean of the synaptic excitatory barrage) (red), and the somatic spike time (blue), as a function of the temporal input offset between the mean timing of the excitatory and the inhibitory barrages. Output jitter is shown by the

shaded area. **(B)** In the gating inhibition case, excitation impinges on the dendritic-unit while inhibition impinges on the somatic-unit where it interacts with the plateau-conductance. (Right) Same as (A) for the gating inhibition case. The timing of the plateau event does not depend on the input offset, while the timing of the somatic spike decreases with increasing offset between excitation and inhibition. Note that the spatially separated inputs give rise to steady low-jitter spike time modulation compared to the direct inhibition case. **(C)** Scatter plots of every data point tested in the 1LIF (**Figure 29**) and 2LIF (**Figure 31**) showing how jitter varies as a function of offset spike time control. Ellipses show center of mass with height and width of +/- 1 standard deviation. Lines show linear best fits.

In Figure 5, we observe how Δ_{IE} modulates the plateau time (the time when the dendrite reaches threshold, blue curves) as well as the spike time (red curves). In the direct case (**Figure 32**A), a small spike time modulation in the plateau time becomes increasingly noisy as inhibition becomes more in phase with excitation. Here, the dendrite acts as a 1LIF, so that the results are similar to those of **Figure 29**, where zero Δ_{IE} has high jitter (**Figure 29**F), and increasing Δ_{IE} decreases the mean spike time, although importantly at a slower rate (ST_{Δ} in **Figure 29**B compared to **Figure 31**B). Moreover, without somatic inhibition, the plateau potential can only transform plateau time into spike time by adding a fixed temporal offset (due to the fixed rise-time of the plateau-conductance). Because of this, the direct case features spike time modulation that is equivalent to plateau time modulation with a fixed added time.

In the gating case (**Figure 32**B), somatic inhibition does not influence the dendritic membrane potential because somato-dendritic interaction only occurs in one direction in our model.

Therefore, the plateau time does not depend on Δ_{IE}. The monotonically changing spike timing is attributed to somatic inhibition and spike timing can be modulated by more than 2.5 σ_{in} by temporal input offsets in the gating case, compared to about 1 σ_{in} spike time modulation in the direct case. Additionally, we find that the jitter remains within 0.3 σ_{in} in the gating case, while ranging from 0.3 σ to 0.6 σ in the direct case.

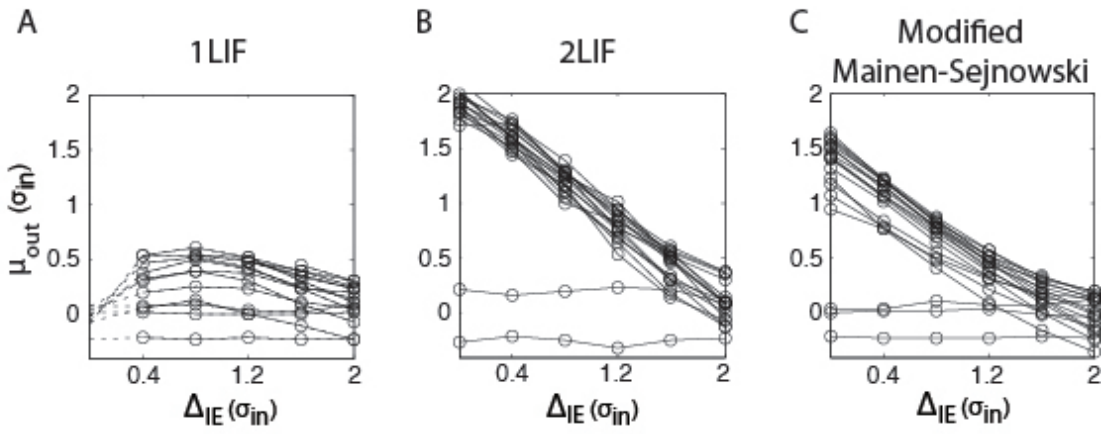

Figure 33: Comparison of spike time control in different models. Mean spike time changes linearly as a function of temporal input offset in the 1LIF (A), 2LIF (B), and Modified Mainen-Sejnowski model (C). Plotted are the mean spike times (circles) for each of 6 input offsets (x-axis), for 25 different choices of excitation and inhibition strength evenly spaced across the entirety of those tested. In the 1LIF case (A), the 0 input offset values were not included since they did not follow the linear trend and would have underestimated STΔ values, but are shown here with dotted lines. Filled lines directly connect mean spike times of the nearest input offsets tested, obtained from simulations with the same excitatory and inhibitory strength values (these are not the best fit lines).

How well can a neuron simultaneously control mean spike time and reduce jitter? To answer this question we plotted jitter as a function of ST_{Δ} for all simulations conducted in the 1LIF (equivalent to direct inhibition) and 2LIF (equivalent to gating inhibition) cases (**Figure 32**C). For direct inhibition, where the postsynaptic potentials of both excitatory and inhibitory inputs directly interact in a single compartment, jitter increases linearly as ST_{Δ} increases. Thus, finding a point in parameter space where spike time is modulated with little noise is difficult. Alternatively, for gating inhibition, where excitatory and inhibitory barrages are separated into distinct spatial compartments, a large portion of parameter space simultaneously modulates spike timing by temporal input offset with attenuated noise.

Discussion

In the first part of our study, we explore the response of conventional LIF units to barrages of inputs. A previous study found that barrages of inhibition increase jitter in LIF units due to an increase in degrees of freedom (Marsalek et al., 1997). Since the time of that computational work, experiments looking at the temporal offset of different current sinks and sources have given credence towards the idea that different barrages of inputs can arrive separated by certain intervals of time (Klausberger & Somogyi, 2008; Mizuseki et al., 2009). Thus, in this study we included temporal input offsets and find that increases in jitter are tempered if inhibitory barrages are sufficiently offset in time from excitatory barrages (**Figure 29**). We further find a tradeoff between control of spike timing by temporal input offset and the ability to decrease spike jitter (**Figure 32**C, blue). In other words, although jitter can be reduced by offsetting inhibition from excitation, the ability of inhibition to shift spike timing is reduced the more

temporally offset synaptic barrages become, in the case where all synaptic input occurs in a single compartment.

Significant synaptic and membrane noise is a relevant phenomenon *in vivo* (Pare, Shink, Gaudreau, Destexhe, & Lang, 1998) rendering the possibility of synaptic fine-tuning (e.g. to balance jitter and temporal control of spikes) remote. Additionally, pyramidal neurons do not act as isopotential units. Experiments reveal the existence of a Ca-hotzone in the apical dendrites, as well as voltage dependent sodium channels and NMDA receptors that can induce long-lasting plateau potentials and cause somatic depolarizations (Antic et al., 2010; Larkum et al., 1999; Larkum et al., 2009; Milojkovic, Zhou, & Antic, 2007; Schiller, Schiller, Stuart, & Sakmann, 1997l; Seamans, Gorelova, & Yang, 1997). We modeled the effects of these dendritic spikes on spike time control first in a biophysical two-compartment (**Figure 30**) model, and then in an abstracted two-component LIF model (2LIF, **Figure 31**), and found that a spatial separation of inhibitory and excitatory barrages into a single neuron that supports dendritic plateau potentials can manipulate spike timing while reducing jitter (**Figure 32**).

The 2LIF model proposed herein lies between simple 1LIF models and more biophysically realistic multicompartmental models (Hay et al., 2011; Koch, 1999; Poirazi, Brannon, & Mel, 2003a) by keeping the parameter space limited while preserving important biophysical realities such as plateau potentials and spatially segregated synaptic input. In the *somatic-unit* of the 2LIF, a depolarizing plateau-conductance is activated whenever the *dendritic-unit* reaches threshold. Dendritic excitation activates the plateau-conductance in the soma, which, in turn, can be gated by somatic inhibition leading to precise spike timing (**Figure 31**,5). Such a mechanism

depends on the spatial separation of synaptic inputs (L. M. Palmer et al., 2012; Pouille & Scanziani, 2001) as well as their communication via the plateau-conductance (**Figure 32**). Here we argue that dendritic nonlinearities confer distinct functionalities to dendritic and somatic input with respect to the somatic action potential. Because this causes the input-output function of neurons to be a mapping from a (at least) two-dimensional input space to a one-dimensional output space, it would be difficult to reproduce the results shown here in a 1LIF model that lacks additional degrees of freedom for the input.

Several multi-component models have been proposed as abstractions of pyramidal neurons to account for properties of dendrites. The sigma-pi unit features groups of inputs that multiply before being summed by weight and have been used to model spatio-temporal clustering needed for local NMDA-spike generation in dendrites (B. W. Mel, 1992). The *clusteron* model (B. Mel, 1992) features a spatial window of supralinearity, allowing for continuous spatio-temporal clustering effects in the dendrites. Similarly, single-neuron computation has been represented by two-layer neural networks (Poirazi, Brannon, & Mel, 2003b) allowing individual dendritic branches to act as a first layer of independent computation whose outputs are fed into the threshold operation at the soma. Here we aim to model the effect of dendritic plateau potentials, and the effect of the resultant plateau potentials on somatic spiking.

It has been proposed that multiple and independent computations (often NMDA-mediated) can provide input to the Ca-hotzone (Polsky, Mel, & Schiller, 2004). Extensions to the 2LIF might be needed to capture more detailed or complicated single-neuron functionalities. For instance, extra "NMDA-compartments" can be added which feed into the dendritic

compartment. These extensions, as well as other details like morphology, spines, plasticity, adaptation, backpropagation, etc. could be added at will to increase the level of detail (for a review on how active dendritic conductance relate to these concepts see (Papoutsi, Kastellakis, Psarrou, Anastasakis, & Poirazi, 2013)). Here we provide a simple conceptual model that accounts for the basic nonlinear layout of ion channels in a cell.

There are a number of two-compartment models with several ionic conductances that focus on interactions between soma and dendrites (Jadi, Polsky, Schiller, & Mel, 2010; Larkum, Senn, & Luscher, 2004; Mainen & Sejnowski, 1996; Murayama et al., 2009; Pinsky & Rinzel, 1994). Here, we feature a non-traditional two-compartment model (2LIF), since the somatic and dendritic components are not "coupled" by a linear resistance but instead by a rectifying diode (the plateau conductance). Our 2LIF model has no explicitly simulated ionic conductances except a passive leak and the plateau-conductance, greatly decreasing the number of parameters needed to define our cell. Additionally, the plateau-event in our model is abstracted as a stereotyped, voltage-independent conductance change in the soma, as opposed to a voltage-dependent conductance change in the dendrites. Thus, our model is designed to be as simple as possible while still allowing for the range of behaviors relevant to spike timing control.

In particular, we compared two types of spike timing control mechanisms, one by changing the temporal input offset (ST_{Δ}), and the other by changing the inhibitory strength (ST_{inh}). We found that ST_{inh} was associated with a tradeoff between controlling spike time and reducing jitter. Though this tradeoff existed in both the 1LIF and 2LIF cases, it was largely tempered

in the 2LIF case (compare **Figure 29**C to **Figure 31**C and **Figure 29**F to **Figure 31**F). In both cases, the no temporal input offset cases were especially poor at controlling spike timing and reducing output jitter simultaneously. The difference between the 1LIF and 2LIF case was especially stark in ST_{Δ}. In 95.9% of the parameter space tested, ST_{Δ} values were higher in the 2LIF than in the 1LIF, and in the majority of parameter space the 2LIF ST_{Δ} values were at least 3 times higher than in the 1LIF.

We focused on the timing of the first action potential, neglecting other aspects of neural coding such as frequency modulation. We did so chiefly because such spike timing is particularly relevant to areas of the brain like the hippocampus, where robust relationships between spatial location and spike timing exist (O'Keefe & Recce, 1993). (O'Keefe & Recce, 1993). Additionally, despite *in vitro* evidence that dendritic electrogenesis contributes to frequency control in pyramidal neurons, our model lacks the complexity to capture such effects. These are highly nonlinear, resulting from a number of nonlinear voltage dependant currents acting in concert (Williams and Stuart 1999; Su, Alroy et al. 2001; Metz, Spruston et al. 2007). Instead of instantiating these complexities, we focused on making the model as simple as possible and relegated ourselves to studying only spike timing.

Our findings have important ramifications for the temporal encoding of neurons in the presence of barrage-like synaptic input. For example, the "dual-oscillator interference model" (Burgess, Barry, & O'Keefe, 2007) used to explain phase precession in entorhinal cortex grid cells features spatial segregation of inputs into the dendrites and soma. The inputs are of slightly different frequencies, causing an interference pattern and a modulation of spike phase.

We likewise observe monotonically increasing spike timing modulation in our 2LIF model by changing the input offset (phase) of the inhibitory barrage relative to the excitatory barrage (**Figure 32**B).

Of particular note is a study looking at the relationship between local dendritic and global neuronal processing in dual-oscillator interference models, considering the realistic electrogenic structure of stellate cells (Remme, Lengyel, & Gutkin, 2010). In that study, an important tradeoff was found between local and global processing as a function of the coupling between the different compartments of the cell. Any dual-oscillator interference model needs both independent oscillations to exist in each compartment (local processing) as well as their interaction in order to create interference (global processing). If, instead, the electrotonic structure is such that multiple compartments can phase lock, then local oscillations cannot independently exist and phase precession cannot be realized. While stellate cells have a soma with a single group of dendrites radiating outward from it, pyramidal neurons have an elongated apical trunk that bifurcates into a second group of thin dendritic tufts. The apical trunk hosts a number of nonlinear channels. Relevant to this discussion are the voltage-dependent sodium channels that only turn on for propagating suprathreshold signals, and the HCN channels, which act to lengthen the electrotonic distance of the neuron, especially with respect to subthreshold events. Finally, pyramidal neurons uniquely possess the calcium "hot-zone" at the apical bifurcation that supports the long-lasting calcium spike. Taken together, these facts point to a compartmentalization of the neuron into independent compartments that can interact exclusively with suprathreshold events. Thus, in our study, both local and global processing can coexist in the same neuron. Our result is wholly dependent on the

subthreshold independence of the two compartments that only interact via suprathreshold signaling.

A more thorough explanation of the "one-way communication" assumption is provided in the discussion where we say: "In our model we considered exclusively the dendrite-to-soma propagation of the calcium spike, and not the back propagation of action potentials. This assumption is valid in regimes where somatic spiking is largely induced by apical dendrite input, and not basal dendrite input. Indeed, axons from Schaffer collaterals and the perforant pathway both send strong inputs into the apical dendrites of pyramidal neurons in the hippocampus (Jarsky, Roxin, Kath, & Spruston, 2005). In more recent *in vivo* work, it has been shown that apical dendritic signals correlate much better to action potential output than do signals in the closer basal dendrites in pyramidal neurons (L. M. Palmer et al., 2014).

Moreover, it is known that theta-locked entorhinal cortex spiking co-exists in time with a current sink in their targets, *stratum lacunosum moleculare* in CA1, where the apical tuft of CA1 pyramidal neurons lie. These cells spike between 90° to 180° of theta (i.e. 50-150 ms) later (Mizuseki et al., 2009). Such a lag, hypothesized to provide temporal windows for local circuit computation (Buzsaki, 2010), is inconsistent with passive integration of synaptic inputs. Our results support the notion that in addition to the possibility of local circuit computation, the spatiotemporal distribution of spiking and current sources/sinks during navigation in the entorhinal/hippocampal circuit (in particular the lag between synaptic input and postsynaptic firing in CA1 cells) and the distribution of membrane channels that support plateau potentials in pyramidal neurons can be explained by a mechanism where dendritic inputs cause a

sustained depolarization in the soma that can be manipulated via somatic inhibition over longer timespans.

Computational network models and some theoretical work have suggested that perisomatic and dendritic inhibition have distinct roles in the generation of spikes during sharp wave ripples in the hippocampus (Cutsuridis & Taxidis, 2013; Taxidis, Mizuseki, Mason, & Owen, 2013). Experimental work by Royer and colleagues (Royer et al., 2012) has explored these distinct effects in the CA1 pyramidal neurons during navigation. Upon suppression of soma-targeting, but not dendrite-targeting, interneurons, the range of phase precession was reduced during navigation by more than a factor of 2 ((Royer et al., 2012) their Fig. 6). Similarly, in the 2LIF model, a decrease in somatic inhibitory strength has a detrimental effect on spike timing control, since the ability to gate the plateau-conductance decreases (Fig 4 and 5). Importantly, manipulating dendritic inhibition in our model does not drastically curtail the cell's phase modulation, since the majority of the spike timing control is due to gating of the plateau-conductance by somatic inhibition, in agreement with findings of Royer and colleagues.

In our study, input distributions were fixed at an input jitter of 40 ms, and thus the results may only be relevant for brain states supporting inputs with similar temporal characteristics. The 40 ms input jitter used here is comparable to the distribution of presynaptic cell firing in entorhinal cortex that project to the hippocampus (Mizuseki et al., 2009). In general, the parameter space of the input is large and multidimensional, involving the numbers of synaptic events, their strengths, temporal distribution shape and frequency, and the relative amount of excitation and inhibition. We neglected to search this space exhaustively and instead chose

parameters with physiological relevance to sustained depolarizations in the cortex. However, due to the ubiquity of the dual integration zone feature in neurons throughout the brain, a model such as ours presented here may describe computation in other brain areas, with synaptic noise of different temporal characteristics, or where temporal coding is not the predominant mode of computation.

THE COMPOSITE MODEL

A phenomenological model

In the previous chapter, we established a biophysical model based on a set of *in vitro* whole-cell patch clamp experiments in layer 5 pyramidal neurons of the mouse neocortex. To conceptually address the single-neuron computation that this biophysical setup performs, we establish a phenomenological model. We compare three models: a composite, multiplicative, and an additive model (**Figure 34**a top). Each of these models uses two sigmoidal functions to perform intermediate computations, and is justified by the existence of the two separate (one dendritic and one somatic) spiking zones in the neuron. In the composite model, basal input is transformed to output frequency via a sigmoid that has its maximum and threshold defined by tuft input (**Figure 34**a, second from left). The interaction of the sigmoids in the composite model is justified by the experimental results suggesting that the result of dendritic electrogenesis is to lower the threshold for a high-frequency burst at the soma. Thus, the mathematical form used in the composite model has a dendritic sigmoid that changes the threshold and maximum firing rate of the somatic sigmoid. The multiplicative and additive models have two independent sigmoids, one of which takes tuft synapses as input, and the other which takes basal synapses as input. The result of these sigmoids is then either multiplied or summed (**Figure 34**a third and fourth from the left). The least-squares best-fits are shown for each of the models in the bottom of **Figure 34**a. The composite model outperforms both the multiplicative and additive models, though less so when Ca^{2+} conductance is decreased by 75%, suggesting that the inability of the

multiplicative and additive models to represent the input-output relationship depends on dendritic electrogenesis (**Figure 34**b). By directly fitting tuft-constant planes of the simulation data (horizontal planes of **Figure 34**a left), to sigmoidal functions, a maximum frequency (M) and threshold (T) can be extracted for each amount of tuft input (**Figure 34**c), and are shown explicitly as the open circles in **Figure 34**d. The sigmoidal functions found by fitting the form of the entire composite equation to the simulation data fit the extracted M and T values well (**Figure 34**d). This points to the strength of the composite model, as the same parameters can be found from the simulation data in two different ways. The effect of tuft input is to increase the maximum possible output frequency (**Figure 34**d left) and decrease the threshold of basal input needed to elicit high frequency firing (**Figure 34**d right). Importantly, both M and T become increasingly linear as apical dendrite Ca^{2+} conductance is decreased (**Figure 34**d brown lines), suggesting a reason why the simpler additive and multiplicative models perform better under those conditions (**Figure 34**b). The composite model describes a coincidence detector between basal and tuft input, since only when both input streams are active in sufficient amounts is the resultant output high frequency.

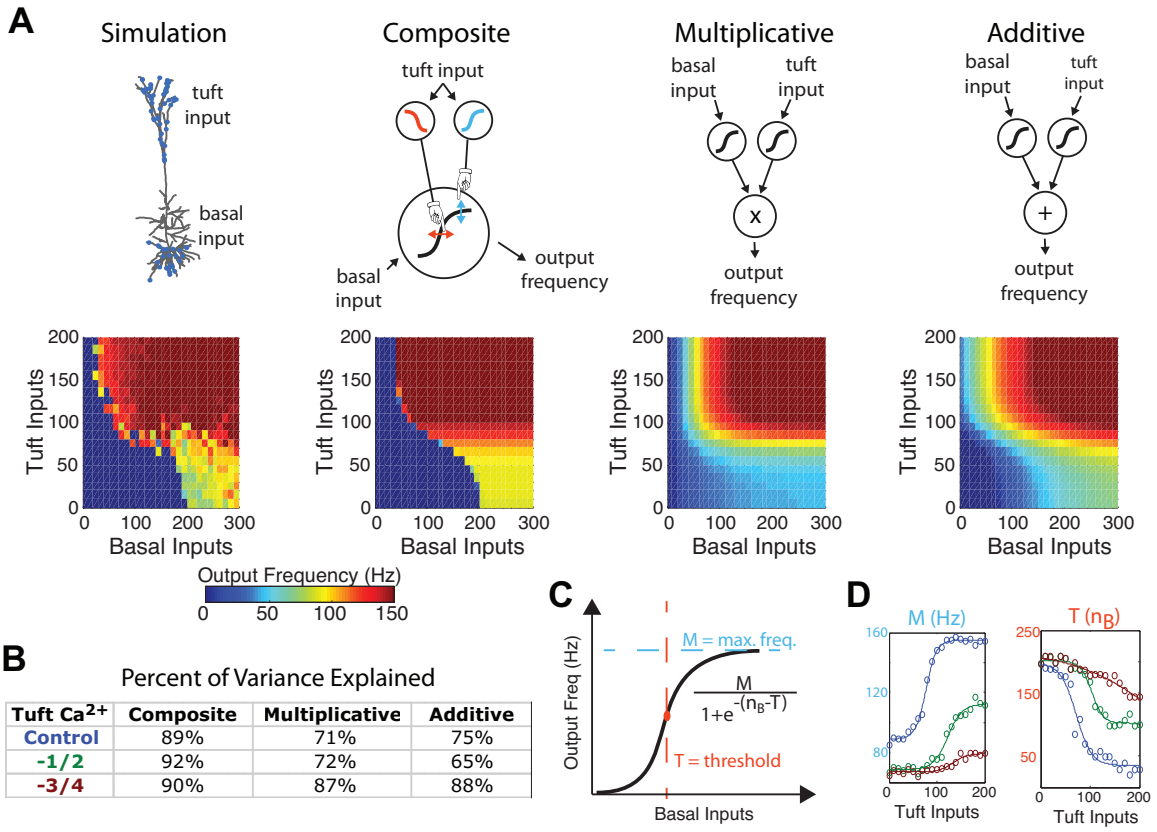

Tuft Ca^{2+}	Composite	Multiplicative	Additive
Control	89%	71%	75%
-1/2	92%	72%	65%
-3/4	90%	87%	88%

Figure 34: Phenomenological models. (a) (Top) Different phenomenological models of a L5 pyramidal cell (left to right): the detailed multi-compartmental simulation; a composite model where the maximum and threshold of the sigmoidal transformation of basal input to spike frequency are defined by tuft input; a multiplicative model which multiplies the independent sigmoidal transformations of basal and tuft output, and an additive model that adds the sigmoidal transformations of basal and tuft output. (Bottom) The output frequencies of the simulation and nonlinear least-squares best-fit models for each of the model types as a function of tuft and basal input. Note that in the composite model, the sigmoid relating tuft input to high-frequency threshold is decreasing while the sigmoid relating tuft input to maximum frequency is increasing, since tuft input acts to lower the threshold and increase the frequency of somatic output. (b) The percentage of variance explained of each of

the three phenomenological model types. (c) The parameters of the composite model can be interpreted as defining the sigmoidal transformation of basal input to output frequency, where the maximum (M) and threshold (T) of that transformation is defined by the tuft input. (d) Plotting the maximum (left) and threshold (right) of the nonlinear least-squares fit to the simulation data (curves) agrees with tuft-constant slices of the simulation (open circles). This gives a method for interpreting and deriving the parameters of the phenomenological model. Colors refer to apical dendrite Ca2+ conductance amounts, as defined in (b).

Potential mechanisms of tuning

How might such single cell computation be involved in visual processing? To explore tuning properties of cells employing a variety of mechanisms, we used circular distributions (von Mises distributions, see Methods and **Figure 35** and **Figure 4**) to model inputs as a function of stimulus orientation. We compared four different mechanisms (**Figure 35**a): a composite sigmoid as described previously; a purely multiplicative where the number of tuft and basal inputs are simply multiplied to get output; a purely additive, where the number of tuft and basal inputs are simply added to get output; and a single sigmoid mechanism, where either the tuft or the basal input is put through a sigmoid function to get the output. The circular distributions used as inputs are normalized such that their maximums (always set to be 0 radians) are 90 synapses (**Figure 35**b). When such inputs are applied to the models we see that the composite mechanism gives the tightest orientation, followed by the sigmoid,

multiplicative, and additive mechanisms (**Figure 35**c). This holds true for a range of input parameters (**Figure 35**d).

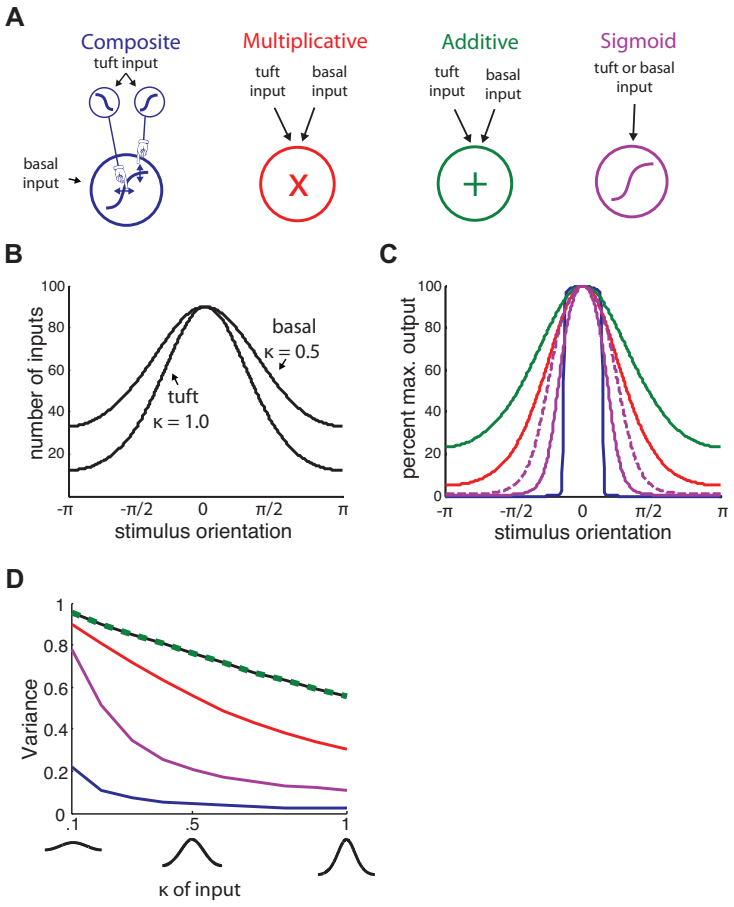

Figure 35: Potential mechanisms of tuning in pyramidal neurons. (a) Four mechanisms are compared (from left to right): composite sigmoid, purely multiplicative where the amount of tuft and basal input are simply multiplied to arrive at the final output, purely additive, where the amount of tuft and basal input are simply added to arrive at the final output, and single-sigmoid, where either the tuft or the basal input is input into a sigmoid function to arrive at the final output. (b) The input into these mechanisms is given by a von Mises distribution (circular analog of a normal distribution) with varying compression parameter (k) and the preferred orientation always set to 0 radians. An example of tuft and basal input

distributions as a function of stimulus orientation is shown with tuft input k = 1.0 and basal input k = 0.5. (c) The output of the different mechanisms with the inputs shown in (b). Colors indicate the different mechanisms as defined in (a). The single-sigmoid mechanism acts on either the tuft (solid purple) or basal (dashed purple) inputs. (d) The circular variance of the output of the different mechanisms as a function of the width of inputs. In this plot, both tuft and basal inputs have the same k, given on the x-axis. The circular variance of the input is shown in black. Note the additive mechanism has the same output variance as the input. At all parameters of the input tested, the composite sigmoid mechanism features the tightest tuning.

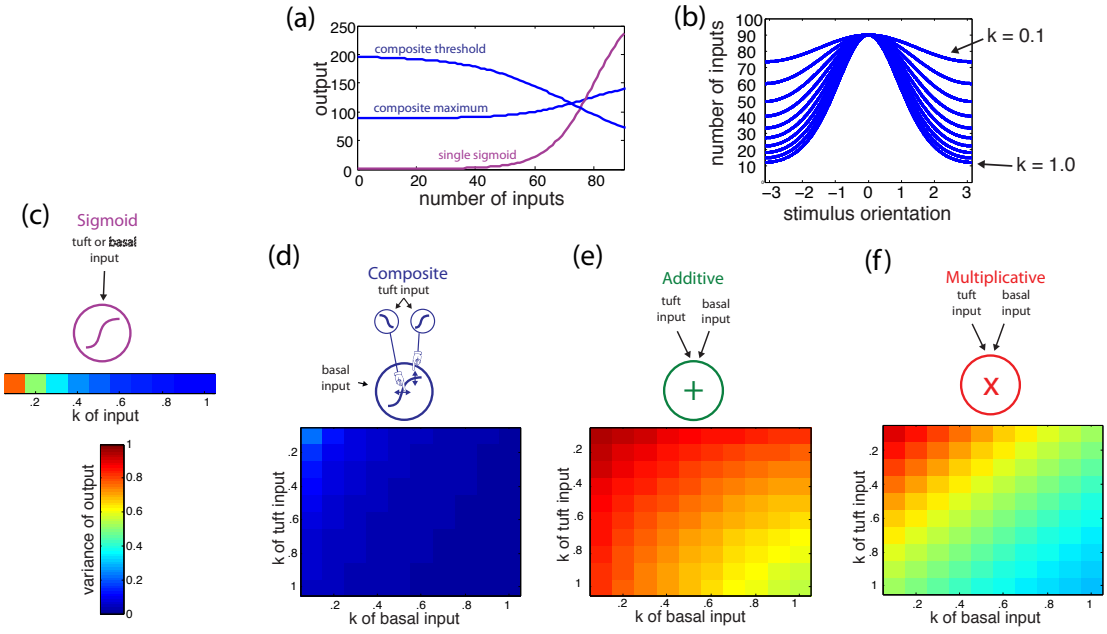

Figure 36: Details of tuning mechanisms. (a) The sigmoid functions used for the composite (blue) and single sigmoid (purple) mechanisms. **(b)** The number of inputs is defined by a von Mises

distribution always centered at 0 radians normalized such that the maximum number of inputs is 90. The only parameter varied for the input is the compression parameter k (where 1/k is the circular analog to the variance of a normal distribution). The output variance of the four different mechanisms is given in **(c-f).**

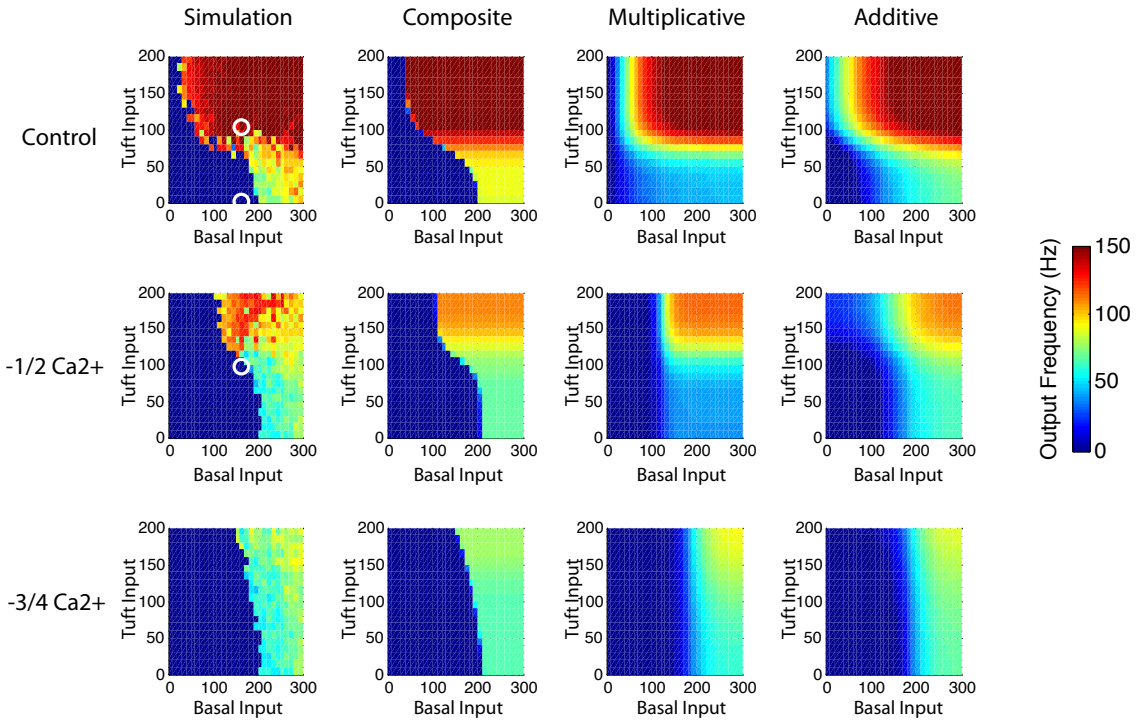

Figure 37: Phenomenological Model Outputs. Shown are the output frequencies as a function of tuft and basal inputs into the simulated morphological neuron, and the three tested phenomenological models , during control and reduced Ca2+ conductance conditions.

Discussion

We introduce a simple phenomenological model that reduces the coincidence detection mechanism and modulation by apical GABAergic input to the simplest possible form. A composite of sigmoids whereby input to the upper layers increases the maximum frequency and decreases the low-to-high frequency threshold of basal inputs (**Figure 34**) explains the data better than more traditional multiplicative or additive models (**Figure 34**) (Gabbiani, Krapp, Koch, & Laurent, 2002; Koch, 1999). It is precisely because the effect of excitatory tuft inputs is to increase the maximum frequency and decrease the threshold of the basal drive needed to elicit that maximum frequency (**Figure 31**) in a Ca^{2+} spike-dependent manner that the composite model outperforms the additive and multiplicative models. In other words, the dendritic, spike-dependent manner in which tuft input changes the input-output relationship between basal input and frequency output is explicitly accounted for in the form of the composite equation. Because many aspects of the model can be interpreted in correspondence with the biophysics of the model (e.g. the maximum and threshold functions are parameterized by Ca^{2+} conductance, and the distinct inputs into the equation are distinct apical and basal excitatory synaptic pathways), this phenomenological model can be tested experimentally. Additionally, the simplicity of the model calls for it to be used in larger simulations of inter-column computation. It is important to note that while apical Ca^{2+} channels play an important role in the burst firing of pyramidal neurons (Williams & Stuart, 1999), other ionic currents, like Na^{+} channels (Oviedo & Reyes, 2002), might also contribute. The existence of such mechanisms, acting either independently or in concert with Ca^{2+} channels, could also support similar computations in pyramidal neurons.

In the last part of our work we present a mechanism where dendritic spikes contribute to the orientation tuning of the cell (**Figure 36**). Importantly, this mechanism is based on the biophysics we found in the *in vitro experiments* (**Figure 7** and **Figure 8**) and the phenomenological model we establish (**Figure 34**), and is dependent on apical tuft input. For a wide range of input parameters (**Figure 36**d and **Figure 37**), including imprecise inputs with large variance, output variance for the composite-sigmoid model was small compared to other mechanisms.

In addition to excitatory inputs, inhibitory inputs across cortical layers are diverse. Genetically and morphologically distinct groups of interneurons contribute inhibitory inputs to specific layers of neocortex, and perform different roles (Jiang, Wang, Lee, Stornetta, & Zhu, 2013; L. Palmer, Murayama, & Larkum, 2012). Although no consensus has been reached about the contribution of specific inhibitory cell types to orientation tuning in mouse V1, multiple papers show that optogenetic excitation of different inhibitory cell types can influence tuning properties of nearby pyramidal neurons (Atallah, Scanziani, & Carandini, 2014; El-Boustani, Wilson, Runyan, & Sur, 2014; Lee, Kwan, & Dan, 2014; Lee et al., 2012). It is plausible that, like excitatory input into the apical dendrites, inhibition located in spatially distinct regions of the pyramidal neuron also contribute to orientation tuning. Layer 1 (L1) is of special interest since it contains neurogliaform cells, which release GABA nonsynaptically. Through a $GABA_B$ metabotropic mechanism, the GABA ultimately causes the blockade of voltage-dependent Ca^{2+} channels, and Ca^{2+} spiking is inhibited (Chalifoux & Carter, 2011). Thus, the simulations where we reduce the conductance of voltage-gated Ca^{2+} channels in the apical dendrite can be interpreted as the physiological consequence of neurogliaform activity in L1.

In this study we found the single-cell biophysics in layer 5 pyramidal neurons supports a nonlinear coincidence detection mechanism whereby tuft input and basal input can integrate in composite-sigmoid manner. This computation can in principle explain how tuft inputs contribute to the tuning properties of pyramidal neurons in the primary visual cortex. Importantly, because the composite-sigmoid model derives closely from the biophysics of the pyramidal neuron, our results are experimentally testable. For example, electric or optogenetic manipulations of inputs onto the tuft dendrites of pyramidal neurons can be used to determine what effect those inputs have on tuning properties. Additionally, the simplicity of the phenomenological model allows it to be used in large-scale network simulations that take into account columnar structure.

Chapter 5

TOWARDS NETWORK LEVEL UNDERSTANDING OF PYRAMIDAL NEURONS

So far in this thesis we have explored the electrophysiology of single pyramidal neurons, created detailed biophysical models, and quantified the computational properties of those neurons using both the biophysical models and more abstracted neurons. In this final chapter of the thesis, we wish to put the single neuron into the larger cortical network. We will first discuss a series of experiments attempting to test the influence of feedback axons in layer 1 on the dendritic nonlinearities of pyramidal neurons. In particular, we will see how layer 1 electrical stimulation, stimulating feedback axons in layer 1, can combine with feedforward sensory input in order to create dendritic NMDA spikes and action potential output. Then we will focus our attention on using channelrhodopsin for precise control of a specific set of feedback axons into layer 1, and test the effects such input can have on the calcium spike in pyramidal neurons. These results, alongside the modeling and experimental results of the previous chapters, will then be combined into a conceptual framework for perceptual binding. Finally, more theoretical concerns will be discussed, especially as they relate to open questions regarding the topics in this thesis.

EXPERIMENTS ON LAYER 1 INPUT IN LAYER 2/3 PYRAMIDAL NEURONS

As shown in previous chapters, NMDA spikes have a causal influence on action potential generation in L2/3 pyramidal neurons. Distal tuft dendrites are the target of feedback input (Felleman & Van Essen, 1991). How does such feedback integrate with feedforward sensory input *in vivo*? We could simulate such input by placing an extracellular stimulating pipette into L1 approximately above the recorded cell and applying paired-pulse stimulation (50 Hz) (**Figure 38a**). For details of the experimental setup, see Methods in Chapter 2. L1 stimulation alone did not evoke a Ca^{2+} response in tuft dendrites however when paired with hindpaw stimulation, a Ca^{2+} response was evoked in 53 ± 8% of the trials which was significantly more frequent than hindpaw stimulation alone ($n = 6$; $p < 0.05$; **Figure 38b** and **c**). These paired L1 and sensory stimulation responses were completely abolished by local NMDA receptor block (**Figure 38b** and **c**) and had similar amplitudes to spontaneous Ca^{2+} transients (1.01 ± 0.22 F/F vs 1.23 ± 0.10 F/F; $n = 6$; $p > 0.05$; **Figure 38d**). This therefore suggests that NMDA spikes can associate top-down input (recruited by L1 stimulation) and bottom-up input (recruited by hindpaw stimulation) arriving simultaneously.

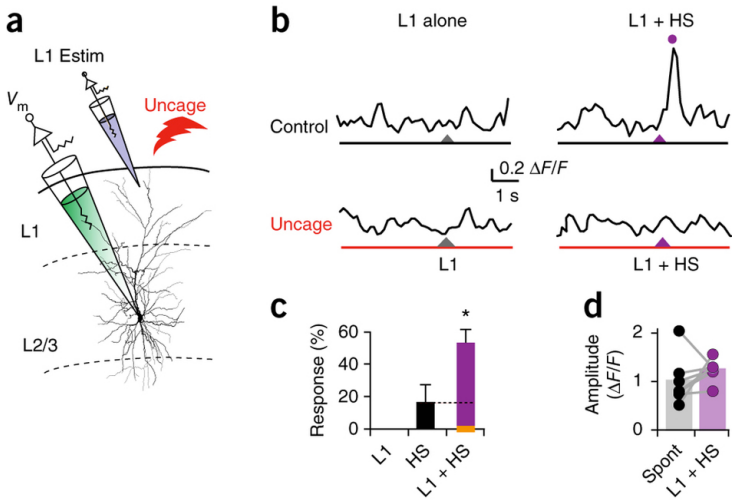

Figure 38: Tuft Ca2+ events report coincident input. (a) Experimental design showing reconstructed L2/3 pyramidal neuron filled with tc-MK801 and placement of extracellular stimulating pipette into layer 1 in vivo. (b) Ca2+ transients during 50-Hz paired-pulse stimulation of L1 alone (L1, left) and together with contralateral hindpaw stimulation (L1 + HS, right) before (top) and after (bottom) block of NMDA receptors by two-photon uncaging (690 nm). (c) Average percentage of trials with a Ca2+ response during L1 stimulation alone, contralateral hindpaw stimulation alone (HS) and L1 and hindpaw stimulation together. Data is paired. Orange line indicates L1 + HS during global NMDA block by intracellular MK801. (d) Amplitude of spontaneous (left) and evoked L1 + HS (right) Ca2+ transients. *P < 0.05. Error bars represent s.e.m.

Long-range fibers conveying feedback information tend to target cortical L1(Felleman & Van Essen, 1991), a fact that has long seemed mysterious(Hubel, 1982). It has been suggested that NMDA receptors in the tuft dendrites might serve to compensate for the remoteness of this important synaptic input(Cauller & Connors, 1994; Larkum, Nevian, Sandler, Polsky, & Schiller, 2009). We found that the response in L2/3 pyramidal neurons to sensory input was

greatly enhanced by coincident NMDA-dependent synaptic input to the tuft region. A recent study has demonstrated the importance of NMDA receptors for processing feedback signals arriving in L1(Self, Kooijmans, Super, Lamme, & Roelfsema, 2012). The results shown here are entirely consistent with that study and suggest that NMDA-receptor-dependent input to this region of the cell not only increases its effectiveness on AP output but also makes this influence conditional on the association of feed-forward and feedback information streams.

The electrical stimulation used in this experiment gives local electrical stimulation to L1, but it does not differentiate between any of the processes that are in the vicinity. Next, we will use an *ex vvo* optogenetic technique in order to specifically target long-range feedback axons.

EXPERIMENTS ON FEEDBACK TO V1 IN MOUSE L5 PYRAMIDAL NEURONS

Abstract

Long-range cortico-cortical feedback axons carry information from higher order areas back to primary sensory areas. Such feedback pathways in the visual system have been implicated in top-down attention, sensory representation, and consciousness. Alongside these concerns about network anatomy, much work has been carried out elucidating the bio-physiology of single. In this work we study the effects of feedback axons on single cell physiology, in order to combine network and single cell aspects of cortical processing, and work towards an integrated view of the cortex from single neurons to cognition. In particular we focus on layer 5 pyramidal neurons, one of the main integrators of the local cortical column. We find that feedback axons can manipulate the dendritic calcium spike of these pyramidal neurons.

Introduction

The cortex is a structured lattice made up of canonical circuits arranged in a sheet. These circuits are composed of hundreds of cells organized across the six layers that make up the cortical depth (~1 mm) and extending out in a cylinder estimated to be ~ 300 um in diameter. Sensory input of different types directly drive specific groups of these circuits (often via the thalamus), and from there the signal propagates to other areas of cortex. The massive

interconnectedness of the cortex soon allows the information to flow not only in a feedforward manner, but also in a recurrent feedback manner, from later stages of the cortical hierarchy back to the earlier areas that are driven directly by bottom up sensory input.

In particular, much attention has been paid to the visual system, tracing both anatomically and physiologically the flow of sensory information, often in primates. These studies show that the posterior pole of the cortex (the primary visual cortex, V1), receives the majority of the initial sensory drive into cortex about 50 ms after the visual stimulus. Later, V1 receives a late, often 100s of ms post-stimulus, signal that is often thought to represent long-range feedback inputs. The role of such feedback has been postulated to be important for many higher order cognitive functions, including top-down attention, perception, and even consciousness.

How exactly feedback would mediate these cognitive functions is still an open question. In this study, we aim to see what the physiological role of long-range feedback to V1 is in terms of physiology, and how this might be relevant to the building up of sensory representations. We focus on two higher-order cortical areas of mouse, the lateromedial visual area (LM), often considered to be the first stage of the ventral stream in the mouse, and the anterior cingulate cortex (ACC) in the frontal pole. Postsynaptically, we focus on layer 5 pyramidal neurons of V1. These neurons have extensive dendritic arborization of all six layers of cortex, and so act as one of the main integrators of the cortical column. Additionally, they send long-range axons to other areas of cortex and to subcortical areas as well as the spinal column, making them a main decision makers of the local column, potentially useful not only in internal representation and perception, but also for behavior.

We find that feedback inputs into V1 from both ACC and LM both synapse mainly in L5 and L1. Given the electrical distance between L1 and the spike initiation zone of a L5 pyramidal neuron, we focused our attention on the interaction of long-range feedback inputs and the dendritic nonlinearities of the cell. By stimulating feedback fibers in conjunction with somatic whole-cell patch stimulation, we were able to monitor the interaction of backpropagating action potentials and dendritic spikes. We found that L1 stimulation decreased the threshold for dendritic spiking. Thus the dendritic spike acts as a readout of concurrent action potential and L1 input. We conclude by discussing how this single-cell setup could be used to create bound percepts distributed across the cortex.

Methods

In order to control long-range axons into V1, we inject adeno-associated virus (AAV; serotype 1 or DJ) into either anterior cingulate cortex (ACC) or the latero-medial visual area (VisL). The virus expresses a fluorophore-channelrhodopsin fusion (either ChIEF-tdTomato or ChETA-mVenus) under the CAG promoter. In this way, axons can be traced anterograde from the injection site to V1. Injections are performed in C57BL/6J mice (Jackson Labs) at p35-p55. Mice were anesthetized with isoflurance and placed in a stereotax. A small hole was drilled into the skull, and virus was injected through a glass pipette. VisL coordinates are 4.1 mm from the midline and 1.4 mm anterior of the transverse sinus, and two injections were performed at a depth of 250 and 650 microns from the pia. ACA coordinates are 0.26 mm from the midline and 0.27 mm posterior of lambda, and two injections were performed at a depth of 600 and 1,250 microns from the pia.

Coronal slices of the brain were taken at least 3 weeks after the injection. Slices of 350 microns were taken from the posterior cortical pole at an angle of 10-15 degrees in order to keep the dendrites parallel in the slice. Before slicing the mouse was anesthetized using isoflurance and perfused with a solution of Tris-ACSF containing, in mM, 73 Tris HCl, 28 Tris Base, 2.5 KCl, 1.2 NaH2PO4, 30 NaHCO3, 20 HEPES, 25 Glucose, 5 Na-ascorbate, 2 Thiourea, 3 Na-pyruvate, 12 N-acetyl-L-cysteine, 10 MgSO4, 0.5 CaCl2. The brain was then excised from the skull and sliced in the same Tris-ACSF at room temperature with a Compresstome Vf-200 (Precisionary Instruments). Slices were incubated at 34C in Tris-ACSF for 5 minutes, and then transferred to room temperature recording ACSF containing 126 NaCl, 2.5 KCl, 2 CaCl2, 1 MgSO4, 1.25 NaH2PO4, 26 NaHCO3, 12.5 Glucose. Slices were kept for at least 45 minutes in recording ACSF before patching.

Whole cell patches were made with borosilicate pipettes between 4 and 7 MOhm, with an Axopatch 700B Amplifier. Internal solution contained, in mM: 115 K-Gluconate; 20 KCl; 10 Hepes; 10 Phospho-Kreatine; 4 ATP-Mg; 0.3 GTP, and had a pH of 7.3 and osmolality of 280 mOsm. The Matlab based acquisition software Ephus (www.ephus.org) was used (slightly modified) for all electrophysiology and laser stimulation.

After whole-cell patching, a 473 nm laser was controlled with a set of galvos (Thorlabs) and projected onto the slice through a 10x air objective. The laser path was designed to be set up on a small custom breadboard (shown in Figure), and consisted of 3 mirrors for alignment and a 4x telescope in order to fill (not completely) the back of the objective. This allowed for

the control of long-range axons from the injection site to V1. Laser pulses were 0.5 ms in length, and were between 20 and 50 uW. In some experiments, TTX and 4-AP were put in the recording solution in order to make sure that the laser was evoking synaptic terminals, and not axons of passage.

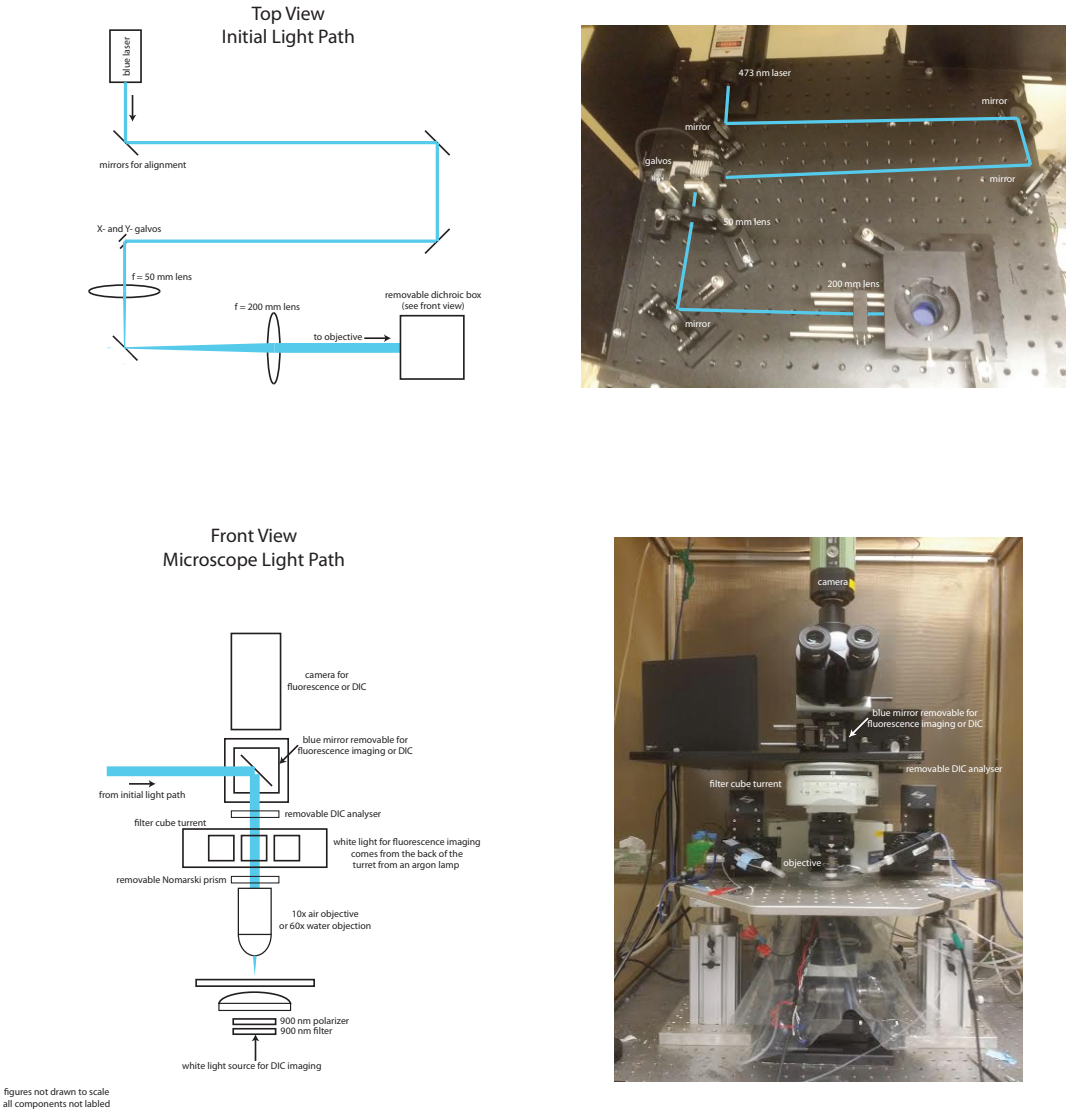

Figure 39: The optical and electrophysiological rig for the experiment. Top Left: The light path for the blue optogenetics laser,

featuring a telescope and galvo-mirrors to stear the laser beam in XY. Top Right: A picture of the built optical setup. Bottom Left: A diagram of the DIC microscope used for electrophysiology. Bottom Right: A picture of the built electrophysiologycail rig.

A critical frequency protocol was used to monitor the dendritic calcium spike of the patched cell. This protocol consists of 3 or 4, 2-ms pulses in current clamp, at threshold for eliciting a single action potential per pulse. Trains of 3 pulses are given from 10 to 200 Hz, in intervals of 10 Hz. The afterdepolarization following the last action potential serves as a readout for the nonlinear dendritic spike. When laser pulses were coupled with critical frequency, the laser pulse always came 1 ms before the second whole-cell pulse.

Analysis of the data was performed in Matlab.

Results

In order to study the effects of feedback pathways in the mouse cortex, we used an *ex vivo* optogenetic approach, summarized in **Figure 41**. Virus carrying an opsin-fluorophore payload was injected into the presynaptic area of interest (either ACA or LM). After waiting at least 3 weeks for the virus to infect and express in presynaptic neurons and their axons, slices were taken for patch electrophysiology. Layer 5 pyramidal neurons in V1 were target for patch

recording. In either the voltage or current clamp configuration, a blue laser was spatially and temporally modulated in order to elicit synaptic events from the presynaptically targeted axons onto the patched cell in V1. In this way, we monitored the effect of long-range feedback synapses on pyramidal neurons in V1.

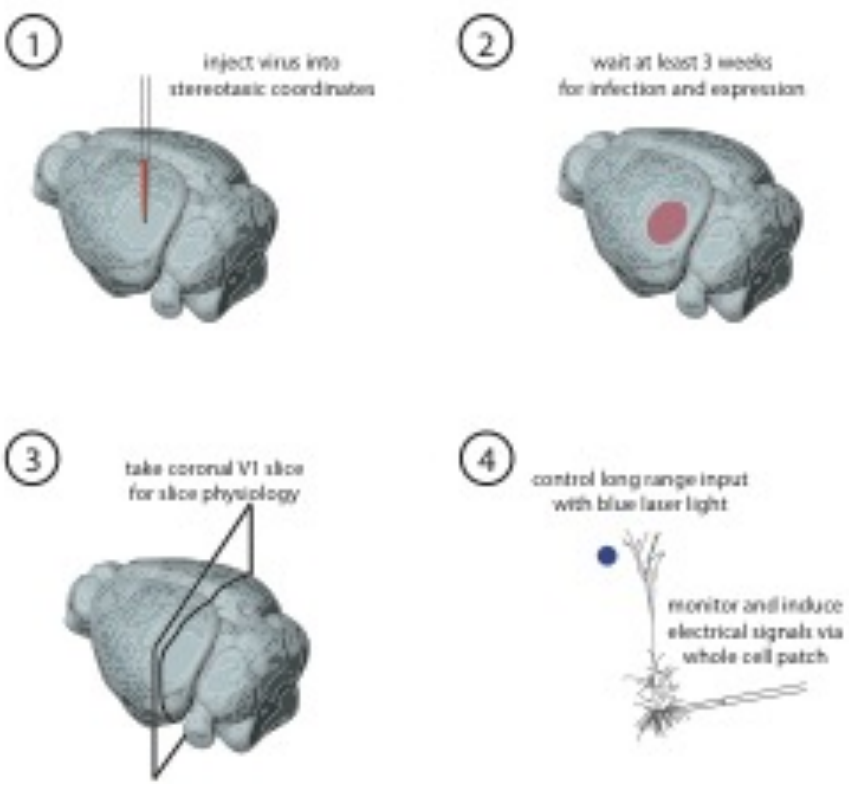

Figure 41: The general experimental procedure. (1) Virus carrying a fluorophore-opsin payload is injected into either ACC or LM. (2) The virus is given at least 3 weeks to infect cells in the targeted areas and express proteins throughout the axons of those cells. (3) Coronal slices of 350 um are taken of the primary visual cortex. Special care is taken to keep pyramidal neuron dendrites parallel to the cut surface so as to preserve the apical dendrites as much as possible. (4) Layer 5 pyramidal neurons in V1 are targeted with whole-cell patch pipettes.

Using a laser that is spatially and temporally modulated to control the long-range feedback inputs in combination with whole-cell patch, we can monitor the laminar structure of feedback inputs or the effect of feedback input on somatic current injections.

As a first step, we looked at the anatomy of feedback projections into V1, using light microscopy. Virus carrying a fluorophore-ChR2 payload was injected into LM or ACA. 350 micron coronal slices were taken of V1, fixed, and then imaged using either a widefield fluorescence or confocal microscope. Both LM (**Figure 42**, **Figure 43**) and ACA (**Figure 43**) projections send axons to V1. The laminar structure of these projections can be seen by looking at the density of fluorescence across the depth of V1 (**Figure 43**). Both LM and ACA projections show strong fluorescent density in L1 of V1.

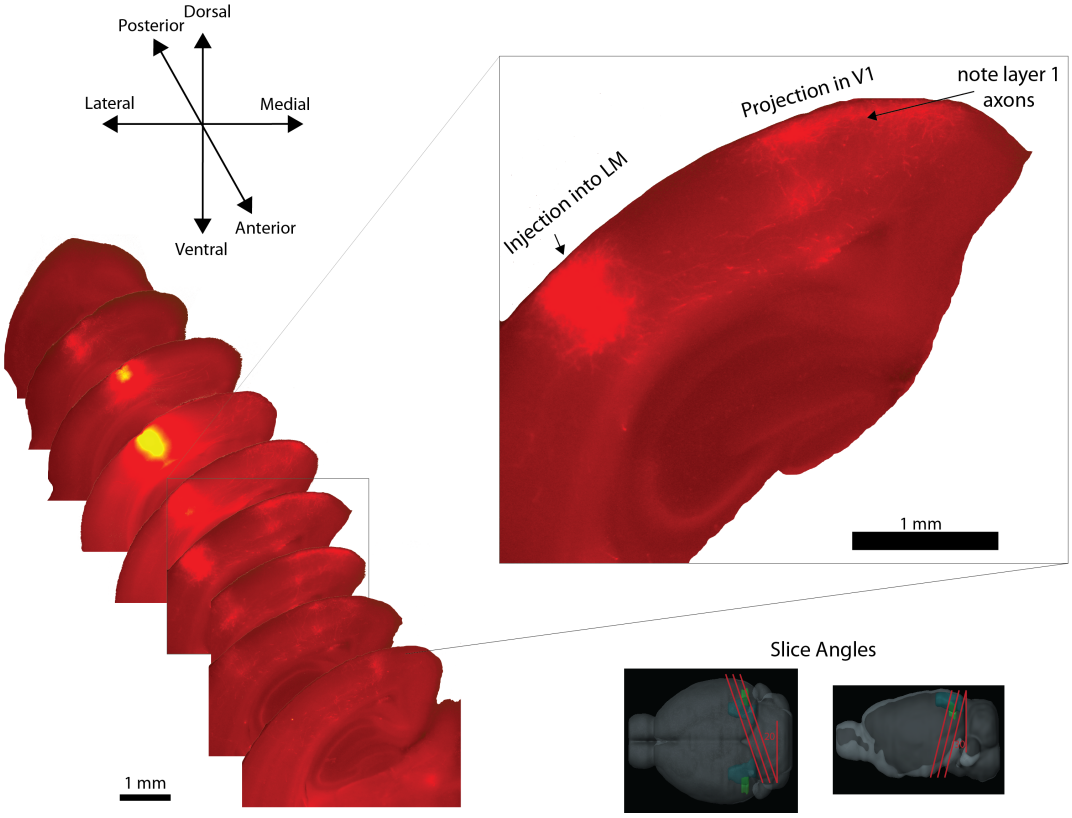

Figure 42: Anatomy of the LM to V1 pathway. Bottom Left: Slices from posterior to anterior of an injection of anterograde tracing virus into area LM. Top Right: A slice showing the anterograde projections from LM to V1, hitting mainly layer 1 but also layer 5.

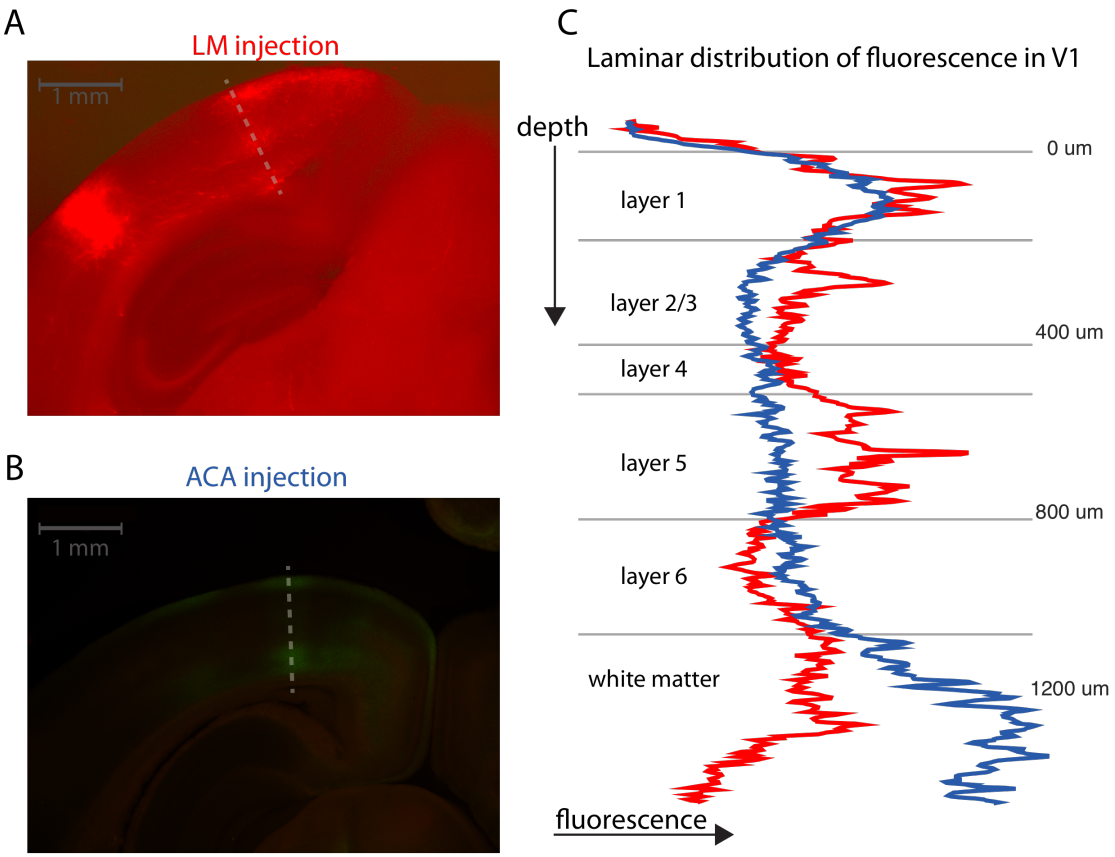

Figure 43: The laminar distributions of LM and ACA projection axons in V1. (A) Fluorescent image of anterograde LM injection. (B) Fluorescent image of ACA axons projecting to V1. (C) The laminar distribution of axons from LM (red) and ACA (blue) to V1.

Although anterograde labeling from both ACA and LM results in strong axonal fluorescence in layer 1 of V1, differences can be seen in lower layers. In particular, while injections in LM resulted in a distinct band in layer 5, injections in ACA had no such band, and instead had labeling in layer 6. The lack of fluorescence from ACA to V1 in layer 5 does not necessarily mean that active synapses do not exist.

In order to test where functional connections exist, a method called channelrhodopsin-assisted circuit mapping (CRACM) was used (**Figure 44**). Channelrhodopsin-fluorophore was expressed in area ACA, a layer 5 pyramidal neuron was patched, and a laser was used to stimulate axons within V1 in a local area (~75 um diameter) at a point at a time in a grid (**Figure 44**A). The neuron was voltage-clamped at -70 mV, in order to measure excitatory currents. The results clearly show two spatially distinct groups of excitatory inputs, one in the basal dendrites, and another in the tuft dendrites (**Figure 44**B). When increasing the laser power, input into the tuft dendrites elicits action potentials at the soma, while basal inputs do not (**Figure 44**C).

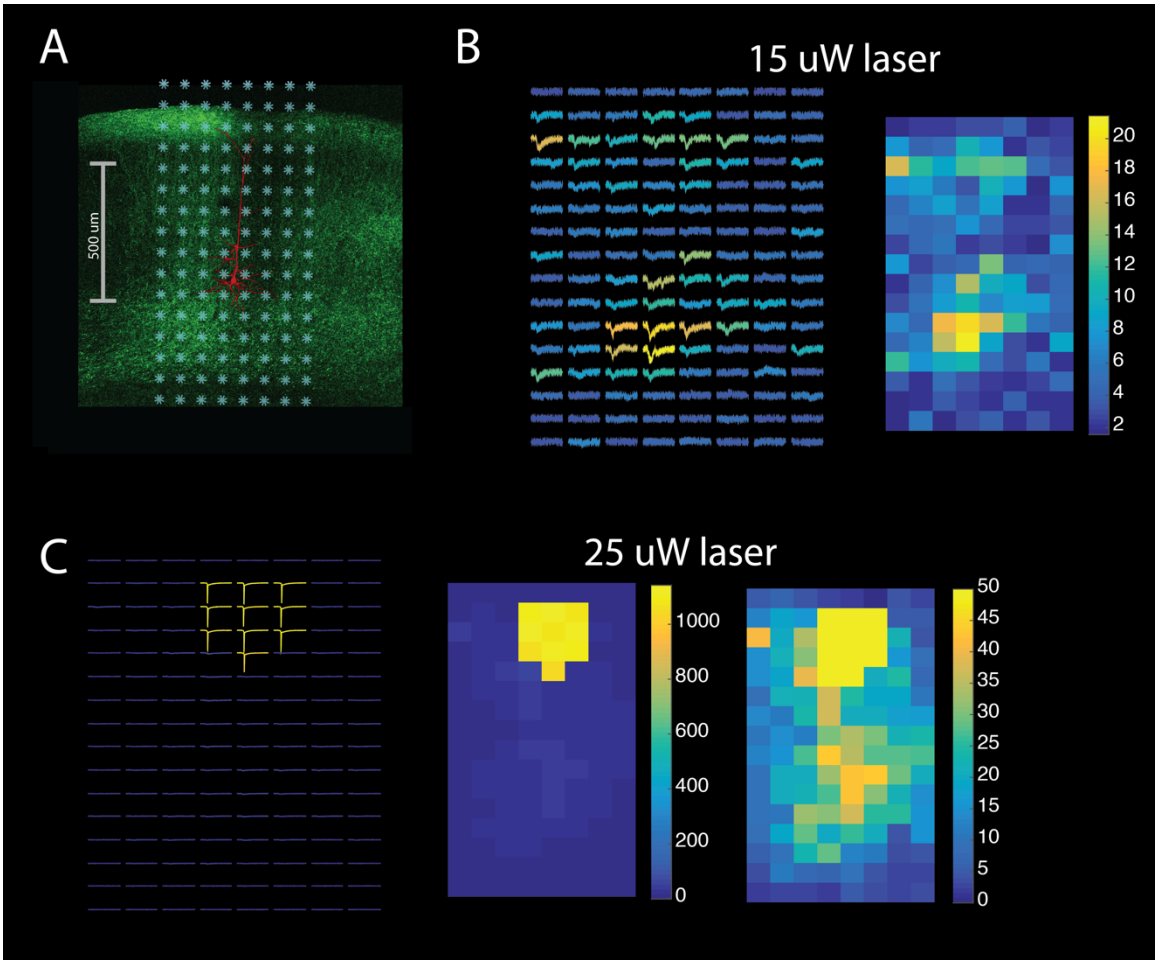

Figure 44: CRACM from ACA to a V1 layer 5 pyramidal neuron. A) Axons from ACA (green) express a fluorophore and opsin. A neuron in V1 (red) was patched, and laser pulses of blue light were given individually in a grid pattern (teal stars) to elicit postsynaptic responses in the patched cell. B) At 15 uW laser power, two groups of synapses can clearly be seen, one at the basal dendrites, and one in the tuft dendrites. C) When laser power is increased to 25 uW, the tuft inputs are strong enough to elicit an action potential, while the basal inputs are not.

How strong are the inputs into these two compartments? The spatially extended nature of the neuron, alongside the nonlinearities along the dendritic extent, makes voltage clamping at a single point insufficient for accurate current readings, an issue called *space clamp*. However, there are two results that already hint at the tuft inputs being incredibly strong relative to the basal inputs. First, despite issues regarding spatial extent (remember that the tuft dendrite is ~3 length constants from the patch, meaning that only ~5% of the signal will passively reach the patch pipette), the amplitudes of tuft and basal inputs are similar. This might be due to stronger synaptic input itself, or by virtue of dendritic nonlinearities that amplify the signal so that passive attenuation of the EPSPs are inverted. Second, action potential generation is seen with stimulation of the tuft dendrites, but not with stimulation of the closer basal dendrites, again suggesting that feedback inputs into the tufts have a larger influence on spiking output than feedback input into the basal dendrites.

In these CRACM experiments, it is possible that the laser is stimulating axons of passage instead of axon terminals. To correct for this, TTX and 4AP can be perfused through the tissue, in order to achieve a method called subcellular CRACM (sCRACM). Performing sCRACM reveals a similar pattern of two distinct spatial locations for excitatory input from ACA to V1 (**Figure 45**).

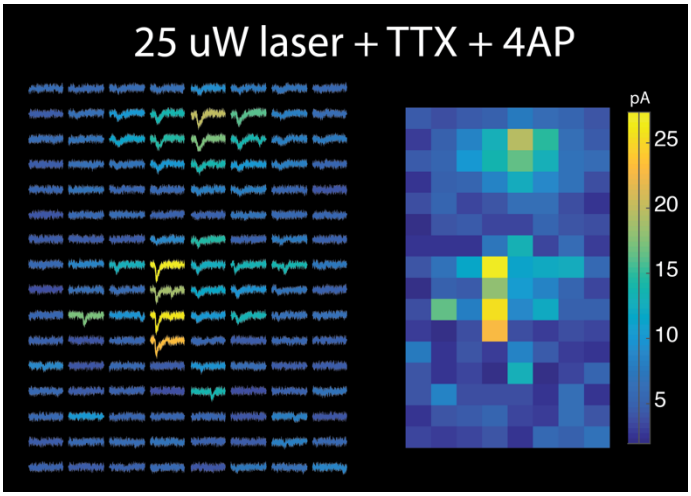

Figure 45: sCRACM reveals the locations of synaptic inputs from ACA. The basic structure of two groups of inputs is preserved, with one group in the tuft dendrites, and the other in the basal dendrites.

What is the effect of feedback input on the dendritic nonlinearities in a layer 5 pyramidal neuron? One possibility is that input into the apical tufts could shift the critical frequency lower, such that it is easier to elicit a dendritic Ca-spike when long-range feedback axons are active. To test this possibility, critical frequency experiments were conducted alongside laser stimulation of layer 1. A 1 ms light pulse was given 10 ms before the last action potential was elicited. As can be seen in **Figure 46**, laser stimulation was able to shift the critical frequency lower.

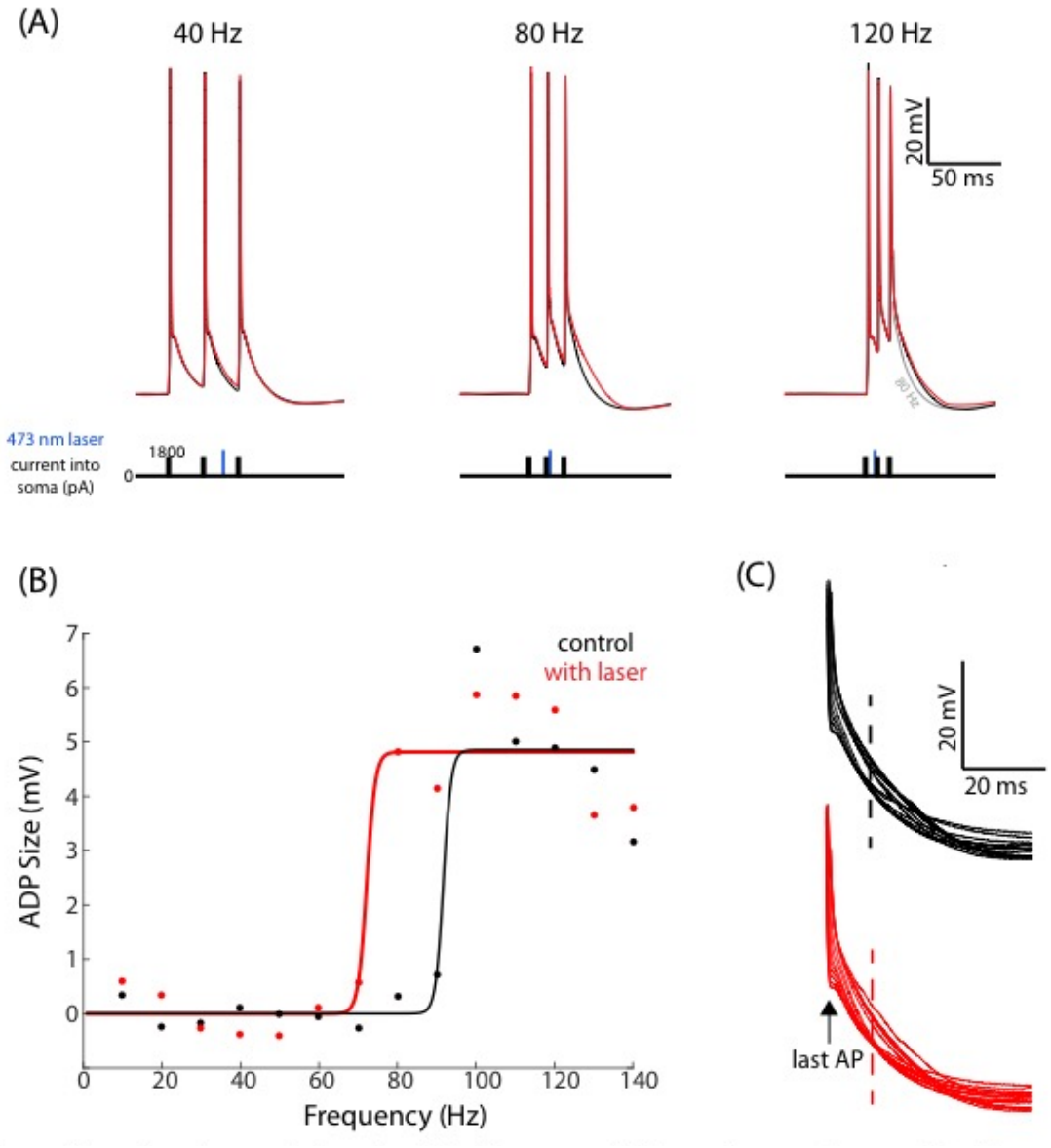

Figure 46: Axons from cingulate modulate the critical frequency. (A) Somatic traces from a critical frequency experiment. 3 current pulses (2 ms) are given into the soma of a patched L5 pyramidal neuron in V1. In red traces, a 473 nm laser pulse (0.5 ms) is given in layer 1 of V1 after the second current pulse. At 40 Hz there is little different in the after-depolarization (ADP) preceding the last spike. At 80 Hz, the laser stimulation increases the ADP, and at

120 Hz, both control and laser stimulated conditions have raised ADP. (B) Ploting the ADP as a function of frequency defines a sigmoid. The inflection point of that sigmoid is called the critical frequency. Laser stimulation of feedback axons from cingulate back to V1 shifts the critical frequncy ~20 Hz to the left. (C) Comparing the ADPs aligned by the last spike shows similar ADP shapes in the control and laser stimulated cases.

Higher laser powers, presumably recruiting more presynaptic axons, were able to shift the critical frequency more (**Figure 47**), in a monotonic fashion.

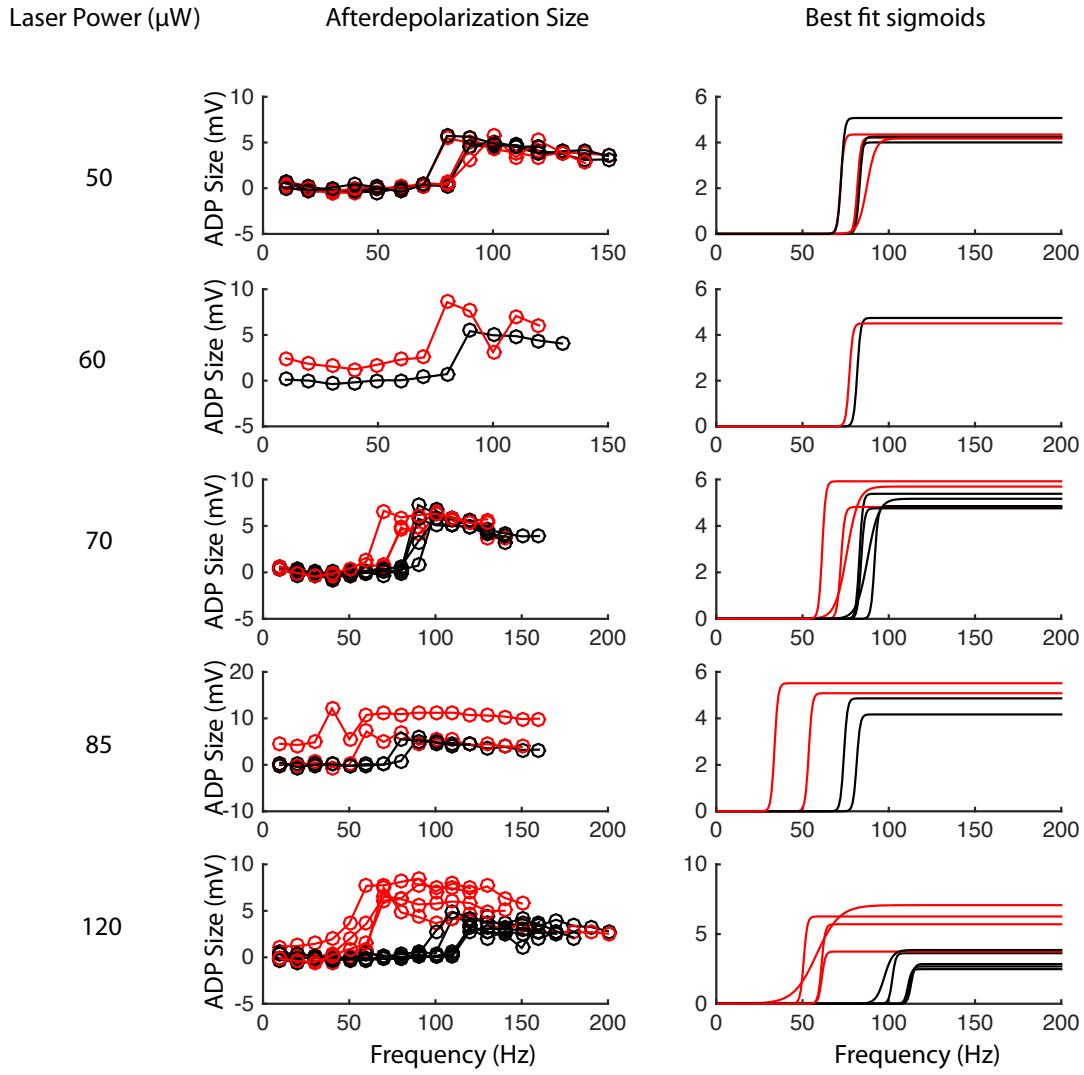

Figure 47: Stimulation of layer 1 axons from ACA in V1 increasingly shift the critical frequency with increasing laser power. Experiments with increasing laswer power are shown in rows from top to bottom. The middle column shows the last spike afterdepolarization size for different frequencies of 3 elicited APs at the soma. The right column shows best fit sigmoid to the raw data shown in the middle column.

Quantification of these results show that while the critical frequency is decreased with increasing laser power, the size of the after depolarization modestly increases linearly. This might be due to increased calcium conductance or more directly from the increased synaptic input itself.

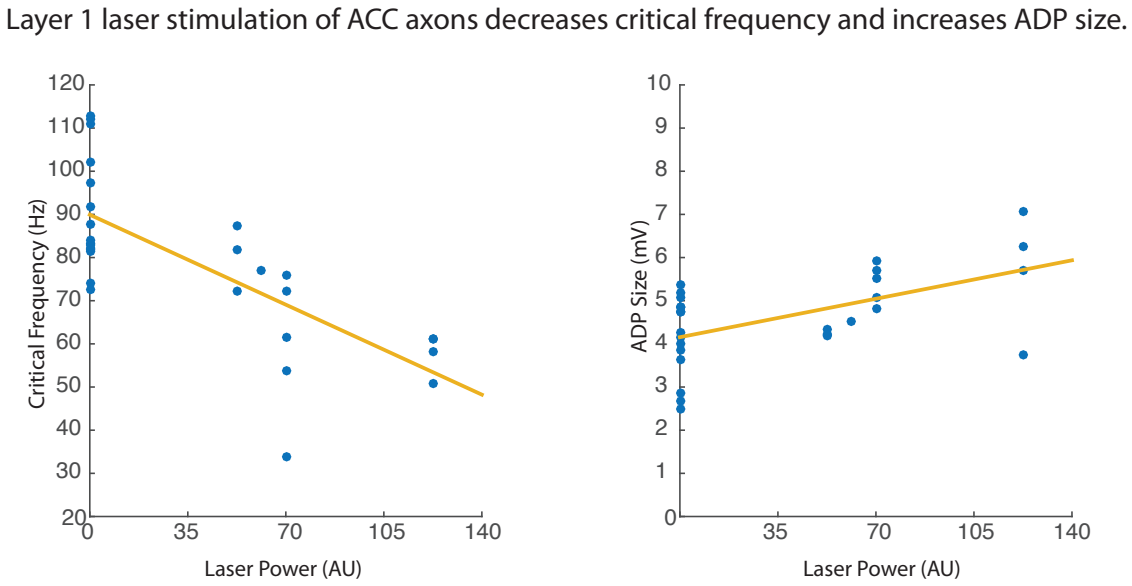

Figure 48: Layer 1 stimulation of ACC axons decreases ritical frequency and increases ADP size. The left panel shows the critical frequency decreasing as a function of laser power in layer 1. The right panel shows an increase in the afterdepolarization size with increasing laser power.

One interesting phenomenon that was unexpected can be seen by looking at the critical frequency on trials without laser stimulation over time. Here we see a clear and linear decrease in critical frequency over time. This potentially plastic effect is necessarily non-synaptic, since the critical frequency experiment requires no synapses to be active. However, in the vast majority of cells patched in which there was no laser stimulation of the dendrites, critical frequency became higher over time, eventually disappearing. The control experiments necessary to untangle this phenomenon were not a focus of this study, and require further inquiry.

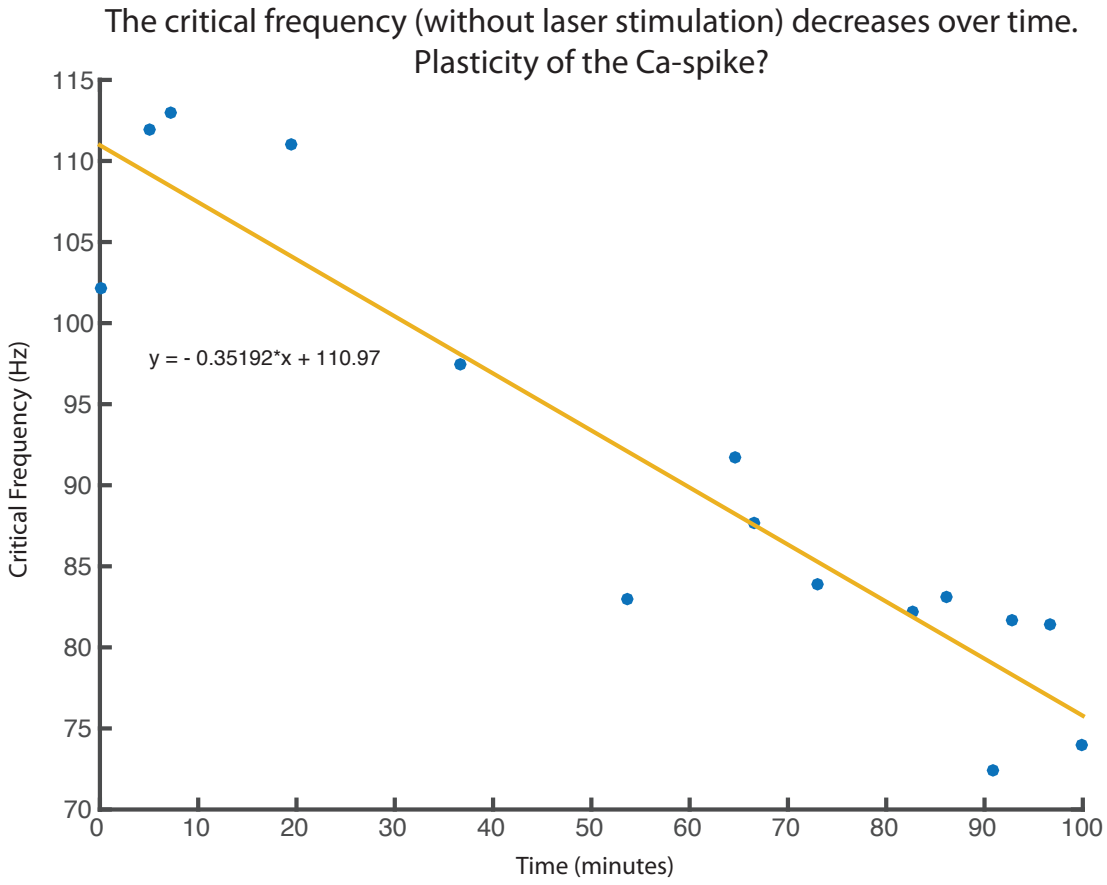

Figure 49: The critical freuqnecy of trials without laser stimulation decreases over time.

The results shown here, while promising, require a few control experiments, and certainly more replication. It is possible that what is measured as a change in critical frequency is really just a linear summation of a normal spike after-depolarization with tuft EPSPs. These experiments were low-yeild, for a number of reasons, which I will list now, alongside some advice, in order to inform any future graduate student thinking about these kinds of experiments:

1. Finding the right virus. Multiple viral constructs, from multiple vendors, were tested over the course of a year. Some simply wouldn't infect/express, some would not infect or express at high enough rates, some would infect but not express. There did not seem to be an easily understood reason for this, other than variability in the construct. One mistake, in retrospect, was to try using the newest and best tools, when older tried and true tools would have sufficed. One should try using the simplest tool that will yield results. Later, the method can be refined if need be.

2. Injection of the virus. In addition to the virus, the method of injection of the virus is also important. I tried iontophoresis, a nanoject, and a pump, all with varying parameter settings. In short, injecting as slow as possible (over the course of minutes) with the pump seemed to yield the most reliable results. Injection volume also mattered, though this depends on the virus. Some virus required as little as 10s of nL, while others required up to 500 nL.

3. Slice health. Studying the long dendrites of pyramidal neurons requires healthy cells, in slices where the dendrites are preserved. Time should be taken in the initial stages of the experiment to make sure slice technique is such that the dendrites are preserved in close

to 100% of experiments. Additionally, because virus infection takes 3-6 weeks, this prep is necessarily older, making slice health a substantially more difficult issue. In order to counterbalance this, several Na-replacement techniques were used during the slicing procedure, to varying degrees of success. In particular, while NMDG replacement kept cells incredibly healthy, they also seemed to be more bursty. In many cases, even a single 2ms current injection at threshold would produce 100-200 ms of high frequency firing.

4. Timing. Related to the previous point, in older slices the physiological properties of the dendritic Ca-spike tend to change quickly after patching. Typically, there was ~10 minutes of reliable critical frequency behavior available before the Ca-spike would disappear. Moreover, over this 10 minutes the critical frequency would often change, making it hard to attribute changes to the laser.

These are the main reasons for the paucity of replicated data in these experiments. Nevertheless, these experiments do show good reason to believe that the critical frequency can be manipulated by long-range feedback tuft input. The CRACM and sCRACM data both imply that feedback tuft input is stronger than feedback input into the basal dendrites. Alongside the modeling results of synaptic barrages into the multicompartmental model, it is entirely plausible that feedback input acts to control burst firing via its effect on the Ca-spike in the dendrites of pyramidal neurons.

THEORETICAL IMPLICATIONS: A POTENTIAL MECHANISM FOR BINDING

One result from the experimental and modeling work of this thesis was a single-cell mechanism for spike bursting via the dendritic Ca-spike of pyramidal neurons. The experimental and modeling results from this thesis clearly show the synapses in layer 1 to be well suited to manipulate the Ca-spike (**Figure 21**, **Figure 46**, **Figure 47**, and **Figure 48**). Additionally, modeling results show that the extracellular signature of the Ca-spike is a large current sink in the upper layers of cortex (**Figure 23**), such as the neural correlate of consciousness discussed in the Introduction. L1 is unique in that it is extremely sparse, and the vast majority (upwards of 90%, (Hubel 1982)) of the synapses there are from long-range inputs, rather than from the local circuit. Importantly, the pyramidal neurons whose dendrites support Ca-spikes are precisely those neurons that make long-range connections themselves, both cortically (feedforward, horizontal, and feedback[9]) and subcortically. What computational role could be played by such physiological and anatomical setup?

One intriguing possibility, which I will call tiger theory, is described by Matthew Larkum (Larkum 2013). Tiger theory takes a largely bottom-up approach, starting from the detailed physiology of pyramidal neurons and the anatomy of long-range connections in the cortex. Of particular importance is the laminar structure of long-range feedforward and feedback axons

[9] There is an "indirect" pathway for cortico-cortico information flow through the thalamus, and some argue that this might be the main way information is transferred from one area of cortex to another ((Sherman and Guillery 2011b)).

in the cortex. There is now ample evidence that feedforward connections strongly innervate the basal dendrites of layer 5 pyramidal neurons with excitatory synapses. Feedback axons innervate layer 1, as shown in **Figure 43**, **Figure 44**, and **Figure 45**, where the dendritic tufts of pyramidal neurons reside. As discussed previously, the physiology of layer 5 pyramidal neurons allows for a coincidence detection mechanism (**Figure 21** and **Figure 22**), whereby concurrent excitatory input into both the basal and apical tuft dendrites causes a high frequency burst.

Additionally, the local inhibitory circuit consists of a number of different cell types that can generally be classified into distinct groups based on their specific effects on either the somatic or apical areas of the pyramidal neuron. For instance, neurogliaform cells in layer 1 metabotropically inhibit voltage-gated calcium channels in the apical dendrites (Palmer et al. 2012; Pérez-Garci, Larkum, and Nevian 2013), whereas single bouquet cells in layer 1 disinhibit the apical dendrite via their inhibitory effects on layer ⅔ inhibitory cells (Jiang et al. 2013). Somatostatin positive inhibitory neurons are known to directly inhibit the apical dendrites, whereas parvalbumin positive inhibitory neurons directly inhibit the basal dendrites, affording these groups of neurons distinct computational roles in the regulation of pyramidal neuron output (Royer et al. 2012; Shai, Koch, and Anastassiou 2014). In this way, inhibition of the apical dendrites by neurogliaform cells,or somatostatin positive interneurons can act as a form of gain control, regulating the frequency of firing in pyramidal neurons. Alternatively, the inhibition of neurogliaform cells, for instance via cholinergic action (though under certain conditions, acetylcholine can have opposite effects, REF BROMBAS), can predispose pyramidal neurons to high frequency firing.

Taken together, pyramidal neurons and the local inhibitory circuit that surrounds them are well suited to associate feedback and feedforward information streams (**Figure 50**). That association, signaled via a high-frequency spike burst in a pyramidal neuron, is then communicated to other areas of the brain, including other areas of cortex. For instance, a pyramidal neuron receiving feedforward orientation information from V1 and motion information via feedback from V5 can bind these two information streams. These associated signals can then contribute, via their influence on the apical or basal dendrites of far-away pyramidal neurons, to other associations. The single-cell mechanism through which concurrent basal and tuft excitatory input creates spike bursting has been named the BAC mechanism (Larkum 2013). In this way, the BAC mechanism causes high-frequency burst firing, as is often seen *in vivo* (de Kock and Sakmann 2008; Buzsáki and Mizuseki 2014), whereas input into only the basal dendrites will only cause tonic low-frequency firing (**Figure 21**, **Figure 22**, and **Figure 50**). Long-range input can also robustly regulate the BAC mechanism indirectly by recruiting the effect of the different cell types in the local inhibitory circuit.

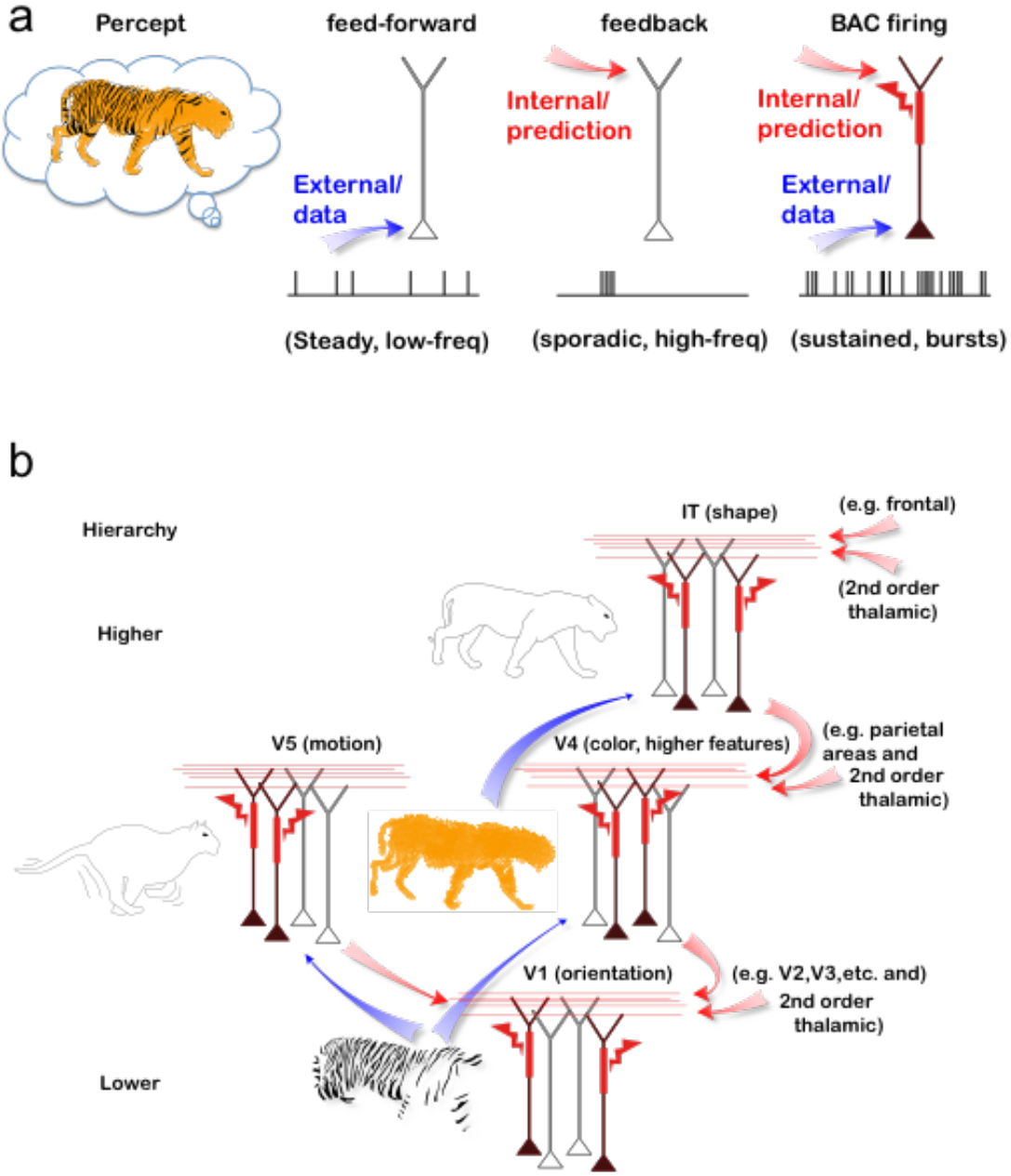

Figure 50: Tiger theory connects physiological and anatomical details to network level computation and perceptual representation in the cortex. A) Input into the basal dendrites of a cell causes steady low-frequency firing in a pyramidal neuron. This feedforward input into the basal dendrites, when combined with feedback input into the apical tufts causes high frequency burst firing.

In the scheme of tiger theory, feedforward input into the basal dendrites carries sensory information from the periphery, while feedback input into the apical tufts carries predictive information about the stimulus. B) The parallel feedforward/feedback interactions in multiple areas acts as a selection mechanism to choose which pyramidal neurons are in a state of high frequency firing, ultimately binding different aspects to represent the percept, in this case a tiger. Figure from (Larkum 2013)

Importantly, low-frequency firing is still available as a unit of information transfer in cases where excitatory input exists into the basal dendrites in the absence of excitation in the apical tufts or when the BAC mechanism is inhibited. These different modes of firing (low-frequency vs. high frequency bursting) can have substantially different influences postsynaptically (Buzsáki and Mizuseki 2014; Lisman 1997). For instance, different short-term plasticity mechanisms act as filters allowing only certain frequencies to effectively communicate with downstream neurons (Markram et al. 1998; Tsodyks and Markram 1997; Tsodyks, Pawelzik, and Markram 1998). There is evidence that presynaptic bursts cause postsynaptic potentials with substantially greater efficacy (>90%) than single action potentials (~40%) (Lisman 1997). In this way, the coincident excitatory input into a pyramidal neuron, representing the association of information from different areas of cortex, can create a unique signal that has different influence on other cortical areas than the integration of a purely feedforward (basal dendrite) input.

Tiger theory importantly serves as a concrete mechanism linking details of electrophysiology and anatomy to larger-scale concepts like perceptual binding and the representation of conscious percepts. Let us take into account the different facts that are put together here. The most basic start with the distribution of nonlinear channels in the apical dendrites of pyramidal neurons, that support nonlinear regenerative spiking, and act as a mechanism for high frequency burst firing in those cells. Anatomically, these cells make long range connections, both in feedforward pathways, where they synapse onto the basal dendrites of other pyramidal neurons, and in feedback pathways, where they synapse into layer 1, and can act to manipulate the apical dendrites of pyramidal neurons. The extracellular signature of such manipulation, in particular, the dendritic Ca spike, is a large current sink in the upper layers. Psychophysics experiments have found that such a signal correlates to conscious perception. In terms of cortical computation, the association of feedforward and feedback signals might act to bind different aspects of a percept together, though the exact details of such a process at the network level remain elusive. In the next section we discuss some theoretical frameworks that might be able to describe such a process in the cortex .

THEORETICAL CONCERNS

Before delving into the details of theoretical considerations, it will be useful to quickly review some ideas that have been covered in this thesis so far. We began by looking at psychophysical results describing signals that correlate to conscious perception. In particular, late extracellular signals that occur in the superficial layers as well as distributed information processing between different cortical regions were presented as candidate NCC. Dendrites of pyramidal neurons, supporting highly nonlinear NMDA and Ca-spiking, are as a likely origin for late extracellular signals in the superficial layers. Next, we asked what computational role such electrogenic structure can play in terms of single neuron processing of synaptic inputs, and discussed how pyramidal neurons and their dendrites act as coincidence detectors between inputs into the basal and apical dendrites, and additionally have powerful mechanisms to regulate such a coincidence mechanism. Importantly, the output of this single cell mechanism is given by a nonlinear increase in the frequency of action potential outputs, in the form of a burst at 100 Hz or greater. As discussed elsewhere (Larkum 2013) and in the previous section, the network implication of such a single cell mechanism is a general principle by which pyramidal neurons distributed across the cortex can be associated with each other, ultimately serving as the physical representation of any given conscious percept.

This series of connections - from psychology to signals, signals to neural biophysics, from biophysics to single cell computation, and single cell computation to network level computation - is built upon more than a century of work in a variety of fields. Still, the

connections between these levels of understanding require substantial amounts of work to be sufficiently fleshed out before becoming widely agreed upon scientific fact. Instead, what has been presented so far should be understood as an attempt to combine results from psychology to the physiology in a coherent and testable framework. The testability of this framework is of special import, as this requires (in the best case) taking the somewhat ineffable topic of consciousness into the realm of neurons and their functions.

As an important part of that project, a number of theoretical (and often mathematical) frameworks emerged attempting to describe the abstract underpinnings of representation and consciousness in the brain, ultimately providing a description for what it means, in terms of algorithm or function, to create a representation, or to be conscious. In the subsection that follows, we will discuss some of these frameworks and explore how they might be related to the ideas mentioned so far. This discussion will not be an in depth review, but will instead feature a largely conceptual overview. Importantly, the discussion that follows should not be interpreted as arguing for an equivalence between these various theories. Instead, what follows is a discussion of the potential areas of conceptual overlap between seemingly disparate ideas, and how they might be brought together, at least at certain points of conceptual intersection.

Hayek's theoretical psychology

We will frame this section with Friedrich Hayek's contributions to theoretical psychology, most explicitly given in his 1953 work *The Sensory Order: An Inquiry into the Foundations of Theoretical Psychology*. The reasons for this are multifold. First, Hayek's contributions mark a

stark departure from multiple theoretical frameworks of that time, for instance behaviorism[10] and the theory of psycho-physical parallelism[11], ultimately arriving at the modern understanding of the role of the brain in perception. Second, as we will see, there are direct conceptual parallels between his ideas and many of the more mathematically rigorous modern ideas. Third, Hayek's work in theoretical psychology is underappreciated, especially given both its breadth and depth. We will see that Hayek's work provides a conceptual framework that suggests overlap between a number of modern theoretical ideas, and tiger theory. With regards to tiger theory, the main point here is the connection between computation at the single cell level (e.g. as discussed, coincidence-detection, association) and more network level implications. This link is what Hayek explores.

Hayek's foundational idea is given quite straightforwardly. Hayek posited three orders: (1) the external world (which he called the physical order), (2) the brain (which he called the sensory order), and (3) the mind (which he called the phenomenal order), and focused his efforts on figuring out the relationship between the three. In Hayek's formulation, the state of the brain has an isomorphic correspondence with that of the mind. The structure of the psychological realm, for Hayek, was relational[12], and as such, that structure of relationships that make up the psyche had to be recapitulated in the structure of the neural network and its activity. This strict correspondence contrasts with the correspondence between the outside world and the

[10] In its' most extreme form behaviorism studies the link between sensory input and behavioral output, and denies that anything is really going on in the mind.

[11] Psycho-physical parallelism is the idea that there is a one-to-one correspondence between sensory input and the contents of the psyche.

[12]

structure of the brain (and thus the mind), which is imperfect, as shown by the existence of sensory illusions. The problem for Hayek was then to describe how the relational network that is the psyche can be encoded in the structure and activity of a neural network, given the computational properties of single neurons that make up that network. Although this might seem trivial to today's standards, it cannot be overstated how important this development was, especially given prevailing ideas at the time. In the end, we will see that Hayek's solution comes in a form that is in many ways remarkably similar (though missing the details of biophysics and anatomy that were not uncovered until the 1990s) to the ideas of Tiger Theory, Integrated Information theory, and Predictive Coding. We will discuss these connections. For Hayek the main questions were:

1) How can a relational network be encoded in the structure and activity of a neural network?[13]
2) How are the relations between objects in the outside world learned and encoded (imperfectly) in the neural network of the brain[14]?

[13] Quote from Hayek: "The question which thus arises for us is how it is possible to construct from the known elements of the neural system a structure which would be capable of performing such discrimination in its response to stimuli as we know our mind in fact to perform." (Hayek 1999)

[14] Quote from Hayek: "Our task will be to show how the kind of mechanism which the central nervous system provides may arrange this set of undifferentiated events in an order which possesses the same formal structure as the order of sensory qualities," and "Our task will thus be to show how these undifferentiated individual impulses or groups of impulses may obtain such a position in a system of relations to each other that in their functional significance they will resemble on eachother in a manner which corresponds strictly to the relations between the sensory qualities which are evoked by them."

The answers to these question came by positing that a foundational computation the brain performs is classification[15]. Hayek described types of classification of increasing complexity (**Figure 51**). *Simple classification* is the sorting of externally different objects into one of a set of different classes by virtue of their differing effects. One example of this is a machine that sorts balls of even diameter into a bin marked A, and balls of an odd diameter into a bin marked B. The machine is said to have classified each ball into either group A or B. Simple classification of this sort can describe simple reflexes, which act to group external stimuli by the behaviors that are produced, often by a chain of very few neurons. *Hierarchical classification*[16] occurs when successive acts of classification occur in successive stages. In this way, the groupings that occur in a previous stage become the objects to be grouped in the next stage. *Multiple classification* allows for stimuli to be in multiple groups at once, and also for multiple stimuli to be classified differently than when they occur individually[17].

[15] Quote from Hayek: "All the different events which whenever they occur produce the same effect will be said to be events of the same class, and the fact that every one of them produces the same effect will be the sole criterion which makes them members of the same class."

[16] Hayek does not use the term hierarchical in his description, and instead just treats it as a more complicated form of multiple classification.

[17] This classification may thus be 'multiple' in more than one respect. Not only may each individual event belong to more than one class, but it may also contribute to produce different responses of the machine if and only if it occurs in combination with certain other events.

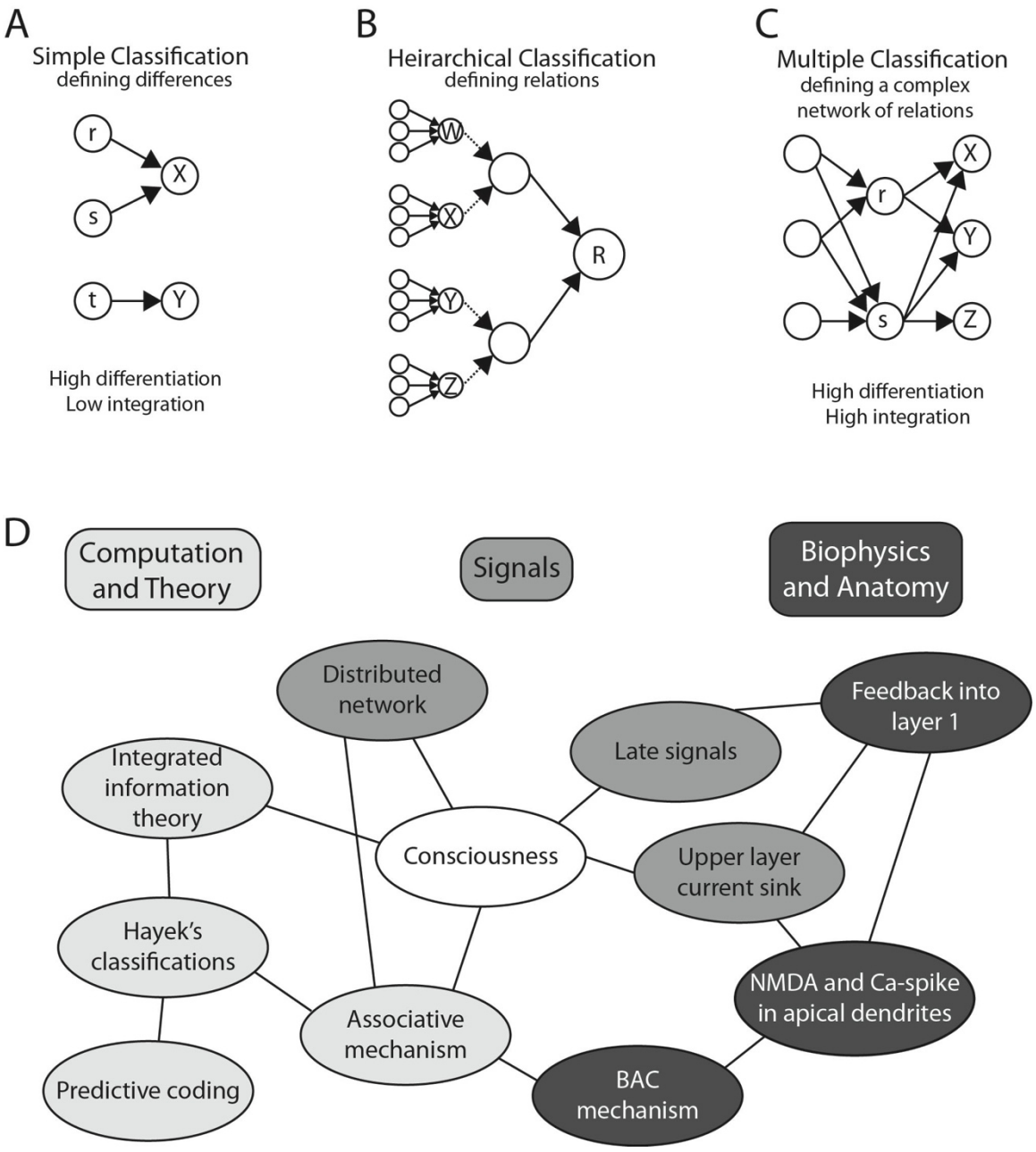

Figure 51: Combining theoretical, biophysical, and psychological aspects of neuroscience. In Hayek's theory of cortical function, neurons perform a classification function by grouping presynaptic cells that have similar postsynaptic effects together. A) In simple classification, classes are defined via their different effects on different cells. Here neuron X defines a class {r,s},

because each of that class causes neuron X to fire. Similarly, neuron Y defines a different class {t}. In the conceptual framework of integrated information theory, these "differences that cause a difference" (ie. the groups {r,s} and {t} each cause different cells to fire, confer the network with high differentiation, but not high integration. B) In hierarchical classification, simple classification occurs in multiple stages. This allows the network to create classes of classes, and importantly, to classify the relationships between different classes. For example, each of neurons W, X, Y, and Z define a class made up of three cells. The cells postsynaptic to W, X, Y, and Z require two simultaneous inputs to fire, signified by the dotted lines. This defines {W&X}, and {Y&Z} as two groups. The neuron R defines a group {W&X,Y&Z}. In this way, the neuron R requires any one of the three cells in groups W and any one of the three cells in group X, or, any one of Y and any one of Z, to fire. In this way, the cell R is said to fire to the relationship between W and X, or to the relationship between Y and Z. Because each of these relationships similarly causes R to fire, these relationships are thus the same. C) In multiple classifications, neurons can be in multiple classes, and different classes can have overlapping members. In this way, neuron r is in groups X and in group Y, and neuron s is in groups X, Y, and Z. In terms of information theory, this type of classification confers the network with integrated information, since neurons r and s have distinct, but semi-overlapping, causal effects. Thus the network has "differences that cause a difference" but also causal dependencies. D) A conceptual representation of the connections between different psychophysical signals, biophysics, and theoretical concerns.

It is this classification, carried out by the activity of postsynaptic neurons (as a function of presynaptic activity and the structure of anatomical connections), that build up a system of relations. Here, we already see a conceptual overlap with some modern ideas. For instance, Guyri Buszaki's *reader* concept is a framework for defining cell assemblies by virtue of postsynaptic effects (e.g. by collective effects on reader neurons) (Buzsáki 2010). Similarly, an important aspect of *integrated information theory*, which will be discussed more soon, is the defining of *causal groups* as *differences that make a difference*, in other words, defined by their causal postsynaptic effects (Oizumi, Albantakis, and Tononi 2014). There are even mathematical theories of computation in dynamical systems, which have not been created or even used in thinking about neural systems, which use the same conceptual idea, such as epsilon machine reconstruction (Crutchfield 1994), that may have the potential to further link these ideas to the more formal aspects of theory of computation.

In the simplest case classification, two neurons which individually cause the same postsynaptic effect are seen by the network as being equivalent, that is, as being in one class[18]. Thus, the position of these two neurons in the entire system of relationships is the same. Different neurons will in general have varying degrees of overlap in their postsynaptic effects, making it possible to talk about varying degrees of similarity with respect to their position in the system of relations. In this way, Hayek spoke of the postsynaptic activity *representing* the common attributes of presynatpic impulses that bring about that postsynaptic effect, though he preferred to say that the postsynatpic activity *constitutes* the attribute, rather than *represents* it.

This was in order to make the ontological point that these neural systems *are* what the common attributes actually are, and that they do not exist outside of the neural network. In other words, the contents of consciousness have a one-to-one correspondence not only with the activity of neurons, but also in the structure of the network in which that activity exists. Importantly, this theory differed radically from contemporaneous theories where the qualitative aspects of the mind were somehow attached to the properties of electrical signals themselves. Here, instead, we see the beginnings of an understanding of the psyche that has at its core relations and information: "it is thus the position of the individual impulse or group of impulses in the whole system of connections which gives it its distinctive quality." (Hayek 1999)

Indeed, it is important here to point out that there are separable aspects of this scheme (**Figure 51**). The first is the (simple) classification of different signals by their differing effects ("to respond differently to different impulses"). In this way if each of a group of cells causes the firing of a postsynaptic cell A, and each of a different group of cells causes the firing of a different cell B, then the network has classified these groups of cells into two distinct classes. This alone, however, does not make up a system of relations, because so far we have only described distinct attributes, A and B, with no real relationship between them. The second aspect is then that of putting those attributes in a relationship with one another. This is where multiple classification comes in. By way of example, this process occurs for instance when a postsynaptic cell requires the concurrent input of any of a member of class A alongside any of a member of class B, or the concurrent input of any member of class C and any member of

class D. In such a case, we can say that the postsynaptic cell responds to the relationship between A and B, which is the same relationship as between C and D.

These two processes have been put to quantitative work in a modern theory of consciousness, called integrated information theory (IIT), proposed by Giulio Tononi. We will not be able to describe the theory in all of its conceptual and mathematical detail here. For our purposes, it is important to point out the conceptual overlap with Hayek's ideas of classification, even though the two theories start from a very different set of considerations. The two concepts necessary for Hayek's scheme to set up a network of relations - that of setting up distinct attributes by virtue of them having distinct postsynaptic effects - and that of relating these attributes to each other by virtue of their overlapping (classifying classes) and diverging (being in multiple classes at once) inputs onto postsynaptic cells, can be conceptually reformulated into the language of information theory. In an information theoretic framework, the setting up of distinct postsynaptic effects (simple classification) confers a high entropy to the network, and thus a high informational content (information here can be estimated as the negative logarithm of the number of different potential states of the system). On the other hand, this information needs to somehow be put in a relational network. This is done by the cooperative effects of different classes both postsynaptically and on each other (multiple classification). This informational dependency is called integration in IIT. Importantly, for a system to have both high information content and high integration, and thus high integrated information, the system must simultaneously have dependencies between different attributes in order to put them in a relation with one another, but not so much dependency as to erase distinctions

between different attributes. Because of a set of principled reasons, IIT posits that systems with high integrated information are conscious (Oizumi, Albantakis, and Tononi 2014).

The exact physiological underpinnings of the thalamocortical system that give the brain high amounts of integrated information, and thus consciousness, are still illusive. However, by considering the similiarities between integrated information and classification, a way forward is seen whereby specific network and physiological structures are found to be plausible candidates. In particular, we will find that by considering increasingly complex structures of classification (and by extension increasingly complex amounts of integrated information), a hierarchical network of feedforward and feedback interactions can work as the substrate for the representation of conscious percepts, and perhaps high amounts of integrated information.

After the general description of classification and how it can be used to set up a series of relationships (**Figure 51**), Hayek goes on to find implications for this idea in terms of the structure of the cortex, and how it might act to build representations. He begins by considering the simplest of automatic reflexes, which performs a simple classification by grouping sensory inputs by the movements they produce. The evolution of the brain led to the pathways of these reflexes, often carried out by a small number of nerve cells from the periphery to the afferent, branching off and sending axons to higher areas of the brain[19]. This allows the brain

[19] It is in this idea, which is the main focus of Chapter 4 in Hayek's book, where Hayek posits a potential use for axons that send the same information to the spinal cord and back to within the cortex. Hayek talks of how there is no evidence for such axons; however, we now know that layer 5b pyramidal neurons have axons which split, sending the same information directly to the spinal cord and to relay cells in the thalamus which feedback into the cortex. The implications of this has been put into a theory of thalamocortical function, with many parallels to the ideas of Hayek, described by Sherman and Guillery (Sherman and Guillery 2002).

to receive information about both the state of the periphery and the actions which the organism is about to take. Unlike pure afferent information, information in the higher centers is available to be used for multiple classification, which can eventually send out motor commands.

Hayek posited a hierarchical scheme whereby the cortex would perform classification in successive layers, and could even perform classifications on relationships themselves, thus providing a highly complex and structured substrate for the psyche. As classifications continue on up the hierarchy, classes become more general and abstracted (classes of classes of classes, and classes of relations between classes, etc.). In the case of the evolution of more complicated control of motor-responses, the higher levels can thus act to represent and control more general groups or motor commands. Importantly, sensory input comes into an already active network, and thus interacts not only with the anatomical structure of the network, but with the activity already present in the network. Hayek describes the type of information processing that feedforward and feedback connections might serve in such a case:

> *The position of the highest centres [of the brain] in this respect is somewhat like that of the commander of an army (or the head of any other hierarchical organization), who knows that his subordinates will respond to various events in a particular manner, and who will often recognize the character of what has happened as much from the response of his subordinates as from direct observation. It will also be similar in the sense that, so long as the decision taken by his subordinates in the light of their limited but perhaps more detailed observation seems appropriate in view of his more comprehensive knowledge,*

> *he will not need to interfere; and that only if something known only to him but not to his subordinates makes those normal responses inappropriate will he have to overrule their decisions by issuing special orders.*

In this way, certain cells (or groups of cells) in the brain act by comparing their knowledge with that they receive from sensorium, only interfering in the network when there is a mismatch. A framework for neural computation, called *predictive coding*, is the mathematical description of such a process. The predictive coding framework posits that the brain uses an efficient coding scheme to represent the external world. In particular, this idea posits that natural redundancies in the external environment acting on the sensory apparatus are not explicitly represented in the brain, and instead what is represented is the deviation of the sensory drive from what is predicted. Rao and Ballard have used this idea to explain the tuning properties of cells in the retina, LGN, and V1. Importantly, this framework puts an emphasis on efficient coding in the brain, something that Hayek did not consider. Despite this, we will see that the biophysical mechanism in which feedforward and feedback signals interact in order to represent sensory perceptions, such as in the BAC mechanism described in sections 3 and 4, is conceptually consistent with the predicting coding framework.

In the parlance of predictive coding, feedback signals, from higher to lower levels in the hierarchy, convey predictions of the activity of the lower levels to which they project to, that is, predictions of general classes of motor commands given the sensory input. In turn, cells compare predictions with information from lower levels and send error signals forward in the hierarchy. In this way the predictions are continually refined. The diction here becomes

conceptually important. A restatement of the processes of refining predictions via error signals representing the comparison of prediction and feedforward sensory driven information puts the ideas regarding network level computation discussed earlier in the chapter squarely in the framework of predictive coding. Indeed, a *comparison* is biophysically nothing more than the local *integration* of feedforward and feedback signals that occur in a single pyramidal neurons (and influenced by the surrounding local circuit). A *prediction* is the *feedback activity* which predispose specific neurons in lower areas to varying degrees of activity (or inactivity). An *error* signal is then the result of the integration of feedforward and feedback signals, which are then broadcasted to higher areas of the hierarchy. Feedback activity, and its robust control over the output of pyramidal neurons via dendritic nonlinearities (NMDA and Ca-spikes), serves here as a physiological mechanism in which these kinds of computation might be carried out in the brain. Importantly, NMDA and Ca-spikes are physical mechanisms that can be both monitored and exquisitely manipulated in experiment, and thus provide a way to test hypothesis about how the cortex implements predicting coding.

In thinking of the further evolution of cortex, Hayek posits that there is fundamentally no difference between the increased control of more complicated motor responses (for instance being able to account for context), and the representation of complex percepts. Indeed, the addition of more and more layers alongside more complicated forms of classification in the network, allows for the network to form a map of the outside world. In this way the role of convergent fibers to higher levels of the hierarchy confers the binding of different attributes into more abstract attributes, while divergence confers the distribution of common attributes

to different categories (Fuster 2003; Hayek 1999). *Associations* between different attributes are given by connections that predispose, but do not on their own elicit, activity in a postsynaptic cell or group of cells. Excitatory feedback input into the apical dendrites of pyramidal neurons can serve this function (**Figure 21** and **Figure 22**). Associations of this type can occur in any direction of the hierarchy . An important aspect of such a distributed network is that higher levels of the hierarchy can, through feedback connectivity to lower areas, act to predispose certain cells in the lower areas to fire. Hayek describes the process through which multiple categorization and multiple associations interact to create a dynamic and ongoing *selection* of categories at multiple levels of the hierarchy:

> *The different associations attaching to individual impulses… will often not only not be convergent but even conflicting; and not all the representations which will form part of the following [ie. postsynaptic effects] of the elements of the complete situation will be capable of simultaneous realization, or would produce a significant new pattern if they did. Since from each element of the structure of connected fibers impulses can pass in a great variety of directions, the initial stream of impulses would merely diffuse and dissipate itself if the overlapping of the following [ie postsynaptic effects] did not determine a selection of some among the many potential paths on which they might travel.*

This type of selection, which occurs on account of multiple associations interacting with each other is consistent with the network level computation which follows from the single-cell biophysics of pyramidal neurons discussed. The main single cell computation in tiger theory,

the BAC mechanism, is that of coincident detection, or more generally stated, of integration from multiple axonal pathways. Individually, these pathways bias, but do not cause, the neuron to fire a burst of high-frequency action potentials (**Figure 21** and **Figure 22**). The pyramidal neuron thus acts as a highly nonlinear classifier of the thousands of excitatory and inhibitory inputs (and in reality even neuromodulatory inputs[20]) that impinge on the basal and tuft dendrites. These classifying neurons then send their own long-range axons to many cells in far away areas, establishing hierarchical and multiple classification. In direct analogy to what Hayek discussed, it is the collective action of this process that works to select which pyramidal neurons are active in different areas of the cortex, and which acts to form the bound representation of percepts in the brain. Here again the physiology of axons in layer 1, NMDA, and Ca-spikes serve as an experimental testbed for theories of perception in the brain.

The ideas presented in this section are all active areas of research. In the coming decade, it will be important to establish exactly where, in both mathematical and physiological foundations, these ideas overlap and differ. At the very least, Hayek's stream of thought suggests that there are connections waiting to be uncovered. Ultimately, understanding the cortical network implications of single cell and local network computation, would be made easier if a more direct connection between ideas like tiger theory, which explicitly take into account physiological and anatomical details of the type that are experimentally measurable and readily manipulated, and the more theoretical ideas of network computation like predictive coding and IIT were better understood.

[20] There is a growing literature on the various of ways neuromodulation specifically alters dendritic integration, and the inhibitory circuit that controls dendritic integration in pyramidal neurons.

Open Questions

In this final section I will list some open questions. Take notice of the diverse levels of neuroscience in which they occur in. Going forward, it will undoubtedly be important to connect these multiple levels.

1. Are single cells from ACA to V1 projecting to both L5 and L1, or only to one or the other? Are there two populations of feedback cells, one that projects to L5, and another that projects to L1?

2. Higher order thalamus projects precisely to L1. Do these fibers affect pyramidal neuron dendrites similarly or differently than cortico-corical feedback?

3. How do feedback axons influence the inhibitory circuit? Are there specific inhibitory cell types that feedback preferentially recruits?

4. What are the plastic effects of the Ca-spike in pyramidal neurons? In general, can plasticity effect intrinsic channels (e.g. Ih and the hotzone) instead of synapses? One intriguing possibility is a tight relationship between perceptual binding and learning, where both occur via the same mechanism – the Ca-spike.

5. What is the relationship between Ca-spiking and burst firing *in-vivo*?

6. How exactly can tiger theory implement predictive coding?

7. Can a network model made of abstracted neurons, like those discussed in Chapter 4, be used to show a solution to the binding problem? Do these networks necessarily have high integrated information?

8. What are the expected population level statistics expected from tiger theory? Can these be experimentally verified and tested against other theories?

9. Is the Ca-spike burst-firing mechanism necessary for contextual modulation?

10. What are the neuromodulatory effects on dendritic processing?

11. Various drugs specifically affect receptors known to be localized to the apical dendrites of pyramidal neurons. In particular, the 5HT2A (serotonin) receptor has been shown to be present in high densities specifically in dendrites that reside in the upper layers of cortex. Interestingly, drugs that target these receptors are used to treat conditions that have large changes on perception, like Schizophrenia. Indeed, drugs like DOI, LSD, mescaline, and psilocybin, all have intense perceptual effects that have been shown to be due to 5HT2A receptor activity. How do these drugs work to change affect and perception? What is the role of dendritic signaling, both in drug-induced perceptual changes, and in disease states like Schizophrenia?

APPENDIX

Layer 2/3 pyramidal neurons during sensory input

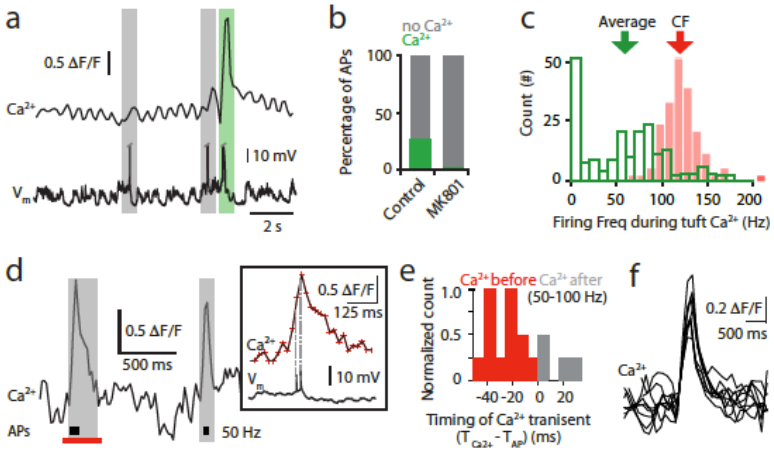

Figure 52: Tuft Ca2+ transients are not from bAPs. Backpropagating action potentials (bAPs) cause Ca2+ inux into the dendrites of layer 2/3 pyramidal neurons in a distance-dependent manner (Svoboda et al, 1999; Waters et al, 2003). We tested the possibility that bAPs cause Ca2+ transients in tuft dendrites. (a) Tuft Ca2+ trace (top) and simultaneous somatic voltage (bottom). Bars highlight somatic APs with (green) and without (grey) associated tuft Ca2+ inux. APs truncated. (b) Only 26 ± 4 % of all somatic APs were associated with a Ca2+ transient in control tuft dendrites (n = 28). Although there were still spontaneous APs when all NMDA channels were blocked by internal MK801, there were no tuft Ca2+ transients illustrating the requirement of active NMDA channels (n = 6 dendrites). (c) Histogram of -ring frequency recorded during tuft Ca2+ transients. The average -ring frequency (60 ± 3 Hz) during tuft

Ca2+ transients is considerably lower than the reported critical frequency (CF; red arrow) for evoking Ca2+ spikes in layer 2/3 pyramidal neurons (Larkum et al, 2007). Therefore bAPs alone could not evoke Ca2+ spikes which would cause Ca2+ inux into the tuft dendrites. (d) To investigate the timing of APs with dendritic Ca2+ activity, imaging frequency was increased to a maximum of 100 Hz. Typical tuft Ca2+ transients recorded at 50 Hz and somatic APs (black dashes). Grey bars, timing of Ca2+ transients compared to APs. Box, magni-cation of Ca2+ transient (top) and simultaneous somatic voltage (bottom) from the region marked with a red bar (left). Red markers on Ca2+ transient, data points (3 data points on the rising phase of the Ca2+ transient). (e) Histogram of the timing of Ca2+ transients recorded at 50-100 Hz compared to the timing of somatic APs. Timing was determined as the difference in time (ms) between the -rst data point on the rising phase of the tuft Ca2+ transient and the time at 10 % of the AP threshold for the -rst AP. On average, the onset of the tuft Ca2+ transient was 16 ± 6 ms before the somatic AP (n=17). (f) Overlay of spontaneous Ca2+ transients from a single tuft dendrite illustrating their stereotypic waveform (n=9). The amplitude of Ca2+ transients recorded in all dendrites were within one standard deviation of the mean.

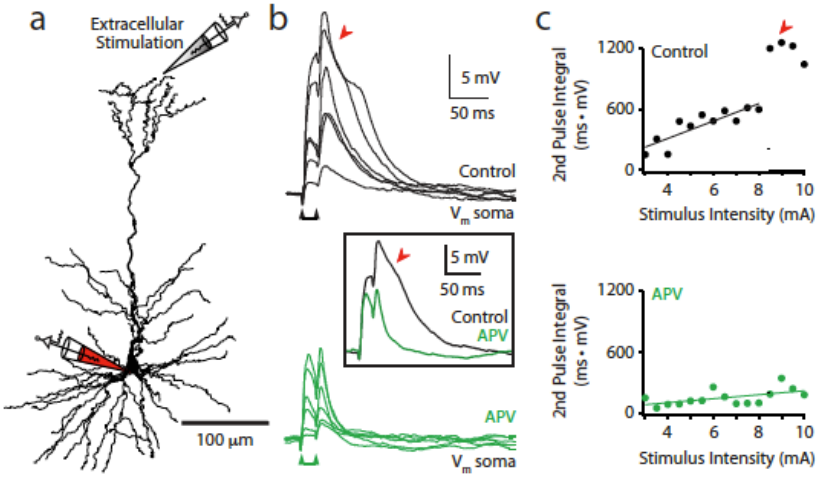

Figure 53: NMDA spikes occur in tuft dendrites of layer 2/3 pyramidal neurons in vitro. NMDA spikes have been shown in the basal dendrites of layer 2/3 pyramidal neurons but not in the tuft dendrite. (a) Experimental paradigm. Somatic recordings were made from layer 2/3 pyramidal neurons filled with Alexa Fluor 594 (50 -M) to aid the placement of an extracellular stimulation pipette in close proximity to a tuft dendrite. (b) Sequentially increasing the intensity of paired pulses (2x 1 ms pulses at 50 Hz) applied to the tuft dendrite shown in (a) resulted in a supralinear voltage response (top; black) which was blocked by bath application of APV (100 -M; bottom; green). Inset, overlay of somatic voltage during supralinear stimulation during control (black) and APV (green). (c) Integral of the somatic voltage during sequential increase in stimulus intensity for the neuron shown in (a) and (b). Block of NMDA channels by APV signficantly decreased the integral of the somatic voltage during a NMDA spike by on average 69 ± 10 % (2nd pulse; $n = 3$; $p < 0.05$; Data not shown). Data fitted with linear regression. Red arrows indicate suprathreshold response.

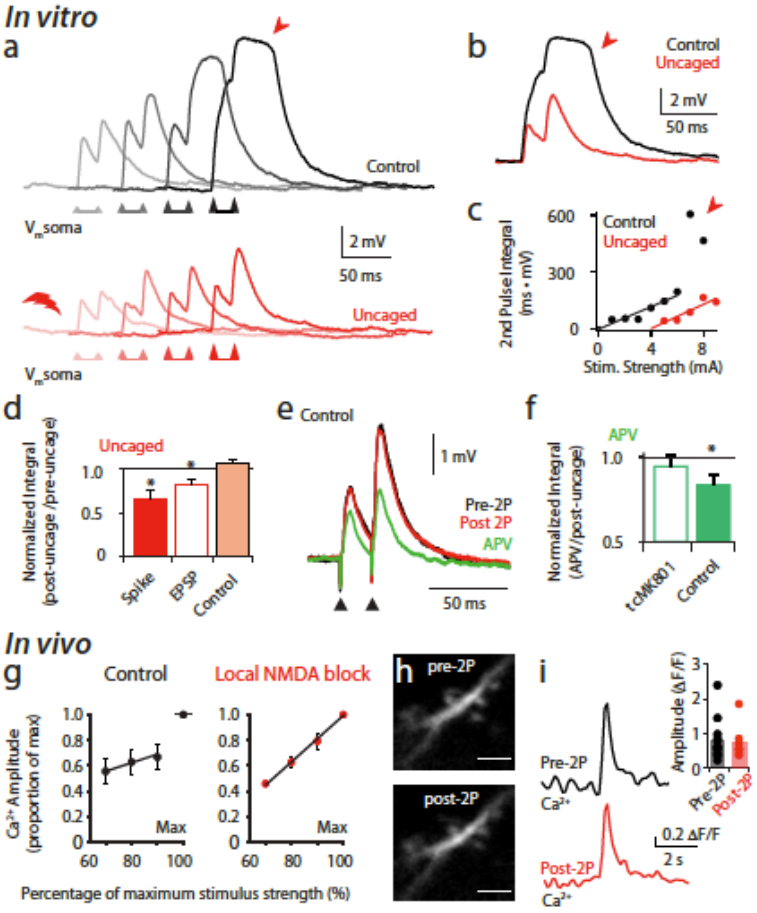

Figure 54: Two-photon uncaging of tc-MK801 blocks NMDA spikes in vitro and in vivo. (a) Somatic voltage responses to sequentially increasing intensity of extracellular stimulation (2x 1 ms pulses at 50 Hz) before (black; top) and after (red; bottom) twophoton activation (710-730 nm) of a caged NMDA channel agonist (tc-MK801) at the stimulated branch in vitro. Arrow indicates a suprathreshold response. (b) Overlay of NMDA spike before (black) and after (red) uncaging tc-MK801 for the dendrite in (a). (c) Integral of the voltage response to increasing stimulus strength for the example shown in (a) and (b) before (black) and after (red) two-photon uncaging. Data tted with linear regression. (d) Normalized integral after two-photon uncaging during a NMDA spike (red solid;

n = 5), EPSP (red empty; n = 11) and control (laser exposure in neurons without tc-MK801; light red; n = 8). (e) Example of extracellularly stimulated potentials from a control neuron (no tc-MK801) before (black) and after (red) two-photon exposure (730 nm for ~3 min) and during bath application of APV (100 -M; green). (f) Normalized integral during bath application of APV after two-photon exposure in neurons lled with tc-MK801 (empty bar; n = 3) and in control (solid bar; n = 5). (g) Amplitude of Ca2+ responses to local extracellular stimulation (2x 1ms pulses at 50 Hz) normalized to the maximum evoked response before (black; left) and after (red; right) two-photon activation of the caged NMDA channel agonist tc-MK801 in vivo (n = 6 dendrites from 3 neurons). Uncaging tc-MK801 abolishes the supralinear response to increasing extracellular stimulation intensity. (h) Here, we show that exposure to twophoton excitation alone had no measureable adverse eects on the dendritic morphology or amplitude of Ca2+ transients. Dendritic morphology before (top) and after (bottom) twophoton laser exposure (690 nm, ~ 3 min). Scale bar, 2 μm. (i) Ca2+ transients before (black; top) and after (red; bottom) exposure to two-photon light (690 nm for ~3 min) from a control layer 2/3 pyramidal neuron lled with OGB1 and Alexa Fluor 594 (and not tc-MK801). Inset, there was no difference in the peak amplitudes of Ca2+ transients before (black) and after (red) exposure to two-photon excitation in control layer 2/3 pyramidal neuron dendrites. * indicates $p < 0.05$. Error bars represent S.E.M.

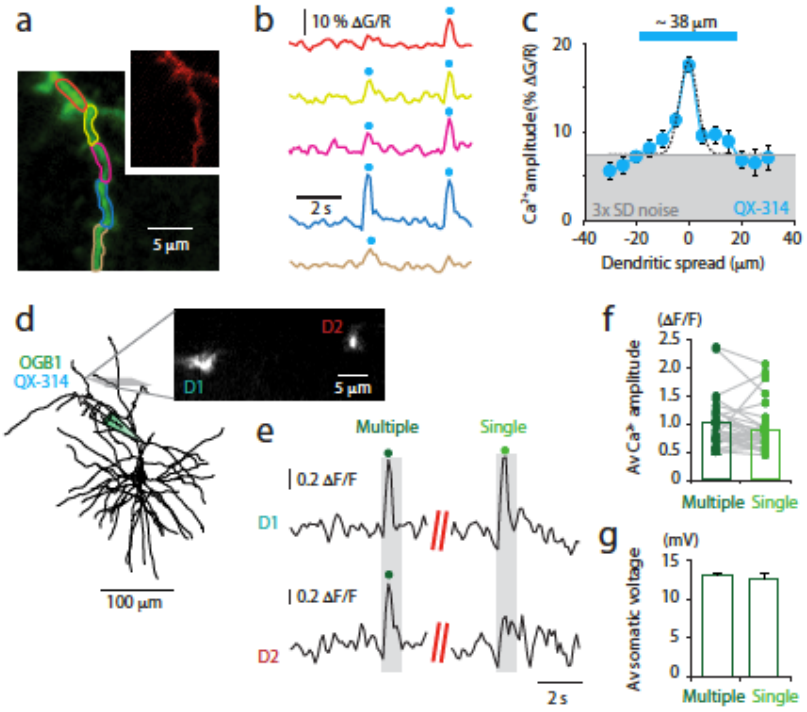

Figure 55: Ca2+ transients in the presence of the Na+ channel blocker QX-314 are similar to control - they are spatially restricted and occur in both single and multiple branches. In theory, backpropagating APs from the cell body can invade the tuft dendrite and inuence dendritic electrogenesis. We therefore tested whether tuft Ca2+ transients were inuenced by somatic activity by adding the Na+ channel blocker QX-314 to the patch pipette. (a) Two-photon image illustrating a tuft branch with 5 µm regions of interest. Inset, red - uorescence. (b) Spontaneous Ca2+ transients from the dendrite shown in (a). Note the di-erent spatial spread of the two transients. To compare di-erent dendritic regions, transients are reported as ΔG/R. (c) Average Ca2+ transient spatial spread along dendritic tuft branches (5 µm regions of interest; n = 40 transients). Data tted with

Gaussian t; dashed line. Grey line; threshold for events (> 3x standard deviation of the noise). (d) Reconstruction of layer 2/3 pyramidal neuron lled with QX-314 and two-photon image of two tuft dendrites. (e) Spontaneous Ca2+ transients which occurred in only one (single) or both (multiple) of the dendrites shown in (d). (f) Average peak amplitudes of the Ca2+ transients which occurred in single (light green) and multiple (dark green) branches (n = 508 transients in 41 branches). (g) Average somatic voltage during Ca2+ transients which occurred in single (light green) and multiple (dark green) branches (n = 9 branches) corrected for the increase in input resistance during QX-314 (see Fig. 3 and S9). Error bars represent S.E.M.

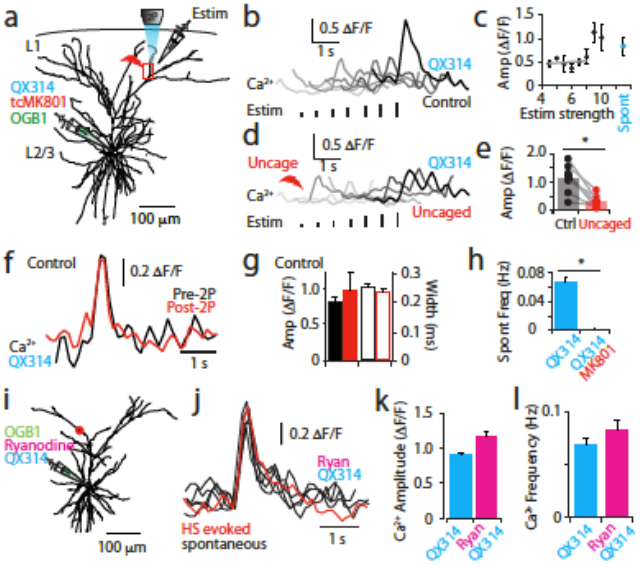

Figure 56: Extracellular stimulation evokes large Ca2+ transients in tuft dendrites which is dependent on NMDA and not voltage-sensitive channels nor internal stores. Action potential (AP) initiation was blocked by including QX-314 in the patch pipette which completely or partially blocks Na+, Ih, K+ and

Ca2+ channels (Perkins and Wong, 1995; Talbot and Sayer, 1996). (a) Reconstruction of a layer 2/3 pyramidal neuron illustrating the experimental design. Neurons were lled with QX-314 and the caged NMDA channel blocker tc-MK801, and an extracellular stimulating pipette was placed in close proximity to a branch of interest. (b) Overlay (spatially shifted for display purposes) of Ca2+ transients in response to increasing stimulus intensity from the tuft dendrite boxed in (a). (c) Average Ca2+ transient amplitude during focal extracellular stimulation of increasing intensity (black, n = 7) and during spontaneous activity (blue; n = 7). Linear regression for subthreshold responses is shown by grey line. (d) Overlay (spatially shifted for display purposes) of Ca2+ transients in response to increasing stimulus intensity after (bottom) block of NMDA receptors by twophoton (690 nm) uncaging of tc-MK801 from the boxed tuft dendrite in (a). (e) The evoked Ca2+ transient amplitude to the same suprathreshold stimulation strength was signicantly larger before (black) than after (red) block of NMDA receptors by two-photon (690 nm) uncaging of tc-MK801. (f) Two-photon laser alone doesn't a-ect Ca2+ activity. Here, we show that exposure to two-photon excitation alone had no measureable adverse e-ect on the amplitude or width of Ca2+ transients in neurons lled with QX-314. Ca2+ transients before (black) and after (red) exposure to two-photon light (690 nm for ~3 min) from a layer 2/3 pyramidal neuron lled with QX-314 (and not tc-MK801). (g) Peak amplitudes (left) and width (right) of Ca2+ transients before (black) and after (red) exposure to two-photon excitation from control layer 2/3 pyramidal neurons (n = 9). (h) Average frequency of spontaneous tuft Ca2+ transients during QX-314 alone (blue; n=40 dendrites) and QX-314 and MK801 (red; n=11 dendrites) in the patch pipette. (i) In addition to synaptic input, large Ca2+ events in the apical dendrites of layer 2/3 neurons have also been shown in vitro to be due to Ca2+ release from ryanodine-

sensitive intracellular stores (Larkum et al, 2003). We therefore tested whether the large Ca2+ events we measured in vivo were ryanodine sensitive. Reconstruction of layer 2/3 pyramidal neuron lled with ryanodine (10 M) and QX-314 (1 mM). (j) Spontaneous (black) and evoked (hindlimb stimulation; red) Ca2+ transients recorded from the neuron shown in (i). The location of the imaged tuft dendrite is indicated by a red circle in (i). (k) Average peak amplitude and (l) frequency of the Ca2+ transients in neurons lled with QX-314 alone (blue; n = 465 transients from 8 dendrites) and both QX-314 and ryanodine (fuchsia; n = 117 transients from 42 dendrites). * $p < 0.05$. Error bars represent S.E.M.

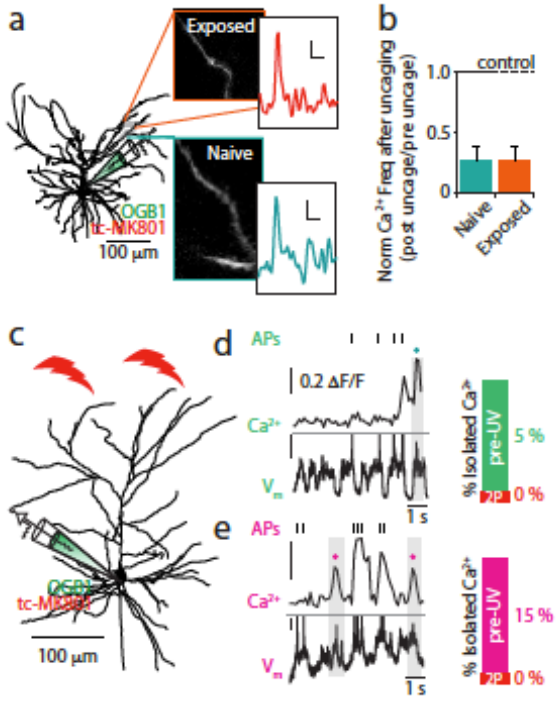

Figure 57: Uncaging of tc-MK801 locally blocks NMDA channels. Here, we show that two-photon uncaging of tc-MK801 locally blocked NMDA channels by comparing the frequency of Ca2+ transients (a & b) and the occurrence of isolated Ca2+ transients (c-e) after subsequent uncaging at a neighboring branch. (a) Neurons were lled with the caged NMDA channel blocker tc-MK801. Ca2+ transients were recorded in both naïve dendrites (no prior two-photon uncaging anywhere in the neuron; green; n = 8 dendrites) and exposed dendrites (neighboring dendrites had local NMDA channels blocked by uncaging tc-MK801; orange; n = 16 dendrites). Insets, control (pre uncaging) Ca2+ transients; scale, 0.2 ΔF/F, 1 s. The local block of NMDA channels by two-photon uncaging of tc-MK801 did not a-ect the frequency of spontaneous control Ca2+ transients in neighboring tuft dendrites (naive, 0.06 ± 0.02 Hz; exposed, 0.06 ±

0.03 Hz). (b) The frequency of spontaneous Ca2+ transients after local NMDA channel block (normalized to the control frequency) in naïve dendrites (green) compared to exposed dendrites (orange). Note, block of NMDA channels does not a-ect the e-ectiveness of uncaging tc-MK801 in neighboring tuft dendrites. (c) Reconstruction of a L2/3 pyramidal neuron lled with tc-MK801. (d) & (e), Dendritic Ca2+ trace and simultaneous somatic voltage from two di-erent tuft dendrites from the neuron shown in (c). Both dendrites have Ca2+ transients in the absence of somatic APs (indicated by colored dots). APs are indicated by dashes and are truncated. Both dendrites had Ca2+ transients (ie not correlated with a somatic AP) before (color) but not after (red) activation of tc-MK801 with two-photon laser. Error bars represent S.E.M.

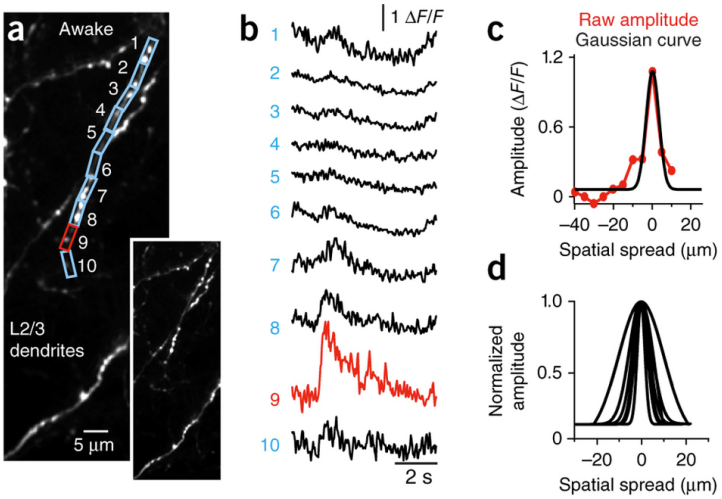

Figure 58: Dendritic Ca2+ activity can also be spatially restricted in the awake state. Layer 2/3 pyramidal neurons were transfected with the genetic Ca2+ indicator GCaMP6 and the spatial spread of spontaneous Ca2+ transients along tuft dendrites was

measured through a chronic imaging window in awake head-restrained mice. (a) Two-photon image of tuft dendrites infected with GCaMP6. (b) Dendritic Ca2+ fluorescence measured from small regions of interest (5 μm) shown in a. (c) The peak amplitude of Ca2+ transients along the dendrite shown in a and b fitted with a Gaussian curve. (d) Gaussian curves plotted from a subset of dendrites illustrating restricted Ca2+ spatial spread along dendrites in the awake state indicative of local dendritic activity.

BIBLIOGRAPHY

Chapter 1

Aru, Jaan, Nikolai Axmacher, Anne T. A. Do Lam, Juergen Fell, Christian E. Elger, Wolf Singer, and Lucia Melloni. "Local Category-Specific Gamma Band Responses in the Visual Cortex Do Not Reflect Conscious Perception." *The Journal of Neuroscience* 32, no. 43 (October 24, 2012): 14909–14. doi:10.1523/JNEUROSCI.2051-12.2012.

Baars, Bernard J. "Global Workspace Theory of Consciousness: Toward a Cognitive Neuroscience of Human Experience." *Progress in Brain Research* 150 (2005): 45–53.

Blake, Randolph, and Robert Fox. "Binocular Rivalry Suppression: Insensitive to Spatial Frequency and Orientation Change." *Vision Research* 14, no. 8 (1974): 687–92.

Breitmeyer, Bruno G., and Haluk Ogmen. "Recent Models and Findings in Visual Backward Masking: A Comparison, Review, and Update." *Perception & Psychophysics* 62, no. 8 (December 2000): 1572–95. doi:10.3758/BF03212157.

Butos, William N., and Roger G. Koppl. "Does the Sensory Order Have a Useful Economic Future." *Cognition and Economics. Advances in Austrian Economics* 9 (2007): 19–50.

Caldwell, Bruce. "Some Reflections on FA Hayek's the Sensory Order." *Journal of Bioeconomics* 6, no. 3 (2004): 239–54.

Carandini, Matteo, and Dario L. Ringach. "Predictions of a Recurrent Model of Orientation Selectivity." *Vision Research* 37, no. 21 (November 1997): 3061–71. doi:10.1016/S0042-6989(97)00100-4.

Casali, Adenauer G., Olivia Gosseries, Mario Rosanova, Mélanie Boly, Simone Sarasso, Karina R. Casali, Silvia Casarotto, et al. "A Theoretically Based Index of Consciousness Independent of Sensory Processing and Behavior." *Science Translational Medicine* 5, no. 198 (2013): 198ra105–98ra105.

Cauller, L. J., and A. T. Kulics. "A Comparison of Awake and Sleeping Cortical States by Analysis of the Somatosensory-Evoked Response of Postcentral Area 1 in Rhesus Monkey." *Experimental Brain Research* 72, no. 3 (1988): 584–92.

Crick, Francis, and Christof Koch. "A Framework for Consciousness." *Nature Neuroscience* 6, no. 2 (2003): 119–26.

———. "Are We Aware of Neural Activity in Primary Visual Cortex?" *Nature* 375, no. 6527 (1995): 121–23.

———. "Towards a Neurobiological Theory of Consciousness." In *Seminars in the Neurosciences*, 2:263–75. Saunders Scientific Publications, 1990. http://authors.library.caltech.edu/40352/.

Cumming, B. G., and A. J. Parker. "Responses of Primary Visual Cortical Neurons to Binocular Disparity without Depth Perception." *Nature* 389, no. 6648 (1997): 280–83.

De Graaf, Tom A., Po-Jang Hsieh, and Alexander T. Sack. "The 'Correlates' in Neural Correlates of Consciousness." *Neuroscience and Biobehavioral Reviews* 36, no. 1 (January 2012): 191–97. doi:10.1016/j.neubiorev.2011.05.012.

Edelman, Gerald M. "Neural Darwinism: Selection and Reentrant Signaling in Higher Brain Function." *Neuron* 10, no. 2 (1993): 115–25.

Fisch, Lior, Eran Privman, Michal Ramot, Michal Harel, Yuval Nir, Svetlana Kipervasser, Fani Andelman, et al. "Neural 'Ignition': Enhanced Activation Linked to Perceptual Awareness in Human Ventral Stream Visual Cortex." *Neuron* 64, no. 4 (November 25, 2009): 562–74. doi:10.1016/j.neuron.2009.11.001.

Flourens, Pierre. *Recherches Expérimentales Sur Les Propriétés et Les Fonctions Du Système Nerveux Dans Les Animaux Vertébrés*. Ballière, 1842. https://books.google.com/books?hl=en&lr=&id=_WRZW_d4R0IC&oi=fnd&pg=PA1&dq=flourens&ots=VVspXxOcml&sig=UEZm6vPd4Sy0rjO35u0YRTnuquU.

Friston, Karl. "The Free-Energy Principle: A Unified Brain Theory?" *Nature Reviews Neuroscience* 11, no. 2 (2010): 127–38.

Fuster, JoaquÃn M. *Cortex and Mind: Unifying Cognition*. Oxford university press, 2003. http://psycnet.apa.org/psycinfo/2002-18891-000.

Fuster, Joaquín M. "The Cognit: A Network Model of Cortical Representation." *International Journal of Psychophysiology* 60, no. 2 (2006): 125–32.

Gaillard, Raphaël, Stanislas Dehaene, Claude Adam, Stéphane Clémenceau, Dominique Hasboun, Michel Baulac, Laurent Cohen, and Lionel Naccache. "Converging Intracranial Markers of Conscious Access." *PLoS Biol* 7, no. 3 (March 17, 2009): e1000061. doi:10.1371/journal.pbio.1000061.

Gawne, Timothy J., and Julie M. Martin. "Activity of Primate V1 Cortical Neurons during Blinks." *Journal of Neurophysiology* 84, no. 5 (2000): 2691–94.

Goldstein, Kurt. "Aftereffects of Brain Injuries in War: Their Evaluation and Treatment. The Application of Psychologic Methods in the Clinic.," 1942. http://psycnet.apa.org/psycinfo/1943-00160-000.

Haider, Manfred, Paul Spong, and Donald B. Lindsley. "Attention, Vigilance, and Cortical Evoked-Potentials in Humans." *Science* 145, no. 3628 (1964): 180–82.

Hameroff, Stuart R. "Quantum Coherence in Microtubules: A Neural Basis for Emergent Consciousness?" *Journal of Consciousness Studies* 1, no. 1 (1994): 91–118.

Harlow, J. M. "Passage of an Iron Rod through the Head. 1848." *Journal of Neuropsychiatry and Clinical Neurosciences* 11, no. 2 (1999): 281–83.

Hayek, Friedrich A. "Contributions to a Theory of How Consciousness Develops." *Translated by Grete Heinz. Hoover Institution, Hayek Archives, Box* 92 (1991).

Hayek, Friedrich August. *The Sensory Order: An Inquiry into the Foundations of Theoretical Psychology*. University of Chicago Press, 1999. https://books.google.com/books?hl=en&lr=&id=UFazm1Xy_j4C&oi=fnd&pg=PR6&dq=The+Sensory+Order:+An+Inquiry+into+the+Foundations+of+Theoretical+Psychology+&ots=8M8XQppbR1&sig=X8dwgbN0lvfxmJklkhsSbTNS9iI.

Heinen, Klaartje, Jacob Jolij, and Victor A. F. Lamme. "Figure???ground Segregation Requires Two Distinct Periods of Activity in V1: A Transcranial Magnetic Stimulation Study:" *NeuroReport* 16, no. 13 (September 2005): 1483–87. doi:10.1097/01.wnr.0000175611.26485.c8.

Horwitz, Steven. "From The Sensory Order to the Liberal Order: Hayek's Non-Rationalist Liberalism." *The Review of Austrian Economics* 13, no. 1 (2000): 23–40.

Imas, Olga A., Kristina M. Ropella, B. Douglas Ward, James D. Wood, and Anthony G. Hudetz. "Volatile Anesthetics Disrupt Frontal-Posterior Recurrent Information Transfer at Gamma Frequencies in Rat." *Neuroscience Letters* 387, no. 3 (October 28, 2005): 145–50. doi:10.1016/j.neulet.2005.06.018.

Juan, Chi-Hung, and Vincent Walsh. "Feedback to V1: A Reverse Hierarchy in Vision." *Experimental Brain Research* 150, no. 2 (2003): 259–63.

King, Jean-Rémi, Jacobo D. Sitt, Frédéric Faugeras, Benjamin Rohaut, Imen El Karoui, Laurent Cohen, Lionel Naccache, and Stanislas Dehaene. "Information Sharing in the Brain Indexes Consciousness in Noncommunicative Patients." *Current Biology* 23, no. 19 (2013): 1914–19.

Knill, David C., and Alexandre Pouget. "The Bayesian Brain: The Role of Uncertainty in Neural Coding and Computation." *TRENDS in Neurosciences* 27, no. 12 (2004): 712–19.

Koivisto, Mika, Mikko Lähteenmäki, Thomas Alrik Sørensen, Signe Vangkilde, Morten Overgaard, and Antti Revonsuo. "The Earliest Electrophysiological Correlate of Visual Awareness?" *Brain and Cognition* 66, no. 1 (February 2008): 91–103. doi:10.1016/j.bandc.2007.05.010.

Koivisto, Mika, and Antti Revonsuo. "Event-Related Brain Potential Correlates of Visual Awareness." *Neuroscience & Biobehavioral Reviews*, Special Section: Developmental determinants of sensitivity and resistance to stress: A tribute to Seymour "Gig" Levine, 34, no. 6 (May 2010): 922–34. doi:10.1016/j.neubiorev.2009.12.002.

Kulics, ALBERT T., and LAWRENCE J. Cauller. "Multielectrode Exploration of Somatosensory Cortex Function in the Awake Monkey." *Sensory Processing in the Mammalian Brain: Neural Substrates and Experimental Strategies, CNUP Neuroscience Reviews*, 1989, 85–115.

Kulics, A. T., and L. J. Cauller. "Cerebral Cortical Somatosensory Evoked Responses, Multiple Unit Activity and Current Source-Densities: Their Interrelationships and Significance to Somatic Sensation as Revealed by Stimulation of the Awake Monkey's Hand." *Experimental Brain Research* 62, no. 1 (1986): 46–60.

Lamme, Victor AF. "Blindsight: The Role of Feedforward and Feedback Corticocortical Connections." *Acta Psychologica* 107, no. 1 (2001): 209–28.

———. "Towards a True Neural Stance on Consciousness." *Trends in Cognitive Sciences* 10, no. 11 (2006): 494–501.

Lamme, Victor A. F., Karl Zipser, and Henk Spekreijse. "Figure-Ground Activity in Primary Visual Cortex Is Suppressed by Anesthesia." *Proceedings of the National Academy of Sciences* 95, no. 6 (March 17, 1998): 3263–68.

Lashley, Karl S. "In Search of the Engram," 1950. http://gureckislab.org/courses/fall13/learnmem/papers/Lashley1950.pdf.

Lashley, Karl Spencer. "Brain Mechanisms and Intelligence: A Quantitative Study of Injuries to the Brain.," 1929. http://psycnet.apa.org/psycinfo/2004-16230-000/.

Massimini, Marcello, Fabio Ferrarelli, Reto Huber, Steve K. Esser, Harpreet Singh, and Giulio Tononi. "Breakdown of Cortical Effective Connectivity during Sleep." *Science (New York, N.Y.)* 309, no. 5744 (September 30, 2005): 2228–32. doi:10.1126/science.1117256.

Ma, Wei Ji, Jeffrey M. Beck, Peter E. Latham, and Alexandre Pouget. "Bayesian Inference with Probabilistic Population Codes." *Nature Neuroscience* 9, no. 11 (2006): 1432–38.

McFadden, Johnjoe. "The Conscious Electromagnetic Information (cemi) Field Theory: The Hard Problem Made Easy?" *Journal of Consciousness Studies* 9, no. 8 (2002): 45–60.

Melloni, Lucia, Caspar M. Schwiedrzik, Notger Müller, Eugenio Rodriguez, and Wolf Singer. "Expectations Change the Signatures and Timing of Electrophysiological Correlates of Perceptual Awareness." *The Journal of Neuroscience* 31, no. 4 (January 26, 2011): 1386–96. doi:10.1523/JNEUROSCI.4570-10.2011.

Nowak, Lionel G., and Jean Bullier. "The Timing of Information Transfer in the Visual System." In *Extrastriate Cortex in Primates*, 205–41. Springer, 1997. http://link.springer.com/chapter/10.1007/978-1-4757-9625-4_5.

Oizumi, Masafumi, Larissa Albantakis, and Giulio Tononi. "From the Phenomenology to the Mechanisms of Consciousness: Integrated Information Theory 3.0," 2014. http://dx.plos.org/10.1371/journal.pcbi.1003588.

Pascual-Leone, Alvaro, and Vincent Walsh. "Fast Backprojections from the Motion to the Primary Visual Area Necessary for Visual Awareness." *Science* 292, no. 5516 (2001): 510–12.

Pearce, J. M. S. "Marie-Jean-Pierre Flourens (1794-1867) and Cortical Localization." *European Neurology* 61, no. 5 (2009): 311–14. doi:10.1159/000206858.

Pockett, Susan. "The Electromagnetic Field Theory of Consciousness A Testable Hypothesis about the Characteristics of Conscious as Opposed to Non-Conscious Fields." *Journal of Consciousness Studies* 19, no. 11–12 (2012): 191–223.

Railo, Henry, Mika Koivisto, and Antti Revonsuo. "Tracking the Processes behind Conscious Perception: A Review of Event-Related Potential Correlates of Visual Consciousness." *Consciousness and Cognition* 20, no. 3 (September 2011): 972–83. doi:10.1016/j.concog.2011.03.019.

Rao, Rajesh PN, and Dana H. Ballard. "Predictive Coding in the Visual Cortex: A Functional Interpretation of Some Extra-Classical Receptive-Field Effects." *Nature Neuroscience* 2, no. 1 (1999): 79–87.

Rees, Geraint, Gabriel Kreiman, and Christof Koch. "Neural Correlates of Consciousness in Humans." *Nature Reviews Neuroscience* 3, no. 4 (2002): 261–70.

Ringach, Dario L., Michael J. Hawken, Robert Shapley, and others. "Dynamics of Orientation Tuning in Macaque Primary Visual Cortex." *Nature* 387, no. 6630 (1997): 281–84.

Sachidhanandam, Shankar, Varun Sreenivasan, Alexandros Kyriakatos, Yves Kremer, and Carl C. H. Petersen. "Membrane Potential Correlates of Sensory Perception in Mouse Barrel Cortex." *Nature Neuroscience* 16, no. 11 (November 2013): 1671–77. doi:10.1038/nn.3532.

Salti, Moti, Simo Monto, Lucie Charles, Jean-Remi King, Lauri Parkkonen, and Stanislas Dehaene. "Distinct Cortical Codes and Temporal Dynamics for Conscious and Unconscious Percepts." *eLife*, May 21, 2015, e05652. doi:10.7554/eLife.05652.

Sarasso, Simone, Melanie Boly, Martino Napolitani, Olivia Gosseries, Vanessa Charland-Verville, Silvia Casarotto, Mario Rosanova, et al. "Consciousness and Complexity during Unresponsiveness Induced by Propofol, Xenon, and Ketamine." *Current Biology* 0, no. 0. Accessed November 20, 2015. doi:10.1016/j.cub.2015.10.014.

Sherman, S. Murray, and R. W. Guillery. "Distinct Functions for Direct and Transthalamic Corticocortical Connections." *Journal of Neurophysiology* 106, no. 3 (September 1, 2011): 1068–77. doi:10.1152/jn.00429.2011.

———. "The Role of the Thalamus in the Flow of Information to the Cortex." *Philosophical Transactions of the Royal Society B: Biological Sciences* 357, no. 1428 (2002): 1695–1708.

Silverstein, Brian H., Michael Snodgrass, Howard Shevrin, and Ramesh Kushwaha. "P3b, Consciousness, and Complex Unconscious Processing." *Cortex* 73 (December 2015): 216–27. doi:10.1016/j.cortex.2015.09.004.

Spong, Paul, Manfred Haider, and Donald B. Lindsley. "Selective Attentiveness and Cortical Evoked Responses to Visual and Auditory Stimuli." *Science* 148, no. 3668 (1965): 395–97.

Sugase, Y., S. Yamane, S. Ueno, and K. Kawano. "Global and Fine Information Coded by Single Neurons in the Temporal Visual Cortex." *Nature* 400, no. 6747 (August 26, 1999): 869–73. doi:10.1038/23703.

Tsuchiya, Naotsugu, Melanie Wilke, Stefan Frässle, and Victor A. F. Lamme. "No-Report Paradigms: Extracting the True Neural Correlates of Consciousness." *Trends in Cognitive Sciences*. Accessed November 20, 2015. doi:10.1016/j.tics.2015.10.002.

Weiskrantz, Lawrence. *Blindsight: A Case Study and Implications*. Oxford University Press, 1986.

Yuille, Alan, and Daniel Kersten. "Vision as Bayesian Inference: Analysis by Synthesis?" *Trends in Cognitive Sciences* 10, no. 7 (2006): 301–8.

Zipser, Karl, Victor AF Lamme, and Peter H. Schiller. "Contextual Modulation in Primary Visual Cortex." *The Journal of Neuroscience* 16, no. 22 (1996): 7376–89.

Chapter 2

Andrade, R. (1991). Blockade of neurotransmitter-activated K+ conductance by QX-314 in the rat hippocampus. *Eur J Pharmacol, 199*(2), 259-262. doi: 0014-2999(91)90467-5 [pii]

Andrew D. Huberman, C. M. N. (2011). What can mice tell us about how vision works? *Trends in Neurosciences, 34*(9), 464-473.

Antic, S. D., Zhou, W. L., Moore, A. R., Short, S. M., & Ikonomu, K. D. (2010). The decade of the dendritic NMDA spike. *J Neurosci Res, 88*(14), 2991-3001.

Berger, T., Larkum, M. E., & Luscher, H. R. (2001). High I(h) channel density in the distal apical dendrite of layer V pyramidal cells increases bidirectional attenuation of EPSPs. *J Neurophysiol, 85*(2), 855-868.

Bock, D. D., Lee, W. C., Kerlin, A. M., Andermann, M. L., Hood, G., Wetzel, A. W., . . . Reid, R. C. (2011). Network anatomy and in vivo physiology of visual cortical neurons. *Nature, 471*(7337), 177-182. doi: nature09802 [pii]

10.1038/nature09802

Branco, T., Clark, B. A., & Hausser, M. (2010). Dendritic discrimination of temporal input sequences in cortical neurons. *Science, 329*(5999), 1671-1675. doi: 10.1126/science.1189664

science.1189664 [pii]

Branco, T., & Hausser, M. (2011). Synaptic integration gradients in single cortical pyramidal cell dendrites. *Neuron, 69*(5), 885-892. doi: 10.1016/j.neuron.2011.02.006

S0896-6273(11)00103-6 [pii]

Carandini, M. (2012). From circuits to behavior: a bridge too far? *Nat Neurosci, 15*(4), 507-509. doi: nn.3043 [pii]

10.1038/nn.3043

Chen, T. W., Wardill, T. J., Sun, Y., Pulver, S. R., Renninger, S. L., Baohan, A., . . . Kim, D. S. (2013). Ultrasensitive fluorescent proteins for imaging neuronal activity. *Nature, 499*(7458), 295-300. doi: 10.1038/nature12354
nature12354 [pii]
Chen, X., Leischner, U., Rochefort, N. L., Nelken, I., & Konnerth, A. (2011). Functional mapping of single spines in cortical neurons in vivo. *Nature, 475*(7357), 501-505. doi: 10.1038/nature10193
nature10193 [pii]
Chen, X., Rochefort, N. L., Sakmann, B., & Konnerth, A. (2013). Reactivation of the same synapses during spontaneous up states and sensory stimuli. *Cell Rep, 4*(1), 31-39. doi: 10.1016/j.celrep.2013.05.042
S2211-1247(13)00275-1 [pii]
Connors, B. W., & Prince, D. A. (1982). Effects of local anesthetic QX-314 on the membrane properties of hippocampal pyramidal neurons. *J Pharmacol Exp Ther, 220*(3), 476-481.
Dong, H. W. (2008). *The Allen reference atlas: A digital color brain atlas of the C57Bl/6J male mouse.*: John Wiley & Sons Inc.
Glickfeld, L. L., Andermann, M. L., Bonin, V., & Reid, R. C. (2013). Cortico-cortical projections in mouse visual cortex are functionally target specific. *Nat Neurosci, 16*(2), 219-226. doi: nn.3300 [pii]
10.1038/nn.3300
Gordon, U., Polsky, A., & Schiller, J. (2006). Plasticity compartments in basal dendrites of neocortical pyramidal neurons. *J Neurosci, 26*(49), 12717-12726. doi: 26/49/12717 [pii]
10.1523/JNEUROSCI.3502-06.2006
Hill, D. N., Varga, Z., Jia, H., Sakmann, B., & Konnerth, A. (2013). Multibranch activity in basal and tuft dendrites during firing of layer 5 cortical neurons in vivo. *Proc Natl Acad Sci U S A, 110*(33), 13618-13623. doi: 10.1073/pnas.1312599110
1312599110 [pii]
Jia, H., Rochefort, N. L., Chen, X., & Konnerth, A. (2010). Dendritic organization of sensory input to cortical neurons in vivo. *Nature, 464*(7293), 1307-1312. doi: nature08947 [pii]
10.1038/nature08947
Koch, C. (1999). *Biophysics of Computation, Information Processing in Single Neurons*: Oxford University Press.
Kole, M. H., Hallermann, S., & Stuart, G. J. (2006). Single Ih channels in pyramidal neuron dendrites: properties, distribution, and impact on action potential output. *J Neurosci, 26*(6), 1677-1687. doi: 26/6/1677 [pii]
10.1523/JNEUROSCI.3664-05.2006
Larkum, M. E., Kaiser, K. M., & Sakmann, B. (1999). Calcium electrogenesis in distal apical dendrites of layer 5 pyramidal cells at a critical frequency of back-propagating action potentials. *Proc Natl Acad Sci U S A, 96*(25), 14600-14604.
Larkum, M. E., & Nevian, T. (2008). Synaptic clustering by dendritic signalling mechanisms. *Curr Opin Neurobiol, 18*(3), 321-331. doi: 10.1016/j.conb.2008.08.013
S0959-4388(08)00086-X [pii]
Larkum, M. E., Nevian, T., Sandler, M., Polsky, A., & Schiller, J. (2009). Synaptic integration in tuft dendrites of layer 5 pyramidal neurons: a new unifying principle. *Science, 325*(5941), 756-760.
Larkum, M. E., Waters, J., Sakmann, B., & Helmchen, F. (2007a). Dendritic spikes in apical Dendrites of neocortical layer 2/3 pyramidal neurons. *Journal of Neuroscience, 27*(34), 8999-9008. doi: Doi 10.1523/Jneurosci.1717-07.2007
Larkum, M. E., Waters, J., Sakmann, B., & Helmchen, F. (2007b). Dendritic spikes in apical dendrites of neocortical layer 2/3 pyramidal neurons. *J Neurosci, 27*(34), 8999-9008. doi: 27/34/8999 [pii]
10.1523/JNEUROSCI.1717-07.2007
Larkum, M. E., & Zhu, J. J. (2002). Signaling of layer 1 and whisker-evoked Ca2+ and Na+ action potentials in distal and terminal dendrites of rat neocortical pyramidal neurons in vitro and in vivo. *J Neurosci, 22*(16), 6991-7005. doi: 20026717
22/16/6991 [pii]

Lavzin, M., Rapoport, S., Polsky, A., Garion, L., & Schiller, J. (2012). Nonlinear dendritic processing determines angular tuning of barrel cortex neurons in vivo. *Nature, 490*(7420), 397-401. doi: 10.1038/nature11451

nature11451 [pii]

Ledergerber, D., & Larkum, M. E. (2010a). Properties of layer 6 pyramidal neuron apical dendrites. *J Neurosci, 30*(39), 13031-13044. doi: 10.1523/JNEUROSCI.2254-10.2010

30/39/13031 [pii]

Ledergerber, D., & Larkum, M. E. (2010b). Properties of Layer 6 Pyramidal Neuron Apical Dendrites. *Journal of Neuroscience, 30*(39), 13031-13044. doi: Doi 10.1523/Jneurosci.2254-10.2010

Ledergerber, D., & Larkum, M. E. (2012). The time window for generation of dendritic spikes by coincidence of action potentials and EPSPs is layer specific in somatosensory cortex. *PLoS One, 7*(3), e33146. doi: 10.1371/journal.pone.0033146

PONE-D-11-10306 [pii]

Magee, J., Hoffman, D., Colbert, C., & Johnston, D. (1998). Electrical and calcium signaling in dendrites of hippocampal pyramidal neurons. *Annu Rev Physiol, 60*, 327-346. doi: 10.1146/annurev.physiol.60.1.327

Major, G., Larkum, M. E., & Schiller, J. (2013). Active properties of neocortical pyramidal neuron dendrites. *Annu Rev Neurosci, 36*, 1-24. doi: 10.1146/annurev-neuro-062111-150343

Major, G., Polsky, A., Denk, W., Schiller, J., & Tank, D. W. (2008). Spatiotemporally graded NMDA spike/plateau potentials in basal dendrites of neocortical pyramidal neurons. *J Neurophysiol, 99*(5), 2584-2601. doi: 10.1152/jn.00011.2008

00011.2008 [pii]

Marshel, J. H., Garrett, M. E., Nauhaus, I., & Callaway, E. M. (2011). Functional specialization of seven mouse visual cortical areas. *Neuron, 72*(6), 1040-1054. doi: S0896-6273(11)01046-4 [pii]

10.1016/j.neuron.2011.12.004

Mayer, M. L., Westbrook, G. L., & Guthrie, P. B. (1984). Voltage-dependent block by Mg2+ of NMDA responses in spinal cord neurones. *Nature, 309*(5965), 261-263.

Mel, B. W. (1993). Synaptic integration in an excitable dendritic tree. *J Neurophysiol, 70*(3), 1086-1101.

Milojkovic, B. A., Zhou, W. L., & Antic, S. D. (2007). Voltage and calcium transients in basal dendrites of the rat prefrontal cortex. *Journal of Physiology-London, 585*(2), 447-468. doi: Doi 10.1113/Jphysiol.2007.142315

Nevian, T., Larkum, M. E., Polsky, A., & Schiller, J. (2007). Properties of basal dendrites of layer 5 pyramidal neurons: a direct patch-clamp recording study. *Nat Neurosci, 10*(2), 206-214.

Perkins, K. L., & Wong, R. K. (1995). Intracellular QX-314 blocks the hyperpolarization-activated inward current Iq in hippocampal CA1 pyramidal cells. *J Neurophysiol, 73*(2), 911-915.

Plotkin, J. L., Day, M., & Surmeier, D. J. (2011). Synaptically driven state transitions in distal dendrites of striatal spiny neurons. *Nat Neurosci, 14*(7), 881-888. doi: 10.1038/nn.2848

nn.2848 [pii]

Polsky, A., Mel, B. W., & Schiller, J. (2004). Computational subunits in thin dendrites of pyramidal cells. *Nat Neurosci, 7*(6), 621-627.

Reeve, J. E., Kohl, M. M., Rodriguez-Moreno, A., Paulsen, O., & Anderson, H. L. (2012a). Addendum: Caged intracellular NMDA receptor blockers for the study of subcellular ion channel function. *Commun Integrat Biol, 5*(3), 1-3.

Reeve, J. E., Kohl, M. M., Rodriguez-Moreno, A., Paulsen, O., & Anderson, H. L. (2012b). Caged intracellular NMDA receptor blockers for the study of subcellular ion channel function. *Commun Integr Biol, 5*(3), 240-242. doi: 10.4161/cib.19400

2011CIB0208R [pii]

Rhodes, P. (2006). The properties and implications of NMDA spikes in neocortical pyramidal cells. *J Neurosci, 26*(25), 6704-6715. doi: 26/25/6704 [pii]

10.1523/JNEUROSCI.3791-05.2006

Rodriguez-Moreno, A., Kohl, M. M., Reeve, J. E., Eaton, T. R., Collins, H. A., Anderson, H. L., & Paulsen, O. (2011). Presynaptic induction and expression of timing-dependent long-term depression demonstrated by compartment-specific photorelease of a use-dependent NMDA receptor antagonist. *J Neurosci, 31*(23), 8564-8569. doi: 10.1523/JNEUROSCI.0274-11.2011

31/23/8564 [pii]

Schiller, J., Major, G., Koester, H. J., & Schiller, Y. (2000). NMDA spikes in basal dendrites of cortical pyramidal neurons. *Nature, 404*(6775), 285-289. doi: Doi 10.1038/35005094

Schiller, J., & Schiller, Y. (2001). NMDA receptor-mediated dendritic spikes and coincident signal amplification. *Curr Opin Neurobiol, 11*(3), 343-348. doi: S0959-4388(00)00217-8 [pii]

Schiller, J., Schiller, Y., Stuart, G., & Sakmann, B. (1997). Calcium action potentials restricted to distal apical dendrites of rat neocortical pyramidal neurons. *Journal of Physiology-London, 505*(3), 605-616. doi: Doi 10.1111/J.1469-7793.1997.605ba.X

Seamans, J. K., Gorelova, N. A., & Yang, C. R. (1997). Contributions of voltage-gated Ca2+ channels in the proximal versus distal dendrites to synaptic integration in prefrontal cortical neurons. *J Neurosci, 17*(15), 5936-5948.

Self, M. W., Kooijmans, R. N., Super, H., Lamme, V. A., & Roelfsema, P. R. (2012). Different glutamate receptors convey feedforward and recurrent processing in macaque V1. *Proc Natl Acad Sci U S A, 109*(27), 11031-11036. doi: 10.1073/pnas.1119527109

1119527109 [pii]

Smith, S. L., Smith, I. T., Branco, T., & Hausser, M. (2013). Dendritic spikes enhance stimulus selectivity in cortical neurons in vivo. *Nature, 503*(7474), 115-120. doi: nature12600 [pii]

10.1038/nature12600

Stuart, G., Spruston, N., Sakmann, B., & Hausser, M. (1997). Action potential initiation and backpropagation in neurons of the mammalian CNS. *Trends Neurosci, 20*(3), 125-131.

Stuart, G. J., & Sakmann, B. (1994). Active Propagation of Somatic Action-Potentials into Neocortical Pyramidal Cell Dendrites. *Nature, 367*(6458), 69-72. doi: Doi 10.1038/367069a0

Svoboda, K., Denk, W., Kleinfeld, D., & Tank, D. W. (1997). In vivo dendritic calcium dynamics in neocortical pyramidal neurons. *Nature, 385*(6612), 161-165. doi: 10.1038/385161a0

Svoboda, K., Helmchen, F., Denk, W., & Tank, D. W. (1999). Spread of dendritic excitation in layer 2/3 pyramidal neurons in rat barrel cortex in vivo. *Nat Neurosci, 2*(1), 65-73. doi: 10.1038/4569

Talbot, M. J., & Sayer, R. J. (1996). Intracellular QX-314 inhibits calcium currents in hippocampal CA1 pyramidal neurons. *J Neurophysiol, 76*(3), 2120-2124.

Taylor, R. E. (1959). Effect of procaine on electrical properties of squid axon membrane. *Am J Physiol, 196*(5), 1071-1078.

Waters, J., & Helmchen, F. (2006). Background synaptic activity is sparse in neocortex. *Journal of Neuroscience, 26*(32), 8267-8277. doi: Doi 10.1523/Jneurosci.2152-06.2006

Waters, J., Larkum, M., Sakmann, B., & Helmchen, F. (2003). Supralinear Ca2+ influx into dendritic tufts of layer 2/3 neocortical pyramidal neurons in vitro and in vivo. *J Neurosci, 23*(24), 8558-8567. doi: 23/24/8558 [pii]

Williams, S. R., & Stuart, G. J. (1999). Mechanisms and consequences of action potential burst firing in rat neocortical pyramidal neurons. *J Physiol, 521 Pt 2*, 467-482. doi: PHY_9930 [pii]

Williams, S. R., & Stuart, G. J. (2002). Dependence of EPSP efficacy on synapse location in neocortical pyramidal neurons. *Science, 295*(5561), 1907-1910. doi: 10.1126/science.1067903

295/5561/1907 [pii]

Xu, N. L., Harnett, M. T., Williams, S. R., Huber, D., O'Connor, D. H., Svoboda, K., & Magee, J. C. (2012). Nonlinear dendritic integration of sensory and motor input during an active sensing task. *Nature*. doi: 10.1038/nature11601

nature11601 [pii]

Zhu, J. J. (2000). Maturation of layer 5 neocortical pyramidal neurons: amplifying salient layer 1 and layer 4 inputs by Ca2+ action potentials in adult rat tuft dendrites. *J Physiol, 526 Pt 3*, 571-587. doi: PHY_0791 [pii]

Chapter 3

Anderson, E. B., Mitchell, J. F., & Reynolds, J. H. (2011). Attentional modulation of firing rate varies with burstiness across putative pyramidal neurons in macaque visual area V4. *J Neurosci, 31*(30), 10983-10992. doi: 31/30/10983 [pii]

10.1523/JNEUROSCI.0027-11.2011

Andrade, R. (1991). Blockade of neurotransmitter-activated K+ conductance by QX-314 in the rat hippocampus. *Eur J Pharmacol, 199*(2), 259-262. doi: 0014-2999(91)90467-5 [pii]

Bair, W., Koch, C., Newsome, W., & Britten, K. (1994). Power spectrum analysis of bursting cells in area MT in the behaving monkey. *J Neurosci, 14*(5 Pt 1), 2870-2892.

Berger, T., Larkum, M. E., & Luscher, H. R. (2001). High I(h) channel density in the distal apical dendrite of layer V pyramidal cells increases bidirectional attenuation of EPSPs. *J Neurophysiol, 85*(2), 855-868.

Cattaneo, A., Maffei, L., & Morrone, C. (1981). Two firing patterns in the discharge of complex cells encoding different attributes of the visual stimulus. *Exp Brain Res, 43*(1), 115-118.

Chalifoux, J. R., & Carter, A. G. (2011). GABAB receptor modulation of voltage-sensitive calcium channels in spines and dendrites. *J Neurosci, 31*(11), 4221-4232. doi: 31/11/4221 [pii]

10.1523/JNEUROSCI.4561-10.2011

Connors, B. W., & Prince, D. A. (1982). Effects of local anesthetic QX-314 on the membrane properties of hippocampal pyramidal neurons. *J Pharmacol Exp Ther, 220*(3), 476-481.

de Kock, C. P., & Sakmann, B. (2008). High frequency action potential bursts (>or= 100 Hz) in L2/3 and L5B thick tufted neurons in anaesthetized and awake rat primary somatosensory cortex. *J Physiol, 586*(14), 3353-3364. doi: jphysiol.2008.155580 [pii]

10.1113/jphysiol.2008.155580

Hay, E., Hill, S., Schurmann, F., Markram, H., & Segev, I. (2011). Models of neocortical layer 5b pyramidal cells capturing a wide range of dendritic and perisomatic active properties. *PLoS Comput Biol, 7*(7), e1002107. doi: 10.1371/journal.pcbi.1002107

PCOMPBIOL-D-10-00224 [pii]

Hines, M. L. (1998). The Neurosimulator NEURON. In C. Koch & I. Segev (Eds.), *Methods in Neuronal Modeling* (pp. 129-136). Cambridge, MA: MIT Press. (Reprinted from: NOT IN FILE).

Kole, M. H., Hallermann, S., & Stuart, G. J. (2006). Single Ih channels in pyramidal neuron dendrites: properties, distribution, and impact on action potential output. *J Neurosci, 26*(6), 1677-1687. doi: 26/6/1677 [pii]

10.1523/JNEUROSCI.3664-05.2006

Larkum, M. E., Nevian, T., Sandler, M., Polsky, A., & Schiller, J. (2009). Synaptic integration in tuft dendrites of layer 5 pyramidal neurons: a new unifying principle. *Science, 325*(5941), 756-760.

Larkum, M. E., Waters, J., Sakmann, B., & Helmchen, F. (2007). Dendritic spikes in apical dendrites of neocortical layer 2/3 pyramidal neurons. *J Neurosci, 27*(34), 8999-9008.

Livingstone, M. S., Freeman, D. C., & Hubel, D. H. (1996). Visual responses in V1 of freely viewing monkeys. *Cold Spring Harb Symp Quant Biol, 61*, 27-37.

Palmer, L., Murayama, M., & Larkum, M. (2012). Inhibitory regulation of dendritic activity in vivo. *Frontiers in Neural Circuits, 6*. doi: Artn 26

Doi 10.3389/Fncir.2012.00026

Palmer, L. M., Shai, A. S., Reeve, J. E., Anderson, H. L., Paulsen, O., & Larkum, M. E. (2014). NMDA spikes enhance action potential generation during sensory input. *Nat Neurosci, 17*(3), 383-390. doi: nn.3646 [pii]

10.1038/nn.3646

Perkins, K. L., & Wong, R. K. (1995). Intracellular QX-314 blocks the hyperpolarization-activated inward current Iq in hippocampal CA1 pyramidal cells. *J Neurophysiol, 73*(2), 911-915.

Smith, S. L., Smith, I. T., Branco, T., & Hausser, M. (2013). Dendritic spikes enhance stimulus selectivity in cortical neurons in vivo. *Nature, 503*(7474), 115-120. doi: nature12600 [pii]

10.1038/nature12600

Stuart, G., & Spruston, N. (1998). Determinants of voltage attenuation in neocortical pyramidal neuron dendrites. *J Neurosci, 18*(10), 3501-3510.

Talbot, M. J., & Sayer, R. J. (1996). Intracellular QX-314 inhibits calcium currents in hippocampal CA1 pyramidal neurons. *J Neurophysiol, 76*(3), 2120-2124.

Taylor, R. E. (1959). Effect of procaine on electrical properties of squid axon membrane. *Am J Physiol, 196*(5), 1071-1078.

Waters, J., Larkum, M., Sakmann, B., & Helmchen, F. (2003). Supralinear Ca2+ influx into dendritic tufts of layer 2/3 neocortical pyramidal neurons in vitro and in vivo. *J Neurosci, 23*(24), 8558-8567. doi: 23/24/8558 [pii]

Zador, A. M., Agmon-Snir, H., & Segev, I. (1995). The morphoelectrotonic transform: a graphical approach to dendritic function. *J Neurosci, 15*(3 Pt 1), 1669-1682.

Zhu, J. J. (2000). Maturation of layer 5 neocortical pyramidal neurons: amplifying salient layer 1 and layer 4 inputs by Ca2+ action potentials in adult rat tuft dendrites. *J Physiol, 526 Pt 3*, 571-587. doi: PHY_0791 [pii]

Chapter 4

Antic, S. D., Zhou, W. L., Moore, A. R., Short, S. M., & Ikonomu, K. D. (2010). The decade of the dendritic NMDA spike. *J Neurosci Res, 88*(14), 2991-3001.

Ascoli, G. A., Alonso-Nanclares, L., Anderson, S. A., Barrionuevo, G., Benavides-Piccione, R., Burkhalter, A., . . . Yuste, R. (2008). Petilla terminology: nomenclature of features of GABAergic interneurons of the cerebral cortex. *Nat Rev Neurosci, 9*(7), 557-568. doi: nrn2402 [pii]

10.1038/nrn2402

Atallah, B. V., Scanziani, M., & Carandini, M. (2014). Atallah et al. reply. *Nature, 508*(7494), E3. doi: nature13129 [pii]

10.1038/nature13129

Burgess, N., Barry, C., & O'Keefe, J. (2007). An oscillatory interference model of grid cell firing. *Hippocampus, 17*(9), 801-812. doi: 10.1002/hipo.20327

Buzsaki, G. (2010). Neural syntax: cell assemblies, synapsembles, and readers. *Neuron, 68*(3), 362-385. doi: S0896-6273(10)00765-8 [pii]

10.1016/j.neuron.2010.09.023

Carnevale, N. T., Hines, M.L. (2006). *The NEURON book*. Cambridge, UK: Cambridge University Press.

Chalifoux, J. R., & Carter, A. G. (2011). GABAB receptor modulation of voltage-sensitive calcium channels in spines and dendrites. *J Neurosci, 31*(11), 4221-4232. doi: 31/11/4221 [pii]

10.1523/JNEUROSCI.4561-10.2011

Cutsuridis, V., & Taxidis, J. (2013). Deciphering the role of CA1 inhibitory circuits in sharp wave-ripple complexes. *Front Syst Neurosci, 7*, 13. doi: 10.3389/fnsys.2013.00013

El-Boustani, S., Wilson, N. R., Runyan, C. A., & Sur, M. (2014). El-Boustani et al. reply. *Nature, 508*(7494), E3-4. doi: nature13130 [pii]

10.1038/nature13130

Freund, T. F., & Buzsáki, G. (1996). Interneurons of the hippocampus. *Hippocampus, 6*(4), 347-470. doi: 10.1002/(sici)1098-1063(1996)6:4<347::aid-hipo1>3.0.co;2-i

Gabbiani, F., Krapp, H. G., Koch, C., & Laurent, G. (2002). Multiplicative computation in a visual neuron sensitive to looming. *Nature, 420*(6913), 320-324. doi: 10.1038/nature01190

nature01190 [pii]

Gidon, A., & Segev, I. (2012). Principles Governing the Operation of Synaptic Inhibition in Dendrites. *Neuron, 75*(2), 330-341. doi: Doi 10.1016/J.Neuron.2012.05.015

Hay, E., Hill, S., Schurmann, F., Markram, H., & Segev, I. (2011). Models of neocortical layer 5b pyramidal cells capturing a wide range of dendritic and perisomatic active properties. *PLoS Comput Biol, 7*(7), e1002107. doi: 10.1371/journal.pcbi.1002107

PCOMPBIOL-D-10-00224 [pii]

Jadi, M., Polsky, A., Schiller, J., & Mel, B. (2010). *Effect of location of inhibition on NMDA spikes in pyramidal cells*. Paper presented at the Society for Neuroscience 2010, San Diego, CA.

Jadi, M., Polsky, A., Schiller, J., & Mel, B. W. (2012). Location-Dependent Effects of Inhibition on Local Spiking in Pyramidal Neuron Dendrites. *Plos Computational Biology, 8*(6). doi: Artn E1002550

Doi 10.1371/Journal.Pcbi.1002550

Jarsky, T., Roxin, A., Kath, W. L., & Spruston, N. (2005). Conditional dendritic spike propagation following distal synaptic activation of hippocampal CA1 pyramidal neurons. *Nat Neurosci, 8*(12), 1667-1676. doi: nn1599 [pii]

10.1038/nn1599
Jiang, X. L., Wang, G. F., Lee, A. J., Stornetta, R. L., & Zhu, J. J. (2013). The organization of two new cortical interneuronal circuits. *Nature Neuroscience, 16*(2), 210-218. doi: Doi 10.1038/Nn.3305
Kamondi, A., Acsady, L., Wang, X. J., & Buzsaki, G. (1998). Theta oscillations in somata and dendrites of hippocampal pyramidal cells in vivo: activity-dependent phase-precession of action potentials. *Hippocampus, 8*(3), 244-261. doi: 10.1002/(SICI)1098-1063(1998)8:3<244::AID-HIPO7>3.0.CO;2-J
Klausberger, T., & Somogyi, P. (2008). Neuronal diversity and temporal dynamics: the unity of hippocampal circuit operations. *Science, 321*(5885), 53-57. doi: 321/5885/53 [pii]
10.1126/science.1149381
Koch, C. (1999). *Biophysics of Computation, Information Processing in Single Neurons*: Oxford University Press.
Larkum, M. E., Kaiser, K. M., & Sakmann, B. (1999). Calcium electrogenesis in distal apical dendrites of layer 5 pyramidal cells at a critical frequency of back-propagating action potentials. *Proc Natl Acad Sci U S A, 96*(25), 14600-14604.
Larkum, M. E., Nevian, T., Sandler, M., Polsky, A., & Schiller, J. (2009). Synaptic integration in tuft dendrites of layer 5 pyramidal neurons: a new unifying principle. *Science, 325*(5941), 756-760.
Larkum, M. E., Senn, W., & Luscher, H. R. (2004). Top-down dendritic input increases the gain of layer 5 pyramidal neurons. *Cerebral Cortex, 14*(10), 1059-1070. doi: 10.1093/cercor/bhh065
bhh065 [pii]
Larkum, M. E., Waters, J., Sakmann, B., & Helmchen, F. (2007). Dendritic spikes in apical Dendrites of neocortical layer 2/3 pyramidal neurons. *Journal of Neuroscience, 27*(34), 8999-9008. doi: Doi 10.1523/Jneurosci.1717-07.2007
Lee, S. H., Kwan, A. C., & Dan, Y. (2014). Interneuron subtypes and orientation tuning. *Nature, 508*(7494), E1-2. doi: nature13128 [pii]
10.1038/nature13128
Lee, S. H., Kwan, A. C., Zhang, S., Phoumthipphavong, V., Flannery, J. G., Masmanidis, S. C., . . . Dan, Y. (2012). Activation of specific interneurons improves V1 feature selectivity and visual perception. *Nature, 488*(7411), 379-383. doi: nature11312 [pii]
10.1038/nature11312
Magee, J., Hoffman, D., Colbert, C., & Johnston, D. (1998). Electrical and calcium signaling in dendrites of hippocampal pyramidal neurons. *Annu Rev Physiol, 60*, 327-346. doi: 10.1146/annurev.physiol.60.1.327
Mainen, Z. F., & Sejnowski, T. J. (1996). Influence of dendritic structure on firing pattern in model neocortical neurons. *Nature, 382*(6589), 363-366. doi: 10.1038/382363a0
Markram, H., & Sakmann, B. (1994). Calcium transients in dendrites of neocortical neurons evoked by single subthreshold excitatory postsynaptic potentials via low-voltage-activated calcium channels. *Proc Natl Acad Sci U S A, 91*(11), 5207-5211.
Marsalek, P., Koch, C., & Maunsell, J. (1997). On the relationship between synaptic input and spike output jitter in individual neurons. *Proc. Natl. Acad. Sci., 94*, 735-740.
Mel, B. (Ed.). (1992). *The clusteron: toward a simple abstraction for a complex neuron* (Vol. 4). San Matea, CA.
Mel, B. W. (1992). Nmda-Based Pattern-Discrimination in a Modeled Cortical Neuron. *Neural Computation, 4*(4), 502-517. doi: Doi 10.1162/Neco.1992.4.4.502
Milojkovic, B. A., Zhou, W. L., & Antic, S. D. (2007). Voltage and calcium transients in basal dendrites of the rat prefrontal cortex. *Journal of Physiology-London, 585*(2), 447-468. doi: Doi 10.1113/Jphysiol.2007.142315
Mizuseki, K., Sirota, A., Pastalkova, E., & Buzsaki, G. (2009). Theta oscillations provide temporal windows for local circuit computation in the entorhinal-hippocampal loop. *Neuron, 64*(2), 267-280. doi: S0896-6273(09)00673-4 [pii]
10.1016/j.neuron.2009.08.037
Murayama, M., Perez-Garci, E., Nevian, T., Bock, T., Senn, W., & Larkum, M. E. (2009). Dendritic encoding of sensory stimuli controlled by deep cortical interneurons. *Nature, 457*(7233), 1137-1141. doi: nature07663 [pii]
10.1038/nature07663

O'Keefe, J., & Recce, M. L. (1993). Phase relationship between hippocampal place units and the EEG theta rhythm. *Hippocampus, 3*(3), 317-330.

Oviedo, H., & Reyes, A. D. (2002). Boosting of neuronal firing evoked with asynchronous and synchronous inputs to the dendrite. *Nat Neurosci, 5*(3), 261-266. doi: 10.1038/nn807
nn807 [pii]

Palmer, L., Murayama, M., & Larkum, M. (2012). Inhibitory regulation of dendritic activity in vivo. *Frontiers in Neural Circuits, 6*. doi: Artn 26
Doi 10.3389/Fncir.2012.00026

Palmer, L. M., Schulz, J. M., Murphy, S. C., Ledergerber, D., Murayama, M., & Larkum, M. E. (2012). The Cellular Basis of GABA(B)-Mediated Interhemispheric Inhibition. *Science, 335*(6071), 989-993. doi: Doi 10.1126/Science.1217276

Palmer, L. M., Shai, A. S., Reeve, J. E., Anderson, H. L., Paulsen, O., & Larkum, M. E. (2014). NMDA spikes enhance action potential generation during sensory input. *Nat Neurosci, 17*(3), 383-390. doi: nn.3646 [pii]
10.1038/nn.3646

Papoutsi, A., Kastellakis, G., Psarrou, M., Anastasakis, S., & Poirazi, P. (2013). Coding and decoding with dendrites. *J Physiol Paris*. doi: S0928-4257(13)00033-8 [pii]
10.1016/j.jphysparis.2013.05.003

Pare, D., Shink, E., Gaudreau, H., Destexhe, A., & Lang, E. J. (1998). Impact of spontaneous synaptic activity on the resting properties of cat neocortical pyramidal neurons In vivo. *J Neurophysiol, 79*(3), 1450-1460.

Perez-Garci, E., Larkum, M. E., & Nevian, T. (2013). Inhibition of dendritic Ca2+ spikes by GABAB receptors in cortical pyramidal neurons is mediated by a direct Gi/o-beta-subunit interaction with Cav1 channels. *J Physiol, 591*(Pt 7), 1599-1612. doi: jphysiol.2012.245464 [pii]
10.1113/jphysiol.2012.245464

Pinsky, P. F., & Rinzel, J. (1994). Intrinsic and network rhythmogenesis in a reduced Traub model for CA3 neurons. *J Comput Neurosci, 1*(1-2), 39-60.

Poirazi, P., Brannon, T., & Mel, B. (2003a). Arithmetic of subthreshold synaptic summation in a model CA1 pyramidal cell. *Neuron, 37*, 977-987.

Poirazi, P., Brannon, T., & Mel, B. (2003b). Pyramidal neuron as two-layer neural network. *Neuron, 37*, 989-999.

Polsky, A., Mel, B. W., & Schiller, J. (2004). Computational subunits in thin dendrites of pyramidal cells. *Nat Neurosci, 7*(6), 621-627.

Pouille, F., & Scanziani, M. (2001). Enforcement of temporal fidelity in pyramidal cells by somatic feed-forward inhibition. *Science, 293*(5532), 1159-1163. doi: 10.1126/science.1060342
293/5532/1159 [pii]

Remme, M. W., Lengyel, M., & Gutkin, B. S. (2010). Democracy-independence trade-off in oscillating dendrites and its implications for grid cells. *Neuron, 66*(3), 429-437. doi: S0896-6273(10)00298-9 [pii]
10.1016/j.neuron.2010.04.027

Royer, S., Zemelman, B. V., Losonczy, A., Kim, J., Chance, F., Magee, J. C., & Buzsaki, G. (2012). Control of timing, rate and bursts of hippocampal place cells by dendritic and somatic inhibition. *Nat Neurosci, 15*(5), 769-775. doi: nn.3077 [pii]
10.1038/nn.3077

Schiller, J., Schiller, Y., Stuart, G., & Sakmann, B. (1997). Calcium action potentials restricted to distal apical dendrites of rat neocortical pyramidal neurons. *Journal of Physiology-London, 505*(3), 605-616. doi: Doi 10.1111/J.1469-7793.1997.605ba.X

Seamans, J. K., Gorelova, N. A., & Yang, C. R. (1997). Contributions of voltage-gated Ca2+ channels in the proximal versus distal dendrites to synaptic integration in prefrontal cortical neurons. *J Neurosci, 17*(15), 5936-5948.

Taxidis, J., Mizuseki, K., Mason, R., & Owen, M. R. (2013). Influence of slow oscillation on hippocampal activity and ripples through cortico-hippocampal synaptic interactions, analyzed by a cortical-CA3-CA1 network model. *Front Comput Neurosci, 7*, 3. doi: 10.3389/fncom.2013.00003

Williams, S. R., & Stuart, G. J. (1999). Mechanisms and consequences of action potential burst firing in rat neocortical pyramidal neurons. *J Physiol, 521 Pt 2*, 467-482. doi: PHY_9930 [pii]

Chapter 5

Cauller, L. J., & Connors, B. W. (1994). Synaptic physiology of horizontal afferents to layer I in slices of rat SI neocortex. *J Neurosci, 14*(2), 751-762.

Felleman, D. J., & Van Essen, D. C. (1991). Distributed hierarchical processing in the primate cerebral cortex. *Cereb Cortex, 1*(1), 1-47.

Hubel, D. H. (1982). Cortical neurobiology: a slanted historical perspective. *Annu Rev Neurosci, 5*, 363-370. doi: 10.1146/annurev.ne.05.030182.002051

Larkum, M. E., Nevian, T., Sandler, M., Polsky, A., & Schiller, J. (2009). Synaptic integration in tuft dendrites of layer 5 pyramidal neurons: a new unifying principle. *Science, 325*(5941), 756-760.

Self, M. W., Kooijmans, R. N., Super, H., Lamme, V. A., & Roelfsema, P. R. (2012). Different glutamate receptors convey feedforward and recurrent processing in macaque V1. *Proc Natl Acad Sci U S A, 109*(27), 11031-11036. doi: 10.1073/pnas.1119527109
1119527109 [pii]

Buzsáki, György. "Neural Syntax: Cell Assemblies, Synapsembles, and Readers." *Neuron* 68, no. 3 (2010): 362–85.

Buzsáki, György, and Kenji Mizuseki. "The Log-Dynamic Brain: How Skewed Distributions Affect Network Operations." *Nature Reviews Neuroscience* 15, no. 4 (2014): 264–78.

Crutchfield, James P. "The Calculi of Emergence: Computation, Dynamics and Induction." *Physica D: Nonlinear Phenomena* 75, no. 1 (1994): 11–54.

De Kock, C P J, and B Sakmann. "High Frequency Action Potential Bursts (≥ 100 Hz) in L2/3 and L5B Thick Tufted Neurons in Anaesthetized and Awake Rat Primary Somatosensory Cortex." *The Journal of Physiology* 586, no. Pt 14 (July 15, 2008): 3353–64. doi:10.1113/jphysiol.2008.155580.

Fuster, JoaquÃn M. *Cortex and Mind: Unifying Cognition*. Oxford university press, 2003. http://psycnet.apa.org/psycinfo/2002-18891-000.

Hayek, Friedrich August. *The Sensory Order: An Inquiry into the Foundations of Theoretical Psychology*. University of Chicago Press, 1999. https://books.google.com/books?hl=en&lr=&id=UFazm1Xy_j4C&oi=fnd&pg=PR6&dq=The+Sensory+Order:+An+Inquiry+into+the+Foundations+of+Theoretical+Psychology+&ots=8M8XQppbR1&sig=X8dwgbN0lvfxmJklkhsSbTNS9iI.

Hubel, David H. "Cortical Neurobiology: A Slanted Historical Perspective." *Annual Review of Neuroscience* 5, no. 1 (1982): 363–70.

Jiang, Xiaolong, Guangfu Wang, Alice J. Lee, Ruth L. Stornetta, and J. Julius Zhu. "The Organization of Two New Cortical Interneuronal Circuits." *Nature Neuroscience* 16, no. 2 (2013): 210–18.

Larkum, Matthew. "A Cellular Mechanism for Cortical Associations: An Organizing Principle for the Cerebral Cortex." *Trends in Neurosciences* 36, no. 3 (2013): 141–51.

Lisman, John E. "Bursts as a Unit of Neural Information: Making Unreliable Synapses Reliable." *Trends in Neurosciences* 20, no. 1 (1997): 38–43.

Markram, Henry, Anirudh Gupta, Asher Uziel, Yun Wang, and Misha Tsodyks. "Information Processing with Frequency-Dependent Synaptic Connections." *Neurobiology of Learning and Memory* 70, no. 1 (1998): 101–12.

Oizumi, Masafumi, Larissa Albantakis, and Giulio Tononi. "From the Phenomenology to the Mechanisms of Consciousness: Integrated Information Theory 3.0," 2014. http://dx.plos.org/10.1371/journal.pcbi.1003588.

Palmer, Lucy M., Jan M. Schulz, Sean C. Murphy, Debora Ledergerber, Masanori Murayama, and Matthew E. Larkum. "The Cellular Basis of GABAB-Mediated Interhemispheric Inhibition." *Science* 335, no. 6071 (2012): 989–93.

Pérez-Garci, Enrique, Matthew E. Larkum, and Thomas Nevian. "Inhibition of Dendritic Ca2+ Spikes by GABAB Receptors in Cortical Pyramidal Neurons Is Mediated by a Direct Gi/o-

Bγ-Subunit Interaction with Cav1 Channels." *The Journal of Physiology* 591, no. 7 (2013): 1599–1612.

Royer, Sébastien, Boris V. Zemelman, Attila Losonczy, Jinhyun Kim, Frances Chance, Jeffrey C. Magee, and György Buzsáki. "Control of Timing, Rate and Bursts of Hippocampal Place Cells by Dendritic and Somatic Inhibition." *Nature Neuroscience* 15, no. 5 (2012): 769–75.

Shai, Adam S., Christof Koch, and Costas A. Anastassiou. "Spike-Timing Control by Dendritic Plateau Potentials in the Presence of Synaptic Barrages." *Frontiers in Computational Neuroscience* 8 (2014). http://www.ncbi.nlm.nih.gov/pmc/articles/PMC4132263/.

Sherman, S. Murray, and R. W. Guillery. "Distinct Functions for Direct and Transthalamic Corticocortical Connections." *Journal of Neurophysiology* 106, no. 3 (September 1, 2011): 1068–77. doi:10.1152/jn.00429.2011.

———. "The Role of the Thalamus in the Flow of Information to the Cortex." *Philosophical Transactions of the Royal Society B: Biological Sciences* 357, no. 1428 (2002): 1695–1708.

Tsodyks, Misha, Klaus Pawelzik, and Henry Markram. "Neural Networks with Dynamic Synapses." *Neural Computation* 10, no. 4 (1998): 821–35.

Tsodyks, Misha V., and Henry Markram. "The Neural Code between Neocortical Pyramidal Neurons Depends on Neurotransmitter Release Probability." *Proceedings of the National Academy of Sciences* 94, no. 2 (1997): 719–23.